Author:
Beesley, Mair E W

Title:
A framework for assessing parameter variability of soil stress-strain data using triaxial test databases

A framework for assessing parameter variability of soil stress-strain data using triaxial test databases

BY

MAIR BEESLEY

DEPARTMENT OF CIVIL ENGINEERING

UNIVERSITY OF BRISTOL

A dissertation submitted to the University of Bristol in accordance with the requirements of the degree of DOCTOR OF PHILOSOPHY in the Faculty of Engineering.

October 2019

59351 words

Abstract

Manufacture of construction materials accounts for around 10% of total UK carbon emissions. Specification and installation of smaller design elements, such as foundations and retaining walls, would enable a significant part of the UK government's target 80% reduction in greenhouse gas emissions by 2050. To this end, the rationale for applying high factors of safety in civil engineering should be challenged by academics and practitioners by considering new design and management processes for buildings and infrastructure.

An assessment of foundation safety requires the prediction of reserve capacity of the geotechnical structure under extreme loading. However, since loads are difficult to measure, assessing the real safety margin is usually achieved by examining the extent of ground displacements and building damage after an extreme event has taken place. Even under safe conditions, operating a structure may provoke excessive ground movements which cause functional and economic loss in nearby assets. Performance-based methods such as Mobilisable Strength Design (MSD) may present an opportunity to improve design efficiencies if the uncertainty associated with settlement predictions can be reduced.

This thesis presents a method to develop and analyse soil test databases for the purpose of characterising stress-strain variability in soils. Various strength mobilisation models are evaluated for their suitability to characterise nonlinear stress-strain behaviour of soil within the moderate stress range. Behavioural influences are studied using the parameters of the chosen model in the context of a statistical framework using a large laboratory database of reconstituted fine-grained materials collected from various publications. Sensitivity of the parameters to shear mode anisotropy, stress history, strain rate, liquid limit and plastic limit is examined by employing single and multiple linear regression analysis techniques. Results of the database analysis are compared with observations from previously reported tests on intact Bothkennar clay and a laboratory programme of isotropically consolidated triaxial compression and extension tests on Kaolin and Bothkennar clay. The new tests validate the relationships between mobilisation strain and overconsolidation ratio identified by analysis of the database and provide evidence for the causes of parameter variability, including differences in procedure and measurement uncertainty.

Using the framework presented in this study, informed decisions can be made about whether to use an empirical correlation calibrated with a database, accepting that the error range in the prediction represents parameter variability of the various soils in the database, or to invest in more tests to achieve the estimated reduction in variability for a particular soil. The results presented for reconstituted soils and a single deposit of soft clay demonstrate the potential value in using test databases for geotechnical variability analysis which could assist ground characterisation assessments on large-scale infrastructure projects.

Dedication and Acknowledgements

First, I would like to express my gratitude for the financial support of this research project that has been provided through the Engineering and Physical Sciences Research Council (EPSRC) Studentship Award.

I gratefully acknowledge the contributions of my supervisors, Dr. Paul Vardanega and Dr. Erdin Ibraim, and thank them for their recommendations and thoughtful comments on this dissertation. I would also like to thank Paul for being always generous with his time and advice and encouraging many opportunities to debate and present my work. I would like to thank Erdin particularly for his guidance on the experimental investigation and helpful suggestions on the structure of the thesis.

I will always be grateful to Dr. David Nash, who inspired and guided me as a mentor and friend from the start and to whom I owe the pleasure of many illuminating discussions on geotechnical engineering and classical music alike, many taking place after his retirement from the university. David's kindness and inspirational gift for teaching are greatly missed.

For her continued support and generous advice, over many cups of tea, I am indebted to Dr. Liz Holcombe. Liz's wide-ranging insights have taught me how to understand engineering problems from multiple scales and perspectives and how to put research into practice during a hugely rewarding trip to Saint Lucia.

Right up here also is the tremendous Gary Martin, who provided constant support and a patient presence in the laboratory while helping me to develop and manufacture many iterations of equipment designs. Gary taught me how to operate most of the equipment in the laboratory.

There are many friends and colleagues of mine whose excellent company ensured that the PhD experience was rewarding and frustrating in equal measure and made me learn about much more than soil mechanics: Eddie, Hugo, Alex, Sam, Alessandro, Yiota, Greg, Giulio, Charlotte, Jamie, Nicola, David. A special shout out to my fellow lab inhabitants, Marina, Lucas, and Lawrence, all of whom have made working in the lab such a joy and provided many stimulating technical (and far from technical!) discussions. Huge thanks also go to my friends outside the university who watched on with patient incredulity and kept me laughing - Alex, Katy, Elly, Liam, Darius, and Francisco.

To my family – this one's for you. Thank you for your unending love and humour and for cheering me on to the finish line. I could not have done it without you.

Author's Declaration

I declare that the work in this dissertation was carried out in accordance with the requirements of the University's Regulations and Code of Practice for Research Degree Programmes and that it has not been submitted for any other academic award. Except where indicated by specific reference in the text, the work is the candidate's own work. Work done in collaboration with, or with the assistance of, others, is indicated as such. Any views expressed in the dissertation are those of the author.

Signed: .....

Mair Elizabeth Williams Beesley

Date: 14 October 2019

Table of Contents

1. Introduction 1

1.1 Chapter outline 2

2. Literature review 4

2.1 Introduction 4

2.2 Variation of undrained shear strength 5

2.3 Variation of undrained stiffness 8

2.3.1 Undrained stiffness related to moderate strains 8

2.3.2 Undrained stiffness related to small strains 10

2.3.3 Variation of undrained stiffness within a single material 10

2.4 Proposed research objectives 12

3. A method to develop and analyse soil test databases: for the variability characterisation of undrained stress-strain behaviour 13

3.1 Geotechnical variability characterisation 13

3.2 The problem case: stress-strain characterisation in the moderate stress range 14

3.3 Motivation for investigating triaxial tests 15

3.4 A parameter variability assessment framework using test databases 17

3.4.1 Selection of soil materials for database analysis 20

3.4.2 Laboratory test database development 24

3.4.3 Pre-failure stress-strain models in the moderate stress range 33

3.4.4 Evaluation of pre-failure stress-strain models in the moderate stress range 38

3.4.5 Nonlinear stress-strain functions selected for the analytical investigation 40

3.4.6 Statistical techniques to evaluate a database of stress-strain test data 41

3.5 Conclusion 44

4. Parameter variability of consolidated undrained triaxial tests using two databases 45

4.1 Introduction 45
4.2 Selecting a suitable nonlinear model for the parameter database 45
4.2.1 Research objectives: 45
4.2.2 Reasons for curve fitting 45
4.2.3 Assessment of three alternative simple nonlinear models for stress-strain 46
4.2.4 Selected stress-strain model 60
4.3 Analysis of parameter variability with test mode, stress history, composition and test procedure 61
4.3.1 Research objective: 61
4.3.2 Classification of database samples 62
4.3.3 Categorisation of test data by test mode 62
4.3.4 Range of stress-strain behaviour by test mode 64
4.3.5 What is *b*? 67
4.3.6 Correlation of Power Law model parameters with *OCR* by simple linear regression 68
4.3.7 Estimation of intact soil parameters from *OCR* and *YSR* 74
4.3.8 Influence of *OCR* on Power Law model parameters: intact versus reconstituted 76
4.3.9 Relationship between *b*, *OCR*, and point of maximum curvature (max_K) 81
4.3.10 Influence of consolidation stress on Power Law model parameters 84
4.3.11 Influence of strain rate 89
4.3.12 Influence of sampling disturbance 91
4.3.13 Influence of plasticity 93
4.3.14 Multiple Linear Regression Analysis: influence of multiple experimental variables 96
4.3.15 Calculated uncertainty of using parameter transformation models to predict stress-strain 101
4.4 Analysis of shear-mode anisotropy by comparison of compression and extension parameters 120

4.4.1 Comparing shear modes to estimate parameter variation 120
4.4.2 Research objective 120
4.4.3 Comparing average trends in compression and extension parameters..... 120
4.4.4 Parameter transformation models from comparisons of compression and extension…….. 123
4.5 Recommended correlations to describe parameter variability of reconstituted soils 132
4.6 Discussion……..134
5. Developing an experimental strategy to investigate stress-strain variability using two soils 140
5.1 Introduction 140
5.2 Selection of experimental materials 140
5.2.1 Reconstituted Kaolin..... 141
5.2.2 Undisturbed and Reconstituted Bothkennar clay..... 142
5.2.3 Geology of Bothkennar..... 142
5.3 Experimental procedures..... 143
5.3.1 Laboratory infrastructure 143
5.3.2 Experimental apparatus..... 144
5.3.3 Sampling procedure 148
5.3.4 CU Triaxial test procedure..... 151
5.3.5 UU Triaxial test procedure..... 161
5.3.6 Oedometer test procedure 161
5.4 Accuracy of sensors and control system..... 161
5.4.1 Calibration..... 162
5.4.2 Stability..... 162
5.4.3 Control 162
5.4.4 Resolution 162
5.4.5 Combined uncertainty of measured quantities..... 162
5.5 Data calculations and parameter approximations..... 164
5.6 Laboratory test programme 166

6. Experimental results: material behaviour and parameter assessment of Kaolin and Bothkennar in the moderate stress range 170
6.1 Material behaviour of Kaolin and Bothkennar 170
6.1.1 Research objectives: 170
6.1.2 Classification of Kaolin and Bothkennar samples 170
6.1.3 Compressibility of reconstituted Kaolin under K_0 conditions 172
6.1.4 Compressibility of reconstituted Kaolin and Bothkennar under isotropic conditions 175
6.1.5 Shearing behaviour of reconstituted Kaolin 178
6.1.6 Shearing behaviour of reconstituted and intact Bothkennar 184
6.2 Influence of *OCR* and shear mode on parameter variability 186
6.2.1 Variation of c_u/σ'_{v0}, $\gamma_{50\ Power}$ and b with *OCR* 186
6.2.2 Influence of shear mode 191
6.3 Influence of test procedure on parameter variability 192
6.3.1 Effects of consolidation procedure on parameters 192
6.3.2 Effects of shearing procedure on parameters 194
6.4 Influence of data interpretation on parameter variability 195
6.4.1 Assumed deformation shape of triaxial specimen 195
6.4.2 Number of data points between S=0.2 and 0.8 197
6.5 Validation of transformation models from RFG/TXCU-278 197
6.5.1 Validated uncertainty estimation of parameter transformation models 198
6.5.2 Validated uncertainty estimation of using parameter transformation models to predict stress-strain 202
6.5.3 Validated uncertainty estimation of fitted power-law functions 206
6.5.4 Example: using the calibrated factor errors to estimate variable stress-strain behaviour 206
6.6 Conclusions 207
7. Footing settlement predictions with parameter variability assessment 210

7.1 Introduction 210
7.1.1 Research objectives 210
7.2 Mobilisable Strength Design 211
7.3 Design example 211
7.4 Design charts using MSD-MSF and implications for factors of safety 214
8. Conclusions and recommendations for future work 218
References 225
Appendices 242

List of Figures

Figure 2- 1. Power law relationship between normalised shear strain and mobilised stress proposed by Vardanega and Bolton (2011) 9

Figure 3- 1. Sources of variability of a soil test parameter 17

Figure 3- 2. Chart showing relationships between E_{u50}/c_u and *OCR* proposed by Duncan and Buchignani (1976) for estimating undrained modulus of clay based on back-calculated field measurements (digitised from the original publication) 33

Figure 4- 1. Residuals of observed stress ratio for CIUC tests in RFG/TXCU-278 (114 tests) by curve-fitting model: (a) Model 1 (b) Model 2 (c) Model 3. 48

Figure 4- 2. Residuals of observed stress ratio for CKUC tests in RFG/TXCU-278 (34 tests) by curve-fitting model: (a) Model 1 (b) Model 2 (c) Model 3. 49

Figure 4- 3. Residuals of observed stress ratio for CIUE tests in RFG/TXCU-278 (55 tests) by curve-fitting model: (a) Model 1 (b) Model 2 (c) Model 3. 50

Figure 4- 4. Residuals of observed stress ratio for CKUE tests in RFG/TXCU-278 (34 tests) by curve-fitting model: (a) Model 1 (b) Model 2 (c) Model 3. 51

Figure 4- 5. Comparison of model bias introduced by different curve-fitting models using Mean Average. The test data of RFG/TXCU-278 are grouped by test mode and by increments of stress ratio: 0.2-0.225, 0.225-0.275, 0.275-0.325, 0.325-0.375, 0.375-0.425, 0.425-0.475, 0.475-0.525, 0.525-0.575, 0.575-0.625, 0.625-0.675, 0.675-0.725, 0.725-0.775, 0.775-0.8. (a) Model 1 (b) Model 2 (c) Model 3. 52

Figure 4- 6. Comparison of Model 2 and Model 3 per triaxial test using data in RFG/TXCU-278. Histogram bins are categorised by OCR range applicable to the reconstituted soil test. Colours indicate where Model 3 (Logarithmic law) outperforms Model 2 (Power law) and vice versa. 55

Figure 4- 7. Comparison of Model 2 and Model 3 per triaxial test using data in BTK/TXCU-34. Histogram bins are categorised by Sampling Depth range applicable to the Intact triaxial test from the Bothkennar Test Site (SERC 1989). Colours indicate where Model 3 (Logarithmic law) outperforms Model 2 (Power law) and vice versa. 55

Figure 4- 8. Comparison of model error introduced by Model 2 and Model 3 using 10^{th}, 50^{th} (Median), and 90^{th} Percentiles. The test data of RFG/TXCU-278 are grouped by test mode (CIUC) and by increments of stress ratio (see Figure 4- 5). 57

Figure 4- 9. Comparison of model error introduced by Model 2 and Model 3 using 10^{th}, 50^{th} (Median), and 90^{th} Percentiles. The test data of RFG/TXCU-278 are grouped by test mode (CKUC) and by increments of stress ratio (see Figure 4- 5). 57

Figure 4- 10. Comparison of model error introduced by Model 2 and Model 3 using 10^{th}, 50^{th} (Median), and 90^{th} Percentiles. The test data of RFG/TXCU-278 are grouped by test mode (CIUE) and by increments of stress ratio (see Figure 4- 5). 58

Figure 4- 11. Comparison of model error introduced by Model 2 and Model 3 using 10^{th}, 50^{th} (Median), and 90^{th} Percentiles. The test data of RFG/TXCU-278 are grouped by test mode (CKUE) and by increments of stress ratio (see Figure 4- 5). 58

Figure 4- 12. Normalised shear strains within 0.01 of the reference stress ratio, S, indicated by red lines (CIUC test mode data only from RFG/TXCU-278) 59

Figure 4- 12. Distribution of normalised shear strains within 0.01 of the reference stress ratio, *S*, and including data from all 4 test modes in databases RFG/TXCU-278 and BTK/TXCU-34 summarised by minima, maxima, 10^{th}, 50^{th} and 90^{th} percentiles 60

Figure 4- 13. Classification of materials in RFG/TXCU-278 and BTK/TXCU-34 63

Figure 4- 14. Stress ratio (*S*) measurements plotted against shear strain measurements $\gamma=1.5\varepsilon_{axial}$ for 305 triaxial tests, 23 reconstituted fine-grained soils, 1 intact soil (Bothkennar clay) 64

Figure 4- 15. Effect of strain normalisation and Power Law Model characterisation on triaxial compression measurements of stress ratio (*S*) and shear strain ($\gamma=1.5\varepsilon_{axial}$) 65

Figure 4- 16. Effect of strain normalisation and Power Law Model characterisation on triaxial extension measurements of stress ratio (*S*) and shear strain ($\gamma=1.5\varepsilon_{axial}$) 66

Figure 4- 17. Range of normalised strain data plotted against the fitted exponent, *b* (all reconstituted test data shown by test mode) 67

Figure 4- 18. Variation of $\gamma_{50\ Power}$ with *OCR* for reconstituted specimens sheared from (a) isotropic consolidation stresses (b) K_0 consolidation stresses 69

Figure 4- 19. Variation of $\gamma_{50\ Power}$ with sampling depth for intact specimens sheared from K_0 consolidation stresses 69

Figure 4- 20. Variation of *b* with *OCR* for reconstituted specimens sheared from (a) isotropic consolidation stresses (b) K_0 consolidation stresses 71

Figure 4- 21. Variation of *b* with sampling depth for intact specimens sheared from K_0 consolidation stresses 71

Figure 4- 22. Variation of c_u/σ'_{v0} with *OCR* for reconstituted specimens sheared from (a) isotropic consolidation stresses (b) K_0 consolidation stresses 72

Figure 4- 24. Variation of c_u/σ'_{v0} with sampling depth for intact specimens sheared from K_0 consolidation stresses 72

Figure 4- 23. Variation of yield stress ratio (*YSR*) measurements with depth (Nash et al. 1992) and interpreted *YSR* (or apparent *OCR*) profile with depth (Hight et al. 1992a) 74

Figure 4- 24. Variation of estimated $\gamma_{50\ Power\ CKUC}$ using *YSR* profile (Figure 4-25, Hight et al. 1992a) or estimated geological *OCR*=1.2 and Equation 4.3 75

Figure 4- 25. Variation of estimated $c_u/\sigma'_{v0\ CKUC}$ using *YSR* profile (Figure 4-25, Hight et al. 1992a) or estimated geological *OCR* (Figure 4- 25) and Equations 4.7 & 4.9 75

Figure 4- 26. Variation of $\gamma_{50\ Power}$ with *OCR* for reconstituted (various) and intact (Bothkennar) specimens sheared in triaxial compression from K_0 consolidated stresses 77

Figure 4- 27. Variation of $\gamma_{50\ Power}$ with *OCR* for reconstituted (various) and intact (Bothkennar) specimens sheared in triaxial extension from K_0 consolidated stresses 77

Figure 4- 28. Variation of *b* with *OCR* for reconstituted specimens sheared in triaxial compression from K_0 consolidated stresses 78

Figure 4- 29. Variation of *b* with *OCR* for reconstituted specimens sheared in triaxial extension from K_0 consolidated stresses 78

Figure 4- 30. Effect of SHANSEP procedure on the normalised stress-strain behaviour of 4 intact specimens of Bothkennar 79

Figure 4- 31. Normalised stress-strain behaviour of all BTK/TXCU-34 79

Figure 4- 32. Comparison of Power Law model parameters from triaxial tests consolidated under isotropic stress conditions 80

Figure 4- 33. Comparison of Power Law model parameters from triaxial tests consolidated under K_0 stress conditions 80

Figure 4- 34. Variation of the *point of maximum curvature* with *b* from CKUC triaxial tests 82

Figure 4- 35. Variation of the *point of maximum curvature* with *b* from CKUE triaxial tests 83

Figure 4- 36. Variation of the *point of maximum curvature* with *OCR* (applied or apparent) from CKUC triaxial tests 83

Figure 4- 37. Variation of the *point of maximum curvature* with *OCR* (applied or apparent) from CKUE triaxial tests 83

Figure 4- 38. Vertical effective stress in situ (digitised from Nash et al. 1992) and applied to tests in BTK/TXCU-34 85

Figure 4- 39. Variation in $\gamma_{50\ Power\ CKUC}$ with present vertical effective consolidation stress σ'_{v0} 87

Figure 4- 40. Variation in $\gamma_{50\ Power\ CKUE}$ with present vertical effective consolidation stress σ'_{v0} 87

Figure 4- 41. Variation of undrained shear strength (c_u) with present vertical effective consolidation stress (σ'_{v0}) measured in CKUC triaxial tests 88

Figure 4- 42. Variation of undrained shear strength (c_u) with present vertical effective consolidation stress (σ'_{v0}) measured in CKUE triaxial tests 88

Figure 4- 43. Variation of normally consolidated strength ratio $c_u / \sigma'_{VO\ NC}$ with axial strain rate applied during undrained shear 89

Figure 4- 44. Variation of $\gamma_{50\ Power\ NC}$ and b with axial strain rate applied during undrained shear 89

Figure 4- 45. Variation of $\gamma_{50\ Power}$ and c_u / σ'_{VO} with axial strain rate applied during undrained shear 90

Figure 4- 46. Variation of $\gamma_{50\ Power}$ with sampling depth and sampling procedure (positive = triaxial compression; negative = triaxial extension) 92

Figure 4- 47. Variation of b with sampling depth and sampling procedure 92

Figure 4- 48. Relationship between normalised undrained shear strength and plasticity index (I_P) for reconstituted soil samples normally consolidated under isotropic or K_0 conditions and sheared in undrained triaxial compression or extension (SHANSEP tests on intact Bothkennar clay included for comparison) 93

Figure 4- 49. Relationship between $\gamma_{50\ Power}$ and plasticity index (I_P) for reconstituted soil samples normally consolidated under isotropic or K_0 conditions and sheared in undrained triaxial compression or extension (SHANSEP tests on intact Bothkennar clay included for comparison) 94

Figure 4- 50. Variation of classification test results reported for the triaxial test specimens in BTK/TXCU-34 95

Figure 4- 51. Predicted-measured plots of $c_{u\ CIUC}$ (n=115 data points, RFG/TXCU-278) predicted using the best-fit single linear regression with σ'_{v0} 98

Figure 4- 52. Predicted-measured plots of $c_{u\ CIUC}/\sigma'_{v0}$ (n=115 data points, RFG/TXCU-278) predicted using best-fit single and multiple linear regression equations with the following variables: *OCR*, strain rate ($\dot{\varepsilon_a}$), w_L and w_P (see Table 4-8) 98

Figure 4- 53. Predicted-measured plots of $\gamma_{50\ Power,\ CIUC}$ (n=114 data points, RFG/TXCU-278) predicted using best-fit single and multiple linear regression equations with the following variables: σ'_{v0}, *OCR*, strain rate ($\dot{\varepsilon_a}$), w_L and w_P (see Table 4- 9) 99

Figure 4- 56. Predicted-measured plots of $b_{\ CIUC}$ (n=114 data points, RFG/TXCU-278) predicted using best-fit single and multiple linear regression equations with the following variables: $\gamma_{50\ Power,\ CIUC}$, strain rate ($\dot{\varepsilon_a}$), w_L and w_P (see Table 4- 10) 99

Figure 4- 54. Predicted-measured plots of Measured Stress Ratio (S) of *all stress-strain data* between 20%≤S≤80% (n=2069 data points) in the CIUC test database (RFG/TXCU-278), predicted using: (a) Equation 4.10 (b) Equation 4.11 (c) Equation 4.12 (d) model parameters $\gamma_{50\ Power}$ and b of every triaxial test 108

Figure 4- 55. Predicted-measured plots of γ (= $1.5\varepsilon_a$) of *all stress-strain data* between 20%≤S≤80% (n=2069 data points) in the CIUC test database (RFG/TXCU- 109

278), predicted using: (a) Equation 4.10 (b) Equation 4.11 (c) Equation 4.12 (d) model parameters $\gamma_{50\ Power}$ and *b* of every triaxial test

Figure 4- 56. Predicted-measured plots of G_{sec}/c_u (since τ_0=0) of *all stress-strain data* between 20%≤*S*≤80% (*n*=2069 data points) in the CIUC test database (RFG/TXCU-278), predicted using: (a) Equation 4.10 (b) Equation 4.11 (c) Equation 4.12 (d) model parameters $\gamma_{50\ Power}$ and *b* of every triaxial test 110

Figure 4- 57. Predicted-measured plots of Measured Stress Ratio (*S*) of *all stress-strain data* between 20%≤*S*≤80% (*n*=1049 data points) in the CKUC test database (RFG/TXCU-278), predicted using: (a) Equation 4.16 (b) Equation 4.17 (c) Equation 4.18 (d) model parameters $\gamma_{50\ Power}$ and *b* of every triaxial test 111

Figure 4- 58. Predicted-measured plots of γ (= $1.5\varepsilon_a$) of *all stress-strain data* between 20%≤*S*≤80% (*n*=1049 data points) in the CKUC test database (RFG/TXCU-278), predicted using: (a) Equation 4.16 (b) Equation 4.17 (c) Equation 4.18 (d) model parameters $\gamma_{50\ Power}$ and *b* of every triaxial test 112

Figure 4- 59. Predicted-measured plots of $G_{sec}/(c_u-\tau_0)$ of *all stress-strain data* between 20%≤*S*≤80% (*n*=1049 data points) in the CKUC test database (RFG/TXCU-278), predicted using: (a) Equation 4.16 (b) Equation 4.17 (c) Equation 4.18 (d) model parameters $\gamma_{50\ Power}$ and *b* of every triaxial test 113

Figure 4- 60. Predicted-measured plots of Measured Stress Ratio (*S*) of *all stress-strain data* between 20%≤*S*≤80% (*n*=1217 data points) in the CIUE test database (RFG/TXCU-278), predicted using: (a) Equation 4.13 (b) Equation 4.14 (c) Equation 4.15 (d) model parameters $\gamma_{50\ Power}$ and *b* of every triaxial test 114

Figure 4- 61. Predicted-measured plots of γ (= $1.5\varepsilon_a$) of *all stress-strain data* between 20%≤*S*≤80% (*n*=1217 data points) in the CIUE test database (RFG/TXCU-278), predicted using: (a) Equation 4.13 (b) Equation 4.14 (c) Equation 4.15 (d) model parameters $\gamma_{50\ Power}$ and *b* of every triaxial test 115

Figure 4- 62. Predicted-measured plots of G_{sec}/c_u (since τ_0=0) of *all stress-strain data* between 20%≤*S*≤80% (*n*=1217 data points) in the CIUE test database (RFG/TXCU-278), predicted using: (a) Equation 4.13 (b) Equation 4.14 (c) Equation 4.15 (d) model parameters $\gamma_{50\ Power}$ and *b* of every triaxial test 116

Figure 4- 63. Predicted-measured plots of Measured Stress Ratio (*S*) of *all stress-strain data* between 20%≤*S*≤80% (*n*=864 data points) in the CKUE test database (RFG/TXCU-278), predicted using: (a) Equation 4.19 (b) Equation 4.20 (c) Equation 4.21 (d) model parameters $\gamma_{50\ Power}$ and *b* of every triaxial test 117

Figure 4- 64. Predicted-measured plots of γ (= $1.5\varepsilon_a$) of *all stress-strain data* between 20%≤*S*≤80% (*n*=864 data points) in the CKUE test database (RFG/TXCU-278), predicted using: (a) Equation 4.19 (b) Equation 4.20 (c) Equation 4.21 (d) model parameters $\gamma_{50\ Power}$ and *b* of every triaxial test 118

Figure 4- 65. Predicted-measured plots of $G_{sec}/(c_u-\tau_0)$ of *all stress-strain data* between 20%≤*S*≤80% (*n*=864 data points) in the CKUE test database (RFG/TXCU-278), predicted using: (a) Equation 4.19 (b) Equation 4.20 (c) Equation 4.21 (d) model parameters $\gamma_{50\ Power}$ and *b* of every triaxial test 119

Figure 4- 66. Variation of $\gamma_{30\ Power}$, $\gamma_{50\ Power}$ and $\gamma_{70\ Power}$ with *OCR* for triaxial compression and extension tests consolidated under K_0 conditions prior to shear 121

Figure 4- 67. Variation of $\gamma_{30\ Power}$, $\gamma_{50\ Power}$ and $\gamma_{70\ Power}$ with *OCR* for triaxial compression and extension tests consolidated under K_0 conditions prior to shear 122

Figure 4- 68. Comparison of c_u/σ'_{v0} from triaxial extension and compression tests on two similarly reconstituted specimens, or two intact specimens from the same sample depth, tested at the same laboratory and with identical strain rate: (a) CIU tests (b) CKU tests 125

Figure 4- 69. Comparison of $\gamma_{30\ CIU}$ and $\gamma_{30\ CKU}$ from triaxial extension and compression tests on two similarly reconstituted specimens, or two intact specimens 126

from the same sample depth, tested at the same laboratory and with identical strain rate: (a) CIU tests and (b) CKU tests

Figure 4- 70. Comparison of $\gamma_{50\ CIU}$ and $\gamma_{50\ CKU}$ from triaxial extension and compression tests on two similarly reconstituted specimens, or two intact specimens from the same sample depth, tested at the same laboratory and with identical strain rate: (a) CIU tests and (b) CKU tests 127

Figure 4- 71. Comparison of $\gamma_{70\ CIU}$ and $\gamma_{70\ CKU}$ from triaxial extension and compression tests on two similarly reconstituted specimens, or two intact specimens from the same sample depth, tested at the same laboratory and with identical strain rate: (a) CIU tests and (b) CKU tests 128

Figure 4- 72. Comparison of *b*-values from triaxial extension and compression tests on two similarly reconstituted specimens, or two intact specimens from the same sample depth, tested at the same laboratory and with identical strain rate: (a) CIU tests (b) CKU tests 129

Figure 5- 1. Diagram of the conventional triaxial testing system used for CU tests (reproduced with permission from Bialowas 2017) 146

Figure 5- 2. Consolidometers (38mm internal diameter) set up before applying vertical stress to Kaolin slurries 148

Figure 5- 3. Reconstituted sample height and void ratio measured immediately after extrusion from the consolidometer. Trimmed intact Bothkennar specimens also plotted for reference. 150

Figure 5- 4. Location of borehole D1: origin of Bothkennar samples investigated in this study (modified from Hight et al. 1992 and Sukolrat 2007) 152

Figure 5- 5. Preparation of intact Bothkennar triaxial specimens by trimming with a piano wire and lathe 153

Figure 5- 6. Compression test setup of kaolin inside conventional isotropic triaxial cell (Linear displacement transducers are attached to the base and top caps with a lightweight connection system) 154

Figure 5- 7. Extension test setup of Kaolin sample CIUE-8-a-52 inside conventional isotropic triaxial cell with extension cap “Vacuum-1” 157

Figure 5- 8. Extension test setup of Kaolin sample inside conventional isotropic triaxial cell with extension cap “Vacuum-2” 159

Figure 5- 9. Displacement and deviator stress measurements during connection between the loading ram and specimen top cap using (a) Vacuum-1 (b) Vacuum-2 160

Figure 5- 10. Assessment of sensor accuracy; dashed lines indicate refer to a region that encompasses 99% of the data points 163

Figure 6- 1. Measurements of Atterberg Limits and moisture contents reported by SERC (1989) and performed by the author, plotted with sampling depth 171

Figure 6- 2. PSD curves for 5 Kaolin specimens (B2 = Batch 2) and 10 Bothkennar specimens measured by laser diffraction using Mastersizer 3000 (Malvern Instruments 2019) 172

Figure 6- 3. Semi-logarithmic K_0-consolidation (oedometer) curves of reconstituted kaolin mixed at different initial water content 173

Figure 6- 4. Variation of void index (I_v) with vertical effective stress for reconstituted kaolin samples mixed at different initial water contents 175

Figure 6- 5. Semi-logarithmic isotropic-consolidation curves of reconstituted kaolin at different initial water content using procedure (a) 177

Figure 6- 6. Semi-logarithmic isotropic-consolidation curves of reconstituted kaolin at different initial water content using procedure (b) 177

Figure 6- 7. Semi-logarithmic isotropic-consolidation curves of reconstituted Bothkennar and intact Bothkennar (during recompression) 178

Figure 6- 8. Effective stress paths for CIU and UU triaxial tests on reconstituted Kaolin 179

Figure 6- 8. Excess pore pressure-strain curves for CIU and UU triaxial tests on reconstituted Kaolin – comparison of tests by p'_0 normalisation 181

Figure 6- 9. Stress-strain curves for CIU and UU triaxial tests on reconstituted Kaolin – comparison of tests by p'_0 normalisation (assumed cylinder deformation) 182

Figure 6- 10. Effective stress paths for CIU and UU triaxial tests on reconstituted Kaolin – comparison of tests by p'_e normalisation (assumed cylinder deformation) 183

Figure 6- 11. Peak stresses for CIU and UU triaxial tests on reconstituted Kaolin tested with procedures (a) and (b) – comparison of tests by p'_e normalisation (assumed cylinder deformation) 183

Figure 6- 12. Stress-strain curves for CIU and UU triaxial tests on reconstituted and intact Bothkennar – comparison of tests by p'_0 normalisation 185

Figure 6- 13. Excess pore pressure-strain curves for CIU and UU triaxial tests on reconstituted and intact Bothkennar – comparison of tests by p'_0 normalisation 185

Figure 6- 14. Effective stress paths for CIU and UU triaxial tests on reconstituted and intact Bothkennar 185

Figure 6- 15. Effective stress paths for CIU and UU triaxial tests on reconstituted and intact Bothkennar – comparison of tests by p'_e normalisation 186

Figure 6- 16. Peak stresses for CIU and UU triaxial tests on reconstituted and intact Bothkennar – comparison of tests by p'_e normalisation (assumed cylinder deformation) 186

Figure 6- 17. Variation of deformation parameter $\gamma_{50\ \mathrm{Power}}$ with *OCR* 188

Figure 6- 18. Correlations between *OCR* and $\gamma_{50\ \mathrm{Power}}$ by shear mode for Kaolin 188

Figure 6- 19. Comparison of $\gamma_{50\ \mathrm{Power}}$ from the author's CIU tests with values from database RFG/TXCU-278 188

Figure 6- 20. Variation of deformation parameter b with OCR 189

Figure 6- 21. Comparison of deformation parameter b from the author's CIU tests with values from database RFG/TXCU-278 189

Figure 6- 22. Relationship between normalised undrained shear strength $(c_u/\sigma'_{v0})_{CIU}$ and OCR for Kaolin tests by shear mode, following the frameworks of Ladd et al. (1977) and Mayne (1980); UU tests and Bothkennar tests are plotted for reference 190

Figure 6- 23. Comparison of normalised undrained shear strength $(c_u/\sigma'_{v0})_{CIU}$ from the author's CIU tests on reconstituted Kaolin and Bothkennar with values from database RFG/TXCU-278 190

Figure 6- 24. Comparison of normalised undrained shear strength $(c_u/\sigma'_{v0})_{CIU}$ from the author's CIU tests on intact Bothkennar with values from Mayne & Holtz (1985) and the database published by Mayne (1988) 190

Figure 6- 25. Stress-strain curves for CIUC and UU triaxial tests on Kaolin – comparison of tests by c_u normalisation 191

Figure 6- 26. Stress-strain curves for CIUE triaxial tests on Kaolin – comparison of tests by c_u normalisation 191

Figure 6- 27. Stress-strain curves for CIU and UU triaxial tests on reconstituted and intact Bothkennar – comparison of tests by c_u normalisation 192

Figure 6- 28. Relationships between deformation parameter $\gamma_{50\ Power}$ and OCR for kaolin described by gradient Γ 193

Figure 6- 29. Relationships between (c_u/σ'_{v0}) and OCR for kaolin described by gradient Λ 193

Figure 6- 30. Measured and modelled stress-strain curves for intact and reconstituted Bothkennar 195

Figure 6- 31. Comparison of CIU parameters using the assumptions of right cylinder and bulging/necking in parabolic shape 196

Figure 6- 32 (a) Predicted-measured plots of $\gamma_{50\ \text{Power CIUC}}$ and $\gamma_{50\ \text{Power CIUE}}$ predicted using Equations 4.11 and 4.14; (b) Predicted-measured plots of $(c_u/\sigma'_{v0})_{\text{CIUC}}$ and $(c_u/\sigma'_{v0})_{\text{CIUE}}$ predicted using Equations 4.22, 4.23, 4.26 and 4.27 199

Figure 6- 33 (a) Predicted-measured plots of $\gamma_{50\ \text{Power CIUE}}$ predicted using Equation 4.29; (b) Predicted-measured plots of $(c_u/\sigma'_{v0})_{\text{CIUE}}$ predicted using Equation 4.31 200

Figure 6- 34 (a) Predicted-measured plots of $\gamma_{50\ \text{Power CIUC}}$ and $\gamma_{50\ \text{Power CIUE}}$ predicted using Equations 6.2 and 6.3; (b) Predicted-measured plots of $(c_u/\sigma'_{v0})_{\text{CIUC}}$ and $(c_u/\sigma'_{v0})_{\text{CIUE}}$ predicted using Equations 6.4 and 6.5 203

Figure 6- 35. Predicted-measured plots of *all new reconstituted Kaolin and Bothkennar stress-strain data* between 20%≤*S*≤80% tested in CIUC (*n*=144 data points) predicted using: (a) Equation 4.11 (b) model parameters $\gamma_{50\ \text{Power}}$ and *b* of every triaxial test 204

Figure 6- 36. Predicted-measured plots of *all new reconstituted Kaolin stress-strain data* between 20%≤*S*≤80% tested in CIUE (*n*=129 data points) predicted using: (a) Equation 4.14 (b) model parameters $\gamma_{50\ \text{Power}}$ and *b* of every triaxial test 205

Figure 6- 37. Estimated peak undrained shear stress and $\gamma_{50\ \text{Power CIUE}}$ for test RBOT-CIUE-1.5-99 206

Figure 7- 1. Load-settlement predictions using MSD-MSF and data from SERC (1989) with comparison to field measurements (a) predicted stress ratio (b) predicted bearing pressure 213

Figure 7- 2. Load-settlement predictions using MSD-MSF and data from RFG/TXCU-278: expected values by test mode of $\gamma_{50\ \text{Power}}$ for *OCR*=1, 2 and 4 using Equations 4.11, 4.14, 4.17, 4.20 and varying *b*-values using mean ± standard deviation 215

Figure 7- 3. Load-settlement predictions using MSD-MSF and data from RFG/TXCU-278: expected parameter ranges by test mode of $\gamma_{50\ \text{Power}}$ for *OCR*=1, 2 216

and 4 using the factor errors of Equations 4.11, 4.14, 4.17, 4.20 in combination with lower or upper *b*-values

List of Tables

Table 3- 1. A parameter uncertainty assessment framework for shear tests on fine-grained soil 18

Table 3- 2. Qualitative parameter uncertainty assessment of tests on various reconstituted soils by comparison with tests on intact Bothkennar Clay 22

Table 3- 3. Qualitative parameter uncertainty assessment of tests on intact Bothkennar Clay by comparison with tests on various reconstituted soils 23

Table 3- 4. Design considerations for triaxial test databases 26

Table 3- 5. Sources of experimental data in RFG/TXCU-278 30

Table 3- 6. Experimental details of the triaxial tests in RFG/TXCU-278 31

Table 4- 1. Bias factor of S for data in RFG/TXCU-278 ($0.2 \leq S \leq 0.8$) by model and by test mode 47

Table 4- 2. Assessment of curve-fitting models by directly comparing the statistics per triaxial test. 54

Table 4- 3. 10^{th}, 50^{th} (Median), and 90^{th} Percentiles of all residuals in RFG/TXCU-278 from Models 2 and 3 between S=0.275 to 0.325, S=0.475 to 0.525, and S=0.675 to 0.725 for CIUC and CKUC test data. 57

Table 4- 4. 10^{th}, 50^{th} (Median), and 90^{th} Percentiles of all residuals in RFG/TXCU-278 from Models 2 and 3 between S=0.275 to 0.325, S=0.475 to 0.525, and S=0.675 to 0.725 for CIUE and CKUE test data. 58

Table 4- 5. Correlations between *OCR* and ($\gamma_{50\ Power}$) from undrained triaxial compression and extension tests sorted by test mode 73

Table 4- 6. Correlations between OCR and (c_u / σ'_{v0}) from undrained triaxial compression and extension tests sorted by test mode 73

Table 4- 6. Minimum and maximum parameter values of the reconstituted test database by test mode 104

Table 4- 7. Multiple Linear Regression of c_u/σ'_{v0} 105

Table 4- 8. Multiple Linear Regression of $\gamma_{50\ Power}$ 106

Table 4- 9. Multiple Linear Regression of b 107

Table 4- 10. Single Linear Regression of $\gamma_{30\ Power\ Extension}$ with $\gamma_{30\ Power\ Compression}$ 130

Table 4- 11. Single Linear Regression of $\gamma_{50\ Power\ Extension}$ with $\gamma_{50\ Power\ Compression}$ 130

Table 4- 12. Single Linear Regression of $\gamma_{70\ Power\ Extension}$ with $\gamma_{70\ Power\ Compression}$ 130

Table 4- 13. Single Linear Regression of $c_u/\sigma'_{v0\ Extension}$ with $c_u/\sigma'_{v0\ Compression}$ 131

Table 5- 1. t_{100} parameters from a series of isotropic consolidation curves on a single Kaolin specimen 155

Table 5- 2. CIU triaxial test details – sample reconstitution, isotropic consolidation, and undrained shear 167

Table 5- 3. UU triaxial test details – sample reconstitution, pore pressure measurement, and undrained shear 168

Table 5- 4. Oedometer test details (Kaolin only) 169

Table 5- 5. Calibration and precision of transducers 169

Table 6- 1. Classification test results (assumed only if no test data available) 171

Table 6- 2. Calculated compressibility parameters 173

Table 6- 3. Parameter values adopted to determine the intrinsic compression lines of Kaolin and Bothkennar 174

Table 6- 4. Measured parameters of CIU triaxial tests 179

Table 6- 5. Measured parameters of UU triaxial tests 179

Table 6- 6. Summary of differences in test procedures (a) and (b) 192

Table 6- 7. Comparison of model parameters using the assumption of right cylinder and reducing the number of fitted data points (n) 196

Table 7- 1. Stress-strain model parameters for triaxial tests shown in Figure 7- 1 (mean values shown for depth range 2.62-9.02m, specimens from 'Laval' samplers only) 213

List of Symbols

The following notation is used in this thesis:

b = fitted exponent in power-law regression of normalised shear strain (γ / γ_{50}) and stress ratio (τ_{mob}/c_u) of a soil test;

b_{CIU} = fitted exponent in power-law regression of normalised shear strain ($\gamma / \gamma_{50\,CIU}$) and stress ratio ($\tau_{mob}/c_u$) of an isotropically consolidated undrained soil test;

b_{CKU} = fitted exponent in power-law regression of normalised shear strain ($\gamma/\gamma_{50\,CKU}$) and stress ratio ($\tau_{mob}-\tau_0$)/($c_u-\tau_0$) of a K_0-consolidated undrained soil test;

CAU = Anisotropically consolidated undrained test of any shear mode;

CAUC = Anisotropically consolidated undrained triaxial compression;

CAUE = Anisotropically consolidated undrained triaxial extension;

CIU = Isotropically consolidated undrained test of any shear mode;

CIUC = Isotropically consolidated undrained triaxial compression

CIUE = Isotropically consolidated undrained triaxial extension;

CKU = K_0-consolidated undrained test of any shear mode;

CKUC = K_0-consolidated undrained triaxial compression;

CKUE = K_0-consolidated undrained triaxial extension;

c_u = undrained shear strength;

c_u/σ'_{v0} = normalised undrained shear strength;

$(c_u/\sigma'_{v0})_{NC}$ = normalised undrained shear strength of a normally consolidated material;

$(c_u/\sigma'_{v0})_{OC}$ = normalised undrained shear strength of an overconsolidated material;

DSS = Anisotropically consolidated direct simple shear;

I_P = Plasticity index;

K_0 = ratio of horizontal to vertical stress with zero lateral strain;

K_S = the individual ratio of normalised undrained shear strength of a pair of samples sheared in triaxial extension and compression from the same initial states;

$K_{S,NC}$ = the individual ratio of normalised undrained shear strength of a pair of normally consolidated samples sheared in triaxial extension and compression from the same initial states;

$K_{S,OC}$ = the individual ratio of normalised undrained shear strength of a pair of overconsolidated samples sheared in triaxial extension and compression from the same initial states;

K_{γ} = the individual ratio of mobilised reference strain of a pair of samples sheared in triaxial extension and compression from the same initial states (the subscript denotes the relevant stress ratio in %)

m = fitted exponent in power-law regression of normalised undrained strength and *OCR*;

M = mobilisation factor (which is akin to a reduction factor on undrained shear strength);

M_c = Gradient of critical state line in q-p' stress space;

MSD = Mobilisable Strength Design;

MSF = Mobilisation Strain Framework;

n = number of data points;

OCR = overconsolidation ratio (maximum past consolidation stress to present consolidation stress);

p = calculated probability of finding the observed value to be at least as extreme as the test statistic when the null hypothesis H0 is true;

p' = mean effective stress;

p'_0 = present mean effective stress;

p'_e = equivalent mean effective stress on the normal consolidation line;

p_{atm} = atmospheric pressure;

PS = Plane strain;

q = deviator stress;

R^2 = coefficient of correlation;

S.E. = standard error;

SHANSEP = Stress History and Normalized Soil Engineering Properties.

UU = Unconsolidated undrained triaxial test.

w_L = liquid limit;

w_P = plastic limit;

Γ = fitted slope coefficient in linear or power-law regression of γ_{50} and *OCR*;

Λ = fitted exponent in power-law regression of normalised undrained strength and *OCR*;

σ_3 σ_1 = Total minor and major principle stresses

σ'_{v0} = present vertical consolidation stress;

τ = shear stress

τ_0 = initial shear stress;

τ_{mob} = the mobilised shear strength;

Φ = angle of frictional shear resistance;

Φ^*_e = Hvorslev strength parameter;

ε_{50} = axial strain to mobilise $0.5(c_u - \tau_0)$;

$\dot{\varepsilon}_a$ = axial strain rate;

γ = shear strain;

γ_{50} = reference shear strain to mobilise $0.5(c_u - \tau_0)$;

$\gamma_{50\,CIU}$ = reference shear strain to mobilise $0.5c_u$ in an isotropically consolidated undrained test;

$\gamma_{50\,CKU}$ = reference shear strain to mobilise $0.5(c_u - \tau_0)$ in a K_0-consolidated undrained test;

γ_{ref} = a reference shear strain;

1. Introduction

The content of this thesis is structured in two parts:

Part (1) considers the problem of selecting an appropriate method to evaluate parameter variability from soil tests, with the focus on undrained shear parameters and anisotropy. Sources of uncertainty and variation affecting test measurements are examined by a detailed review of published experiments. A large database of digitised triaxial tests compiled from the literature is used to quantify the variability of established and new test parameters. The design of the database is described, and a simple criteria-based framework is suggested that can be used to characterise parameter uncertainty associated with any chosen geotechnical test that measures fine-grained soil behaviour in undrained shear. Importantly this includes recognising how the measurements are affected by the capabilities and limitations of the apparatus and procedure. It is shown by analysis of the test database that measurement uncertainty is an important component of stress-strain parameter variability that should be acknowledged when assessing parameter variability from geographically and geologically diverse soil test databases.

The degree of nonlinearity and onset of yielding are assessed for 271 reconstituted soil tests sheared to peak stress failure. Statistical and residual error analysis techniques are used to evaluate three simple stress-strain models (by curve fitting to the stress-strain test data) and the variability of the chosen model parameters and normalised undrained shear strength in the context of design calculation uncertainty. New strain parameters are introduced which are defined by reference to strength mobilisation ($[\tau-\tau_0]/[c_u-\tau_0]$) of 30% and 70%, and compared to mobilisation strain at 50%: γ_{50} (Vardanega and Bolton 2011, Beesley and Vardanega 2019). The strain parameters are shown to be sensitive to shear mode with more anisotropic behaviour in K_0 consolidated tests observed by comparing compression with extension strain parameters. An alternative empirical approach to the normalised strength framework proposed by Kulhawy and Mayne (1990) and refined by Ching and Phoon (2013) is used to investigate stress-strain variation with different testing conditions by multiple linear regression analysis. It is shown that the measured strength and strain parameters (i.e. parameters that have been objectively derived from experimental data points) can be predicted with reducing error as modifier factors are introduced for overconsolidation ratio (*OCR*) and strain rate although the scatter

cannot be fully explained by the added variables. Using this approach, it is shown that adopting liquid or plastic limits in the multiple linear regression model is not always useful in explaining the variance of c_u/σ'_{v0} of reconstituted soils for all test modes. Using the same test data, neither classification test improves the prediction of the model deformation parameters.

Part (2) serves two purposes: (i) to examine experimental uncertainty in closer detail with new laboratory experiments prepared under similar conditions to those in the database; and (ii) to test the predictive capability of the database framework proposed in Part (1). A programme of laboratory tests is presented: isotropically consolidated (CI) undrained triaxial compression and triaxial extension (CIUC and CIUE), unconsolidated undrained triaxial compression (UU), and one-dimensional (K_0) consolidation oedometer (OED) tests. Reconstituted kaolin is used to investigate the sensitivity of test parameters to different test conditions such as consolidation type, consolidation rate, and type of axial load cap. Four sets of CIUC and CIUE shear mode comparisons using two kaolin specimens with identical stress histories before shearing (at OCR = 1, 2 and 8) are evaluated with the results of the earlier database analysis. Undisturbed and reconstituted Bothkennar samples tested with the same method (CIUC compared with CIUE) are presented with the database framework parameters as a first step at assessing quantitively the differences in stress-strain behaviour between undisturbed and reconstituted (lightly-overconsolidated) material.

Finally, a simple scenario analysis is used to demonstrate the effect of parameter variability on the load-settlement predictions of a shallow footing test at Bothkennar (reported by Jardine et al. 1995).

1.1 Chapter outline

- Chapter 2 reviews the literature on the variability of stress strain in fine-grained soils and defines the broad research motivations for the thesis.
- Chapter 3 describes the motivation for investigating triaxial tests using empirical database analysis to characterise parameter variability. A database development procedure and parameter uncertainty framework are also described. An explanation is provided of the compilation of two test databases. Parts of this chapter have been reported in:

Beesley M.E.W. and Vardanega P.J., 2019. "Parameter variability of undrained shear strength and strain using a database of reconstituted soil tests". *Canadian Geotechnical Journal*. https://dx.doi.org/10.1139/cgj-2019-0424 (ahead of print).

- Chapter 4 reports the results of the database analysis. The chapter is an expansion of the work presented in the following publication:

Beesley M.E.W. and Vardanega P.J., 2019. "Parameter variability of undrained shear strength and strain using a database of reconstituted soil tests". *Canadian Geotechnical Journal*. https://dx.doi.org/10.1139/cgj-2019-0424 (ahead of print).

- Chapter 5 describes the experimental procedures in the laboratory programme. Parts of the chapter have been reported in:

Beesley M.E.W., Vardanega P.J., and Ibraim, E., 2019. "Developing an experimental strategy to investigate stress-strain models using kaolin". In: *Recent Advancements on Expansive Soils, GeoMEast 2018*, McCartney J., Hoyos L. (eds), Springer, Cham, Switzerland: 99-118.

- Chapter 6 presents the results of the laboratory programme and comparison is made with the results of the database analysis in Chapter 4. Parts of the chapter have been presented in the following publication:

Beesley M.E.W., Vardanega P.J., and Ibraim, E., 2019. "Developing an experimental strategy to investigate stress-strain models using kaolin". In: *Recent Advancements on Expansive Soils, GeoMEast 2018*, McCartney J., Hoyos L. (eds), Springer, Cham, Switzerland: 99-118.

- Chapter 7 demonstrates a simple scenario analysis of a load-displacement prediction using an MSD-MSF framework. The work is in part based on the following paper:

Beesley M.E.W. and Vardanega P.J., 2020. "Variability of soil stress-strain non-linearity for use in MSD analyses using databases of triaxial tests on fine-grained soils". *10th International Symposium on Geotechnical Aspects of Underground Construction in Soft Ground* (accepted)

- Chapter 8 presents the conclusions of the thesis and recommendations for future work.

2. Literature review

2.1 Introduction

Civil engineering design requires a balance between safety, function, and economy. Appropriate safety margins minimise the risk of failure occurring for a certain limit state. Limit states may be associated with collapse (of the structure or soil) or unserviceability, and the latter can often govern design if predicted soil strains are large enough to cause undesirable building damage. For an engineer to make a reliable prediction of the limit state, both the mechanism of failure and the pre-failure deformation behaviour must be well understood.

There are numerous challenges to overcome for the reliable predictions of ground displacements and potential collapse. These include: estimation of the in-situ stress state prior to construction; estimation of the change in stresses within the soil mass induced by construction loads (most often computed using idealised elastic stress distributions); assessment of the strains associated with stress changes in various directions of shear; interaction of soil stiffness and structural stiffness and its influence on mobilised stresses and strains in the soil and structure; soil heterogeneity in terms of strength and stiffness inherited from geological processes; the effect of disturbance caused by in-situ or sampling methods on measured engineering parameters. An understanding of the relative significance of these factors, for a particular soil deposit and site location, is a prerequisite to specifying a suitable site investigation.

Valuable qualitative knowledge of these features of soil behaviour can be obtained through years of professional experience. In particular, the monitoring and analysis of field performance data can help engineers with learning how to identify likely behavioural mechanisms; however, as Lambe (1973) warns, engineers should be cautious about using field results to validate predictive techniques. Lambe argues that many geotechnical predictive methods are semi-empirical, and hence the selected design data on which the prediction is based must be appropriate to the specific site conditions.

Given that the conditions are controlled exclusively by the engineer, theoretical models can be used to investigate the sensitivity of key design criteria to the variability of modelled geotechnical

parameters. Good-quality, reproducible laboratory test data provide such parameters for the theoretical model. Theoretical models may be calibrated with physical soil models (e.g. centrifuge tests) of similar imposed boundary conditions and soil type. There is, still, a large step-change from the theoretical model to the field situation, deriving from in-situ geological or environmental features which have not been captured by the 'idealised' soil test results, or from construction-related events (Lambe, 1973). Since geotechnical designs rely on geotechnical measurements or empirical estimates of soil parameters, an understanding of parameter variability arising from different tests and geology is fundamental to practitioners.

2.2 Variation of undrained shear strength

Many previous researchers have focussed their efforts on quantifying the variation of the well-established design parameter for short-term (i.e. prior to drainage) failure of clay – peak undrained shear strength, c_u. For a particular testing technique, the value of c_u is likely to vary within a soil deposit according to depth, orientation of the sample or downhole probe, and stress history expressed as the overconsolidation ratio (*OCR*) of maximum past to present vertical effective stresses. For a given soil element within a soil mass, the value of c_u will also depend on testing technique due to the applied shear mode and strain rate of the test and the degree of sampling or in-situ disturbance. In addition to these mechanically-derived influences, the undrained shear strength will vary between different soil deposits; differences in soil type due to sedimentation and post-sedimentation processes are frequently characterised by material parameters (such as void ratio, liquid limit, liquidity index, clay fraction) and structural characteristics (e.g. fissures). Researchers have recommended value ranges or empirical correlations to estimate c_u values based on shear mode (Mayne and Holtz 1985), strain rate (e.g., Kulhawy and Mayne 1990), *OCR* (Mayne 1980, Ching and Phoon 2014b), plasticity index (Skempton 1954, Skempton 1957, Ching and Phoon 2013), among others. Use of any geotechnical correlations require careful consideration of the associated statistical measures, a large number of test results, and an assessment of whether the soils and soil tests are relevant to the site being investigated - for example, see Mayne (1980) and Ching and Phoon (2014a).

Ladd et al. (1977) proposed a framework for clays exhibiting normalised behaviour that enables the prediction of c_u if in-situ effective vertical stress and *OCR* are known. Based on many experimental observations that samples of natural, low sensitivity clays, consolidated anisotropically to beyond their in-situ stresses, vary with stress history, Equation 2.1 is fundamental to the SHANSEP testing procedure because it assumes a constant variation in c_u/σ'_{v0} with *OCR*:

$$\frac{\left(\frac{c_u}{\sigma'_{v0}}\right)_{OC}}{\left(\frac{c_u}{\sigma'_{v0}}\right)_{NC}} = OCR^m \tag{2.1}$$

Where, m = fitted exponent; σ'_{v0} = present vertical consolidation stress; $(c_u/\sigma'_{v0})_{OC}$ = normalised undrained shear strength of an overconsolidated material; $(c_u/\sigma'_{v0})_{NC}$ = normalised undrained shear strength of a normally consolidated material.

Mayne's extensive body of work (Mayne 1980, Mayne 1985, Mayne and Holtz 1985, Mayne 1988, Mayne et al. 2009) investigates the variation of c_u/σ'_{v0} with *OCR* and different modes of applied consolidation and shear. Using a large database of published experiments, Mayne (1980) demonstrated that the Λ parameter (equivalent to the fitted exponent m shown in Equation 2.1 and derived from SHANSEP measurements of strength ratio) could be obtained by regression analysis of each test series and used to predict the variation of c_u/σ'_{v0} with *OCR* for the particular combination of consolidation mode and shear mode used in the test series.

Mayne (1988) produced generalised empirical values for Λ for anisotropically consolidated direct simple shear (DSS), isotropically consolidated undrained compression (CIUC), anisotropically consolidated undrained compression (CAUC), and anisotropically consolidated undrained extension (CAUE) tests on overconsolidated natural samples by computing the regression coefficients for each test database of c_u/σ'_{v0}. By way of example, the parameters estimated for a single deposit using the empirical trends for CIUC samples (Λ_{CIUC} = 0.70 and normally-consolidated strength ratio, $(c_u/\sigma'_{v0})_{NC}$ = 0.38) were shown by Mayne to predict *OCR* values that were in close agreement to those estimated from companion oedometer tests.

Recognition of the importance of test mode when considering undrained strength assessment has developed over several decades (e.g. Ladd and Bailey 1964, Bjerrum 1972, Bjerrum 1973, Ladd et al. 1977, Mayne 1985, Mayne and Holtz 1985, Mayne 1988, Chandler 1988, Mesri 1989, Ohta and Nishihara 1985, Chen and Kulhawy 1993, Mayne et al. 2009). Strength anisotropy includes the combined and interrelated influences of inherent anisotropy, stress-induced anisotropy, and strain-induced anisotropy. Just before the onset of shearing, a natural sample will be inherently anisotropic as a result of particle deposition and geologically induced strains, and potentially additional strains caused by the sampling and preparation process in the laboratory. As Jovičić and Coop (1998) point out, a reconstituted sample has fabric anisotropy controlled exclusively by strain-induced anisotropy prior to shearing. The stress-induced component of anisotropy takes effect when any sample (natural or reconstituted) is sheared from a $K_0 \neq 1$ effective stress condition and compared to a similar sample sheared from a different point in stress space e.g. at $K_0=1$ (Mayne 1985). Strength anisotropy can be exposed by comparing values of peak strength measured using two or more different shear modes. Likewise, strain anisotropy could be exposed by comparing values of a reference strain measurement related to the onset of shearing in each shear mode. In this study a more general term is adopted to describe anisotropy measured by different shear modes: *shear-mode anisotropy*.

Shear-mode anisotropy has been examined by Mayne and Holtz (1985) using a large experimental database. Individual pairs of natural or artificial samples consolidated in the same manner under isotropic or anisotropic conditions, and subsequently sheared in either compression or extension, were analysed by comparing $(c_u/\sigma'_{v0})_{\text{Extension}}$ with $(c_u/\sigma'_{v0})_{\text{Compression}}$. Based on data from a collection of different test types (including plane strain, triaxial, hollow cylinder), Equations 2.2a and 2.2b were recommended by Mayne and Holtz (1985) to describe the range of ratio observed between normalised undrained strength measured in extension and compression (K_S):

$$0.5 \leq \frac{\left(\frac{c_u}{\sigma'_{v0}}\right)_{\text{CIUE}}}{\left(\frac{c_u}{\sigma'_{v0}}\right)_{\text{CIUC}}} = K_S \leq 1.0 \qquad \text{(For NC and OC clays, } 1 \leq OCR \leq 100\text{)} \tag{2.2a}$$

$$0.25 \leq \frac{\left(\frac{c_u}{\sigma'_{v0}}\right)_{\text{CAUE}}}{\left(\frac{c_u}{\sigma'_{v0}}\right)_{\text{CAUC}}} = K_S \leq 1.0 \quad \text{(For NC clays; reduces to } 0.5 \leq 1.0 \text{ for OC clays, } 1 \leq OCR \leq 20\text{)} \tag{2.2b}$$

2.3 Variation of undrained stiffness

2.3.1 Undrained stiffness related to moderate strains

A survey of the literature relating to undrained clay stiffness reveals that relatively few studies exist that attempt to characterise stiffness, or strains, using global database collection methods similar to those of Mayne. Among the reasons for this may include the relatively recent developments in measuring accurate small-strain stiffness in triaxial tests - with local strain gauges (Jardine et al. 1984) and piezoceramic bender elements (Pennington et al. 1997, Pennington 1999, Jovičić and Coop 1998). Another reason could be that there is not, at present, an established design parameter that characterises the non-linear stiffness degradation over the desired strain range and that is commonly correlated with variables such as K_0 (ratio of present horizontal to vertical effective stress), *OCR*, mode of shear (e.g. triaxial compression/extension, direct shear, plane strain), or strain rate. A qualitative analysis by O'Brien et al. (1992) describes the sensitivity of "mobilised undrained stiffness*"* to recent stress history, stress path direction, structural anisotropy, strain rate, ageing effects (i.e. creep), *OCR*, and boundary conditions.

Vardanega and Bolton (2011) investigated the potential benefit of a new model deformation parameter to characterise stiffness in the 'moderate strain' region (i.e. the strain range appropriate to situations where plastic failure is approached more closely under the mobilised stresses). Based on a large number (115) of undrained shear stress-strain test data from the literature, Vardanega and Bolton (2011) established a simple power-law curve fitting procedure relating mobilised stress ratio (τ_{mob} / c_u) to normalised shear strain (γ / $\gamma_{M=2}$) as shown in Figure 2- 1. Their analysis of the normalisation parameter $\gamma_{M=2}$, defined as the shear strain required to mobilise one-half of the peak strength, demonstrated that the application of Equation 2.3 with a *b*-value equal to 0.6 was capable of predicting the database of strength mobilisation data (between stress ratios of 0.2 and 0.8) to within error bounds of ±40%. Given that the database included tests with different applied shear modes (triaxial compression, direct simple shear, and resonant column) on natural intact samples with different geological and stress histories, the variation is relatively small. An important feature of the database to note is that all samples were tested from isotropic stresses.

$$(\tau_{mob} / c_u) = 0.5(\gamma / \gamma_{M=2})^{b} \quad (2.3)$$

Where, γ = shear strain; $\gamma_{M=2}$ = a reference shear strain mobilising $0.5c_u$ in an isotropically consolidated undrained shear test; b = a fitted exponent.

An alternative approach to characterising stiffness can be done by calculation of an equivalent modulus, E_u, at certain strain levels or stress ratios. Recently, Casey et al. (2016) published a database of reconstituted clays of varying geological origin and plasticity. All tests were K_0-consolidated and sheared only in compression. Casey et al. (2016) showed that E_u of normally consolidated and overconsolidated soils is sensitive to pre-shear vertical effective stress (σ'_{v0}). Their data suggested that an increase in σ'_{v0} produced the same increase in E_u of overconsolidated soils regardless of stress ratio (0.25, 0.5 or 0.75). While normally consolidated soils were less sensitive overall to a change in σ'_{v0}, the recommended correlations varied according to stress ratio. This implies that if the data were normalised by the procedure proposed by Vardanega and Bolton (2011), the stress-strain curve 'shape' parameter, b, would show less variability at $OCR > 1$ than for data where $OCR=1$.

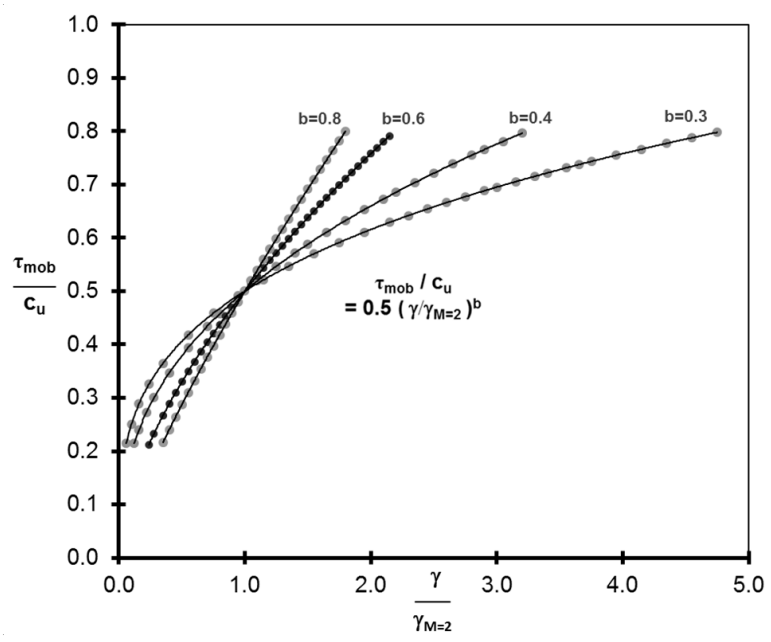

Figure 2- 1. Power law relationship between normalised shear strain and mobilised stress proposed by Vardanega and Bolton (2011)

2.3.2 Undrained stiffness related to small strains

The small-strain stiffness of fine-grained soils has received more attention in recent years. Possibly this is a result of increased awareness of the significance of small-strain non-linearity on serviceability design (e.g. Jardine et al. 1986, Burland 1989). Since Jardine et al. (1984) first proposed a form of the undrained modulus degradation curve - in which the authors normalised the undrained secant modulus (E_u) with undrained shear strength (c_u) - other researchers have published datasets for a tested soil by expressing small to large strain stiffness variation in similar forms (e.g. Jardine et al. 1986, Allman and Atkinson 1992, O'Brien et al. 1992). E_u and the undrained shear modulus G are frequently normalised by p'_0, the initial effective mean stress prior to shear.

The effect of shear mode on undrained stiffness can be examined by observing the scatter in modulus degradation curves. For instance, Jardine et al. (1986) presented data from unconsolidated undrained shear tests on intact samples and K_0-consolidated undrained shear tests on reconstituted samples sheared at various *OCR* (=1 to 7). The axial strain of 0.1% is often taken as the limit of the small strain region. Up to a strain of 0.1%, the K_0- compression samples are significantly stiffer than those sheared in extension; at a strain of 0.1%, the ratio of respective mean values of E_u/p'_o in compression and extension presented by Jardine et al. (1986) is approximately 2 for both intact and reconstituted samples. The difference in mobilised stiffness between shear modes reduces further with increasing strain. Vardanega and Bolton (2013) presented a database of 67 tests on clays and silts for a variety of test types (including triaxial compression, torsional shear, and resonant column). The study demonstrated a significant reduction in scatter of the test data when the normalisation parameter for G was taken as G_{max} instead of p'_0.

2.3.3 Variation of undrained stiffness within a single material

London Clay

Hight et al. (2003) presented a large database of various laboratory and in-situ tests on London Clay. The results of reconsolidated tests on natural samples demonstrated a strong dependence of undrained modulus (E_u/p'_o) on consolidation path. Like Jardine et al. (1986), the authors calculated a ratio of 2 between the stiffness in compression and extension in the small strain region. In this study,

however, the importance of stress path direction is emphasised: the samples are consolidated isotropically then swelled anisotropically to reach the pre-shear state. Hence, the tests in undrained triaxial extension continue in the same direction of stress path, while the compression tests involve a reversal. Additionally, Hight et al. (2003) point out that creep may have a significant influence on small strain stiffness.

Kaolin Clay

Kaolin China clay is a white-coloured, dry-milled clay consisting of a high proportion of kaolinite. Kaolinite is a mineral commonly found in sedimentary and residual soils. Commercial kaolin clay has been used widely by geotechnical researchers, notably by Schofield and Wroth (1968) in the development of the Critical State framework.

Advanced stress path tests on kaolin samples were carried out by Powrie et al. (1998) to investigate the sensitivity of soil stiffness to simulated complex stress paths caused by excavations in clay. They discovered that soil stiffness showed strong dependence on the change in orientation of stress path. For example, where a stress path involved a reversal in stress path direction, a stiffer response was observed. The authors pointed out that this can lead to a more rapid mobilisation of strength with shear strain.

The mobilisation strain framework proposed by Vardanega and Bolton (2011) was examined further by Vardanega et al. (2012) using a series of isotropically consolidated kaolin samples sheared at various *OCR* values. The authors recommended Equations 2.4a and 2.4b to describe $\gamma_{M=2}$ and b which both showed a positive correlation with *OCR* according to the linear regressions

$$\log_{10}(\gamma_{M=2}) = 0.680\log_{10}(OCR) - 2.395 \quad (2.4a)$$

$$(n = 18,\ R^2 = 0.815)$$

$$b = 0.011(OCR) + 0.371 \quad (2.4b)$$

$$(n = 18,\ R^2 = 0.591)$$

2.4 Proposed research objectives

Previous experimental studies have investigated the sensitivity of stiffness and/or strength parameters to one of the following:

- for a particular consolidation history, i.e. either K_0-consolidation or Isotropic consolidation, variation in shear mode (triaxial compression and extension)
- for a particular shear mode, i.e. triaxial compression, variation in anisotropic consolidation path
- *OCR* and/or strain rate in combination with one of the above

Only one research publication was found (Gens 1982) where a reconstituted soil had been tested both from K_0 and isotropic consolidated initial states, for a range of *OCR* (1 to 10) and sheared in compression and extension.

Previous studies have suggested that undrained stiffness is influenced by creep, strain rate, consolidation path, recent stress path rotation, *OCR* and shear mode. The relative influences of these factors are currently unknown. It is likely that some factors will have more influence on the mobilised stiffness at small strains, while others will have greater effect on moderate to large strains. It could be inferred from Germaine and Ladd (1988) that the most important influence on undrained stress-strain behaviour is the anisotropic or isotropic consolidation history; they argue that samples sheared from isotropic consolidation presents considerably misleading behavioural trends. This fundamental mechanical behaviour can be investigated with reconstituted samples. However, significant differences may be observed in the mobilised strains and degree of mobilised strength measured in natural samples and reconstituted samples. A quantitative analysis of deformation behaviour for reconstituted and natural samples for the small to large strain regions could provide considerable value to engineers working on routine serviceability designs for short-term construction.

This thesis investigates the range of nonlinear behaviour in the moderate stress range represented by a stress ratio of 0.2 to 0.8. Such a range represents a factor of safety on undrained collapse of 5 to 1.25. Chapter 3 reviews and describes the selected methods for the variability analysis of deformations in the moderate stress range.

3. A method to develop and analyse soil test databases: for the variability characterisation of undrained stress-strain behaviour

Parts of this chapter have been included in the following publication:

> Beesley M.E.W. and Vardanega P.J., 2019. "Parameter variability of undrained shear strength and strain using a database of reconstituted soil tests". *Canadian Geotechnical Journal*. https://doi.org/10.1139/cgj-2019-0424 (ahead of print)

3.1 Geotechnical variability characterisation

Geotechnical characterisation methods involve inevitable uncertainties. Two types of uncertainty are relevant to geotechnical parameters: aleatoric and epistemic. A geotechnical parameter, such as undrained modulus (E_u), is affected by naturally random geological processes and field conditions (aleatoric uncertainty) and the resulting influence on parameter variation may not be well understood (epistemic uncertainty). Parameter assessment is also affected by epistemic uncertainties related to the method of investigation. For instance, measured deformation properties may be affected to an unknown degree by sampling disturbance or a selected testing procedure (e.g. Duncan 1980, Germaine and Ladd 1988). If site-specific test data are limited, or if their reliability is questioned, it is valuable to know the possible variation and best estimate of a test parameter.

The variability of parameters from soil tests can be characterised by analysing large test databases. Very large numbers of tests sourced on a global scale are needed to realistically represent the full range and distribution of a test parameter (for all soils or a sub-group of soils) (Ching and Phoon 2014a). It may be useful in some cases, however, to develop sub-global databases to characterise the distribution of parameters related to a region or to selected geologies e.g. for a large-scale regional

infrastructure project such as a new metro system. Naturally, it is the local bias and reduced (but well characterised) range of such a parameter database that is sought to develop more accurate and precise parameter distributions for the project.

Characterising the distribution of a test parameter is dependent not only on the geographical spread, and geological conditions, of the test samples, but also on the experimental conditions of the tests. It is well established that c_u is influenced by the depositional material and structure of the soil, historic and present stresses in situ (Ladd et al. 1977, Mayne 1980, Jamiolkowski et al. 1985, Chandler 1988, Ladd 1991), sampling disturbance (e.g. Hight et al. 1992a and 1992b) and measurement procedures, such as shearing the sample from unconsolidated or reconsolidated conditions (Chen and Kulhawy 1993), from isotropic or anisotropic consolidated conditions (Mayne 1985), in different modes of shear (Mayne & Holtz 1985, Mayne 1988, Brosse et al. 2017), and at various strain rates (Sheahan et al. 1996, Kulhawy and Mayne 1990). A method is needed to characterise the variability of parameters so that parameter ranges may be justified for design sensitivity analyses; taking into account geological and testing variability.

3.2 The problem case: stress-strain characterisation in the moderate stress range

In chapter 2 it was observed that, while much of the geotechnical research on fine-grained soils has focussed on understanding the influence of experimental variables on peak and small-strain parameters, there is a gap in the literature concerning the variability characterisation of stress-strain behaviour in the pre-failure moderate stress range. The work presented in this thesis aims to address the problem from the viewpoint of a geotechnical designer faced with a limited number of tests available for site characterisation. To perform load-settlement prediction analyses, within a load factor range of $0.2 < \sigma_{mob}/\sigma_{failure} < 0.8$, as discussed in Chapter 2, deformation parameters are needed that can reliably describe stress-strain response within the soil displacement mechanism. Fine-grained soils are characteristically nonlinear over the full pre-failure range (Jardine et al. 1986, Atkinson 2000, Brosse et al. 2016). Strength anisotropy has been widely investigated (e.g., Mayne and Holtz 1985, Won 2013, Brosse et al. 2017) but less information is available to characterise stiffness anisotropy at pre-failure

loads (Brosse et al. 2016). Here a simple empirical approach to characterising nonlinear stress-strain curves is investigated. The aim is to develop a general framework that can be used by practising engineers to assess possible ranges in stress-strain response using a few routine test parameters, and to evaluate the importance of parameter uncertainties. To do so requires first selecting representative nonlinear deformation parameters and, second, developing a method to characterise their variability.

A procedure for evaluating a choice of nonlinear stress-strain models is demonstrated and the resulting parameters of the chosen model are investigated in relation to known test conditions (consolidation mode, consolidation stresses, *OCR*, shear mode, strain rate) and material characteristics (liquid and plastic limit). Two test databases RFG/TXCU-278 and BTK/TXCU-34 (totalling 312 triaxial tests), these are defined in detail in the following sections, have been assembled from experiments on 24 fine-grained soils from 22 publications. This chapter describes the proposed method of variability characterisation of undrained stress-strain response using consolidated undrained (CU) triaxial tests. However, the test database development procedure and statistical tools that are described may be adopted for characterising the variability of other soil test parameters. Results of the in-depth statistical analysis of the database are presented in Chapter 4.

3.3 Motivation for investigating triaxial tests

The aim of this work is to demonstrate a method to characterise the variability of nonlinear soil behaviour at pre-failure load levels. Variations in stress-strain response and their likely causes are identified using a simple stress-strain relationship and evaluating the effects of model approximation and parameter variability. The method has been developed using the CU triaxial test, since in practice it is the test that has traditionally been used for the measurement of monotonic soil deformation and shear strength (Bishop and Henkel 1962, Germaine and Ladd 1988, Santucci de Magistris et al. 1999, Potts et al. 2002). This is likely to be the result of: the capability of the triaxial apparatus to control drainage and a large range of stresses and therefore replicate – to a limited extent – the boundary conditions and stress paths of the soil in-situ; the relative ease of procedures for transporting and storing tubed cylindrical samples until required for trimming and testing (Bolton 1979) and for measuring

stresses and strains (Tatsuoka 1988); and from the continued development of constitutive models using triaxial data (e.g., Schofield and Wroth 1968, Roscoe and Burland 1968, Banerjee and Stipho 1979, Davies and Newson 1993, Stallebrass and Taylor 1997, Grimstad et al. 2011).

Technical standards BS 1377 Part 8 (BSI 1990) and ASTM D4767–11 (ASTM 2011) describe isotropic consolidation procedures for effective stress triaxial tests and so the differences between CIU and CKU triaxial shear parameters are perhaps not widely appreciated in practice, particularly for stress-strain properties (Baldi et al. 1988). BS EN ISO 17892-9:2018 (ISO 2018), which supersedes BS 1377 Part 8, describes procedures for anisotropic and isotropic consolidation.) Previous studies have investigated strength anisotropy from triaxial tests (Ladd et al. 1977, Mayne and Holtz 1985, Won 2013) but more research is required to understand the anisotropy of strains mobilised beyond the small-strain region (Simpson 1999).

Advanced constitutive models developed by researchers in the last three decades have increasingly focussed on describing anisotropic stress-strain-strength behaviours of soils but often rely on triaxial test data for evaluation of their accuracy (e.g., Banerjee et al. 1985, Graham et al. 1989, Grimstad et al. 2011, Krabbenhøft et al. 2019). Inherent deficiencies of both model and testing apparatus make this challenging (Muir Wood 2017), which must be recognised if practitioners use routine triaxial testing for model calibration. Other models that have gained popularity in industry include analytical boundary element solutions for multiple soil-structure interactions e.g. Repute (Basile 2015). Any serviceability-based calculation procedure of settlement prediction which relies upon the assumption of similarity between the load-settlement relationship and the experimental stress-strain curve (e.g., Skempton 1951, Bolton et al. 1990, Osman and Bolton 2005, Klar and Klein 2014) requires the selection of an ‘average’ characteristic curve. A better understanding of the variability in stress-strain response measured with triaxial tests would lead to more informed parameter selections for such models. Thus, as a first step it is appropriate to consider the variability of stress-strain behaviour from triaxial tests; this is used in a design example in Chapter 7.

3.4 A parameter variability assessment framework using test databases

Variability of a soil test parameter arises from an incomplete knowledge of its variation with different test conditions together with the contribution of natural geological variation (Figure 3- 1). Accordingly, the characterisation of a parameter from any geotechnical test must consider the potential errors and uncertainties in the measured properties that arise from the test procedures. A ground investigation could be viewed as an experimental investigation with measured and unmeasured variables and when considering geotechnical test results the engineer should evaluate the sources of error (Germaine and Ladd 1988). Problems can be caused by the equipment, the operation of a test procedure, and the assumptions used in the interpretation of measurement data. These errors add to the difficulty of assessing the inherent natural variability of soil materials. Germaine and Ladd (1988) review in detail the various sources of triaxial testing errors and categorise them into appropriate solutions for the error: correct, avoid, or (if the error cannot be corrected or avoided) evaluate the error for data interpretation.

It is hypothesised here that any routine soil shear test, whether undertaken in the laboratory or in situ, can be given a parameter uncertainty "rating" to describe uncertainties related to the specific characteristics and procedures of the test. Table 3- 1 lists five primary features of fine-grained soil shear tests and provides examples of how uncertainties associated with each feature affect the following parameters: V_s, G_{50}, c_u. These parameters represent behaviours at increasing strain levels during shear and their sensitivities to the different sources of measurement uncertainty will not necessarily agree. Importantly, items 1 to 5 in Table 3- 1 are not independent and it is the combination of these five features that will determine the measurement uncertainty of the chosen parameter.

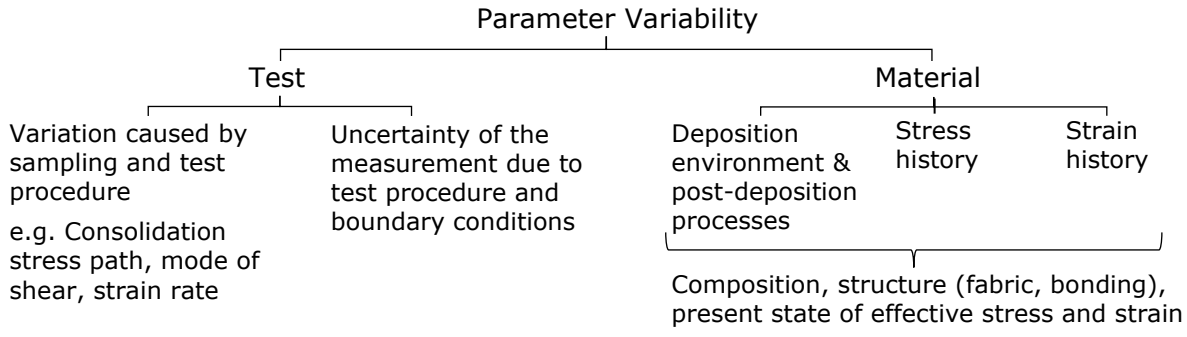

Figure 3- 1. Sources of variability of a soil test parameter

Table 3- 1. A parameter uncertainty assessment framework for shear tests on fine-grained soil

	Small strain parameter: Shear wave velocity $V_s = G_{max} / \rho$	Moderate strain parameter: Undrained secant stiffness G_{50}	Peak stress parameter: Undrained shear strength c_u
1. Principal stress system	Directions of wave propagation and polarisation relative to vertical/horizontal planes e.g. $G_{hv}/\rho = V_{s(hv)}$, $G_{vh}/\rho = V_{s(vh)}$ and $G_{hh}/\rho = V_{s(hh)}$	Directions of applied stresses relative to vertical/horizontal planes	Directions of applied stresses relative to vertical/horizontal planes
2. Stress changes a) Prior to shear	a) Prior to shearing in situ, the test installation method may alter effective stresses in the ground that would need to be approximated or measured. In laboratory tests, an uncertain change in effective stress will have taken place due to the sampling and handling process. In effective stress laboratory tests, changes in effective stress are applied to simulate the consolidation history of the soil deposit. To measure effective stresses, total stresses and pore pressures must be measured.		
b) During shear	b) Effective stress changes are dependent on the capability of the apparatus to measure pore pressure and to control stresses in different directions.		
3. Strain changes a) Prior to shear	a) Prior to shearing in situ, the test installation method may alter strains in the ground that would need to be approximated. In laboratory tests, the sampling and handling process may result in an uncertain degree of specimen swelling if contact is made with fluid and shear disturbance to the soil structure. In effective stress laboratory tests, volumetric strains are controlled by the applied stresses on the specimen and pore pressures within the specimen. To measure strains, volumetric and shear strains must be measured.		
b) During shear	b) If the shear wave velocity test shears the soil at lower strains than the linear elastic limit, then the measurement is insensitive to strain	b) Strain distribution in the soil sample may be nonuniform and difficult to identify with standard test equipment	b) Identified as the peak shear stress, hence dependent on strain which controls the stressed area
4. Uncertainty of the measured quantities	Travel distance and travel time	Deviator stress (deviator load/assumed area of stress) and strain (displacement relative to original length) and assumed relationship to shear stress and shear strain	Deviator stress (deviator load/assumed area of stress) and assumed relationship to shear stress
5. Scale factor (volume of soil tested)	The displacement mechanism and strength of larger samples may be more sensitive to inherent macro structural features and less sensitive to fabric. The reverse may be true for smaller samples.		

The author proposes Table 3- 1 as a framework for characterising parameter uncertainty from shear test data on fine-grained soils. It may be used as a framework to assess measurement uncertainty of a parameter associated with the imposed procedure and boundary conditions of the test, so that a more reliable evaluation of parameter variability associated with natural soil materials can be facilitated. The variation in results due to testing procedures is separate to the variation due to material variability.

Hence, epistemic parameter uncertainties associated with the effects of composition, fabric and structure of a natural soil are excluded from Table 3- 1. Such characteristics of soil are influenced by the environmental conditions experienced during the deposition and subsequent geological history of the formation via a variety of possible processes such as cementation, leaching, ageing, lithification, erosion, and weathering.

There are two possible ways of determining parameter uncertainty related to a chosen type of soil shear test. The first requires a series of tests on identical specimens to quantify the repeatability of a technique and to assess the variation in parameters caused by variations in technique. An evaluation of accuracy would involve selecting the technique that produces a parameter closest to the assessed "true" value, which in research practice would mean selecting the technique that involves the least observable error. In commercial practice, there is no opportunity to investigate testing variation effects this way due to limited budgets and numbers of samples.

However, codes of practice for geotechnical testing permit a necessary degree of flexibility in selecting the test methods for consolidated-undrained triaxial tests so that the method is suitable for the material. Some codes, such as BS 1377 Part 8 (BSI 1990) and ASTM D4767–11 (ASTM 2011), were drafted to test for strength parameters with less focus on the techniques required for stress-strain measurement. For example, lubricated ends are optional and in practice are infrequently used (G. Martin, personal communication 2019; Dr. A. Mandolini, personal communication 2019). Even with frictional ends, both codes specify only that the selection of strain rate should satisfy the condition of equilibration of pore pressure by the estimated time to peak stress failure. The use of frictional ends is likely to result in specimen non-uniformity that would lead to less accurate measurements of stress-strain behaviour (Sheng et al. 1997, Muir Wood 2017). The resulting measurement is an approximation with an accuracy dependent on the assumed shape of specimen deformation; commonly either right-cylinder (Bishop and Henkel 1962), bulging (Germaine and Ladd 1988), or parabolic (Fayad 1986, Germaine and Ladd 1988, Escribano et al. 2019) shapes are assumed. Other testing decisions include selecting the strain and pore pressure measurement systems, rate of consolidation, rate of undrained shear, and time allowed for secondary consolidation prior to undrained shear.

Since it is unlikely that a practising engineer would be afforded the time to evaluate all such sources of parameter uncertainty for each test, it is hypothesised that the development of test databases could provide a rational and practical method for the industry to characterise parameter variability by test type (the term 'test mode' is adopted herein instead of test type – see section 3.4.2.1). This second, alternative, approach is challenging due to the uncertain combination of variations in testing methods and material variability (Figure 3- 1). Added complications include potential disturbance of the material due to sampling and handling methods in the laboratory or as a result of installation methods for the in-situ test. However, the development of test databases with accurate, and consistent, parametric records of the testing and sample details would provide a valuable data store that could facilitate assessments of the effects of different procedures on the measured parameters.

To characterise parameter variability by database analysis requires: (1) a selection of soil materials, (2) a database development procedure, (3) relevant parameters to describe the sample details and test measurements, and (4) a method of database analysis. This general framework is described in the following sections for the reconstituted and intact soil test databases presented in this thesis.

3.4.1 Selection of soil materials for database analysis

Reconstituted soil samples were chosen to populate RFG/TXCU-278, a reconstituted soils test database of 278 consolidated-undrained triaxial tests, thereby controlling for the following experimental variables: maximum and present consolidation stresses in the horizontal and vertical directions (and hence *OCR* and K_0) and orientation of cross-anisotropic axis of symmetry (coincident with the direction of principal stress, σ'_1, following Tatsuoka 1988). Thus, the test parameters in the reconstituted database reflect the natural variability of intact soil samples (including the soil's composition, cross-anisotropy and stress history) absent of the effects of structure and bedding orientation. The reconstituted soil tests were chosen specifically to assess the likely variation of stress-strain response with consolidation type (CIU or CKU) and shear mode (i.e. 90° rotation of principal stress between triaxial compression and triaxial extension). A comparison of compression and extension behaviour may be used to assess strain anisotropy in a similar approach to that adopted by previous researchers to assess stiffness anisotropy

(Brosse et al. 2016) and strength anisotropy (e.g. Low et al. 2011, Ratananikom et al. 2015).

An intact soil test database, BTK/TXCU-34, comprising 34 consolidated-undrained triaxial tests from one well-known ground investigation site - the Bothkennar testing facility in Scotland - has been developed for comparison with the reconstituted test database. The tests were reported by SERC (1989) and undertaken by two laboratories: one at City University and the other located at Imperial College London. Triaxial compression and extension tests are included in the database to investigate parameter variation with shear mode. Hight et al. (1992a) describe the Bothkennar Clay as lightly overconsolidated (*OCR* = 1.25 to 1.15) due to erosion and groundwater lowering. Measurements of yield stress ratio (*YSR*) reported by Nash et al. (1992) indicate a range of apparent *OCR* that exceeds the geological *OCR* at depths greater than 3.5m, which is indicative of the structured nature of the clay. There is little evidence to suggest that the fine-grained soil matrix is bedded at an inclination to the horizontal plane; however, more bedding, laminations, or mottling dominate at different depths (Nash et al. 1992, Paul et al. 1992, Hight et al. 1992a). It is worth noting that the stress-strain curves of samples from different depths have been shown to vary (without using parameters) (Hight et al. 1992a).

For each test database, the variability characterisation of the measured stress-strain response encompasses different sources of variation and uncertainty. The reconstituted soils test database allows an assessment to be made of the significance of stress history, testing procedure and measurement uncertainty to parameter variability. This is because many of the experimental variables were controlled and sampling disturbance effects are eliminated but many different laboratories and operators produced the test data. In contrast, with the intact test database it is expected that limited variation in testing procedure and measurement uncertainty would contribute to parameter variability because only two laboratories were involved in the tests. Hence, the intact soil test database is expected to demonstrate parameter variability that is more strongly influenced by the in-situ state and natural variability of the deposit combined with variable sampling disturbance.

The suggested framework in Table 3- 1 can be used to make a simple qualitative comparison of the sources of parameter uncertainty for each database using parameter range (scatter) with a rating of low or high. The results of the database analysis, presented in chapter 4, updates this preliminary

assessment with quantitative measures of the parameter distributions from each database. The tools used for the quantitative assessment of parameter uncertainty and variability are presented in the next sections of this chapter.

Table 3- 2. Qualitative parameter uncertainty assessment of tests on various reconstituted soils by comparison with tests on intact Bothkennar Clay

Reconstituted soils test database (RFG/TXCU-278)		Uncertainty
1. Principal stress system	Triaxial stress apparatus including conventional cell (CIUC and CIUE) and hydraulic stress path cell (CKUC and CKUE)	
2. Stress changes a) Prior to shear b) During shear	There are no sampling disturbance effects since the consolidation stress history is controlled prior to shear. Therefore, the uncertainty of stress changes is limited to the effects of: • directional stress control of the apparatus, and • non-uniformity within the triaxial sample during the test. Multiple triaxial test apparatus and operators (from 21 publications) are likely to increase the parameter range due to this uncertainty.	2a) None 2b) High
3. Strain changes a) Prior to shear b) During shear	Strain history of the reconstituted samples will vary with reconstitution method and consolidation stress history. By the start of the shear stage of the triaxial test, the materials may be considered to behave like unstructured soils with similar depositional conditions and no sampling disturbance effects. Adopted strain rate is a variable of stress control and strain control during consolidation and shear and becomes significant in undrained shear particularly when frictional ends are used (Sheng et al. 1997). The reconstituted test database includes a range of $\varepsilon_a^{\cdot}$ = 0.02 to 49.6 %/hour. 28% tests were reported to have employed lubricated end platens; 11% were reported to have frictional end restraint; for 61% of the test database, no information concerning specimen end restraint was available. Therefore, the uncertainty of strain changes is limited to the effects of: • Creep at the end of consolidation (2a), • non-uniformity within the triaxial sample during the test (2b). Multiple triaxial test apparatus and operators (from 21 publications) are likely to increase the parameter range due to this uncertainty.	3a) Low 3b) High
4. Uncertainty of the measured quantities	The uncertainty of measured stresses and strains, while clearly dependent on (items 1, 2b and 3b), is also conditional to (following Germaine and Ladd 1988): • the appropriate error corrections made for apparatus compliance • a suitable approximation adopted for geometry of the deforming specimen, • avoidance of tilting/seating/saturation/leakage/temperature errors, • a decision that the use of frictional ends and any appearance of a shear rupture has negligible effect on the measurements.	4) High
5. Scale factor (volume of soil tested)	All triaxial samples have 38-100mm diameter prior to setup in the triaxial cell. Most samples have a H/D ratio of approximately 2, although Liu (2001) used H/D=1 for CIUE tests.	5) Low

Table 3- 3. Qualitative parameter uncertainty assessment of tests on intact Bothkennar Clay by comparison with tests on various reconstituted soils

Intact Bothkennar Clay test database (BTK/TXCU-34)		Uncertainty
1. Principal stress system	Triaxial hydraulic stress path cell (CKUC and CKUE)	
2. Stress changes a) Prior to shear b) During shear	The samples would have experienced uncertain effective stress changes with sampling disturbance effects associated with the sampling depth (1.6 to 17.5 mbgl) and sampling procedure (Sherbrooke, Laval, Piston, and). An effective stress profile was established from bulk density measurements and depth to ground water table (Nash et al. 1992), which was used together with estimated K_0= 0.6 to select the appropriate recompression stresses (Hight et al. 1992a). 2 of the 34 samples were tested using the SHANSEP procedure and consolidated to stresses twice those estimated in-situ (*OCR*=1). A detailed investigation of yield stresses using various one-dimensional consolidation tests (Nash et al. 1992) provided an average *OCR* profile with some scatter (Hight et al. 1992a). Therefore, the uncertainty of stress changes is limited to the effects of: • sampling and sample preparation disturbance (2a), • subsequent changes to effective stress during reconsolidation (2a), • directional stress control of the apparatus (2a, 2b), and • control of stress uniformity within the triaxial specimen during the test (2a, 2b). Compared to Table 3- 2, the parameter uncertainty of stress uniformity during the triaxial test will be lower due to the consistent and high-quality test methods employed by the two laboratories.	2a) High 2b) Low
3. Strain changes a) Prior to shear b) During shear	Shear strains and volumetric strains prior to shear disturb the structure of Bothkennar clay (Hight et al. 1992a). An uncertain strain history was imposed on the samples during the sampling and transportation process. Subsequent reconsolidation in the triaxial cell caused changes in volumetric strains – the largest volumetric strains occurred in the SHANSEP tests. For only 9 of the 34 tests the shear strain rate was recorded: $\dot{\varepsilon}_a$ = 0.04%/hour in 3 tests from 5.3m sampling depth; $\dot{\varepsilon}_a$ = 0.19%/hour in 6 tests from 5.4m and 6m sampling depth. The remaining 25 tests were undertaken by City University and are assumed to have strain rates of $\dot{\varepsilon}_a$ = 0.20%/hour (Hight et al. 1992a) Uncertainty is therefore limited to the methods employed by the ground investigation contractor and two laboratories.	3a) High 3b) Low
4. Uncertainty of the measured quantities	The same errors relating to uncertainty of the measured stresses and strains would apply to the intact test database as for the reconstituted test database (see Table 3- 2, item 4). However, the range can be assumed to be considerably narrower because only 2 laboratories were involved in the intact test database.	4) Low
5. Scale factor (volume of soil tested)	All tests were undertaken using 38mm x 76mm cylindrical samples. Fabric differences may influence the resulting triaxial test deformation parameters, but parameter sensitivity to fabric is probably the same as reconstituted soil	5) Low

3.4.2 Laboratory test database development

3.4.2.1 Categorisation of test data by test mode (consolidation-shear mode)

All geotechnical laboratory test data may be categorised by a test mode. Test mode refers to the combination of consolidation mode (consolidation controlled by isotropic or anisotropic stresses, or by K_0 conditions of zero lateral strain, or no consolidation) and shear mode (direction of principal stresses applied by the testing apparatus) used in the test. By categorising tests into test modes, the variety of test procedures involved in characterising the parameter variability distribution is reduced. Furthermore, different test modes identify the important influence of stress path on the resulting shear parameters in a simplified but practical manner for test databases.

The term 'test mode' has been used by Ching and Phoon (2013) to differentiate between triaxial compression tests with various consolidation modes (isotropic consolidation CIUC, K_0 consolidation CKUC, unconsolidated UU), K_0-consolidated triaxial extension (CKUE), unconsolidated unconfined compression (UC), direct simple shear (DSS), and field vane (FV). This thesis follows the same convention for shear mode (item 1 Table 3- 1) and consolidation mode: isotropically-consolidated (CI), K_0-consolidated (CK), anisotropically-consolidated (CA), unconsolidated (U). In this study only triaxial compression and triaxial extension shear modes are considered but other laboratory shear tests used in practice that may be categorised by item 1 in Table 3- 1 include plane strain compression, plane strain extension, direct simple shear, and torsional shear. A thorough review of laboratory shear testing devices by Tatsuoka (1988) describes the modes of shear relevant for test mode categorisation.

Categorisation of tests can be justified by the different stress paths experienced by a specimen in alternative test modes. During shear (see items 2b and 3b in Table 3- 1), a stress path in triaxial compression is distinct from triaxial extension as the direction of principal stress (σ_1) is respectively vertical ($\delta = 0^\circ$) or horizontal ($\delta = 90^\circ$) and the intermediate principal stress (σ_2) is respectively equal to σ_3 or σ_1. The resulting stress-strain measurements are controlled by shear-mode anisotropy ($\delta = 90^\circ$ or 0°) and by the relative magnitude of intermediate principal stress $(\sigma_2 - \sigma_3)/(\sigma_1 - \sigma_3)$ = 0 or 1 and different procedures must be used to control these parameters during the shear stage of the test. Since

the stress-strain data are affected by experimental errors and uncertainties in procedure (Germaine and Ladd 1988, Silvestri 2001), it would be valuable to characterise, separately, the variability of stress-strain measured in triaxial compression or triaxial extension shear modes.

Prior to shear (see items 2a and 3a in Table 3- 1), different consolidation stress paths may be adopted in the triaxial cell to simulate changes in effective stresses that may occur in situ. In CI triaxial tests on reconstituted specimens, effective stresses are increased and reduced isotropically to control the value of *OCR* prior to shearing. In principle the strains during isotropic consolidation are not actively controlled but an experimentalist's decision to use lubricated ends would aim to mitigate the effect of end restraint on volumetric strains. In contrast, during CK triaxial tests shear stresses are applied to a reconstituted specimen during consolidation explicitly to limit lateral strains to a minimum (approximately zero).

Some differences in fabric anisotropy may be expected between two identically reconstituted specimens that have each subsequently experienced isotropic or K_0 consolidation stress histories in the triaxial cell. A comparison of stress-strain behaviour from the two samples (sheared under identical conditions) would reveal only differences induced by their stress history and initial stresses, if all other experimental variables remained the same. Consider three hypothetically identical intact specimens that have been sampled and set up in a triaxial cell in an identical manner, and then each subjected to one of the following three stress paths prior to shear: (1) reconsolidated under conditions of zero lateral strain to estimated anisotropic in-situ stresses (Recompression method); (2) reconsolidated to estimated mean in-situ effective stress (K_0=1 Isotropic Recompression method); (3) consolidated under conditions of zero lateral strain to a stress 1.5 times or higher than the estimated in-situ effective stress and swelled to known *OCR* (SHANSEP method). In this case, comparing the shear behaviour of each sample (sheared under identical conditions) would result in differences attributed to initial shear stress (1 and 2) and stress history (1 and 3) and associated changes in shear and volumetric strain during consolidation. Without acknowledging these important differences in consolidation test procedure, the stress-induced effect would become an uncontrolled variable in the assessment of parameter characterisation.

3.4.2.2 Database development framework

Organisation and storage of data requires a customised database design. A relational database is a common design form used by commercial businesses as it provides efficient storage of large data tables linked together by common data fields. A relational database is therefore suited to storing various soil tests which require identification by test mode, sample coordinates, sample depth, elevation, geological strata, project code, or any other variable. *HoleBase* is one example of a commercial software platform that uses a relational database system to manage soil test data.

Table 3- 4 outlines the general design considerations for the development of the soil test databases presented in this study (see Tables 3- 2 and 3- 3):

Table 3- 4. Design considerations for triaxial test databases

1. What is the purpose of storing the soil test data?	The purpose of creating an efficient data storage and retrieval system for a large number of triaxial tests was to facilitate the analysis of stress-strain measurements using a computer-based algorithm.
2. What are the present objectives regarding the analysis of the stored test data?	Objectives of the database analysis include: (1) to evaluate different models of undrained stress-strain so that an appropriate model can be chosen to characterise stress-strain variability; (2) to evaluate the variability in the model parameters due to inherent material properties and applied experimental conditions. By quantifying the sources of parameter variability statistically, the objective is to facilitate a more rigorous selection and evaluation process for subsequent soil test modes in future project work.
3. What are the user and time access requirements for the database?	The database allows anyone who is familiar with soil test variables to extract the test data for analysis from a readily accessible and durable digital format (e.g. csv). For each triaxial test, the database stores: (1) a list of index parameters/test variables and (2) tabulated increments of shear stress-strain. A ReadMe.txt file, stored with the csv files, defines units and formulae to ensure that consistency is maintained in later expansion of the database. A unique test ID defines the csv file name (*Material _ Sample Type _ Test Mode _ OCR _ Sample Number*). For long-term expansion of the database, test variables should be avoided in the file name and replaced with a numeric ID (e.g. *Test Mode_0000001*).

4. Which test modes are to be included in the database?

The following test modes are included in the reconstituted database: isotropically-consolidated undrained compression (CIUC), isotropically-consolidated undrained extension (CIUE), K_0-consolidated undrained compression (CKUC), K_0-consolidated undrained extension (CKUE). The intact database includes only CKUC and CKUE test modes. In view of the different stress and strain histories experienced in the SHANSEP tests, intact test data are further categorised as Recompression or SHANSEP tests. Experimental details of all tests are summarised in sections 3.3.2.3 and 3.3.2.4.

5. What are the mandatory index parameters required for test input? (i.e. defining material classification properties and applied experimental conditions)

The following listed parameters must be entered into the database to undertake the analytical procedure presented in this report:

Index parameters [a]	**Unit**
Test Mode	-
Reconstituted R/Intact N	-
Test Operator	-
Date of test	-
Sample location [b]	-
Geological formation	-
Applied *OCR* (R only)	-
Sampling depth (N only) [c]	-
Vertical effective stress after consolidation, σ'_{v0}	kPa
Horizontal effective stress after consolidation, σ'_{h0}	kPa
Undrained strain rate	%/hr
Liquid limit, w_L	/100%
Plastic limit, w_P	/100%

Notes

[a] *Other useful parameters would include: Initial pore pressure (of intact specimens measured before saturation (CU tests) or shearing (UU tests); time taken to consolidate the specimen; time allowed for secondary consolidation before shearing the specimen; initial void ratio; initial specimen dimensions; volumetric strain before shearing.*

[b] *Easting Northing or other location reference is recommended, but unavailable here for reconstituted soils*

[c] *n/r = not relevant to reconstituted (R) soil tests; relevant to intact (N) soil tests*

6. Which test variables are measured in the test? Can this number of variables vary?

Stress-strain data were obtained only from the undrained shear stage of a triaxial test. Most authors published their test data using deviator stress (q) or shear stress ($0.5q = \tau$) and axial strain (ε_a) which was used to calculate shear strain by $\gamma=1.5\varepsilon_a$

	Other measurements during undrained shear such as cell pressure (σ_3), excess pore pressure (Δu) and radial strain (ε_r) would provide valuable information about the stress path and sample deformations; however, this information was not always available (from the 22 publications) and, if available, it was not possible to digitise additional test variables to exactly match the digitised stress-strain increments.
7. How have the test data been digitised?	Test data were digitised from 260 CU triaxial tests on reconstituted soils and 34 CU triaxial tests on intact soils that were published in graphs or tables by the publication authors. Published data plots were digitised using Engauge Digitizer Version 4.1, a free digitising software. Shear stress-strain data from 18 triaxial tests published by Vardanega et al. (2012) were reanalysed and re-filtered from the original data source for this study.
8. For each variable, what is the unit of measurement and how many increments are available? (i.e. number of data points)	Index parameters are entered once into the database per triaxial test (see item 5 for parameters and units). Stresses are recorded in kPa and strains are unitless. The number of digitised data-points per triaxial test ranged from 3 to around 200 with a mean of 24.
9. What are the conditions for analysing different input tests?	The approach taken in this study was to analyse the data under two conditions (a and b): a) Data are categorised by test mode according to section 3.6.1 and different test modes cannot be grouped when developing empirical correlations: $CIUC_{Reconstituted}$, $CIUE_{Reconstituted}$, $CKUC_{Reconstituted}$, $CKUE_{Reconstituted}$, $CKUC_{Intact\ Recompression}$, $CKUE_{Intact\ Recompression}$, $CKUC_{Intact\ SHANSEP}$, $CKUE_{Intact\ SHANSEP}$. b) A comparison can be made of compression and extension behaviour if two tests have the following identical database input fields (see Table 3- 5): *test operator*, *geological formation, sample location, OCR* (reconstituted) or *sampling depth* (intact), and *undrained strain rate*.

3.4.2.3 Experimental details of reconstituted soils test database: RFG/TXCU-278

The new database is named following the convention of Ching and Phoon (2014a). Table 3- 5 lists the sources of data in the reconstituted test database compiled from experiments on 23 fine-grained soils from 21 publications. The selection criteria for the database were:

(i) Multiple experiments using reconstituted samples of natural fine-grained material,

(ii) consolidated at different overconsolidation ratios, under isotropic or K_0 conditions,

(iii) and subsequently sheared in triaxial compression or extension up to peak failure to examine the effect of applied shear mode. (Several datasets included samples sheared in compression only, to increase the range of soil types studied – see Table 3- 5).

Table 3- 5 includes observations of the experimental stress-strain data and notes on the digitisation process. Experimental details of all triaxial tests are summarised in Table 3- 6.

3.4.2.4 Experimental details of intact soil test database: BTK/TXCU-34

An intact soil test database was developed to assess sensitivity of stress-strain parameters to the natural material variability in a single soil deposit. The selection criteria for the soil deposit were:

(i) Multiple CU triaxial tests on fine-grained soil sampled over a large depth range,

(ii) consolidated under in-situ stresses,

(iii) and subsequently sheared in triaxial or extension up to peak failure to examine the effect of applied shear mode,

(iv) by a minimum number of laboratories.

The ground investigation site at Bothkennar was chosen on the basis of these criteria and, additionally, because a block sample of Bothkennar clay was available for experimental investigation (chapter 5 and 6). BTK/TXCU-34 was developed only from triaxial test data reported by SERC (1989). Experimental details of all triaxial tests are summarised in Table 3- 7.

Table 3- 5. Sources of experimental data in RFG/TXCU-278

Reference	Test material	w_L (%)	I_P (%)	Test modes	*OCR*	Strain rate (%/min)	Excluded test data	Experimental comments	Digitisation comments
Parry (1956, 1960)	Weald Clay (n=8)	43	25	CIUC (n=6) CIUE (n=2)	1-12		8 tests available for digitisation included as per criteria in section 2.1 (drained tests excluded).		Tests digitised from plotted data *points* available in the thesis, otherwise from the plotted data *lines* given in the paper (n=2 of 8 tests).
Gasparre (2005)- 6 of 7 tests from Abdulhadi (2004)	London Clay (n=7)	63-67	35-41	CIUC (n=7)	1-12		6 tests excluded from digitisation due to poor resolution.		Tests digitised from plotted data *points* where available, otherwise from the plotted data *lines* (n=5 of 7 tests).
Gens (1982)	Lower Cromer Till (n=10)	25	12	CIUC (n=5) CIUE (n=5)	1-10		All undrained tests included (drained tests excluded).		Stress-strain per test digitised from two separate *line* plots (small strain and large strain); data points unavailable.
Loudon (1967)	Kaolin (n=8)	74	32	CIUC (n=8)	1-8.1			A strain rate 0.0019in/min was used but to estimate in units of %/min an axial length of 3 inches has been assumed.	Tests digitised from plotted data *points* where available, otherwise from the plotted data *lines* (n=1 of 8 tests).
Liu (2004)	Kaolin (n=22)	56	24	CIUC (n=9) CIUE (n=11)	1-8		3 tests excluded from digitisation due to poor resolution. 2 tests excluded from stress-strain curve fitting (n too low) but the digitised c_u is included in c_u database analysis.	"Strain rates for undrained tests conformed to those recommended by ASTM 4767" p.141. No other information available. Assumed rate of 1% per hour as per ASTM D4767 – 11.	Tests digitised from plotted data *points.*
Sachan & Penumadu (2007)	Kaolin (n=12)	62	30	CIUC (n=6) CIUE (n=6)	1-10		6 tests on 'Flocculated' samples included; 6 tests on 'Dispersed' samples excluded.		Tests digitised from plotted data *lines*.
Conn (1988)	Keuper Marl (n=20)	36	17	CIUC (n=9) CIUE (n=11)	1-10				Tests digitised from plotted data *lines*.
Valls-Marquez (2009)	Kaolin (n=11)	65	32	CIUC (n=7) CIUE (n=4)	1-5.1				Tests digitised from plotted data *lines*.
Braathen (1966)	Boston Blue Clay (n=4)	45.5	22.3	CIUC (n=3)	1-8.1	0.0191	4 cyclic tests and 7 anisotropically consolidated tests excluded.	Possible load seating issue in one test (CIUC_R_BBC_2_2).	Tabulated data provided.
Fayad (1986)	Boston Blue Clay (n=1)	42	21	CIUC (n=1)	7.5	0.0083			CIU test digitised from plotted data *line.*
Zhu and Yin (2000)	Hong Kong Marine Clay (n=24)	60	32	CIUC (n=12) CIUE (n=12)	1-8				Tests digitised from plotted data *points.*
Atkinson & Little (1988)	Ware Lodgement Till (n=7)	40	22	CIUC (n=7)	1-32		10 'tubed' (natural) samples excluded.		Tests digitised from plotted data *lines*.
Kamal (2012)	Oxford Clay (n=5)	66	32	CIUC (n=5)	1-10				Tests digitised from plotted data *points.*
Kamal (2012)	Gault Clay (n=3)	74	46	CIUC (n=3)	1-5				Tests digitised from plotted data *points.*
Kamal (2012)	Kimmeridge Clay (n=3)	49	26	CIUC (n=3)	1-5				Tests digitised from plotted data *points.*
Vardanega et al. (2012)	Kaolin (n=18)	62.6	33	CIUC (n=18)	1-20				Experimental data of the triaxial tests published by Vardanega et al. (2012) were reanalysed and re-filtered from the original data source for this study.
Parry & Nadarajah (1974)	Kaolin (n=8)	72	32	CIUC (n=4) CIUE (n=4)	1-2.3				Tests digitised from plotted data *lines,* note c_u is uncertain due to unclear presentation of the data.
Fayad (1986)	Boston Blue Clay (n=7)	42	21	CKUC (n=4) CKUE (n=3)	1-8.2		1 cyclic test excluded.		3 tests digitised (from plotted data *lines*): CKUC_R_BBC_1_1, CKUE_R_BBC_4_1, CKUE_R_BBC_8_1 (note that τ_0 taken from digitisation) otherwise tabulated data provided.
Gens (1982)	Lower Cromer Till (n=10)			CKUC (n=6) CKUE (n=4)	1-10 1-7		All undrained tests included (drained tests excluded).		Stress-strain per test digitised from two separate *line* plots (small strain and large strain).
Valls-Marquez (2009)	Kaolin (n=2)	65	32	CKUC (n=1) CKUE (n=1)	1		CKUC test excluded from stress-strain curve fitting (n too low) but the digitised c_u is included in c_u database analysis.		CKU tests digitised from plotted data *points* including τ_0.
Abdulhadi (2009)	Boston Blue Clay (n=22)	46.5	22.7	CKUC (n=19) CKUE (n=3)	1-4.2 1		1 CKUE test excluded from digitisation due to poor resolution.	Possible gap or bedding error affecting small strain measurements in one test (BBC_R_CKUC_1_9).	Digitised from plotted data *lines* including τ_0 (~0.004% axial strain for OCR=1 tests). Two tests show significant discrepancy between digitised and reported τ_0: BBC_R_CKUC_1_9 and BBC_R_CKUC_1_10.
Kamei & Nakase (1989)	Kawasaki Clay (n=8)	55.3	29.4	CKUC (n=4) CKUE (n=4)	1-9.6		K30_R_CKUC_1_1 excluded from stress-strain curve fitting (n too low) but the digitised c_u is included in c_u database analysis.		Tests digitised from plotted data *points* including τ_0. Authors do not report τ_0. Resolution of digitised plot: ε_a = 0.039%
Hight et al. (1985)	London Clay (n=7)	75	47	CKUC (n=4) CKUE (n=3)	1-7		LDN_R_CKUC_1_1 excluded from stress-strain curve fitting (n too low) but the digitised c_u is included in c_u database analysis.		Tests digitised from strain contours on stress path *line* plots, including τ_0. Authors do not report τ_0. Resolution of digitised plot: p' = 0.27kPa q = 0.26kPa
Hight et al. (1985)	North Sea Clay (n=6)	32	17	CKUC (n=4) CKUE (n=3)	2-8 1-17		NSC_R_CKUC_1_1 and NSC_R_CKUC_1.5_1 excluded from stress-strain curve fitting (n too low) but the digitised c_u is included in c_u database analysis.		Tests digitised from strain contours on stress path *line* plots, including τ_0. Authors do not report τ_0. Resolution of digitised plot: p' = 0.27kPa q = 0.30kPa
Sheahan (1991)	Boston Blue Clay (n=36)	45.1-45.8	23-25.5	CKUC (n=27) CKUE (n=9)	1-8 1-4		1 CKUC test (CTX-21) excluded from stress strain curve fitting (n too low) but the digitised c_u is included in c_u database analysis.		Tabulated data provided.
Parry & Nadarajah (1974)	Kaolin (n=7)	72	32	CKUC (n=3) CKUE (n=4)	1-2.6		1 CKUC test excluded from digitisation due to poor resolution.		Tests digitised from plotted data *lines,* note τ_0 and c_u are uncertain due to unclear presentation of these data.

Table 3- 6. Experimental details of the triaxial tests in RFG/TXCU-278

Reference	Test material	Reconstitution method	Consolidation method	Shear measurement	Area correction	Filter and/or membrane correction	Load cap
Isotropically-consolidated triaxial tests							
Parry (1956, 1960)	Weald Clay (n=8)	The soil was mixed with distilled water at w = 0.8w_L and "pressed in successive layers" into the sample mould.	Porous stones were boiled to reduce the entrenchment of air. All B values achieved 0.96 to 0.98. A single increment of cell pressure applied with a consolidation time of 3-4 days (CIUC) or 7-8 days (CIUE).	Externally measured displacement (global strain)	"Average area" for the measured length and volume (right-cylinder)	Filter strips used. Filter and membrane correction applied to (assumed peak) deviator stress: -13.79kPa (CIUC with vertical filter strips); +1.38 to +2.76kPa (CIUE with spiral filter strips).	Ball bearing (CIUC); threaded rod or bayonet (CIUE)
Gasparre (2005) who describes the method of all tests undertaken by Abdulhadi (2004) under her supervision	London Clay (n=7)	The soil was mixed with water at w = 1.25w_L and compressed in 38mm Perspex consolidometers under σ'_v = ~30kPa	Consolidation rate of 3kPa/hour applied with pauses at 100kPa intervals to allow excess pore pressure dissipation	Inclinometers (local strain)	Right-cylinder $A=A_0/(1-\varepsilon)$ where A_0=area at start of undrained shear	Vertical filter strips used. Membrane stress correction followed La Rochelle et al. (1988) for barrelling and block sliding deformation.	Conventional suction cap, no ball bearing and forced alignment
Gens (1982)	Lower Cromer Till (n=10)	The soil was air dried, ground, then passed through 2mm sieve, before mixing with distilled water at w = 1.26w_L and consolidated isotropically as a block in a large 152mm diameter triaxial cell under 160 or 120kPa before swelling to OCR=4. From the block, 8 specimens were cut to size (38mm diameter) and waxed for storage.	A single increment of cell pressure applied with a consolidation time of 24 hours and an additional 24 hours of drainage prior to undrained shear.	Externally measured displacement corrected by load cell deflection (global strain)	Right-cylinder	Lubricated stainless steel discs were used with spiral filter strips. No correction for filter strips was applied since minimal restraining effect was observed during initial investigations. No membrane correction applied.	No information but reasonable to assume use of ball bearing (CIUC); bayonet or suction cap (CIUE)
Loudon (1967)	Kaolin (n=8)	Prepared from a slurry, no other information.	Discrete increments of 20 lb/in^2 (138kPa) cell pressure applied during consolidation and swelling.	Externally measured displacement assumed due to testing date (global strain)	No information	No information	No information
Liu (2004)	Kaolin (n=22)	Powdered kaolin was mixed with water at w = 150% and consolidated one-dimensionally as a block in a large consolidation tank	Stress controlled continuous rate of isotropic consolidation	Externally measured displacement (global strain)	No information	Lubricated aluminium platens used with either geotextile or inclined slotted whatman filter strips at high/ low confining pressures respectively. Tests on dummy samples provided corrections for the different materials.	Ball bearing (CIUC); threaded rod (CIUE)
Sachan & Penumadu (2007)	Kaolin (n=12)	Powdered kaolin was mixed with de-aired and deionized water at w = 155% and consolidated one-dimensionally in a consolidometer. 102mm diameter 102mm height specimen obtained after 24 hrs.	Limited information - it appears that a single increment of cell pressure was applied, and consolidation monitored to establish primary consolidation behaviour	No information	No information	Lubricated ends and filter paper strips were used	No information other than "fixed" top platen
Conn (1988)	Keuper Marl (n=20)	The soil was air dried, before mixing with distilled water at w = 2w_L (approximately) and consolidated one-dimensionally in a steel 100mm diameter tube under 30kPa vertical stress for 3 days. Extruded to a 38mm triaxial mould and waxed for storage.	Discrete cell pressure increments up to a maximum of 700kPa. Samples were overconsolidated by increasing back pressure.	External dial gauge and displacement transducer. Tests terminated at 20% axial strain.	"standard triaxial area correction" right cylinder used for extension tests	Corrections made for membranes, side drains in compression tests only (spiral drains used for extension tests), apparatus compliance	Threaded bars
Valls-Marquez (2009)	Kaolin (n=11)	Powdered kaolin was mixed with de-aired and deionized water at w = 1.5w_L and consolidated one-dimensionally in an acrylic consolidometer with 50mm internal diameter	100kPa/hour increase in cell pressure	External displacement transucer (possibly)	No information	Membrane correction according to British Standard 1377-7:1990. No info about drainage filters/lubricated ends.	GDS extension cap
Braathen (1966)	Boston Blue Clay (n=4)	Sampled from field pits, air dried, ground, mixed to slurry with w=400%, passed through No 200 sieve, increased salt content from 23 to 24 g/l, settled, heated to 70°C, placed into 241mm diameter consolidometer, consolidated under 1.5kg/cm3 (147.1kPa), submerged in oil and stored (probably in large consolidometer) in humid room until trimmed for experiment.	Discrete cell pressure increments. At least 7000 minutes allowed for final consolidation step including primary consolidation, hence 96 hours assumed to follow primary consolidation of final increment.	Externally measured displacement assumed due to testing date (global strain)	Right-cylinder	Filter strips used with correction applied to deviator stress.	Probably a rigid top cap (same Geonor cell used for cyclic tests).
Fayad (1986)	Boston Blue Clay (n=1)	Identical sedimentation process/equipment to Germaine (1982). Used recycled clay powder from previous experiments on Boston Blue Clay at MIT, air dried, ground, passed through #40 sieve, increased salt content from 9.9 to 16 g/l and slurry with w=100%.	Discrete cell/axial pressure increments (vertical effective stress limited to 20% increases), 8 hours per increment. About 24 hours followed primary consolidation of final increment.	Externally measured displacement transducer shown in Ayan (1985) (global strain)	Parabolic shape used for area correction.	Filter strips used with Filter Correction applied to deviator stress for compression tests.	No information
Zhu and Yin (2000)	Hong Kong Marine Clay (n=24)	Consolidated one-dimensionally from a slurry as a block in a large consolidation tank under 55kPa	Single increments of cell pressure were applied to obtain maximum and minimum effective stresses	No information	No information	Filter strips used	GDS system
Atkinson & Little (1988)	Ware Lodgement Till (n=7)	Chalk clasts removed, air dried, ground, passed through 0.425mm sieve, and mixed with distilled water at w = 20%. Pressed into 38mm sample mould by hand.	Limited information	Externally measured displacement (global strain)	Right-cylinder	Filter paper side drains used. Corrections made for compliance and seating errors	No information
Kamal (2012)	Oxford Clay (n=5)	Trimmings were soaked in water and mixed mechanically to a slurry paste. Consolidated one-dimensionally from slurry as a block in a 230mm diameter consolidation tank under 50kPa then cut into smaller blocks and waxed for storage.	5kPa/hour increase in cell pressure with hold periods after every increment of 100kPa	Internal instruments attached to the specimen: axial LVDTs, mid height pore pressure transducer, radial belt, and mid height bender elements	Right-cylinder or two-wedge sliding mechanism (Chandler 1966)	Filter paper side drains used. No membrane correction applied.	Suction cap connection made before consolidation

Reference	Test material	Reconstitution method	Consolidation method	Shear measurement	Area correction	Filter and/or membrane correction	Load cap
Kamal (2012)	Gault Clay (n=3)	Trimmings were soaked in water and mixed mechanically to a slurry paste. Consolidated one-dimensionally from slurry as a block in a 230mm diameter consolidation tank under 50kPa then cut into smaller blocks and waxed for storage.	5kPa/hour increase in cell pressure with hold periods after every increment of 100kPa	Internal instruments attached to the specimen: axial LVDTs, mid height pore pressure transducer, radial belt, and mid height bender elements	Right-cylinder or two-wedge sliding mechanism (Chandler 1966)	Filter paper side drains used. No membrane correction applied.	Suction cap connection made before consolidation
Kamal (2012)	Kimmeridge Clay (n=3)	Trimmings were mixed with water by hand and consolidated one-dimensionally in 38mm or 50mm floating tube consolidometer.	5kPa/hour increase in cell pressure with hold periods after every increment of 100kPa	Internal instruments attached to the specimen: axial LVDTs, mid height pore pressure transducer, radial belt, and mid height bender elements	Right-cylinder or two-wedge sliding mechanism (Chandler 1966)	Filter paper side drains used. No membrane correction applied.	Suction cap connection made before consolidation
Vardanega et al. (2012)	Kaolin (n=18)	Prepared from a slurry, no other information.	Single increments of cell pressure were applied to obtain maximum and minimum effective stresses while back pressure was maintained at 350kPa	Externally measured displacement (global strain)	No information	No information	No information
Parry & Nadarajah (1974)	Kaolin (n=8)	Powdered kaolin was mixed with water at w = 160% and consolidated one-dimensionally in a 38mm diameter mould under 200kPa	Cell pressure increased and decreased incrementally	Externally measured displacement using dial gauge	No information	Lubricated end platens used. No filter drains.	No information
K_0-consolidated triaxial tests							
Fayad (1986)	Boston Blue Clay (n=7)	Identical sedimentation process/equipment to Germaine (1982). Used recycled clay powder from previous experiments on Boston Blue Clay at MIT, air dried, ground, passed through #40 sieve, increased salt content from 9.9 to 16 g/l and slurry with w=100%.	Discrete cell/axial pressure increments (vertical effective stress limited to 20% increases), 8 hours per increment. About 24 hours followed primary consolidation of final increment.	Externally measured displacement transducer shown in Ayan (1985) (global strain)	Parabolic shape used for area correction.	Filter strips used with Filter Correction applied to deviator stress for compression tests. Helicoidal filter strips used for extension tests with no stress correction applied.	No information
Gens (1982)	Lower Cromer Till (n=10)	The natural material was air dried, ground, then passed through 2mm sieve, before mixing with distilled water at w (%) = $1.26w_L$ and consolidated one-dimensionally as a block in a large 224mm diameter container under 200kPa before swelling to OCR=4. From the block, 8 specimens were cut to size (38mm diameter) and waxed for storage.	Stress controlled hydraulic apparatus used with continuous manual adjustment of cell and chamber pressures. No information about rate of consolidation other than "slow rates of stress change".	Externally measured displacement corrected by load cell deflection (global strain)	Right-cylinder	Lubricated stainless steel discs were used with spiral filter strips. No correction for filter strips was applied since minimal restraining effect was observed during initial investigations. No membrane correction applied	No information but reasonable to assume use of ball bearing (CKUC); bayonet or suction cap (CKUE)
Valls-Marquez (2009)	Kaolin (n=2)	Powdered kaolin was mixed with de-aired and deionized water at w = $1.5w_L$ and consolidated one-dimensionally in an acrylic consolidometer with 50mm internal diameter	Continuous stress increase at about 50kPa/2 days. K_0-conditions controlled by either volume change (CKUC test) or Hall effect transducers (CKUE test)	Local LVDTs for CKUC test and Hall effects transducers for CKUE test	No information	Membrane correction according to British Standard 1377-7:1990. No info about drainage filters/lubricated ends.	GDS extension cap
Abdulhadi (2009)	Boston Blue Clay (n=22)	Natural material was softened with tap water and mixed into slurry, passed through #10 US standard sieve, oven dried, ground, blended into batch containers. The dried powder was then mixed with de-aired water at w = 100% (about $2w_L$) and sodium chloride added to achieve 16 g/l concentration. Slurry was vacuumed and placed into 65mm diameter consolidometer and consolidated one-dimensionally under 100kPa or 1000kPa vertical effective stress then swelled to OCR=4 before extrusion.	One-dimensionally consolidated using volumetric strain rate of 0.15%/hour and algorithm to maintain approximately equal axial and volumetric strains, 24 hours held load, swelled using strain rate of 0.15%/hour, 24 hours held load prior to shearing	Externally measured displacement (global strain)	Parabolic (CKUC), right-cylinder (CKUE)	Frictional end platens were used	No information
Kamei & Nakase (1989)	Kawasaki Clay (n=8)	From Nakase & Kamei (1983): Consolidated one-dimensionally from a slurry as a block in a large consolidation tank under 69kPa, then trimmed into five specimens 50mm dameter 120mm height	Four step process of applying cell pressure and axial pressure increments under predetermined K_0 value.	Externally measured displacement (global strain)	No information	Lubricated ends using membranes and silicone grease.	Threaded bar in diagram (Nakase & Kamei 1983)
Hight et al. (1985)	London Clay (n=7)	No information	No information	No information	No information	No information	No information
Hight et al. (1985)	North Sea Clay (n=6)	No information	No information	No information	No information	No information	No information
Sheahan (1991)	Boston Blue Clay (n=36)	The natural material is wet sieved, oven-dried, processed to powder, mixed with de-aired and distilled water at w (%) = 100 to form a slurry. Salt and phenol added to act as flocculant and antibacterial agents. Mixed under vacuum and dropped into lower chamber (30cm diameter batch consolidometer). Compressed one-dimensionally to 24.5kPa and swelled to OCR=4 before extrusion and cut to size.	One-dimensionally consolidated using volumetric strain rate of 0.1%/hour and algorithm to maintain approximately equal axial and volumetric strains,24 hours held load, swelled using strain rate of 0.05%/hour, 24 hours held load prior to shearing. Measured pore pressure changes during the held load period were <1% of the consolidation stress.	Externally measured displacement (global strain)	Lubricated ends were used, and the deforming geometry was non-cylindrical. Parabolic (CKUC) and right-cylinder (CKUE) corrections were adopted.	Lubricated ends were used. Vertical filter strips (compression) or spiral filter strips (extension) over the top and base thirds of the specimen, with corrections made only for increased resistance in compression (not extension). Membrane corrections were made following Germaine and Ladd (1988).	No information
Parry & Nadarajah (1974)	Kaolin (n=7)	Powdered kaolin was mixed with water at w = 160% and consolidated one-dimensionally in a 38mm diameter mould under 200kPa	Approximate K_0 conditions (0.15% radial strains) were achieved by applying increments of axial and cell pressures to a predetermined K_0 value	Externally measured displacement using dial gauge	No information	Lubricated end platens used. No filter drains.	No information

3.4.3 Pre-failure stress-strain models in the moderate stress range

Duncan and Buchignani (1976) proposed relationships between E_u/c_u and *OCR* for ranges of clay soils categorised by plasticity index (Figure 3- 2, digitised from the original publication). The chart published in 1976 was later reproduced by Jamiolkowski et al. (1979) and Casey et al. (2016) who clarified that the lines shown in Figure 3- 2 correspond to a stress ratio of 0.5, where stress ratio (*S*) is defined by Equation 3.1:

$$\frac{\tau_{mob} - \tau_0}{c_u - \tau_0} = S \tag{3.1}$$

Where, τ_0 = initial shear stress, τ_{mob} = the mobilised shear strength, and c_u = undrained shear strength.

Equation 3.1 was proposed by Casey et al. (2016) to clarify the definition of E_u (secant undrained modulus) according to the mobilised undrained shear strength. Stress ratio is relabelled in this study as *S* (previously defined as *B* by Casey et al. 2016) to avoid confusion with parameters from the original mobilisation framework (Vardanega and Bolton 2011, Vardanega et al. 2012).

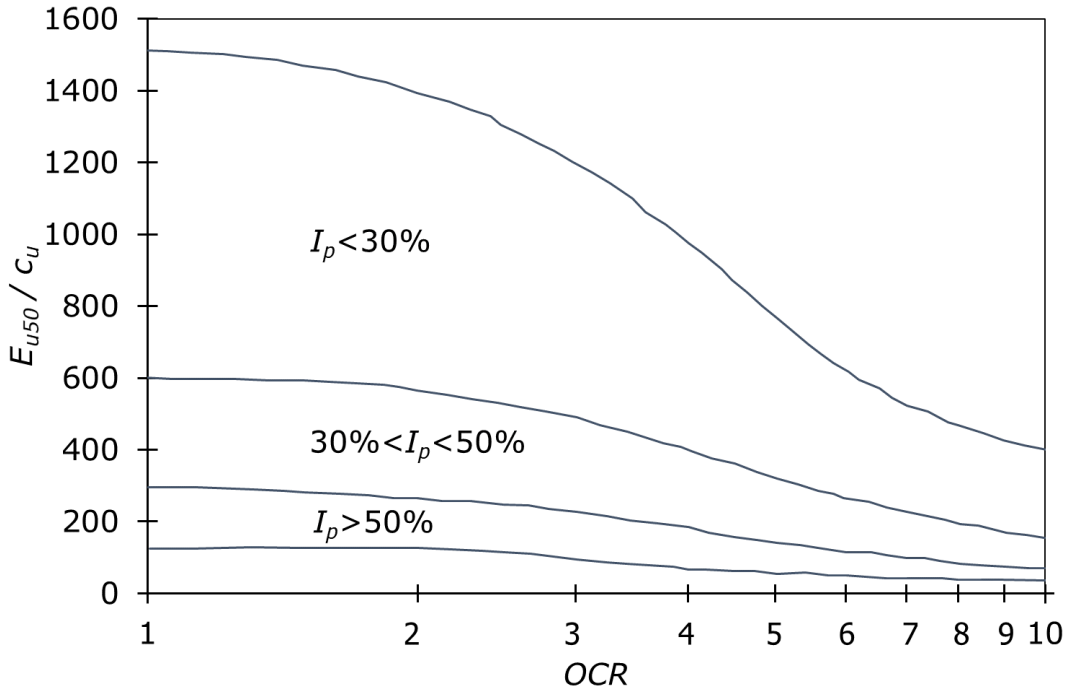

Figure 3- 2. Chart showing relationships between E_{u50}/c_u and *OCR* proposed by Duncan and Buchignani (1976) for estimating undrained modulus of clay based on back-calculated field measurements (digitised from the original publication)

Whereas the parameter ranges recommended by Duncan and Buchignani (1976) were based on field measurements, and give no indication of nonlinear behaviour, Casey et al. (2016) used a reconstituted soils database of CKUC test results to develop new empirical correlations describing the variation of secant undrained modulus (E_u) with stress ratio. To characterise nonlinear behaviour, Casey et al. (2016) adopted equivalent elastic secant modulus values at three points on a soil's stress-strain curve which could be estimated by three different empirical equations. They demonstrated that E_u at S=0.25, 0.50 and 0.75, normalised by a reference effective stress (σ'_{vref} = 100kPa), varied with pre-shear vertical consolidation stress applied in the triaxial test (denoted here by σ'_{v0}):

$$\frac{E_u}{\sigma'_{vref}} = 465\left(\frac{\sigma'_{v0}}{\sigma'_{vref}}\right)^{0.73} \qquad \text{at } S = 0.25 \qquad (3.2a)$$

$$\frac{E_u}{\sigma'_{vref}} = 364\left(\frac{\sigma'_{v0}}{\sigma'_{vref}}\right)^{0.68} \qquad \text{at } S = 0.50 \qquad (3.2b)$$

$$\frac{E_u}{\sigma'_{vref}} = 260\left(\frac{\sigma'_{v0}}{\sigma'_{vref}}\right)^{0.61} \qquad \text{at } S = 0.75 \qquad (3.2c)$$

Nonlinear elasticity is a common approach used by constitutive modellers (Potts et al. 2001). A nonlinear elastic stress-strain model was first implemented with finite element (FE) analysis by Duncan and Chang (1970); in their paper they explained that incremental stress-strain calculation procedures in FE analyses can be well expressed by a formula describing the degradation of tangent modulus (E_t). Their proposed model (Equation 3.3) assumes

- a hyperbolic stress-strain law (recommended by Konder 1963 and many others e.g., Hardin and Drnevich 1972),
- a Mohr-Coulomb failure criterion, and
- an empirical relationship to estimate initial tangent modulus (E_i) from the confining pressure applied in a triaxial test

to mathematically describe the variation of tangent modulus (E_t) with any stress increment up to peak stress (Duncan and Chang 1970):

$$E_t = \left[1 - \frac{R_f(1 - sin\varphi)(\sigma_1 - \sigma_3)}{2c\ cos\varphi + 2\sigma_3 sin\varphi}\right]^2 Kp_a \left(\frac{\sigma_3}{p_a}\right)^n \quad (3.3)$$

Where, σ_1 = major principal stress; σ_3 = minor principal stress; R_f = the failure ratio (always less than unity) defined by the ratio of the measured value of $(\sigma_1 - \sigma_3)_{failure}$ at peak strength to the asymptotic value of $(\sigma_1 - \sigma_3)_{ult}$ as defined by the hyperbolic stress-strain equation; c and φ are Mohr-Coulomb strength parameters; K and n = respectively the intercept and slope coefficients obtained by fitting a straight line through a series of measurements of (E_i) at different confining stresses (σ_3) plotted in transformed axes log(E_i) and log(σ_3).

Both approaches by Duncan and Chang (1970) and Casey et al. (2016) characterise stress-strain by fractions of mobilised shear strength (S) and nonlinear elasticity. The former approach was developed for routine triaxial tests and in principle can simulate stress-strain behaviour incrementally at any stress ratio. However, a greater number of model parameters and at least 3 triaxial tests are needed to calibrate the model for a soil. To the author's knowledge, no database has been published explicitly to interrogate the model accuracy of Equation 3.3. Undertaking such a task would require a large test database that includes measurements of all 5 model parameters for each test. Although adopting the approach by Casey et al. (2016) has the advantage that it has been already calibrated by a large database (73 CKUC tests), their method provides only 3 points on the stress-strain curve.

An alternative representation of stress-strain behaviour is described by Bolton (1993a) as plastic strength (c_u) mobilisation with the development of plastic shear strains (γ_{mob}) and suggested that the relationship may be described by a power law (Bolton 1993b):

$$S = \frac{\Delta\tau}{\Delta\tau_p} = \left(\frac{\Delta\gamma}{\gamma_p}\right)^b \quad (3.4)$$

Where, in undrained soils, $\Delta\tau_p$ = applied shear stress to mobilise peak strength (c_u-τ_0); γ_p = shear strain mobilised at peak strength (c_u); $\Delta\tau$ = an increment of shear stress (τ_{mob}-τ_o); $\Delta\gamma$ = an increment of shear strain; and b = a fitted exponent.

Similar power-law functions were proposed in earlier studies to describe stress-strain relationships observed in laboratory soil tests (Brinch Hansen 1965) and to define p-y curves for offshore structures (Matlock 1970; Zhang and Anderson 2017). Whereas the model by Matlock (1970) assumed a set '*b*' value (of 0.33), the variation of *b* was recognised by Brinch Hansen (1965) and Bolton (1993b) and later formalised by Vardanega and Bolton (2011) who proposed a framework suitable for reliability-based design style approaches (Vardanega and Bolton 2016a):

$$S = \frac{\tau_{mob}}{c_u} = 0.5\left(\frac{\gamma}{\gamma_{50\,CIU}}\right)^{b_{CIU}} \qquad 0.2 \leq \tau_{mob}/c_u \leq 0.8 \quad \text{(CIU conditions)} \qquad (3.5)$$

Where, τ_{mob} = the mobilised shear strength; γ = shear strain; $\gamma_{50\,CIU}$ = shear strain to mobilise $0.5c_u$ under isotropically-consolidated undrained conditions (denoted in the authors' study as $\gamma_{M=2}$); and b_{CIU} is an exponent to describe non-linearity. Since $\tau_0 = 0$, $\tau_{mob}/c_u = S$.

If soil stress-strain may be accurately represented by power-law curves, a varying exponent is indicative of varying stress-strain non-linearity. A similar approach using a power-law and hardening exponent was suggested by Hollomon (1945) to describe ranges of plastic flow (ductility) in metals. Equation 3.5 makes use of a reference mobilisation strain (γ_{50}) at S=0.5 which may be measured in routine triaxial tests.

Vardanega and Bolton (2011) developed the Mobilisation Strain Framework (MSF) i.e. Equation 3.5 with a large test database including 92 isotropically-consolidated undrained shear tests (CIU) on intact soils and demonstrated that b_{CIU} = 0.608 (mean) ± 0.158 (standard deviation). The subscript CIU has been added to the model parameters of Equation 3.5 in this study to acknowledge isotropic (K_0 = 1) consolidation stresses prior to undrained shear (see section 3.4.2.1).

Casey (2016), in response to the discussion of Vardanega and Bolton (2016b), observed that a large difference in mobilised reference strain at S=0.5 measured in triaxial compression may occur as a result of using an isotropic or K_0-consolidation stress path. Vardanega and Bolton (2016b) (following Vardanega 2012) when discussing the work of Casey et al. (2016) acknowledged that a modification of Equation (3.5) is needed when considering K_0-consolidated triaxial tests (expressed here by Equation 3.6). Equation 3.6 reduces to Equation 3.5 if K_0 = 1 (isotropic consolidation stresses).

$$S = \frac{\tau_{mob} - \tau_0}{c_u - \tau_0} = 0.5\left(\frac{\gamma}{\gamma_{50\,CKU}}\right)^{b_{CKU}} \qquad 0.2 \leq S \leq 0.8 \qquad (3.6)$$

Where, τ_0 = initial shear stress; $\gamma_{50\,CKU}$ = shear strain to mobilise $0.5(c_u - \tau_0)$ (denoted in previous works as γ_{ref}); and b_{CKU} is an exponent that describes soil non-linearity.

Klar and Klein (2014) pointed out that expressing stress-strain behaviour with a power-law leads to infinitely high initial stiffness and instead proposed an exponential function to model CIU test results (Equation 3.7):

$$S = \frac{\tau_{mob}}{c_u} = \left(1 - e^{-0.693\frac{\varepsilon_a}{\varepsilon_{50\,CIU}}}\right) \qquad 0.2 \leq S \leq 0.8 \qquad (3.7)$$

Where, ε_a = axial strain; $\varepsilon_{50\,CIU}$ = shear strain to mobilise $0.5c_u$ under isotropically-consolidated undrained conditions. Equation 3.7 may also be expressed in the form of Equation 3.8 by adopting shear strain in place of axial strain. To consider initial stresses where $K_0 \neq 1$, Equation 3.9 may used.

$$S = \frac{\tau_{mob} - \tau_0}{c_u - \tau_0} = \left(1 - e^{-0.693\frac{\gamma}{\gamma_{50\,CIU}}}\right) \qquad 0.2 \leq S \leq 0.8 \qquad (3.8)$$

$$S = \frac{\tau_{mob} - \tau_0}{c_u - \tau_0} = \left(1 - e^{-0.693\frac{\gamma}{\gamma_{50\,CKU}}}\right) \qquad 0.2 \leq S \leq 0.8 \qquad (3.9)$$

A logarithmic function has also been used to describe soil stress-strain curves: Puzrin and Burland (1996) proposed Equation (3.10) to characterise measurements outside the small strain region by defining a lower strain limit as $x_1 = \varepsilon_e + e - 1$, where ε_e = the elastic region limit and e = 2.718. Like Equation 3.4, the stress-strain curve is normalized with respect to a limiting strain and a limiting stress which may be taken as measured at the point of peak stress:

$$\frac{q}{q_p} = \frac{\varepsilon}{\varepsilon_r} - \alpha\frac{\varepsilon}{\varepsilon_r}\left[\ln\left(1 + \frac{\varepsilon}{\varepsilon_r}\right)\right]^R \qquad (3.10)$$

$$\text{Where, } R = \frac{\left(1+\frac{\varepsilon_p}{\varepsilon_r}\right)ln\left(1+\frac{\varepsilon_p}{\varepsilon_r}\right)}{\frac{\varepsilon_p}{\varepsilon_r}\left(\frac{\varepsilon_p}{\varepsilon_r}-1\right)} \text{ and } \alpha = \frac{\left(\frac{\varepsilon_p}{\varepsilon_r}-1\right)}{\frac{\varepsilon_p}{\varepsilon_r}\left[ln\left(1+\frac{\varepsilon_p}{\varepsilon_r}\right)\right]^R}$$

q = deviator stress; q_p = peak deviator stress; ε_p = strain at peak deviator stress; ε_r = a reference strain defined by q_p/E_{max}; and E_{max} = initial stiffness modulus.

(In the same paper, Puzrin and Burland 1996 also demonstrated a separate function for small-strain data. The two adjoined functions, known as L4, was incorporated into a constitutive model to predict pre-failure deformations caused by tunnelling in London Clay; see Addenbrooke et al. 1997).

3.4.4 Evaluation of pre-failure stress-strain models in the moderate stress range

Selection of a suitable stress-strain function requires:

(1) that the model is sufficiently representative of a soil's physical behaviour (e.g. Klar and Klein 2014);

(2) the lowest possible number of model parameters while maintaining reasonable accuracy (Puzrin and Burland 1996);

(3) that the model parameters should be representative of physical properties (Puzrin and Burland 1996);

(4) that the parameters should be simple to derive (Puzrin and Burland 1996);

(5) that the parameters can be evaluated by reliability-based procedures (e.g. Vardanega and Bolton 2011, 2016a).

All models presented by the cited studies use a form of strength mobilisation to describe soil stress-strain behaviour. If Equation 3.1 is used to describe the applied strength mobilisation, it seems plausible that a reasonable description of the resulting normalised-stress-strain data may be achieved by hyperbolic, power, exponential, or logarithmic functions. Only the models proposed by Duncan and Buchignani (1976), Casey et al. (2016), and Duncan and Chang (1970), do not use a form of strain mobilisation.

Power and hyperbolic laws are unlikely to represent realistic soil behaviour close to peak stresses: Vardanega and Bolton (2011) recommended an upper limit of S=0.8; Duncan and Chang (1970) stated that R_f varies between 0.75 and 1.0. If strength mobilisation is represented by an exponential law i.e. Equation (3.8) or (3.9), the initial stiffness is limited to a finite value whereas the power law leads to infinitely high stiffness (Klar and Klein 2014). The stress-strain models proposed by Puzrin and Burland (1996) and Klar and Klein (2014) are defined by a collapse limit but the authors

offer no suggestion on suitable lower limits for stress ratio. Satisfying condition (1) may then be provisional to limiting the modelled range of mobilised strains and mobilised stresses.

To simplify the modelling process, a single model that can simulate stress-strain behaviour over the relevant engineering design range is desirable. The chart proposed by Duncan and Buchignani (1976) is too limiting: the data bounds may be representative of field conditions, but Figure 3-1 provides less information than the other models since the chart can be used to estimate only a single point on the stress-strain curve. The models proposed by Vardanega & Bolton (2011) and Casey et al. (2016) are calibrated with a similar range of stress ratio. The power-law approach was originally defined by Vardanega & Bolton (2011) for the moderate strain region (strains >0.1%) corresponding to a moderate range of mobilised stresses which represent typical factors of safety (of 5 at S=0.2 and 1.25 at S=0.8). For engineering purposes, the prediction of settlements up to a strength mobilisation of 80% is a prudent choice. Vardanega and Bolton (2011) demonstrated with 115 soil tests that Equation 3.5 fits stress-strain data reasonably well in the stress range of $0.2 \leq S \leq 0.8$ with a mean R^2 of about 0.97 (n=115). Outside these bounds, the power-law model should be used with caution, and other functions (e.g., hyperbolic) may be more suitable at lower strain levels.

Equations 3.5, 3.6 and 3.10 require 4 model parameters; Equations 3.7, 3.8 and 3.9 require 3. To predict modulus at a single stress ratio, the framework by Casey et al. (2016) requires 3 parameters which increases to 5 when considering two additional points on the stress-strain curve. Adopting the approach by Duncan and Chang (1970) requires 5 model parameters – and it is doubtful that R_f has physical significance; rather, R_f is simply a manifestation of the model and may be difficult to predict.

There is a similarity between Duncan and Chang (1970) and Puzrin and Burland (1996): the models rely on measured or estimated initial stiffness (E_i). Since the measurement of elastic modulus is uncommon in routine triaxial tests (e.g., with bender element instrumentation – see Pennington et al. 1997), and since its estimate introduces additional uncertainties to the model characterisation process, the approach taken in this study is to restrict the number of investigated model parameters to those that can be measured easily (condition 4) from a single routine triaxial test. The limitations of the compiled test database should also be acknowledged in selecting stress-strain models to be evaluated. Section

3.4.2.2 describes the development of the two test databases and states that only stress-strain increments were digitised. The selected stress-strain models must therefore provide a means of evaluating the non-linearity observed in triaxial test measurements.

3.4.5 Nonlinear stress-strain functions selected for the analytical investigation

In the author's view, any mathematical model may be adopted to predict stress-strain provided that it demonstrably matches the data and the range of physical behaviour for which it was originally developed. The calibrated range of behaviour for a model may be conveniently defined by a limited range of mobilised stress and/or mobilised strain, where mobilised stress is defined by a reference stress and mobilised strain is defined by a reference strain, with each reference value being of clear relevance to the design scenario. For the problem case considered in this study, the relevant reference stress is undrained shear strength, c_u. The reference strain has been chosen to investigate the effect of the c_u normalisation procedure (strength mobilisation as defined by Equation 3.1), on deformation parameter variability. Reference strains at S=0.3 (γ_{30}), 0.5 (γ_{50}) and 0.7 (γ_{70}) are defined by the models fitted to the stress-strain test data and used to investigate strain variability at different strength mobilisation levels.

Considering the preceding discussion, three mathematical functions have been selected to investigate nonlinear stress-strain behaviour in fine-grained soils: power (Equations 3.5 and 3.6), exponential (Equations 3.8 and 3.9), and logarithmic (Equations 3.11 and 3.12).

$$S = \beta \cdot \log10\left(\frac{\gamma_{50\ CIU}}{\gamma}\right) + 0.5 \qquad 0.2 \leq S \leq 0.8 \qquad (3.11)$$

$$S = \beta \cdot \log10\left(\frac{\gamma_{50\ CKU}}{\gamma}\right) + 0.5 \qquad 0.2 \leq S \leq 0.8 \qquad (3.12)$$

It has been shown that simple mathematical expressions can be adapted to describe tests where initial stresses are $K_0 \neq 1$ or isotropic. Tests performed with isotropic consolidation stresses are described by Equations 3.5, 3.8, and 3.11. Tests performed with initial stresses of $K_0 \neq 1$ are described by Equations 3.6, 3.9, and 3.12. The exponential model (Equation 3.8 and 3.9) is inflexible in shape and hence, like Matlocke (1970), a constant soil non-linearity is inherently assumed. The power-law model (Equation 3.5 and 3.6) and logarithmic model (Equation 3.11 and 3.12) include an additional non-linearity

parameter: b or β. By investigating the exponential model as a comparison to the power-law and logarithmic models, it allows an assessment to be made of the significance of non-linearity to modelling soil stress-strain response.

If a model with a variable non-linearity parameter is assessed to be sufficiently accurate, it means that the measured non-linearity and strain magnitude of any triaxial test can be evaluated against a large database of similar test modes.

3.4.6 Statistical techniques to evaluate a database of stress-strain test data

3.4.6.1 Evaluating stress-strain models

The previous sections outlined methods of selecting and categorising triaxial test stress-strain data appropriate for database analysis. Using simple linear regression analysis, any stress strain model may be fitted to the data of each triaxial test if the required model parameters are available in the database. In section 3.4.5, three models were selected to test whether they may be suitable for the variability characterisation of stress-strain behaviour. This section describes statistical tools to evaluate the accuracy of a chosen stress-strain model.

The exponential model (Equation 3.8 and 3.9), power-law model (Equation 3.5 and 3.6) and logarithmic model (Equation 3.11 and 3.12) were fitted to the data points (τ, γ) of 271 reconstituted soil tests (RFG/TXCU-278). Seven tests provided only peak stress data. The same models were fitted to the 34 intact soil tests (SERC 1989). For consistency, in this study the range of stress ratio in all three models is limited to $0.2 \leq S \leq 0.8$. The method of least squares was used to estimate a "best fit" linear regression line using one or two transformed axes ($\log_{10}$) as appropriate to the model. Least squares estimators of the slope and intercept were calculated by minimising the sum of squares of deviations in observed values (y_i) from the regression line. To assess the quality of model fit to the test data, the following statistics were calculated for every test in the two databases.

The coefficient of determination (R^2) describes the variance that can be explained by the model. R^2 is calculated using Equation 3.13:

$$R^2 = 1 - \frac{\sum(y_i - \hat{y}_i)^2}{\sum(y_i - \bar{y}_i)^2} \tag{3.13}$$

(Kvalseth 1983), where y_i = actual (observed) value; $\hat{y}_i$ = sample mean of the fitted y_i values; $\bar{y}_i$ = sample mean of the actual (observed) values.

Equation 3.14 is used to calculate the standard error of the regression (*SE*):

$$SE = \left(\frac{\sum(y_i - \hat{y}_i)^2}{(n-1)} \right)^{\frac{1}{2}} \tag{3.14}$$

where, n = number of y_i values.

Puzrin and Burland (1996) proposed a "quantitative criterion of accuracy", *a*, which can be calculated by the inverse of standard error using Equation 3.15:

$$a = \left(\frac{\sum(y_i - \hat{y}_i)^2}{(n-1)} \right)^{-\frac{1}{2}} \tag{3.15}$$

SE and *a* may both be used as relative measures of accuracy when comparing models. Here, a distinction must be made between evaluating accuracy of the regression and evaluating prediction accuracy of the stress-strain model. The former requires the transformed regressand $\log_{10} y_i$ and $\log_{10} \hat{y}_i$ if transformed axes were used to estimate the best-fit linear regression. When comparing different models fitted to a single triaxial test, Equations 3.14 and 3.15 should be calculated using non-transformed axes. In this case the parameters are not representing accuracies of the regressions but, rather, quantify the average residual error of predicted stress-strain (here in terms of strength mobilisation and strain).

When considering multiple tests, a comparison of observed and predicted data points can be calculated by a ratio (factor) or subtraction (residual) of the two terms. Factor error is defined by Equation 3.16:

$$Factor\ Error = (\text{Observed or actual target value / Predicted target value}) \tag{3.16}$$

where the mean average factor error is termed "bias" (Ching and Phoon 2014b),

$$Bias = Mean(\text{Observed or actual target value / Predicted target value}) \tag{3.17}$$

Residual errors are calculated using Equation 3.18:

$$Residual\ Error = \text{(Predicted target value) - (Observed or actual target value)} \quad (3.18)$$

In this study, average factor errors and average residual errors are calculated by the sample mean (Ching and Phoon 2014b) or sample median (see Chapter 4).

3.4.6.2 Evaluating empirical correlations of model parameters

In Chapter 4, the statistical tools presented in section 3.4.6.1 are used to quantify modelling errors of the exponential model (Equation 3.7 and 3.11), power-law model (Equation 3.4 and 3.5) and logarithmic model (Equation 3.9 and 3.10). On the basis of least modelling error, one model is selected to investigate variability of the model parameters.

Variability of the model parameters for each test mode is investigated using single linear regression analysis to identify empirical correlations (or transformation models) with other experimental variables and by calculating errors (*SE*, factor error, and residual error) to describe scatter in the data. A description of parameter variability using predicted vs. measured plots and bandwidths of prediction error is valuable (Koutsoftas et al. 2017 and Kootahi and Mayne 2017), particularly when evaluating the variability of different parameters (or the uncertainty of different transformation models). All prediction errors quoted in this study refer to a region that encompasses 80% of the data points.

To investigate sensitivity of the parameters to different sources of parameter variability (Figure 3- 1), the method adopted in this thesis is to test the significance of single and multiple regressors in reducing error in the prediction of the parameters. The following hierarchy of regressors was used:

1. σ'_{v0} (present effective stress) using single linear regression analysis
2. *OCR* (applied overconsolidation ratio) using single linear regression analysis and multiple linear regression analysis with
    a. *OCR*, $\dot{\varepsilon_a}$ (strain rate)
    b. *OCR*, $\dot{\varepsilon_a}$, w_L (liquid limit)
    c. *OCR*, $\dot{\varepsilon_a}$, w_L, w_P (plastic limit)

By introducing more regressors to a model, higher R^2 values and larger errors (*SE*) will always result unless the higher order model is in fact a better fit (Montgomery and Runger 2003). Therefore, additional statistical tools were used to assess the value of multiple regressors (Equations 3.16, 3.17, 3.18, 3.19, and 3.20):

$$COV = \text{[Standard Deviation of (Observed target value/Predicted target value)]/Bias} \quad (3.18)$$

$$\cdot/ \textit{Factor Error} = \text{Range of Factor Error in a region that encompasses 80\% of the data points} \quad (3.19)$$

$$\pm \textit{Error (\%)} = \text{Range of Residual Error in a region that encompasses 80\% of the data points} \quad (3.20)$$

3.5 Conclusion

This chapter has described the motivations for investigating triaxial tests using database analysis techniques and a framework to assess parameter uncertainty and variability using empirical methods. Chapter 4 presents the results of detailed statistical analyses of the two soil test databases: RFG/TXCU-278 and BTK/TXCU-34.

4. Parameter variability of consolidated undrained triaxial tests using two databases

4.1 Introduction

In chapter 3, a method is described for the development of triaxial test databases that can be adopted by geotechnical practitioners. Two test databases – one of reconstituted soils (RFG/TXCU-278) and the other intact (BTK/TXCU-34) - have been analysed for the purpose of stress-strain parameter characterisation, using the statistical tools outlined in section 3.4.6. Although an additional test database of CIU and CKU tests on intact specimens (published by Mayne & Holtz 1985) is included for comparison, it was not possible to perform the full analytical procedure on the database since to the author's knowledge only the normalised strength (c_u/σ'_{v0}) data are publicly available.

This chapter presents the results of the stress-strain data analysis in the following order: (1) evaluation and selection of a suitable nonlinear model for triaxial stress-strain in the performance range of $0.2 \leq (\tau-\tau_0)/(c_u-\tau_0) \leq 0.8$; (2) analysis of stress history and testing variation effects by single and multiple linear regression; (3) analysis of shear-mode anisotropy by comparison of compression and extension tests.

4.2 Selecting a suitable nonlinear model for the parameter database

4.2.1 Research objectives:

(1) To develop a method of assessing the suitability of simple models for nonlinear stress-strain behaviour in the performance range of $0.2 \leq (\tau-\tau_0)/(c_u-\tau_0) \leq 0.8$.

(2) To quantify errors associated with the simple model approximation of the relationship between stress and strain.

4.2.2 Reasons for curve fitting

The number of stress-strain data points per triaxial test varies from 3 to 200. It is not possible to identify strains at selected strength mobilisation levels (e.g. at stress ratio = 0.5) without first fitting a mathematical function to the available data points. While many more sophisticated constitutive models

of material behaviour could be adopted for predicting stress-strain, these models require additional parameters (e.g. slope of void ratio and effective stress during normal consolidation) for their calibration. Most of the publications from which RFG/TXCU-278 was compiled provided "typical" consolidation curves instead of the full set of consolidation data measured in the CU triaxial tests. Limited information was also available for the tests compiling BTK/TXCU-34 as the CU consolidation parameters were excluded from the report by SERC (1989). Since the measurement uncertainty of such experimental parameters has received limited attention in the literature, it was not possible to evaluate the modelling uncertainty that would be introduced by including additional model parameters. The approach taken in this work was therefore to restrict the number of sources of uncertainty to the measurement of consolidation stresses, measurement of undrained shear stresses and strains, data digitisation, and model approximation.

4.2.3 Assessment of three alternative simple nonlinear models for stress-strain

The following three simple empirical curve fitting models have been tested:

Model 1 $S = \frac{\tau_{mob}-\tau_0}{c_u-\tau_0} = 1 - e^{-0.693\frac{\gamma}{\gamma_{50}}}$ $0.2 \leq S \leq 0.8$ Exponential Model

2 parameters required for CIU; 3 parameters required for CKU;

Model 2 $S = \frac{\tau_{mob}-\tau_0}{c_u-\tau_0} = 0.5\left(\frac{\gamma}{\gamma_{50}}\right)^b$ $0.2 \leq S \leq 0.8$ Power Law Model

3 parameters required for CIU; 4 parameters required for CKU;

Model 3 $S = \frac{\tau_{mob}-\tau_0}{c_u-\tau_0} = \beta \cdot \log\left(\frac{\gamma_{50}}{\gamma}\right) + 0.5$ $0.2 \leq S \leq 0.8$ Logarithmic Model

3 parameters required for CIU; 4 parameters required for CKU;

Models 1, 2, and 3 require c_u and τ_0 to be available from every test in the database. Since $\tau_0 = 0$ for isotropic stresses, the number of model parameters reduces by 1 for CIU triaxial tests.

Before any observations can be made from model parameters about strain anisotropy and the influence of testing variation and stress history, the curve fitting procedure needs to be evaluated. Empirical curve fitting with a poor model will introduce modelling uncertainty into the subsequent

stress-strain model parameters. While it is possible to quantify modelling uncertainty following the method described in this chapter, which makes use of the residuals from the fitted stress-strain models, a serious error in fit between a model and the test data should be avoided.

Figures 4-1, 4-2, 4-3, and 4-4 show the residuals (Equation 3.17) of each triaxial test on reconstituted soil plotted by model type (1, 2 or 3) and test mode (CIUC, CKUC, CIUE, or CKUE). In each sub-figure, between 864 and 2069 data points are plotted including every digitised data point of stress-strain (i.e. ($\tau-\tau_0$) and $\gamma=1.5\varepsilon_a$) between $0.2\leq S\leq 0.8$, where S = stress ratio (Equation 3.1). Residuals of *S*, plotted against the measured value, show a distinct pattern for each model (BTK/TXCU-34 shows similar patterns: see Appendix 4-1). Model 1, the exponential law model recommended by Klar and Klein (2014), consistently underpredicts *S* up to a value of about 0.7 and appears to be particularly ill-suited to characterising the curvature of CKUE tests. Compared with Model 1, Models 2 and 3 generate smaller residuals in all test modes. A key conclusion that can be drawn from these plots is that the shape of the measured stress-strain curves deviates substantially from the exponential rate function assumed in Model 1 and that including an additional non-linearity (or shape) parameter in Models 2 and 3 reduces the modelling error. However, all three models are biased and will result in biased predictions of *S*.

Bias is indicated by a non-zero mean error. Ching and Phoon (2014b) define bias as the arithmetic mean average ratio of a measured (or "target") value and a predicted value. Bias factors of *S* for all measurements of RFG/TXCU-278 between 0.2 and 0.8, by test mode, shown in Table 4-1 provide quantitative evidence that Model 1 is unsuitable for the stress-strain characterisation of CU triaxial tests. However, in this case, bias cannot facilitate the decision to choose between Model 2 and Model 3.

The bias of Model 2 and 3 is minor when the average is applied to all data between $0.2\leq S\leq 0.8$ (Table 4-1). But Figures 4-1 to 4-4 show that model error is dependent on stress ratio. An alternative measure of modelling approximation (termed "Mean Residual Error") is shown in Figures 4-1 to 4-4 and

Table 4- 1. Bias factor of *S* for data in RFG/TXCU-278 ($0.2\leq S\leq 0.8$) by model and by test mode

Test mode:	CIUC n=2069	CKUC n=1049	CIUE n=1217	CKUE n=864
Model 1 bias factor	0.876	0.928	0.828	0.691
Model 2 bias factor	1.001	1.001	1.001	1.001
Model 3 bias factor	0.998	0.998	0.999	0.998

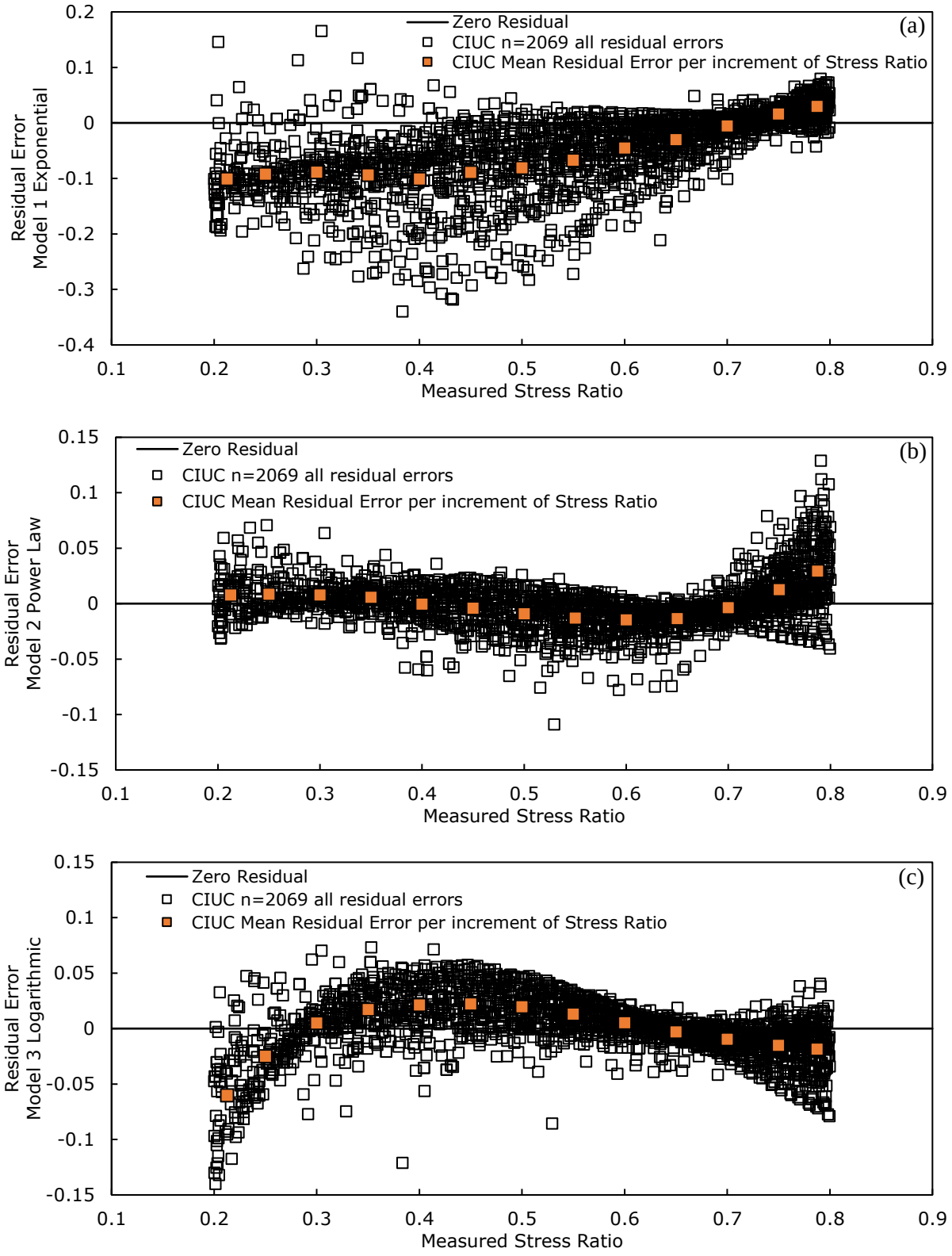

Figure 4- 1. Residuals of observed stress ratio for CIUC tests in RFG/TXCU-278 (114 tests) by curve-fitting model: **(a)** Model 1 **(b)** Model 2 **(c)** Model 3.

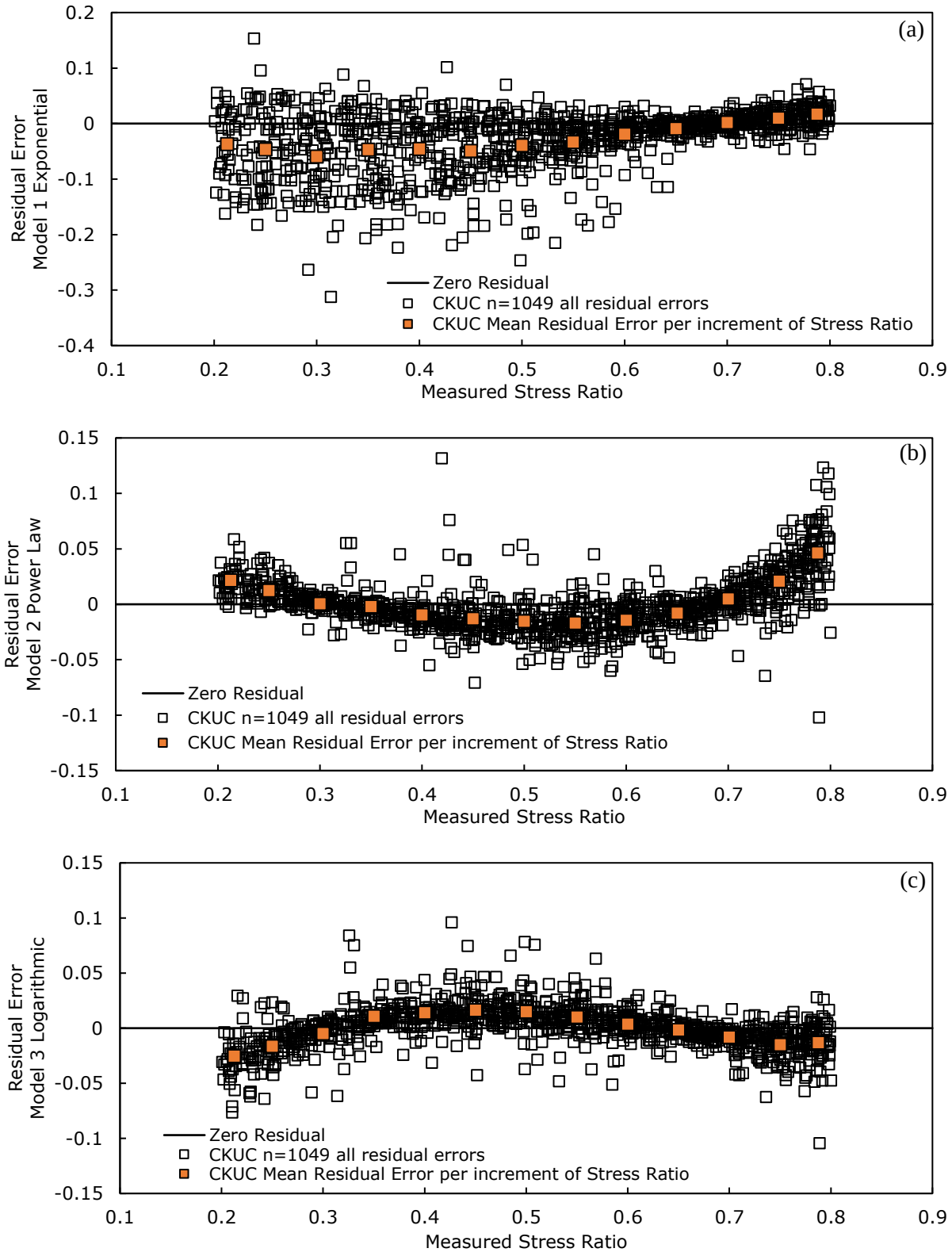

Figure 4- 2. Residuals of observed stress ratio for CKUC tests in RFG/TXCU-278 (34 tests) by curve-fitting model: **(a)** Model 1 **(b)** Model 2 **(c)** Model 3.

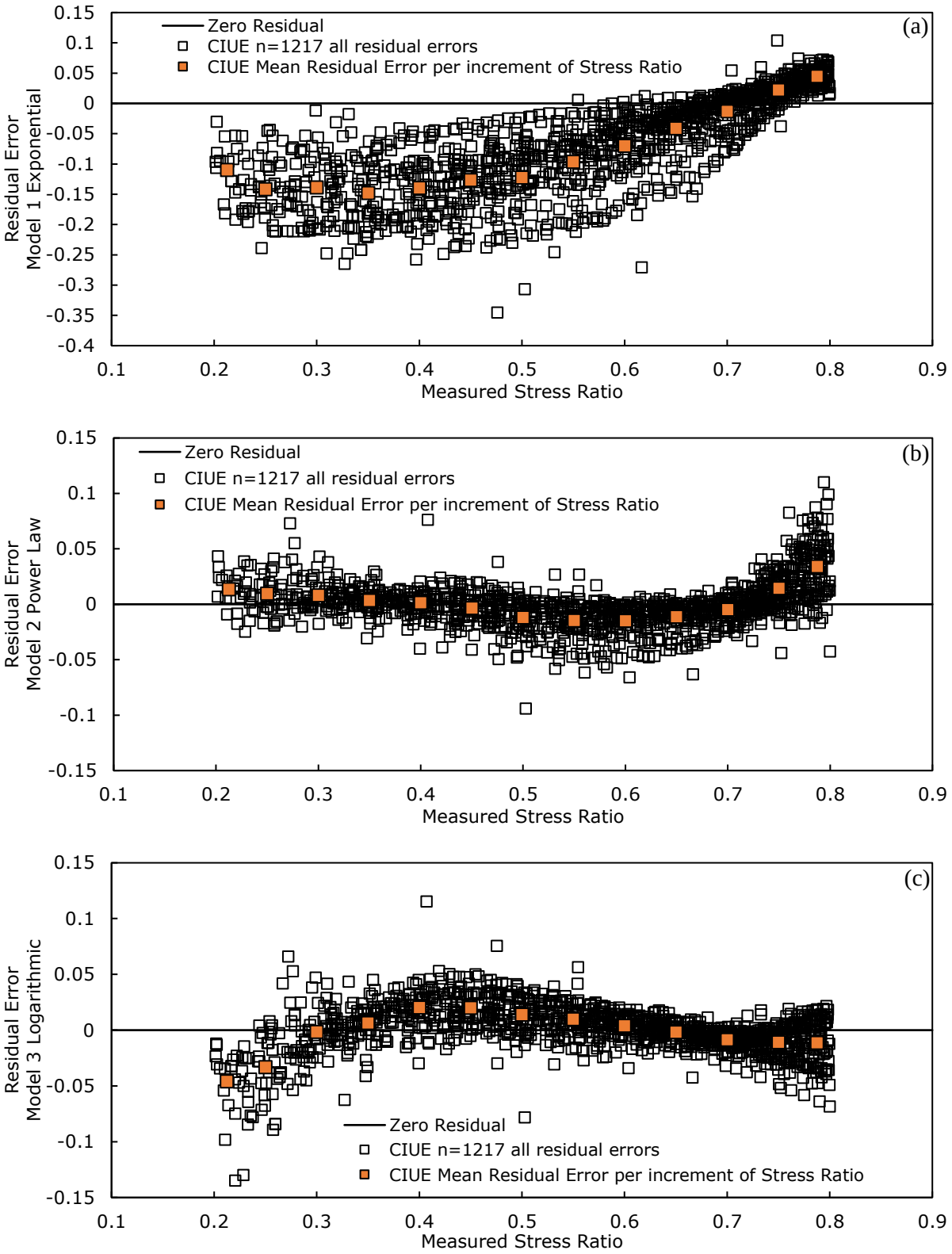

Figure 4- 3. Residuals of observed stress ratio for CIUE tests in RFG/TXCU-278 (55 tests) by curve-fitting model: **(a)** Model 1 **(b)** Model 2 **(c)** Model 3.

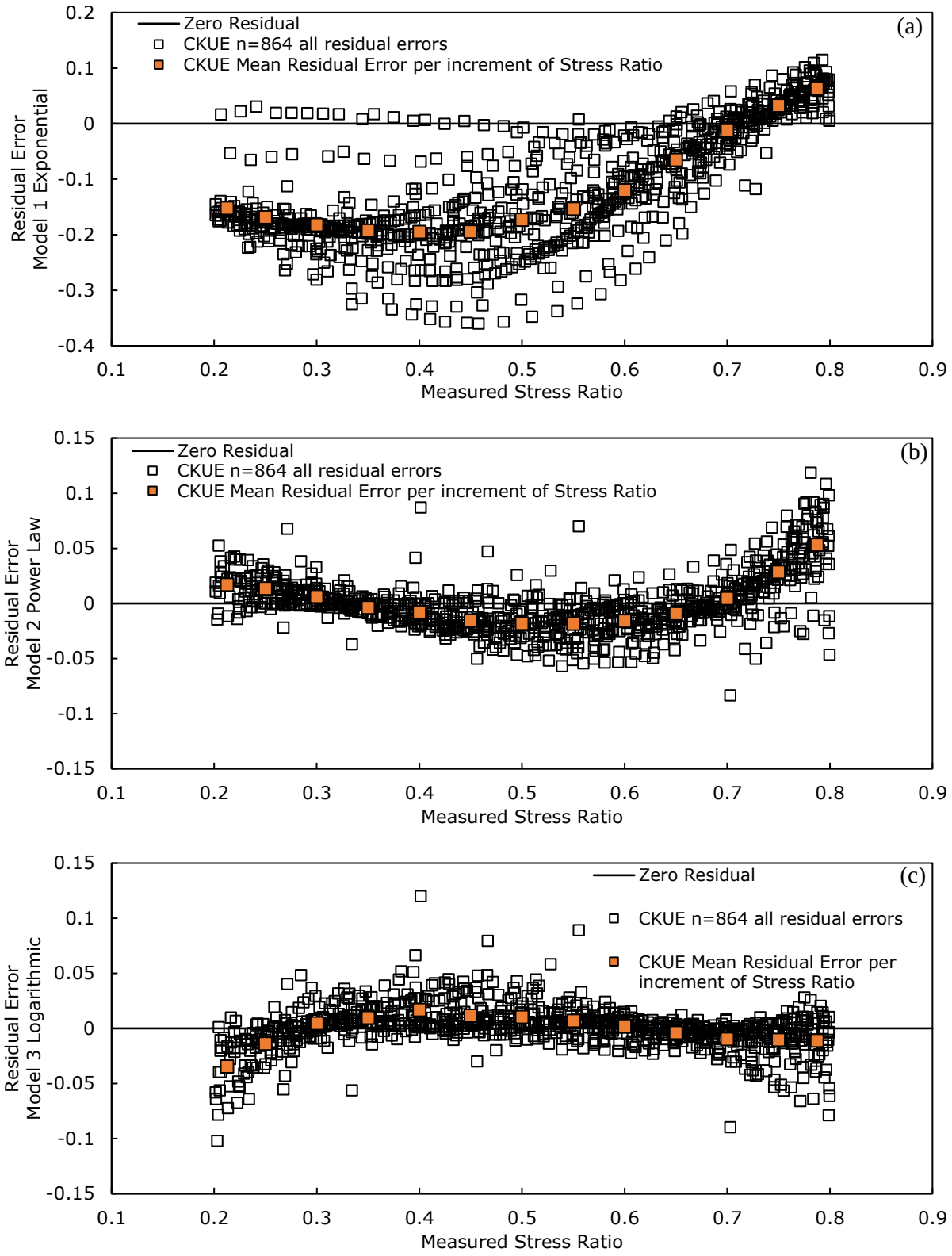

Figure 4- 4. Residuals of observed stress ratio for CKUE tests in RFG/TXCU-278 (34 tests) by curve-fitting model: **(a)** Model 1 **(b)** Model 2 **(c)** Model 3.

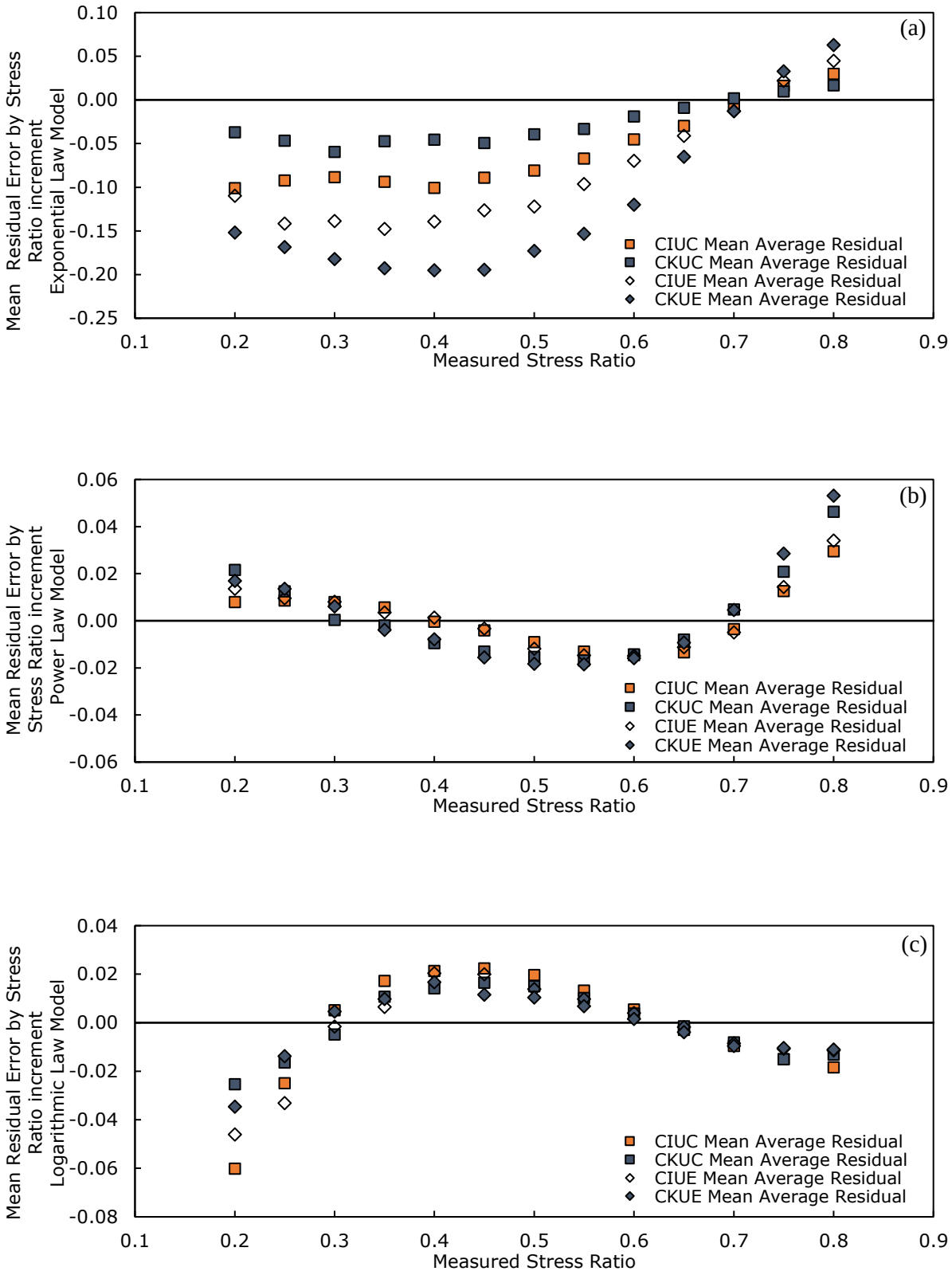

Figure 4- 5. Comparison of model bias introduced by different curve-fitting models using Mean Average. The test data of RFG/TXCU-278 are grouped by test mode and by increments of stress ratio: 0.2-0.225, 0.225-0.275, 0.275-0.325, 0.325-0.375, 0.375-0.425, 0.425-0.475, 0.475-0.525, 0.525-0.575, 0.575-0.625, 0.625-0.675, 0.675-0.725, 0.725-0.775, 0.775-0.8. **(a)** Model 1 **(b)** Model 2 **(c)** Model 3.

summarised for each model in Figure 4-5. The arithmetic mean average of the residuals has been calculated including all residual errors for the test mode database (i.e. CIUC, CIUE, CKUC, or CKUE) grouped by increments of stress ratio. Figure 4-5 shows that Model 1 would include a significant error when used to predict stress ratio measurements below 0.7. Compared with Model 1, Models 2 and 3 produce smaller residuals on average and the mean residuals of each test mode are closer in value, which implies that the characterisation of stress-strain using Model 2 and Model 3 is less sensitive to test mode. However, there are two problems with using the mean to quantify the effect of model error by increment of stress ratio. The first is that there is no information regarding the spread of error; second, the distribution of the residuals may be skewed so that extreme values strongly influence the mean.

To identify and quantify the model error per triaxial test, three descriptive statistics (*SE*, *a*, and R^2) were calculated for each regression. Standard error (*SE*) indicates the average residual error about the regression line for the triaxial test. Proposed by Puzrin and Burland (1996) for the comparison of stress-strain models, *a* is the inverse of *SE* and R^2 identifies the percentage of variance of the independent variable, *S*, that can be explained by the model. The results, presented in Table 4-2, are directly compared between Model 2 (the Power Law model) and Model 3 (Logarithmic) or between Model 2 and Model 1 (Exponential). Model 2 significantly outperformed Model 1 in 90% of all triaxial tests, achieving 73% decrease in *SE* and 82% increase in R^2 on average (*SE* is more informative in this type of evaluation than *a*). However, Model 2 fitted only 44% of the tests on reconstituted soils more accurately than Model 3, increasing to 59% for intact soils - on average improving *SE* and R^2 respectively by 50% and 2%.

a is more useful for comparing different models per triaxial test (Puzrin and Burland 1996). The histograms in Figures 4-6 and 4-7 show the frequency of tests where $a_{\text{Model 3}}$ exceeds $a_{\text{Model 2}}$ and vice versa. Figure 4-6 suggests that Model 3 provides a better fit for test data of reconstituted samples with lower *OCR*. However, the reverse may be true for intact samples, which could suggest that a different shape in the measured stress-strain curve may apply to reconstituted and intact specimen tests of similar *OCR*. It remains unclear at this stage whether Model 3 or Model 2 should be selected for the variability characterisation of stress-strain behaviour, but Model 1 is certainly outperformed by both models and is given no further consideration.

Table 4- 2. Assessment of curve-fitting models by directly comparing the statistics per triaxial test.

	Statistical parameter:	*S.E.*	*a*	R^2	*S.E.*	*a*	R^2
RFG/ TXCU-278	Comparison of alternative model versus Model 2 (Power Law), on average, by statistical parameter	Model 3 (Logarithmic) 153 / 271 tests (56%)			Model 1 (Exponential) 27 / 271 tests (10%)		
		0.49	3.72	1.02	0.60	1.95	1.02
	Comparison of Model 2 (Power Law) versus alternative model, on average, by statistical parameter	Model 3 (Logarithmic) 118 / 271 tests (44%) outperformed by Model 2 (Power Law)			Model 1 (Exponential) 244 / 271 tests (90%) outperformed by Model 2 (Power Law)		
		0.51	2.79	1.02	0.27	7.23	1.82
BTK/ TXCU-34	Comparison of alternative model versus Model 2 (Power Law), on average, by statistical parameter	Model 3 (Logarithmic) 14 / 34 tests (41%)			Model 1 (Exponential) 3 / 34 tests (9%)		
		0.50	2.97	1.02	0.59	1.90	1.02
	Comparison of Model 2 (Power Law) versus alternative model, on average, by statistical parameter	Model 3 (Logarithmic) 20 / 34 tests (59%) outperformed by Model 2 (Power Law)			Model 1 (Exponential) 31 / 34 tests (91%) outperformed by Model 2 (Power Law)		
		0.50	2.91	1.02	0.28	5.66	1.66

Since it is not apparent on a test by test basis which of Models 2 and 3 is more suitable (see Table 4-2), alternative measures of model error are shown in Figures 4-8, 4-9, 4-10, and 4-11. Using the same residual database shown in Figures 4-1 to 4-4 and subdividing the stress ratio measurements into increments as for Figure 4-5, percentiles of the residuals were calculated including the 10^{th}, 90^{th}, and 50^{th} (median). Using these percentiles, the middle 80% of residual data per increment of stress ratio is displayed in Figures 4-8, 4-9, 4-10, and 4-11. The distribution of error shows that Model 2 tends to underpredict stress ratio between 0.3 and 0.7 and to overpredict stress ratio at the extreme ends of the performance range. The reverse tendency is apparent for Model 3, and since the Predicted=Observed line lies between the two medians in almost every case, this suggests that on average the database measurements of triaxial stress-strain sit between the two model approximations. Measurements of shear stress and strain in triaxial extension tests may have higher variability than compression tests as the distribution of error is more skewed, particularly for CKUE tests. Skew could also be related to smaller numbers of CIUE and CKUE tests which are underrepresented in RFG/TXCU-278 compared to compression tests. Within the modelled performance range, the least median bias and the narrowest error bounds occur between S = 0.275-0.375 and 0.625-0.725 for every test mode regardless of the model.

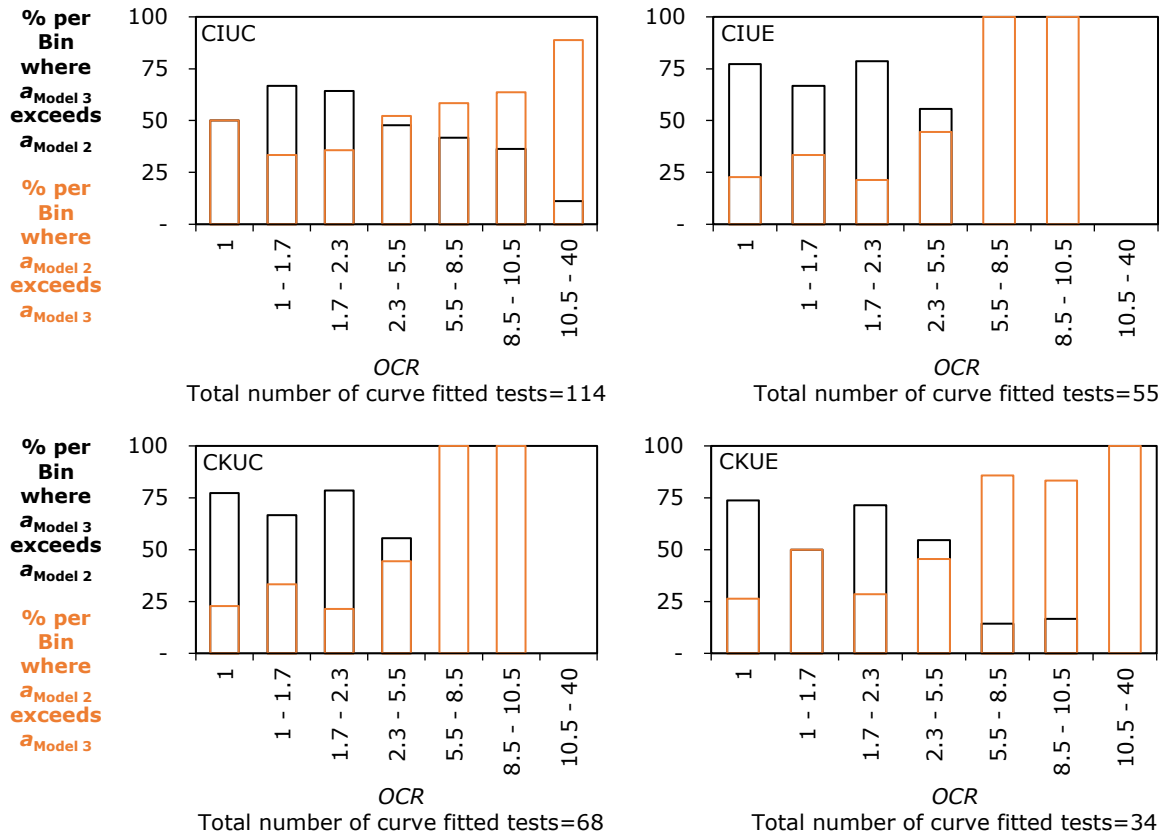

Figure 4- 6. Comparison of Model 2 and Model 3 per triaxial test using data in RFG/TXCU-278. Histogram bins are categorised by *OCR* range applicable to the reconstituted soil test. Colours indicate where Model 3 (Logarithmic law) outperforms Model 2 (Power law) and vice versa.

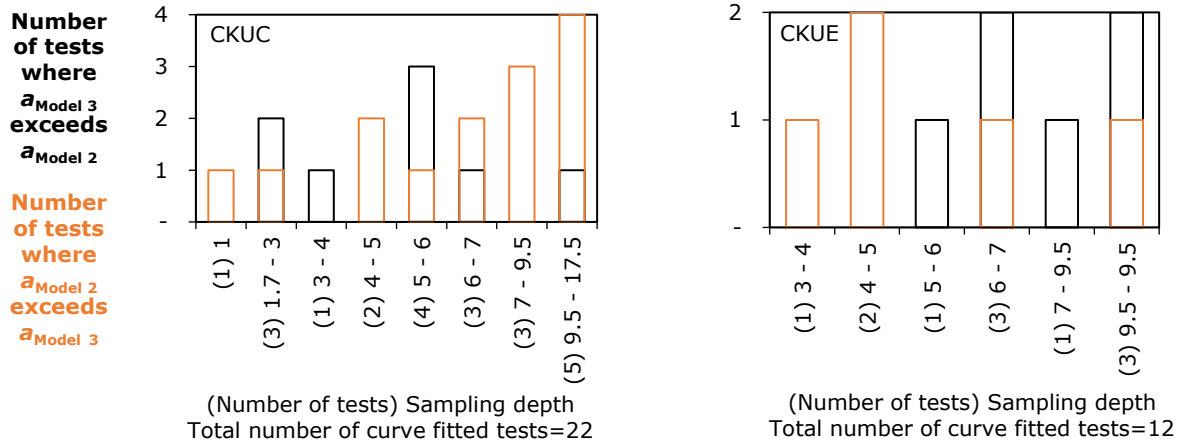

Figure 4- 7. Comparison of Model 2 and Model 3 per triaxial test using data in BTK/TXCU-34. Histogram bins are categorised by *Sampling Depth* range applicable to the Intact triaxial test from the Bothkennar Test Site (SERC 1989). Colours indicate where Model 3 (Logarithmic law) outperforms Model 2 (Power law) and vice versa.

Three stress ratios (0.3, 0.5, and 0.7) were chosen to investigate the effect of model approximation on stress ratio S (Tables 4-3 and 4-4) and strain γ (Figure 4-12 and 4-13). At S = 0.3 and 0.5, the range in error of the prediction of S made using Model 2 is either equal to or less than the error made by Model 3. Model 2 overpredicts measurements of S between 0.675 and 0.725 and with more error than Model 3 which tends to underpredict S with the same test data. Predictions of S in CKUC and CKUE made using Model 2 appear to be significantly biased (underpredicted) at S=0.5 and therefore in most of these tests a biased modelling error in the "pivot strain" (Vardanega and Bolton 2011) must occur during the curve fitting procedure.

In fact, the reference strain at S=0.5 ($\gamma_{50\ \mathrm{Power}}$) is generally overestimated by Model 2 but the effect is not consistent for all reconstituted soil tests. An approximate measure of the error in modelled strain is shown in Figure 4-12 using normalised shear strain. Measurements of γ were normalised by the reference strains predicted by Model 2 and Model 3 at stress ratios of 0.3, 0.5 or 0.7 with the reference strains named γ_{30}, γ_{50} and γ_{70} respectively. When the normalised strain is plotted against measured stress ratio (Figure 4-12), deviation from the target strain value can be observed by a deviation from unity of normalised strain at the reference stress ratio. As an approximation the distribution of normalised strains has been characterised within 0.01 of the reference stress ratio (the bounds of ±0.005 are indicated by red lines in Figure 4-12) by grouping data from all 4 test modes and calculating the percentiles (Figure 4-13). The distributed data in Figure 4-13 shows that there is a wide error range in strain within 0.01 of the reference stress ratio. At all three stress ratios, the normalised strains include values both greater and less than one. On average the power law model (Model 2) produces less biased strains than the logarithmic model (Model 3) and the distributed errors are generally skewed to a lesser extent. Normalised strains predicted by Model 2 are also more precise (i.e. more closely distributed) within the 10^{th} and 90^{th} percentiles than those predicted by Model 3.

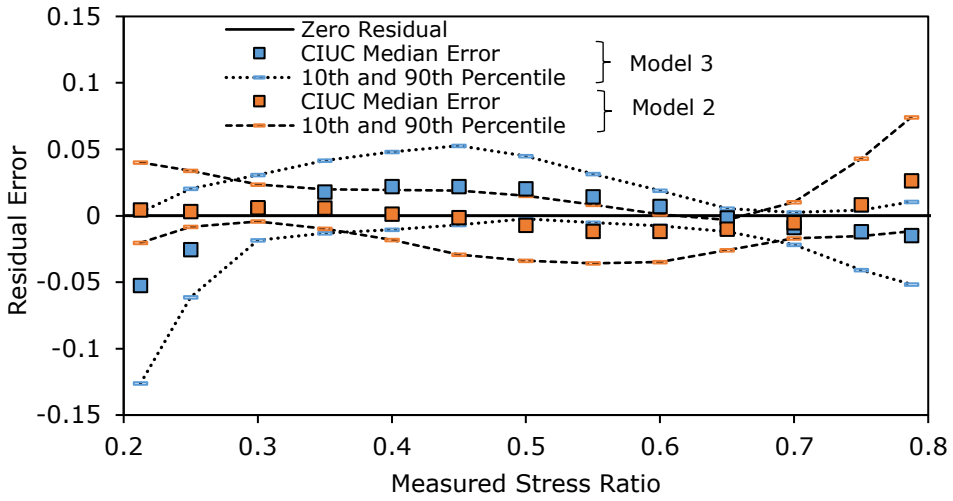

Figure 4- 8. Comparison of model error introduced by Model 2 and Model 3 using 10th, 50th (Median), and 90th Percentiles. The test data of RFG/TXCU-278 are grouped by test mode (CIUC) and by increments of stress ratio (see Figure 4- 5).

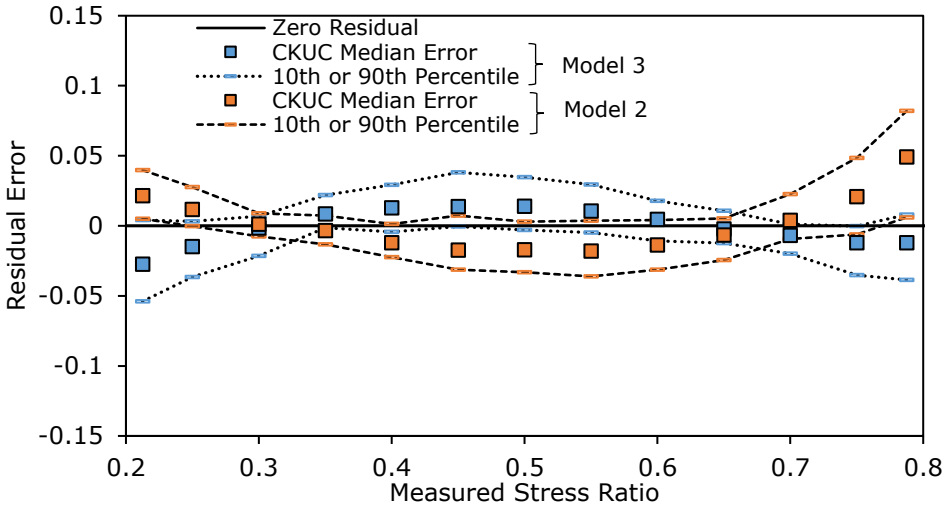

Figure 4- 9. Comparison of model error introduced by Model 2 and Model 3 using 10th, 50th (Median), and 90th Percentiles. The test data of RFG/TXCU-278 are grouped by test mode (CKUC) and by increments of stress ratio (see Figure 4- 5).

Table 4- 3. 10th, 50th (Median), and 90th Percentiles of all residuals in RFG/TXCU-278 from Models 2 and 3 between S=0.275 to 0.325, S=0.475 to 0.525, and S=0.675 to 0.725 for CIUC and CKUC test data.

	Stress Ratio:	S=0.275 to 0.325		S=0.475 to 0.525		S=0.675 to 0.725	
Test Mode	Percentile	Model 3	Model 2	Model 3	Model 2	Model 3	Model 2
CIUC	0.90	+0.031	+0.024	+0.045	+0.015	+0.003	+0.010
	0.50	+0.006	+0.006	+0.020	-0.007	-0.009	-0.005
	0.10	-0.019	-0.004	-0.002	-0.034	-0.022	-0.017
	Range of Error	0.050	0.028	0.047	0.049	0.025	0.027
CKUC	0.90	+0.007	+0.009	+0.035	+0.003	+0.001	+0.023
	0.50	-0.002	+0.001	+0.014	-0.017	-0.007	+0.004
	0.10	-0.020	-0.008	-0.003	-0.033	-0.020	-0.009
	Range of Error	0.027	0.017	0.038	0.036	0.021	0.032

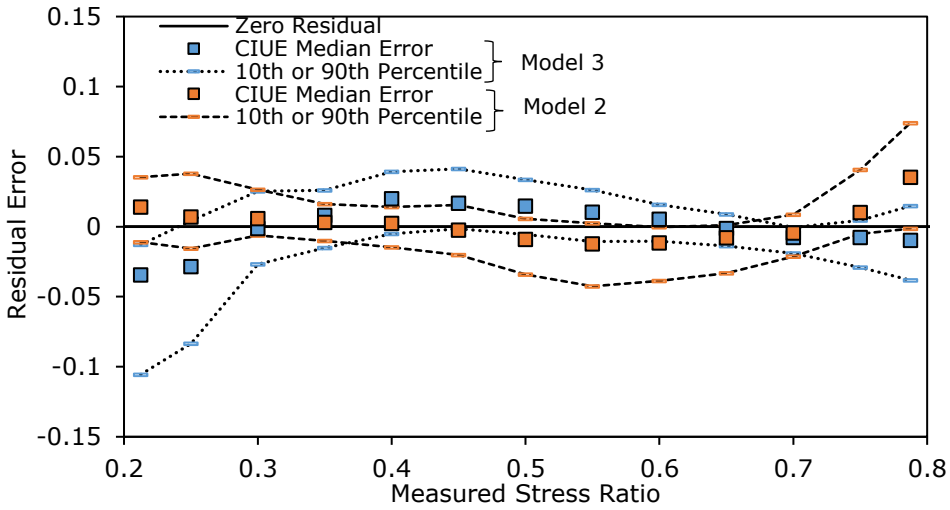

Figure 4- 10. Comparison of model error introduced by Model 2 and Model 3 using 10th, 50th (Median), and 90th Percentiles. The test data of RFG/TXCU-278 are grouped by test mode (CIUE) and by increments of stress ratio (see Figure 4- 5).

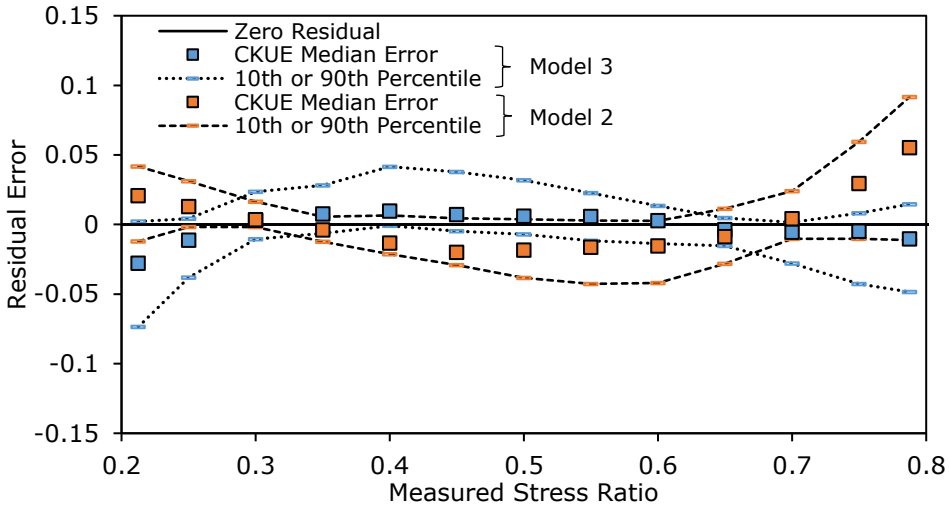

Figure 4- 11. Comparison of model error introduced by Model 2 and Model 3 using 10th, 50th (Median), and 90th Percentiles. The test data of RFG/TXCU-278 are grouped by test mode (CKUE) and by increments of stress ratio (see Figure 4- 5).

Table 4- 4. 10th, 50th (Median), and 90th Percentiles of all residuals in RFG/TXCU-278 from Models 2 and 3 between S=0.275 to 0.325, S=0.475 to 0.525, and S=0.675 to 0.725 for CIUE and CKUE test data.

	Stress Ratio:	S=0.275 to 0.325		S=0.475 to 0.525		S=0.675 to 0.725	
Test Mode	Percentile	Model 3	Model 2	Model 3	Model 2	Model 3	Model 2
CIUE	0.90	+0.025	+0.026	+0.034	+0.006	-0.001	+0.009
	0.50	-0.001	+0.006	+0.015	-0.009	-0.008	-0.004
	0.10	-0.027	-0.006	-0.006	-0.034	-0.019	-0.021
	Range of Error	0.052	0.032	0.040	0.040	0.018	0.030
CKUE	0.90	+0.024	+0.016	+0.032	+0.004	+0.002	+0.024
	0.50	+0.003	+0.004	+0.006	-0.018	-0.005	+0.004
	0.10	-0.010	-0.002	-0.007	-0.038	-0.028	-0.010
	Range of Error	0.034	0.018	0.039	0.042	0.030	0.034

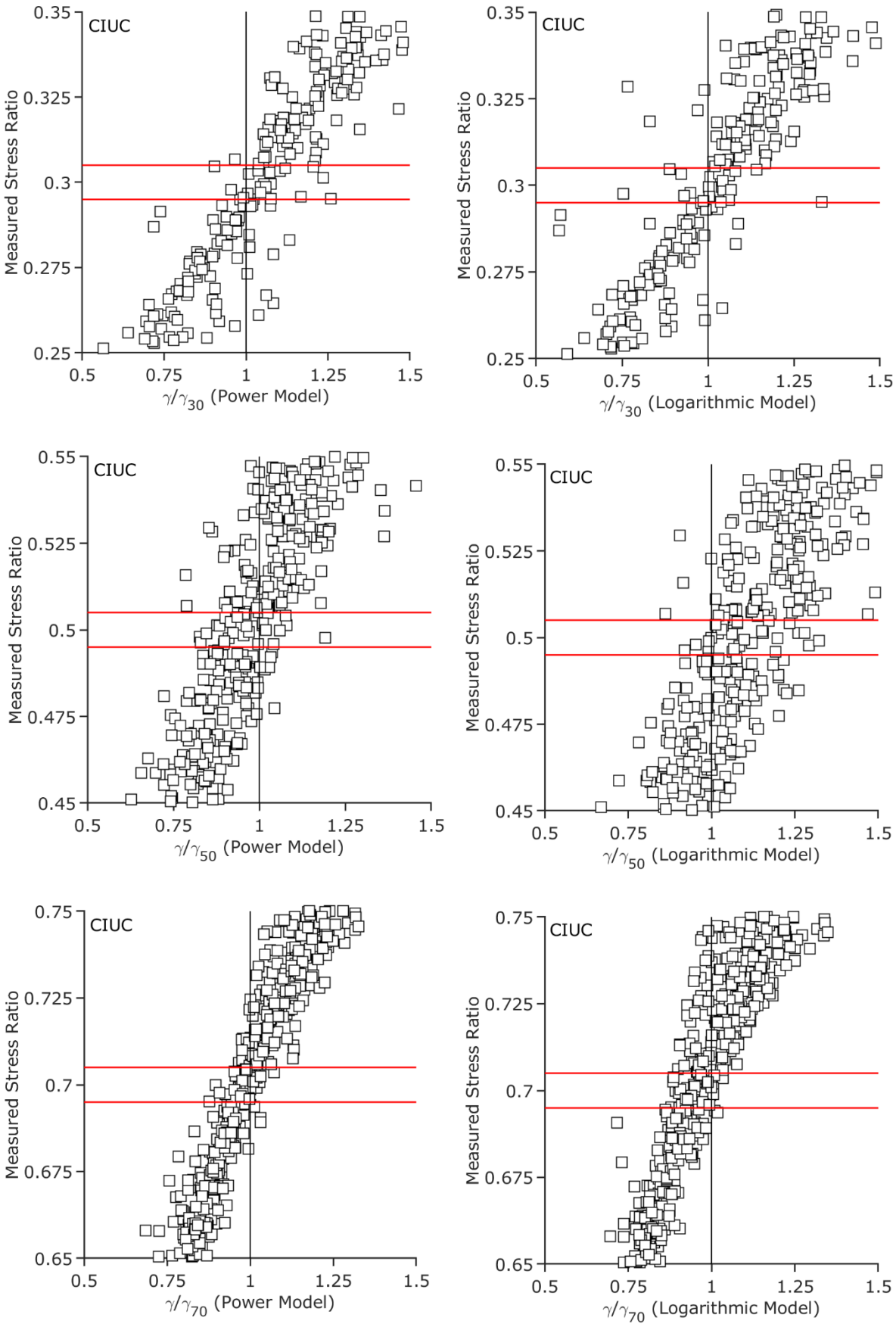

Figure 4- 12. Normalised shear strains within 0.01 of the reference stress ratio, *S*, indicated by red lines (CIUC test mode data only from RFG/TXCU-278)

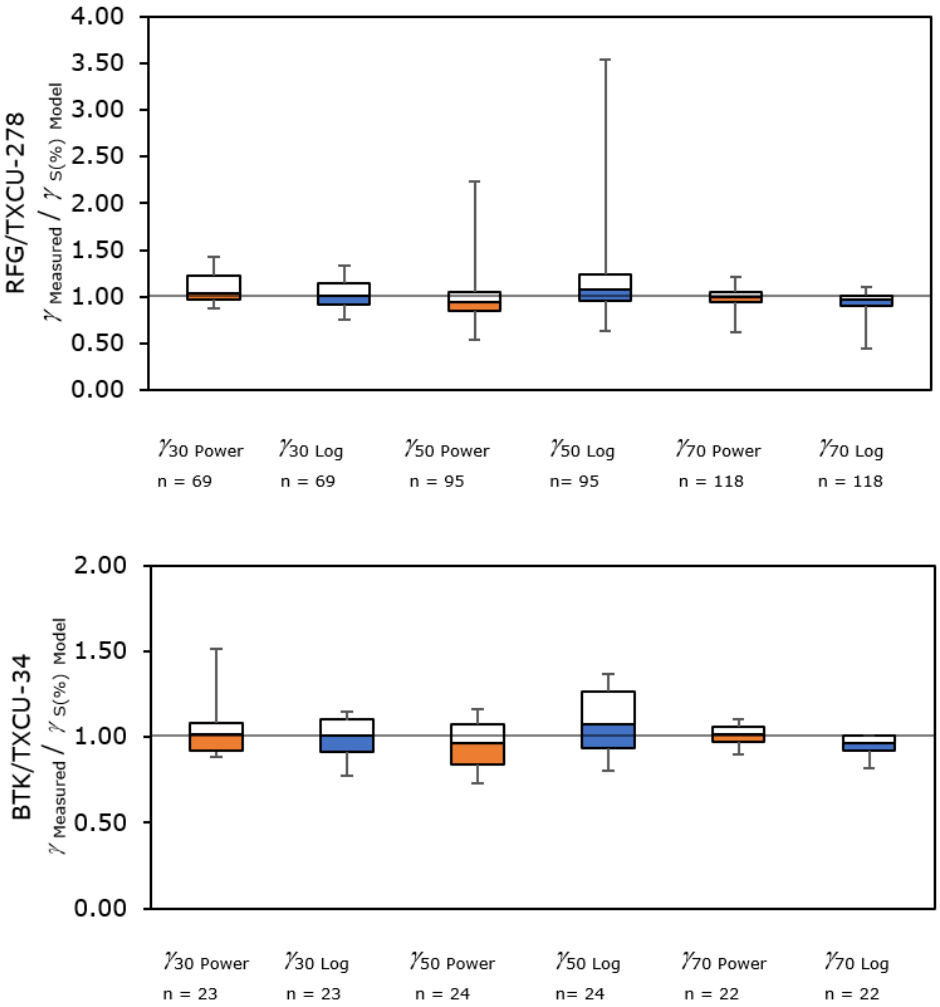

Figure 4- 13. Distribution of normalised shear strains within 0.01 of the reference stress ratio, *S*, and including data from all 4 test modes in databases RFG/TXCU-278 and BTK/TXCU-34 summarised by minima, maxima, 10th, 50th and 90th percentiles

4.2.4 Selected stress-strain model

Although none of the models perfectly replicate the stresses and strains measured in the tests compiled in the databases, Model 2 (Power Law) is most suited to characterising nonlinear stress-strain behaviour between $0.2 \leq S \leq 0.8$. Model 1 is inflexible in shape which means that the behaviour is matched only with the pivot strain (at $S=0.5$) whereas Models 2 and 3 have additional non-linearity parameters (b and β respectively) to capture the variation in stiffness degradation. Strength mobilisation can be represented up to peak stresses ($S=1$) by Model 1 and it is therefore in principle more consistent with measured behaviour at the point of undrained failure than Model 2 or Model 3. While Model 1 has a smaller standard error than Model 2 in one of every ten triaxial tests, there is a clear bias towards underpredicting S at values below 0.7 which shows that the exponential rate assumed in Model 1 differs

significantly from the measured rates of change in stress and strain observed in reconstituted and intact soil tests. The use of Model 1 for predicting triaxial stress-strain cannot therefore be justified from the data in this study.

Shear stresses and strains within $0.2 \leq S \leq 0.8$ are more accurately represented by power or logarithmic functions. Residual error analysis of the power and logarithmic model predictions shows that most measurements of stress ratio have values between the two approximations of behaviour. However, it is not possible to choose between the two models from the calculated bias of all predicted stress-strain data (see Table 4-1). Moreover, when comparing the regression characteristics for each test it appears that Model 2 and Model 3 perform equally well in minimising the standard error of S (by about 50%) and increasing R^2 (by 2%). The decision to choose between the two models is then determined by the distribution of error associated with model bias i.e. an approach should be taken which recognises and quantifies the deficiencies of the model at different mobilisation levels. In this study the errors of predicted strain and stress ratio made by the different models have been quantified using percentiles to evaluate the distributed error within increments of stress ratio. Given the evidence of smaller errors in modelled strain using this approach, Model 2 outperforms Model 3 and the Power Law is therefore selected for parameter variability characterisation.

4.3 Analysis of parameter variability with test mode, stress history, composition and test procedure

4.3.1 Research objective:

(1) To characterise the variability of nonlinear stress-strain behaviour of soil tested in undrained shear using normalised strength (c_u/σ'_{v0}) and the deformation parameters of the selected Power Law model ($\gamma_{50\ \mathrm{Power}}$ and b) by:

   a. investigating the significance of test mode, stress history, composition and variations in triaxial testing methods to the variability characterisation of c_u/σ'_{v0}, $\gamma_{50\ \mathrm{Power}}$ and b

   b. identifying important explanatory variables for the prediction of c_u/σ'_{v0}, $\gamma_{50\ \mathrm{Power}}$ and b

   c. assessing sources of uncertainty in the observed values of c_u/σ'_{v0}, $\gamma_{50\ \mathrm{Power}}$ and b

By extending the application of the MSF framework to different triaxial stress paths, the key contribution of this work is in demonstrating the likely variation in stress-strain response with consolidation type (CIU or CKU) and shear mode (triaxial compression or extension) and uncertainties associated with test procedures.

4.3.2 Classification of database samples

Classification of the 22 reconstituted soils indicate a wide range of plasticity (Figure 4-14), with 73% of materials classified as inorganic and medium-high plasticity. Materials classified outside of this range include the processed kaolin clays, which plot in a cluster close to the A-line, and a low plasticity glacial till investigated by Gens (1982). With the exception of the kaolin materials, all reconstituted soils were sampled from natural deposits.

For comparison with the reconstituted materials, the results of index tests reported by SERC (1989) are also plotted in Figure 4- 14. An index test measurement was provided for every triaxial test specimen in the report. Bothkennar clay samples have a higher plasticity than most of the materials in the reconstituted database. Since the plastic limit range is narrow ($0.29 \leq w_P \leq 0.33$), the range in I_p is caused mainly by the large variation of liquid limit. Higher liquid limits and plastic limits are indicative of higher clay content (Dumbleton and West 1966). The index tests from Bothkennar plot approximately in a straight line that would be expected for soils of similar deposition (Muir Wood 1990). The scatter may be assumed to reflect the natural variability of the deposit at various sampling depths between 1.6m and 17.5m. In section 4.3.13 the origins of fluctuations in index test parameters are discussed and the influence of plasticity and natural variations of the clay deposit at Bothkennar on model parameter variability is explored in further detail.

4.3.3 Categorisation of test data by test mode

The database of 278 consolidated undrained shear (CU) triaxial tests on reconstituted samples and the database of 34 CU triaxial tests on intact Bothkennar samples are presented in sub-databases of sample consolidation type (isotropic or K_0) and shear mode (triaxial compression or triaxial extension) which are identified by test mode: CIUC, CIUE, CKUC, or CKUE. In addition to CKUC and CKUE test modes, test data in the intact Bothkennar database are categorised by “Recompression” or “SHANSEP”

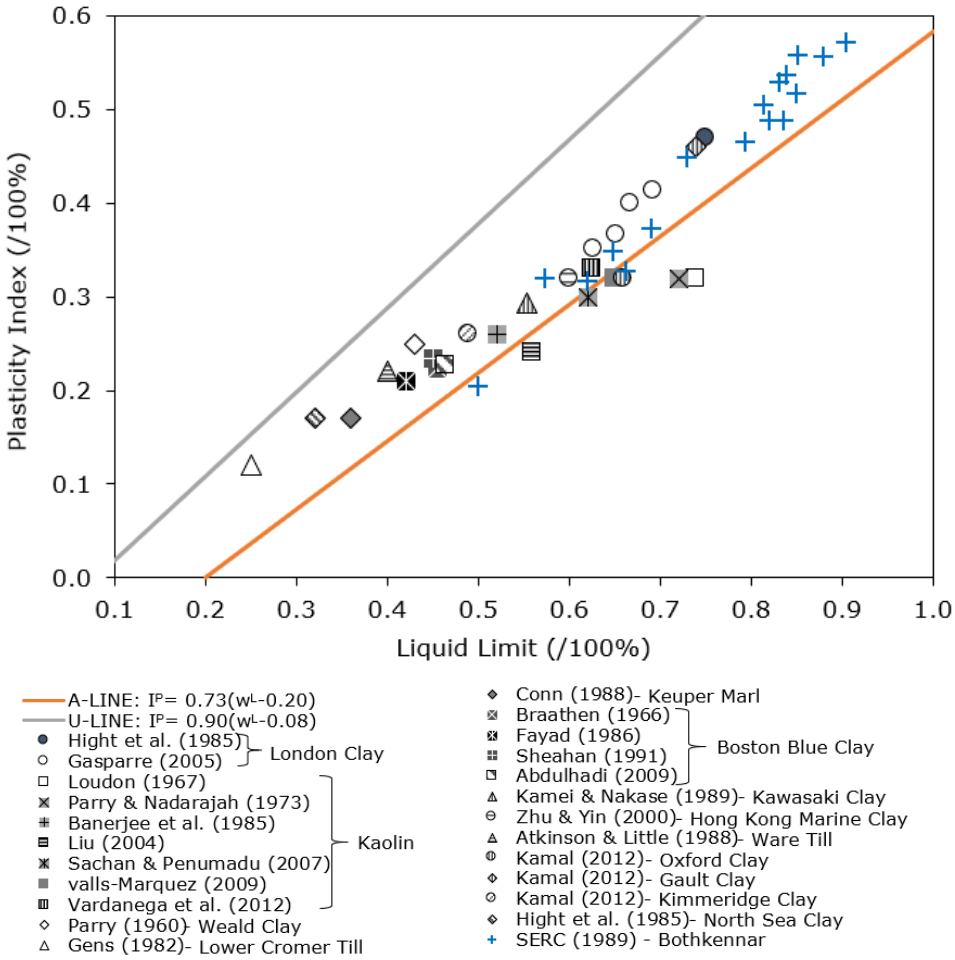

Figure 4- 14. Classification of materials in RFG/TXCU-278 and BTK/TXCU-34

tests owing to the different stress histories prior to shear. Normalised undrained shear strength data from a database of intact triaxial samples, obtained from Mayne & Holtz (1985), are also presented for comparison. With limited information available about the testing procedures adopted during consolidation, the database of c_u/σ'_{v0} measurements published by Mayne & Holtz (1985) are simply categorised as CIUC, CIUE, CKUC, or CKUE and no attempt was made to correlate model parameters with stress history.

Experimental details of all triaxial test data included in RFG/TXCU-278 and BTK/TXCU-34 are summarised in section 3.9. All test data have been categorised and analysed by test mode for the purpose of assessing differences in parameters between test modes. A detailed description of the important differences between test modes and the reasons for categorising test data according to test mode can be found in section 3.6.

4.3.4 Range of stress-strain behaviour by test mode

Figure 4- 15 shows all the test data in the performance range $0.2 \leq S \leq 0.8$. This demonstrates the variability of strains within each test mode that exists in the database. Out of the four test modes, $\gamma_{\text{CKUE Reconstituted}}$ has the largest range of over 3 log cycles. $\gamma_{\text{CIUC Reconstituted}}$ has the second largest range of approximately 2 ½ log cycles and shows similar magnitudes to the CIU database published by Vardanega and Bolton (2011). Comparatively $\gamma_{\text{CIUE Reconstituted}}$ is less variable which is likely to be a consequence of fewer tests – approximately half the number of tests available in the CIUC database. Magnitudes of CIUE strains are within the same region as CIUC measurements but there is a larger discrepancy between CKU shear modes with strains measured in extension generally exceeding those measured in compression. Reconstituted and intact tests of the same test mode show a similar range and magnitude of strains although reconstituted CKUE tests are considerably more variable.

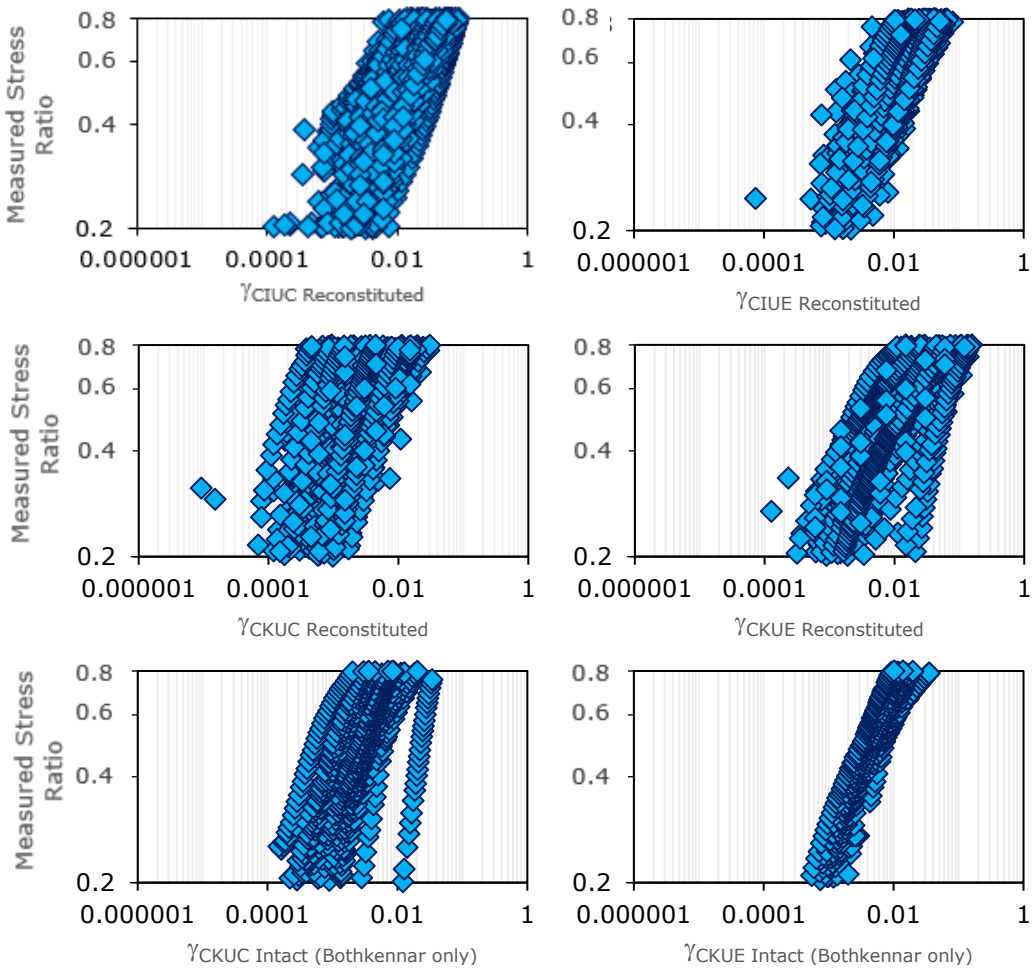

Figure 4- 15. Stress ratio (S) measurements plotted against shear strain measurements $\gamma=1.5\varepsilon_{axial}$ for 305 triaxial tests, 23 reconstituted fine-grained soils, 1 intact soil (Bothkennar clay)

In Figures 4- 16 and 4- 17 the same data are plotted again to demonstrate the effect of using the Power Law (Model 2) characterisation. When viewing the stress ratio and shear strain data plotted on linear axes, the variety of nonlinear behaviour is obvious but the range in non-linearity is shown more clearly by normalised strain ($\gamma/\gamma_{50\ Power}$). Figures 4- 16 and 4- 17 show power law relationships between stress ratio and $\gamma/\gamma_{50\ Power}$ using average (mean), maximum and minimum *b*-values found for the test mode (excluding one outlying CKUC reconstituted test). From these figures the power law appears to characterise the range of stress-strain data quite well although some error about the pivot strain can be observed. This error was identified earlier in figures 4- 12 and 4- 13.

Lower *b*-values indicate more non-linearity, which can be observed by the upper values of

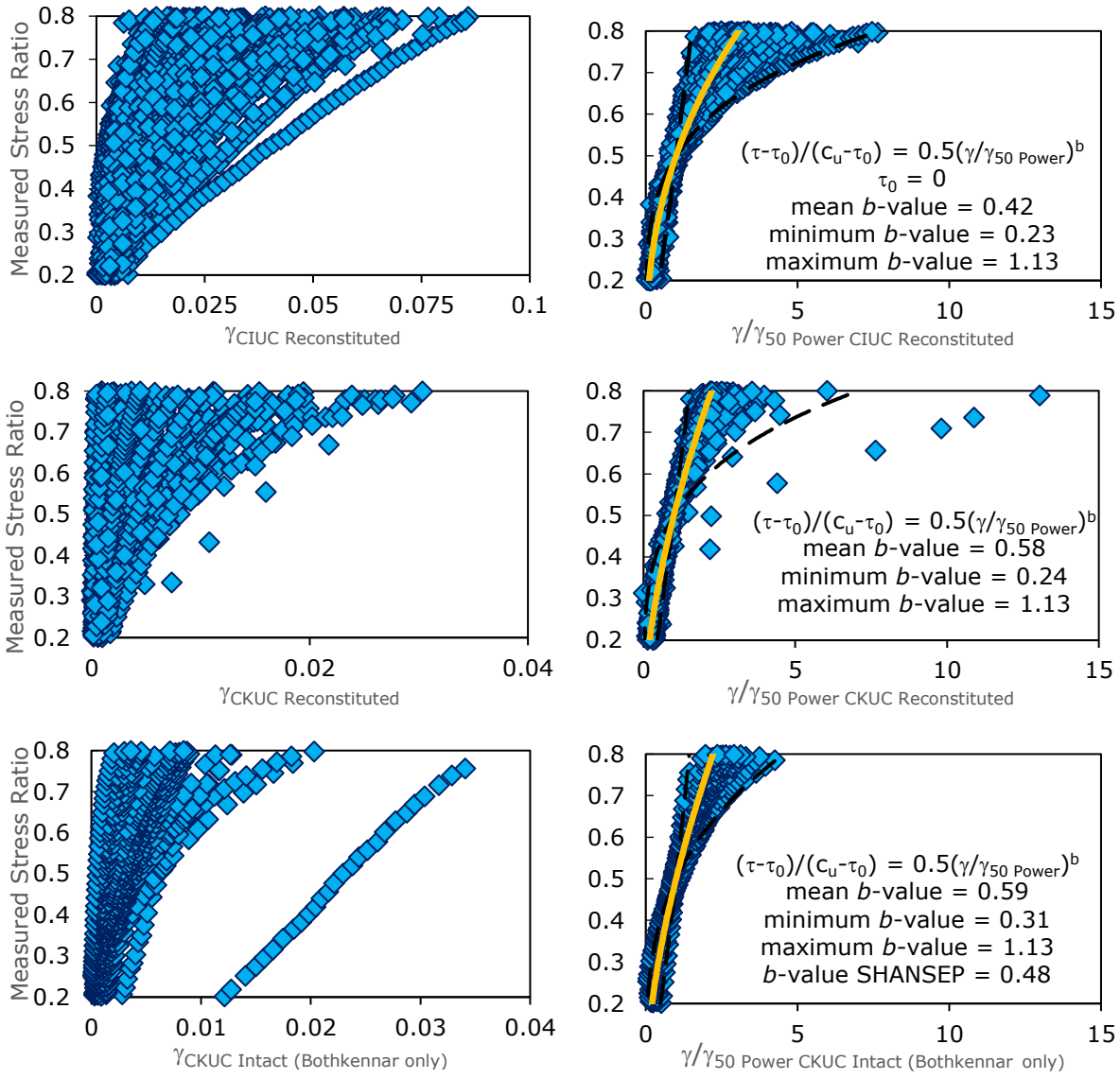

Figure 4- 16. Effect of strain normalisation and Power Law Model characterisation on triaxial compression measurements of stress ratio (*S*) and shear strain ($\gamma=1.5\varepsilon_{axial}$)

$\gamma/\gamma_{50\ Power}$ at stress ratios (S) greater than 0.5. It is interesting to note the similarity in behaviour of CKUC tests on reconstituted and intact specimens - both in the range of strains and b-values – while the CKUE test data do not show evidence of similarity. Measurements of $\gamma_{CKUE\ Intact\ Bothkennar}$ are in the lower range of $\gamma_{CKUE\ Reconstituted}$. This may be explained in part by the smaller number of intact tests in the CKUE database as a narrower range of test results should be expected. However, the intact specimens were sampled from a deposit characterised by geological OCR of about 1.2 (Nash et al. 1992a and Hight et al. 1992a report values of YSR of 1.3 to 4 over the sampling depth); whereas $\gamma_{CKUE\ Reconstituted}$ data were measured from materials with OCR varying from 1 to 17. A stiffer response in triaxial stress-strain would be expected from intact specimens that have not experienced significant destructuration prior to shearing

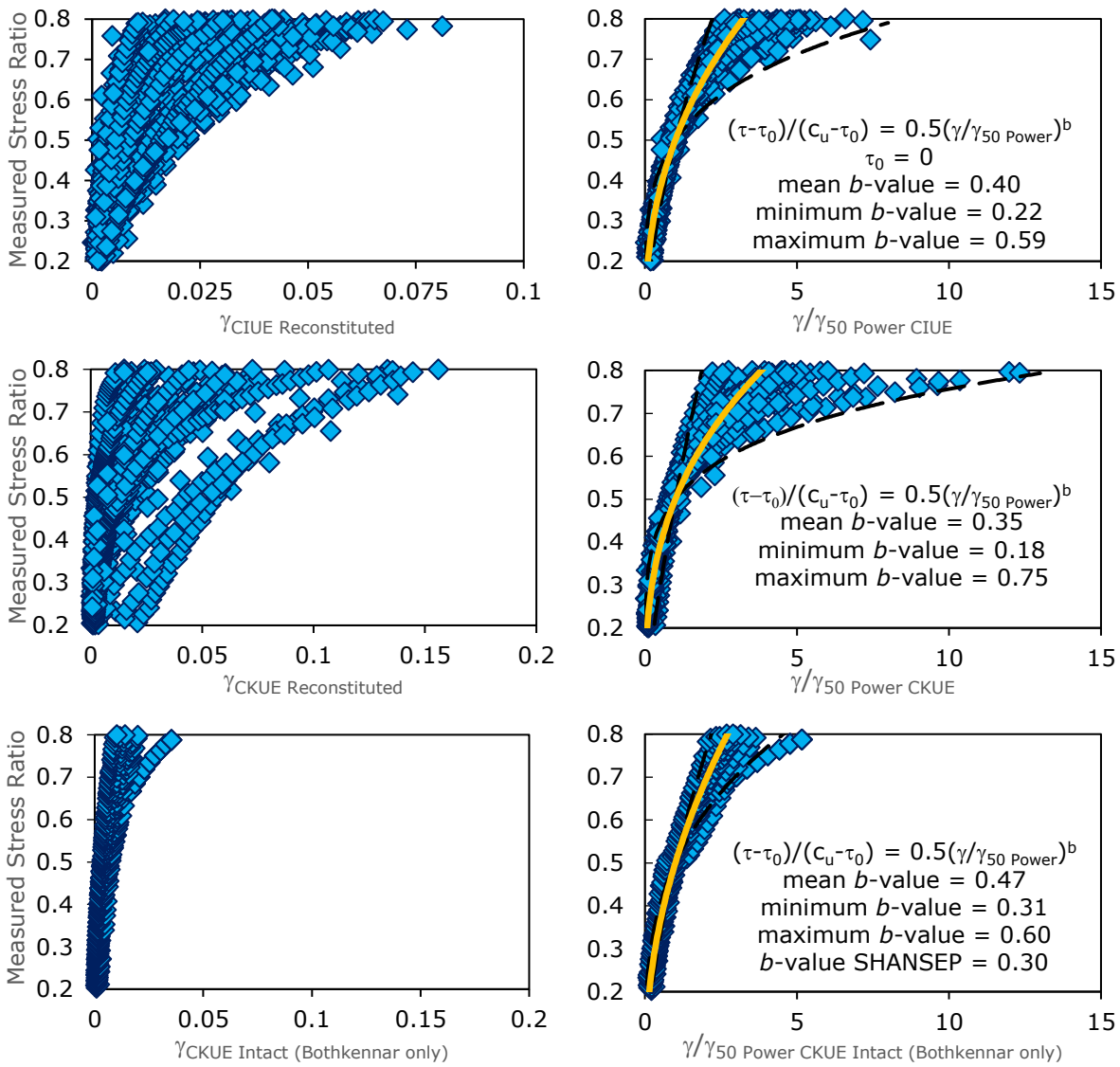

Figure 4- 17. Effect of strain normalisation and Power Law Model characterisation on triaxial extension measurements of stress ratio (S) and shear strain ($\gamma=1.5\varepsilon_{axial}$)

(Hight et al. 1992a). One would expect the mobilisation of S=20% to occur between yield surfaces Y2 and Y3 (Hight et al. 1992a, Hight et al. 2003, Vardanega and Bolton 2011) and so it is unlikely that complete destructuration would have taken place in the intact material. Reconstituted specimens were completely destructured during the reconstitution process although the soil fabric would have been affected by an unknown progression of particle orientation during consolidation. It is therefore unclear why CKUC tests show a similar range in behaviour from reconstituted and intact tests while this is not the case for CKUE tests. Understanding the possible causes of variability in $\gamma_{50\ Power}$ and b-value measured in structured and destructured materials is the focus of the next sections of this report.

4.3.5 What is *b*?

Simply, the model parameter b is a fitted exponent for the power-law relationship between undrained triaxial stress and strain. However, b is also the nonlinear shape parameter of the stress-strain model which may indicate ductility of the soil material. This is illustrated more clearly in Figure 4- 18 which shows all normalised strain data in the reconstituted database plotted against the best-fit b-value for each triaxial test. The value of b is determined by the spread of strain data about the pivot strain: lower b values are found for tests with a larger range of $\gamma/\gamma_{50\ Power}$ in the performance range $0.2 \leq S \leq 0.8$. Values of b = 0.2 to 0.3 are related to approximately 2 log cycles of $\gamma/\gamma_{50\ Power}$. Figure 4- 18 suggests that triaxial extension is characterised by more nonlinear behaviour than triaxial compression but that there is also more similarity in the range of b between CIUC and CIUE than between CKUC and CKUE.

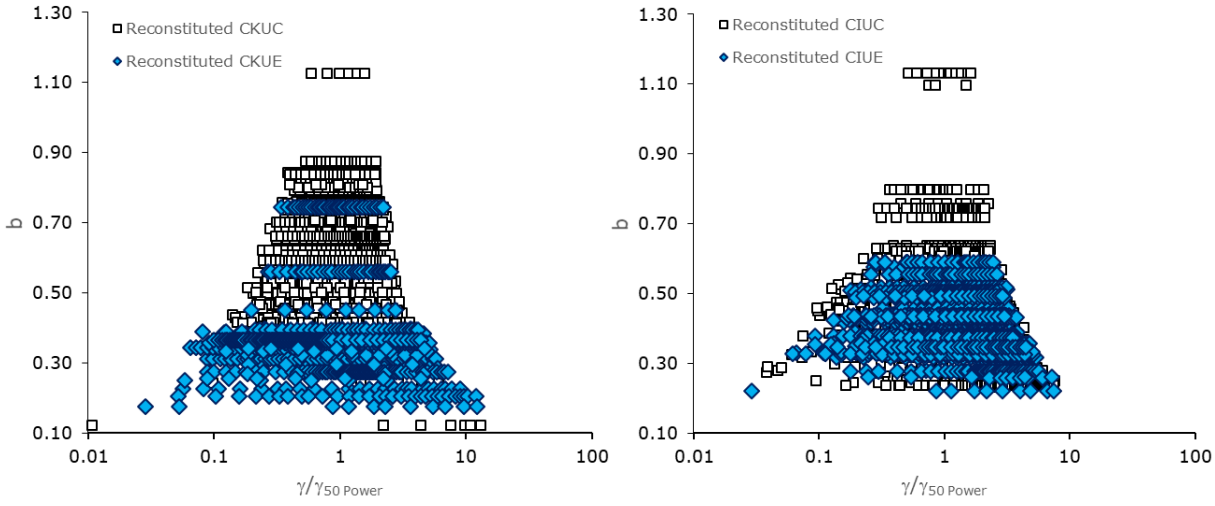

Figure 4- 18. Range of normalised strain data plotted against the fitted exponent, b (all reconstituted test data shown by test mode)

4.3.6 Correlation of Power Law model parameters with *OCR* by simple linear regression

In this section the data in RFG/TXCU-278 have been analysed to evaluate the possibility of using *OCR* as a predictor for model parameters γ_{50} and *b* measured from four triaxial modes of stress and strain (i.e. CIUC, CIUE, CKUC, CKUE). Since it is well known that c_u/σ'_{v0} and *OCR* are closely related (Ladd et al. 1977, Jamiolkowski et al. 1985, Mayne 1980), the relationship between c_u/σ'_{v0} and *OCR* is also investigated for each test mode as it provides a useful comparison of parameter variability. Model 2 was fitted to the stress-strain data for each triaxial test. Using the method of least-squares, power-law relationships were fitted to 271 triaxial tests using the available data points ($n \geq 3$) with a range of $0.779 \leq R^2 \leq 0.9999$ and $0.0017 \leq S.E. \leq 0.0925$. 7 additional triaxial tests provided only peak stress data.

A significant correlation exists between $\gamma_{50\ Power}$ and *OCR* measured during CIUC, CIUE, CKUC and CKUE tests on reconstituted specimens. Lines of best fit are plotted with the data in Figure 4- 19. Positive linear regressions were found between $\gamma_{50\ Power}$ and *OCR* for CIUC, CIUE, and CKUE data and between $\log_{10}(\gamma_{50\ Power})$ and $\log_{10}(OCR)$ for CKUC. Considering any *OCR* value between 1 to 11, on average $\gamma_{50\ Power\ CIUE}$ is up to a factor of 1.5 times smaller than $\gamma_{50\ Power\ CIUC}$ with more disparity at lower values of *OCR*. The trends of reference strain with *OCR* are dissimilar when comparing CKU modes as $\gamma_{50\ Power\ CKUE}$ is about 3.5 to 7.5 times larger on average than $\gamma_{50\ Power\ CKUC}$ for the data in RFG/TXCU-278.

Casey (2016) reported a similar relationship for a database of $n=73$ CKUC tests and a range in $\gamma_{50\ Power\ CKUC}$ that is close to the range observed in the new database. At $OCR=1$ the two average values of $\gamma_{50\ Power\ CKUC}$ are equal to 0.0004 and 0.0005 and the slope coefficients are 1.57 and 1.35 respectively for Casey (2016) and this study. The database published by Casey (2016) includes 9 sources of material whereas this new database includes 7 sources of material from 9 experimental studies and a greater number of samples between $6 < OCR \leq 10$ (10 tests compared to 3 tests). Both databases share test data obtained from Abdulhadi (2009). Table 4- 5 summarises the reported trends between $\gamma_{50\ Power}$ and *OCR*; there is a clear lack of published intact test databases to compare with reconstituted parameter trends.

In Figure 4- 20, the effect of stress history on the model deformation parameter from tests on intact specimens is demonstrated here by plotting $\gamma_{50\ Power}$ against sampling depth. Both $\gamma_{50\ Power\ CKUC}$ and $\gamma_{50\ Power\ CKUE}$ show scatter and an increase in magnitude at depths shallower than 3.38m where higher

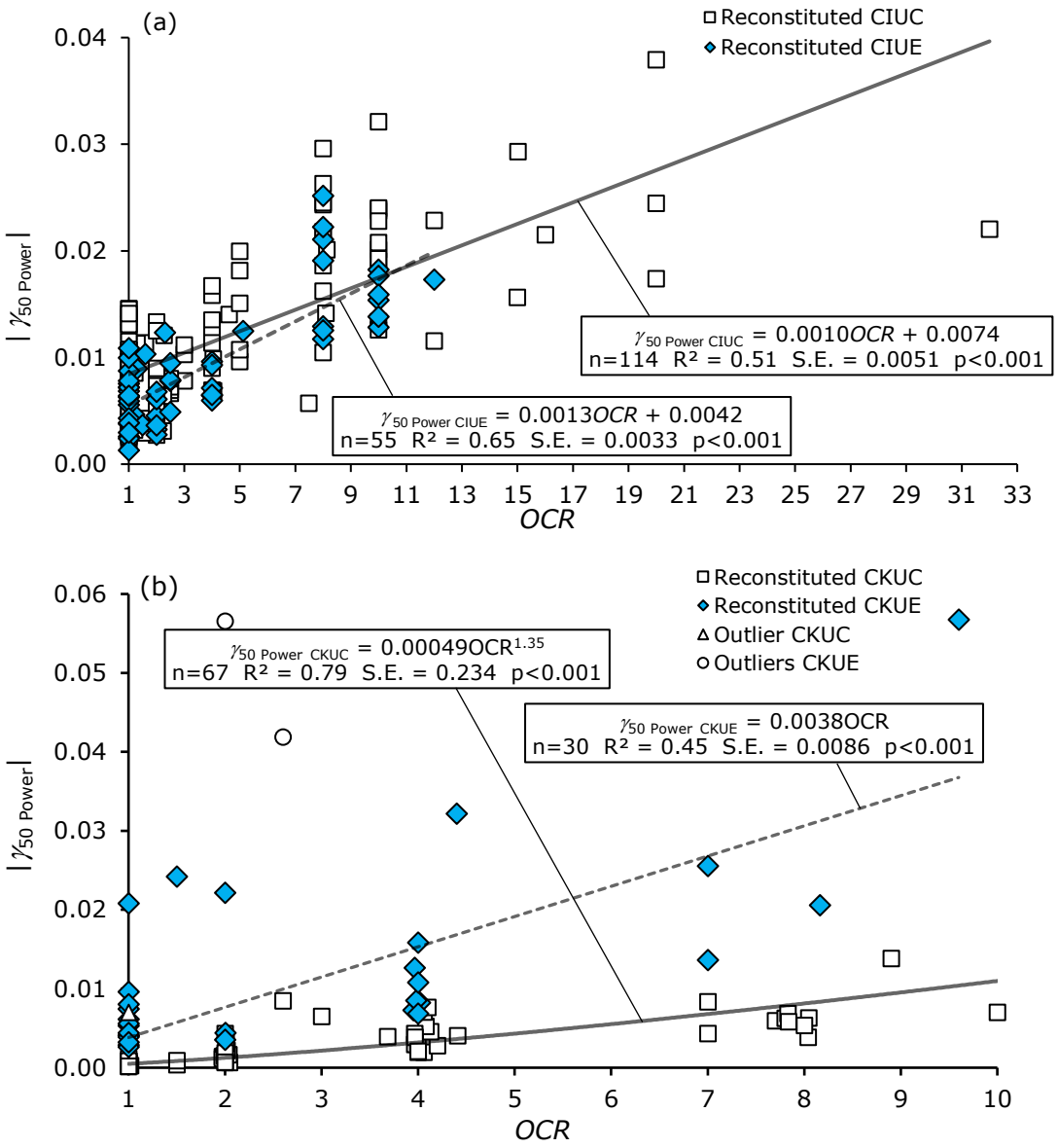

Figure 4- 19. Variation of $\gamma_{50\ Power}$ with *OCR* for reconstituted specimens sheared from (a) isotropic consolidation stresses (b) K_0 consolidation stresses

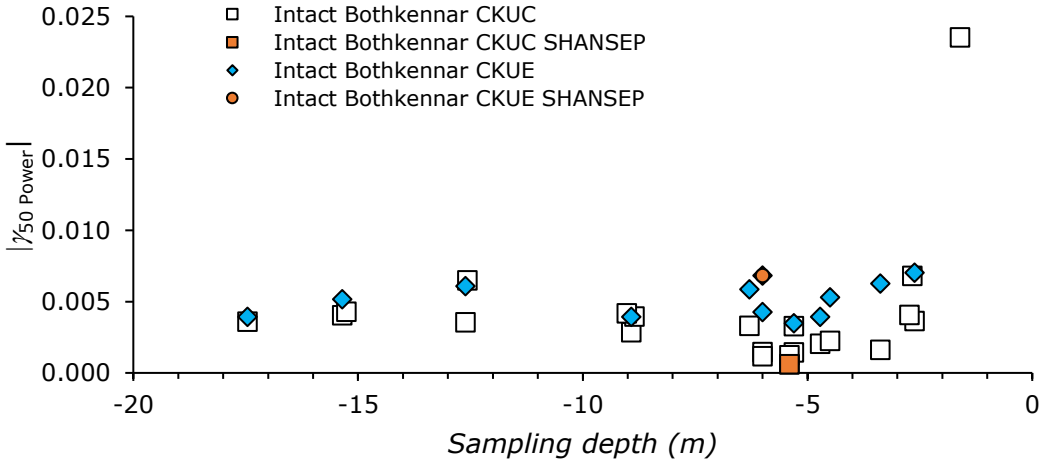

Figure 4- 20. Variation of $\gamma_{50\ Power}$ with sampling depth for intact specimens sheared from K0 consolidation stresses

OCR is expected. The lowest value of $\gamma_{50\ Power\ CKUC}$ was measured in the SHANSEP test (i.e. at *OCR*=1). Whereas the same consolidation procedure applied prior to triaxial extension has produced a value of $\gamma_{50\ Power\ CKUE}$ that is in the upper range of those measured from intact CKUE tests. (Published values of apparent *OCR* or *YSR* from oedometer tests are compared with model parameters in later sections).

No trend was found to correlate *b* and *OCR* for the reconstituted test modes – except only a weak negative correlation that exists for CKUC tests (R^2 = 0.21) and it is not shown in Figure 4- 21. Casey (2016) showed that b_{CKUC} did not correlate with *OCR* and the values shown in Figure 4- 21 are similarly distributed to the database published by Casey (2016) with large scatter at *OCR*=1. The mean values and standard deviations calculated for this new reconstituted soil test database demonstrate a disparity in the distributions of *b* from CKUC and CKUE tests. Tests on intact Bothkennar, however, show no clear disparity in *b*-values by shear mode (Figure 4- 22). On average, b_{CIUE} is slightly lower than b_{CIUC} and less scattered.

Both model parameters $\gamma_{50\ Power}$ and *b* have so far indicated a distinct change in behaviour between reconstituted soils tested in CKUC and CKUE. When the reconstituted soil is stressed monotonically from *S*= 20% to 80%, CKUC tests on average mobilise smaller strains and the normalised strains have a narrower range than CKUE tests. Figure 4- 23 shows that at peak stresses, when the soil has lost all stiffness, the average behaviour in CKUC and CKUE are also distinctly different. Using the results of the new database, CKUC tests on reconstituted soil would be expected to measure smaller peak stresses than an intact sample, with more deviation at low *OCR*; whereas larger measurements of $c_u/\sigma'_{v0\ CKUE}$ would be expected (refer to Table 4- 6 for regressions displayed in Figure 4- 23).

In contrast to CKU measurements on reconstituted soils, the average values of $\gamma_{50\ Power}$ and *b* are relatively similar whether sheared in compression or extension from isotropic conditions. The stress-strain behaviour (using $\gamma_{50\ Power}$ and b of the relevant test mode) would be expected to deviate more between CIUC and CIUE at *OCR* values close to 1 where lower extension strains have been observed (Figure 4- 19a). Compared to CKU tests, there is also less obvious banding shown in Figure 4- 23a indicating that the two distributions of strength data from CIUC and CIUE tests are similar. Apart from a small number of reconstituted specimens tested at *OCR*=1, all values of $c_u/\sigma'_{v0\ CIUE}$ are within the range

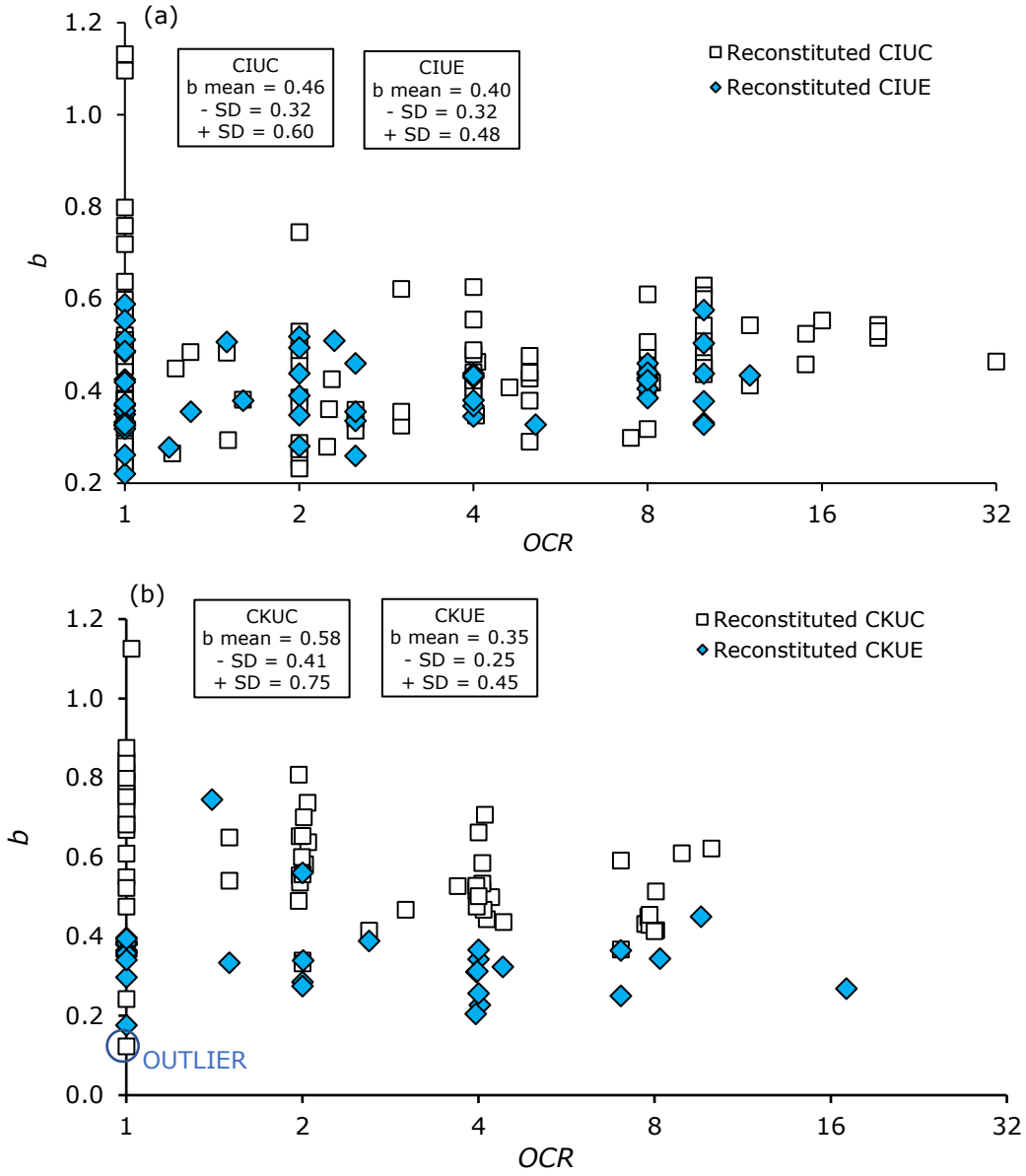

Figure 4- 21. Variation of *b* with *OCR* for reconstituted specimens sheared from (a) isotropic consolidation stresses (b) K_0 consolidation stresses

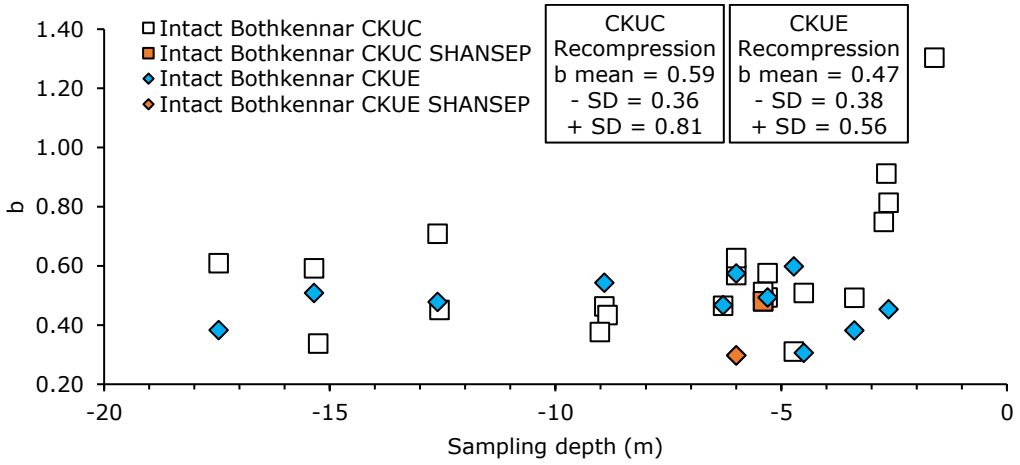

Figure 4- 22. Variation of *b* with sampling depth for intact specimens sheared from K_0 consolidation stresses

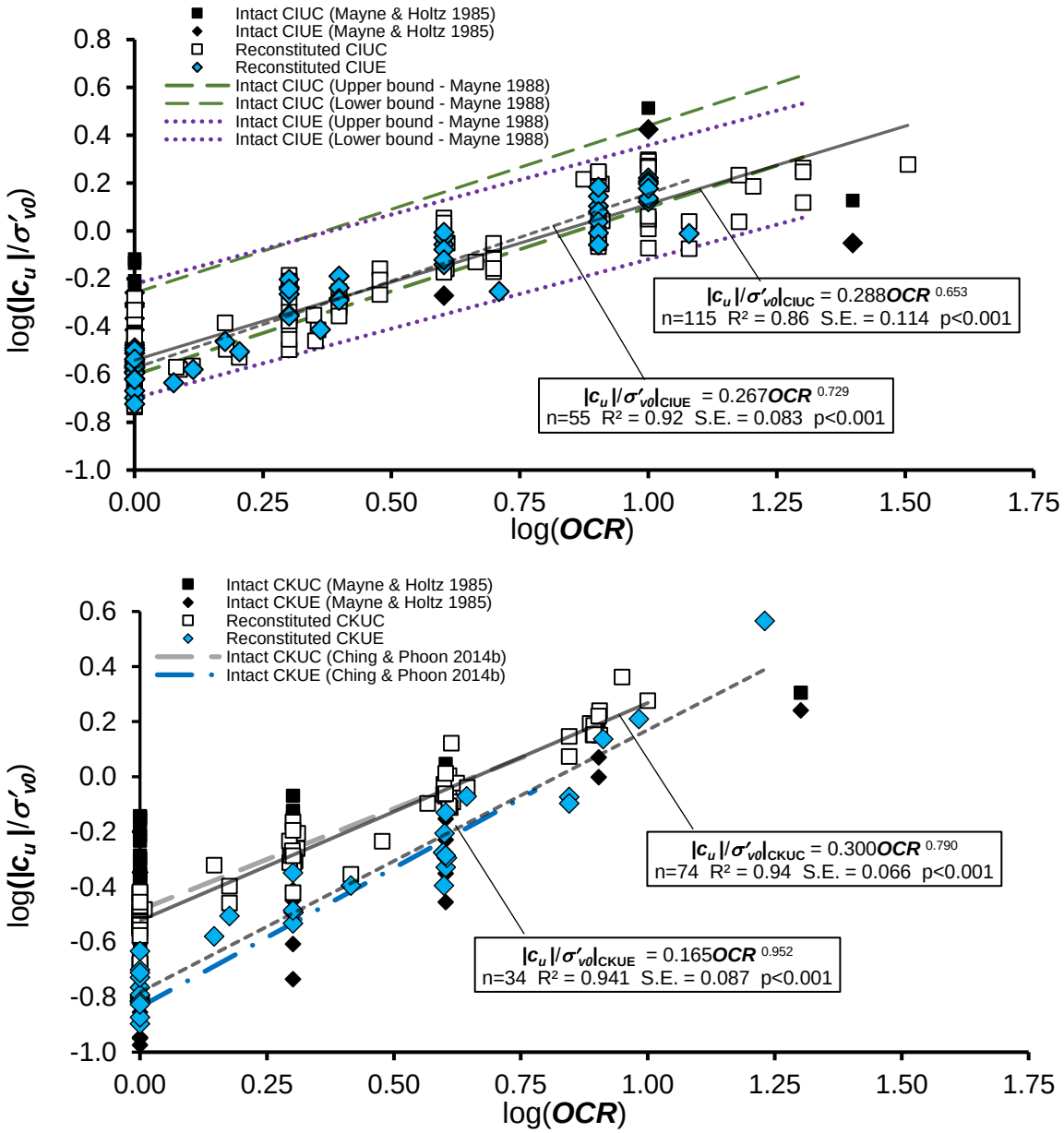

Figure 4- 23. Variation of c_u/σ'_{v0} with *OCR* for reconstituted specimens sheared from (a) isotropic consolidation stresses (b) K_0 consolidation stresses

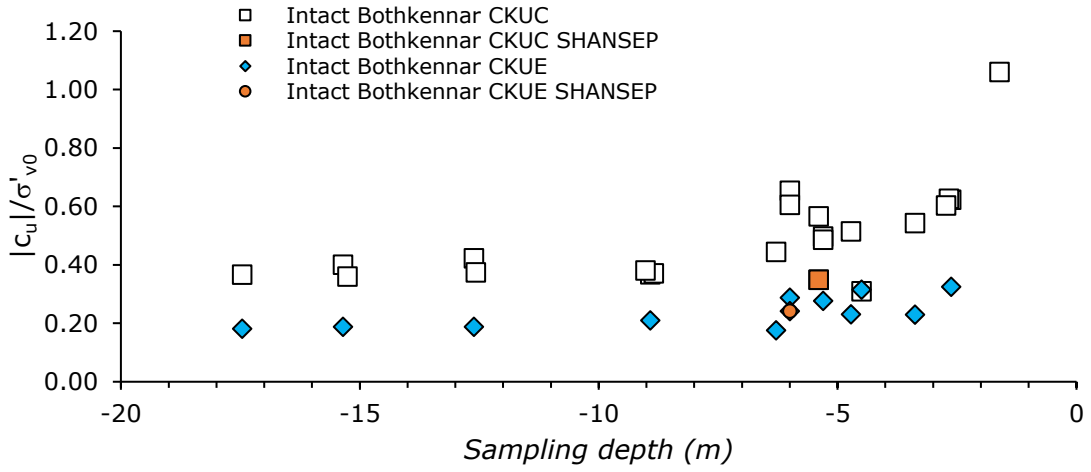

Figure 4- 24. Variation of c_u/σ'_{v0} with sampling depth for intact specimens sheared from K_0 consolidation stresses

Table 4- 5. Correlations between *OCR* and ($\gamma_{50\ Power}$) from undrained triaxial compression and extension tests sorted by test mode

Sample type	Database Reference	*OCR*	CIU, CKU or CAU	Regression axes Natural or Log-Log	$\gamma_{50\ Power\ NC}$	Γ (slope regression coefficient)	(Eq.)	*n*	R^2	*S.E.*	p-value	Data within error bounds	± % Error	Factor Error	Bias	COV
Reconstituted	RFG/TXCU-278	1-32	CIUC	Natural	0.0084	0.0010	(4.1)	114	0.51	0.005	<0.001	81%	60	1.75	1.03	0.40
Reconstituted	RFG/TXCU-278	1-12	CIUE	Natural	0.0055	0.0013	(4.2)	55	0.65	0.003	<0.001	80%	55	1.70	1.00	0.39
Reconstituted	RFG/TXCU-278	1-10	CKUC	Log-Log	0.0005	1.35	(4.3)	67	0.79	0.234	<0.001	81%	60	2.00	1.16	0.65
Reconstituted	RFG/TXCU-278	1-10	CKUE	Natural	0.0038	0.0038	(4.4)	30	0.45	0.0086	<0.001	80%	90	2.10	1.38	0.83
Reconstituted	Casey (2016)	1-9	CKUC	Log-Log	0.0004	1.57		73	0.87		<0.001					

Table 4- 6. Correlations between *OCR* and (c_u/σ'_{v0}) from undrained triaxial compression and extension tests sorted by test mode

Sample type	Database Reference	*OCR*	CIU, CKU or CAU	Regression axes Log-Log	$(c_u/\sigma'_{v0})_{NC}$	Λ (slope regression coefficient)	(Eq.)	*n*	R^2	*S.E.*	p-value	Data within error bounds	± % Error	Factor Error	Bias	COV
Reconstituted	RFG/TXCU-278	1-32	CIUC	Log-Log	0.288	0.653	(4.5)	115	0.86	0.114	<0.001	81%	45	1.45	0.88	0.17
Intact	Mayne 1988 Upper Bound	1-20	CIUC	Log-Log	0.25	0.7										
Intact	Mayne 1988 Lower Bound	1-20	CIUC	Log-Log	0.55	0.7										
Intact	Ching & Phoon 2014b	1-6	CIUC	Log-Log	0.397	0.71		127								
Reconstituted	RFG/TXCU-278	1-12	CIUE	Log-Log	0.267	0.729	(4.6)	55	0.92	0.083	<0.001	80%	25	1.30	1.02	0.18
Intact	Mayne 1988 Upper Bound	1-20	CIUE	Log-Log	0.20	0.58										
Intact	Mayne 1988 Lower Bound	1-20	CIUE	Log-Log	0.60	0.58										
Reconstituted	RFG/TXCU-278	1-10	CKUC	Log-Log	0.300	0.790	(4.7)	74	0.94	0.066	<0.001	80%	20	1.2	0.99	0.19
Intact	Mayne 1988 Upper Bound	1-20	CAUC	Log-Log	0.20	0.78										
Intact	Mayne 1988 Lower Bound	1-20	CAUC	Log-Log	0.45	0.78										
Intact	Ching & Phoon 2014b	1-6	CKUC	Log-Log	0.328	0.736	(4.9)	143								
Reconstituted	RFG/TXCU-278	1-10	CKUE	Log-Log	0.165	0.952	(4.8)	34	0.94	0.087	<0.001	79%	25	1.30	1.02	0.20
Intact	Mayne 1988 Upper Bound	1-20	CAUE	Log-Log	0.12	0.85										
Intact	Mayne 1988 Lower Bound	1-20	CAUE	Log-Log	0.25	0.85										
Intact	Ching & Phoon 2014b	1-6	CKUE	Log-Log	0.146	1.009		83								

of intact strength data reported by Mayne (1988). However, $c_u/\sigma'_{v0\,\mathrm{CIUC}}$ measurements on reconstituted specimens are approximately within or below the lower bound reported by Mayne (1988) for CIUC tests on intact specimens. It is worth noting that the values of Λ reported in this study, for all test modes, significantly exceed those reported by Mayne (1988) for reconstituted artificial clay mixtures.

4.3.7 Estimation of intact soil parameters from *OCR* and *YSR*

A profile of yield stress ratio (also termed "apparent *OCR*" by Hight et al. 1992a) in Bothkennar clay was recommended by Hight et al. (1992a) based on average measurements of yield stress ratio undertaken by Nash et al. (1992b) using Incremental Load (IL) tests on intact specimens from Laval samples (see Figure 4- 25). Where *YSR* values exceed the estimated geological *OCR* (about 1.2 for Bothkennar clay between 5 and 15m below ground level), this suggests that yielding behaviour in the oedometer is influenced by clay structure (Hight et al. 1992a) and ageing (Nash et al. 1992a) in addition to stress history. Figure 4- 25 (digitised from Nash et al. 1992a) suggests that measured yield points in the oedometer are also influenced by test and sampling procedures.

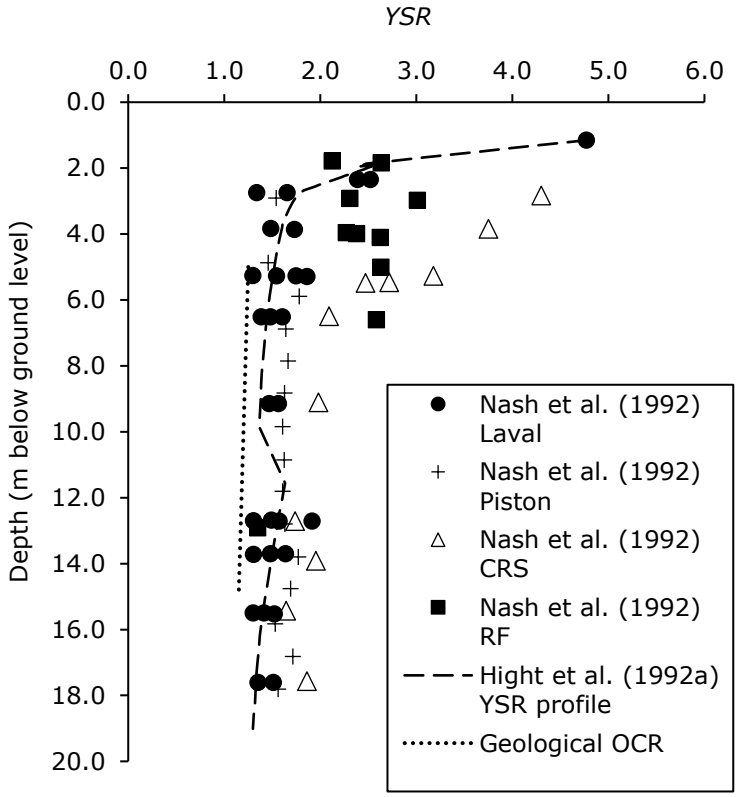

Figure 4- 25. Variation of yield stress ratio (*YSR*) measurements with depth (Nash et al. 1992a) and interpreted *YSR* (or apparent *OCR*) profile with depth (Hight et al. 1992a)

In Figure 4- 26, the measured reference strains ($\gamma_{50\ Power\ CKUC}$) are plotted with their estimates calculated using *OCR*=1.2 or the *YSR* profile shown in Figure 4- 25 in combination with Equation 4.3 (Table 4- 5). A companion plot (Figure 4- 27) shows the variation in normalised undrained shear strength ($c_u/\sigma'_{v0\ CKUC}$) for the same dataset. Using Equations 4.3 and 4.7 and *OCR*=1.15 to 1.25 underpredicts $\gamma_{50\ Power\ CKUC}$ and $c_u/\sigma'_{v0\ CKUC}$ measured using Recompression procedures. The parameters measured from

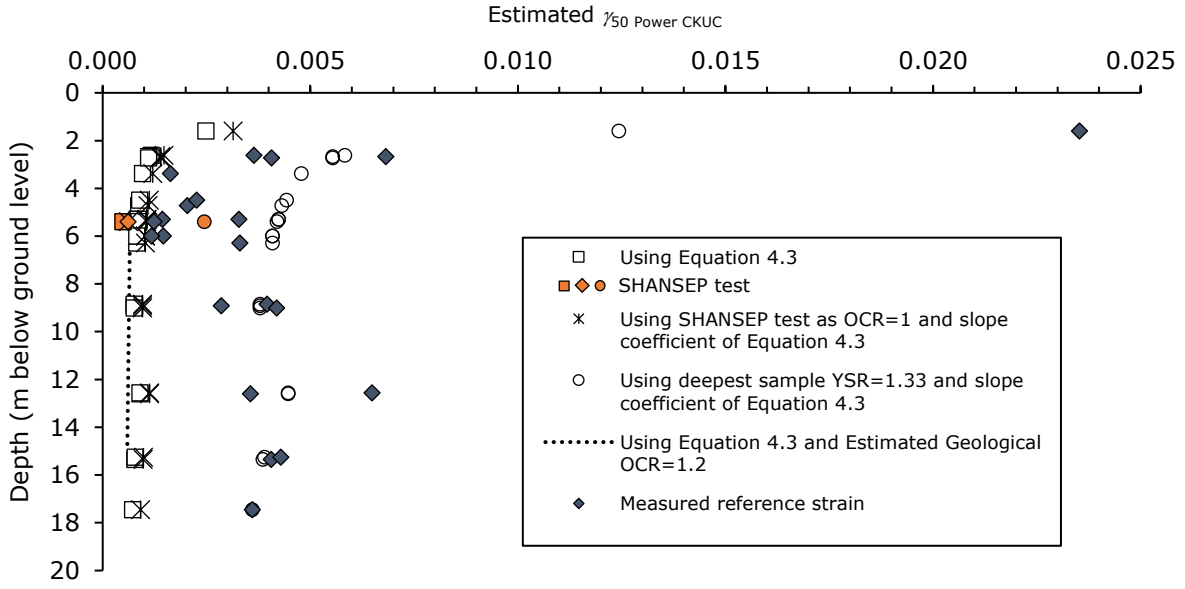

Figure 4- 26. Variation of estimated $\gamma_{50\ Power\ CKUC}$ using *YSR* profile (Figure 4- 25, Hight et al. 1992a) or estimated geological *OCR*=1.2 and Equation 4.3

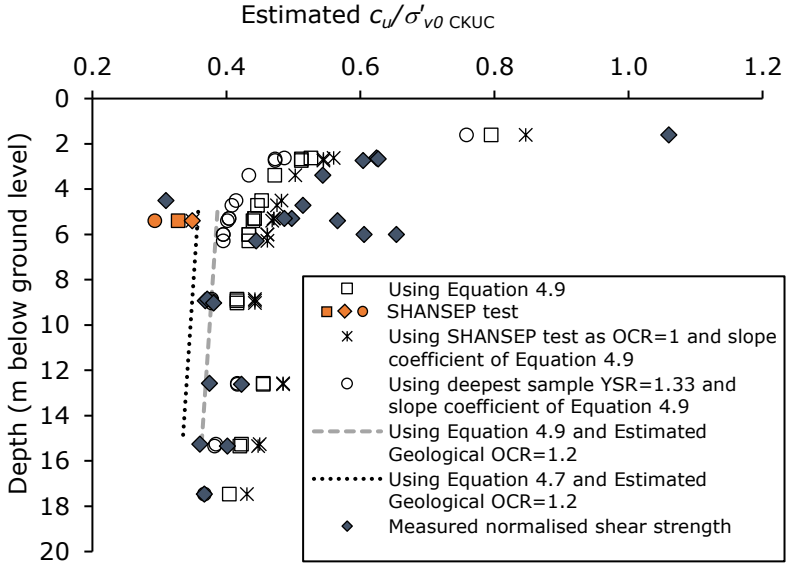

Figure 4- 27. Variation of estimated $c_u/\sigma'_{v0\ CKUC}$ using *YSR* profile (Figure 4- 25, Hight et al. 1992a) or estimated geological *OCR* (Figure 4- 25) and Equations 4.7 & 4.9

SHANSEP tests (indicated by the diamond symbol) are closely approximated by Equations 4.3 and 4.7. The plots suggest that estimating variation of c_u/σ'_{v0} with depth could be achieved by measuring the variation of *YSR* with depth (taken to be equal to the variation of *OCR* with depth) and an empirical slope coefficient (Table 4- 5) - following the method of Mayne (1980). However, when comparing predicted values with those measured from CKUC tests, the error of the prediction is sensitive to the value chosen for the "known *YSR*" measurement of c_u/σ'_{v0}.

The strength and strain parameters plotted in figures 4- 26 and 4- 27 show that the triaxial test data reported by SERC (1989) are variable, particularly between 4.5 and 6m below ground level (bgl). An upswing in both parameters towards the ground surface matches the *YSR* profile which Hight et al. (1992a) suggested to be linked to desiccation shallower than 3.5m bgl - despite a piezometric level of 1.0m bgl throughout the deposit (Nash et al. 1992a). However, $\gamma_{50\ \text{Power CKUC}}$ is more variable than $c_u/\sigma'_{v0\ \text{CKUC}}$ and shows a less obvious trend with depth. Causes of the scatter in both parameters are likely to be linked to sampling disturbance and variations in test procedure, and to some extent to material variability (Figure 3- 1). The next sections of the chapter examine the causes of variation in more detail.

4.3.8 Influence of *OCR* on Power Law model parameters: intact versus reconstituted

In this section, the Power Law model parameters of intact and reconstituted samples are compared to assess the significance of *OCR*. A range of "intrinsic" behaviour of different soils is represented by the reconstituted parameter database, which also represents the variation due to different test procedures followed by the authors of each publication (9 publications in total for CKU tests). Figures 4- 28, 4- 29, 4- 30, and 4- 31 show $\gamma_{50\ \text{Power}}$ and *b* plotted against apparent (intact) or applied (reconstituted) *OCR*. Generally, the intact parameters are similar in magnitude to the expected range of reconstituted parameters at the same *OCR*. Several tests on intact Bothkennar clay resulted in higher $\gamma_{50\ \text{Power CKUC}}$ values than shown by the reconstituted database. The shallowest intact sample has an especially high value which is significant in this respect being the material with largest *OCR*. $\gamma_{50\ \text{Power CKUE}}$ values from intact tests are remarkably close to the trendline described by Equation 4.4. Figures 4- 30 and 4- 31 show that *b* values from intact tests are more variable as they are scattered across and outside the ranges of standard deviation recommended in Figure 4- 21.

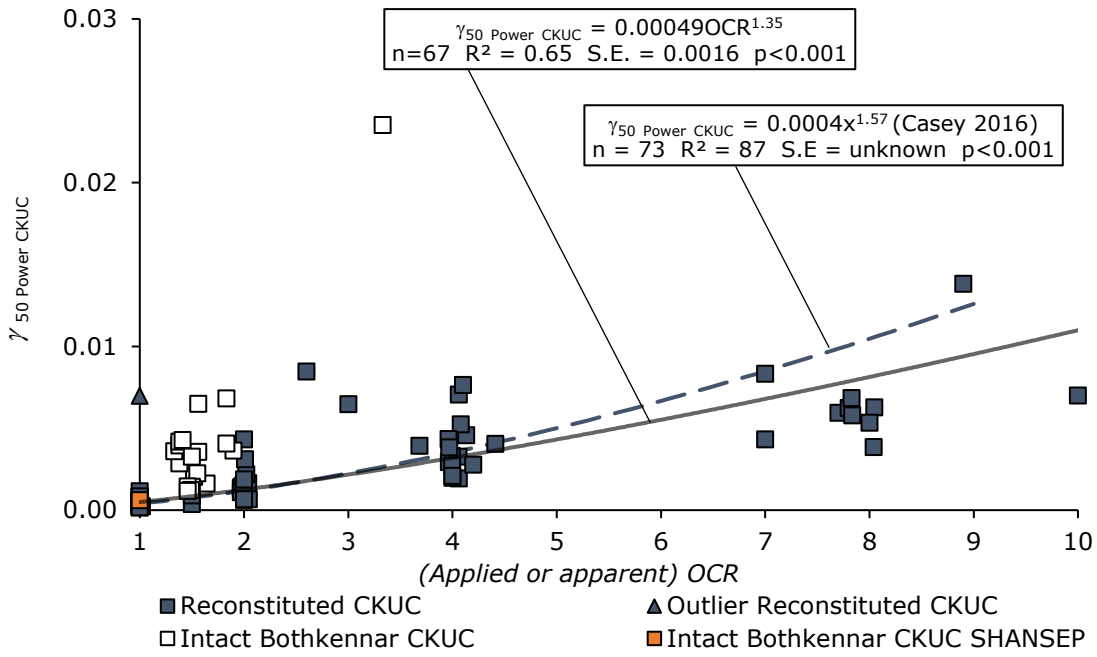

Figure 4- 28. Variation of $\gamma_{50\ Power}$ with *OCR* for reconstituted (various) and intact (Bothkennar) specimens sheared in triaxial compression from K_0 consolidated stresses

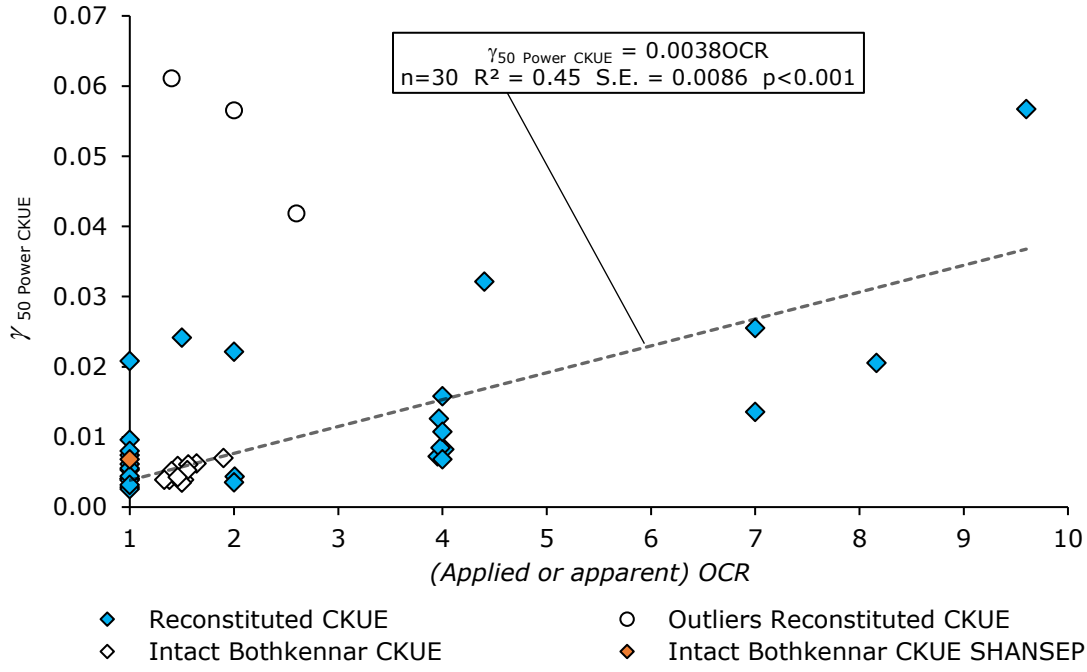

Figure 4- 29. Variation of $\gamma_{50\ Power}$ with *OCR* for reconstituted (various) and intact (Bothkennar) specimens sheared in triaxial extension from K_0 consolidated stresses

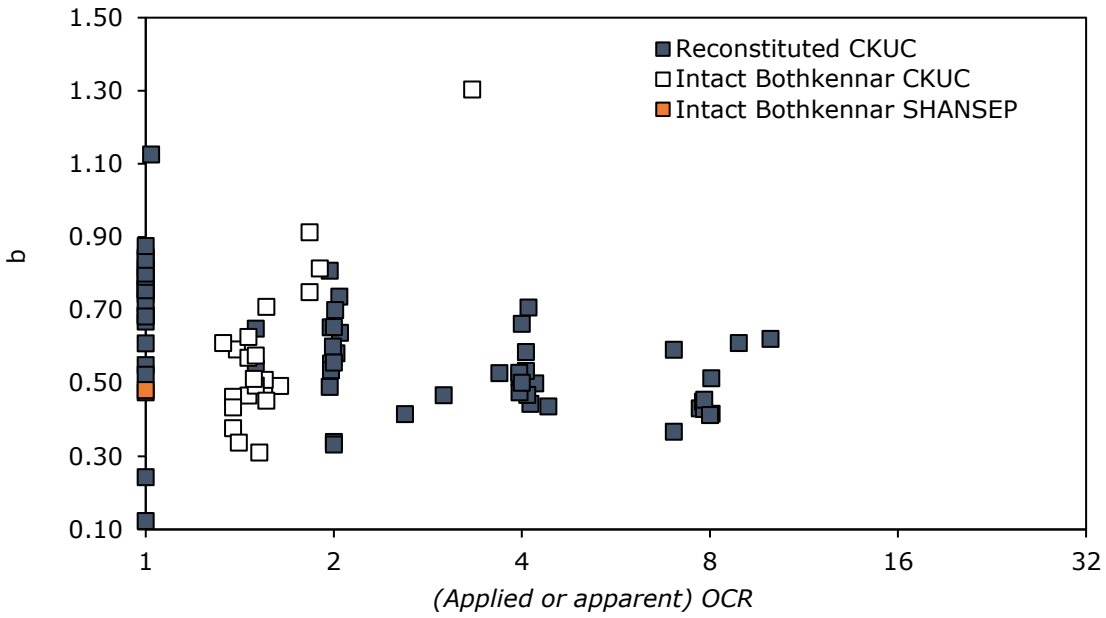

Figure 4- 30. Variation of *b* with *OCR* for reconstituted specimens sheared in triaxial compression from K_0 consolidated stresses

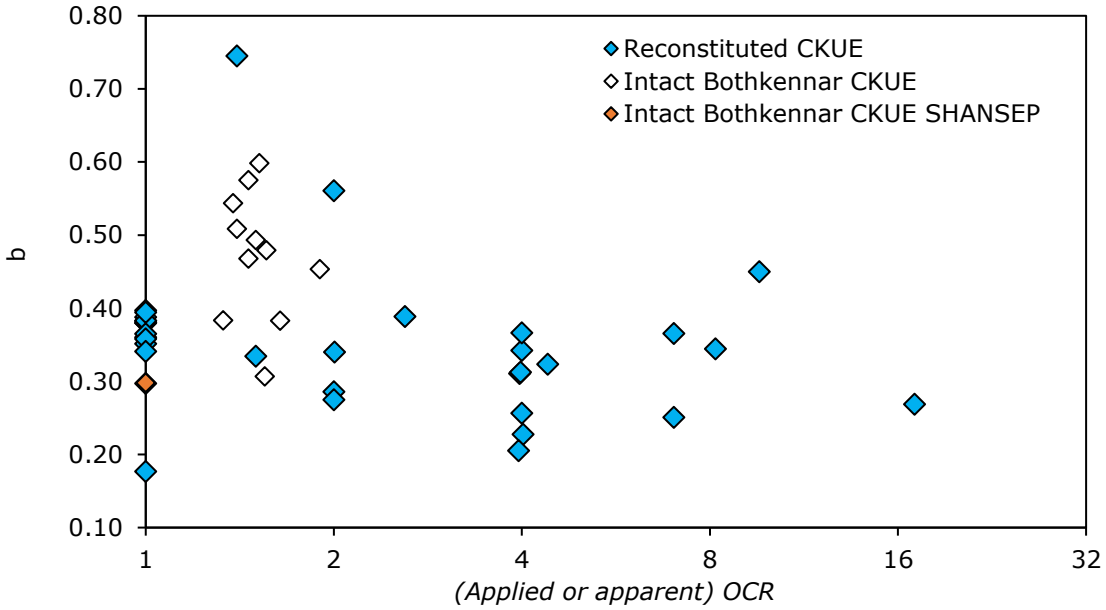

Figure 4- 31. Variation of *b* with *OCR* for reconstituted specimens sheared in triaxial extension from K_0 consolidated stresses

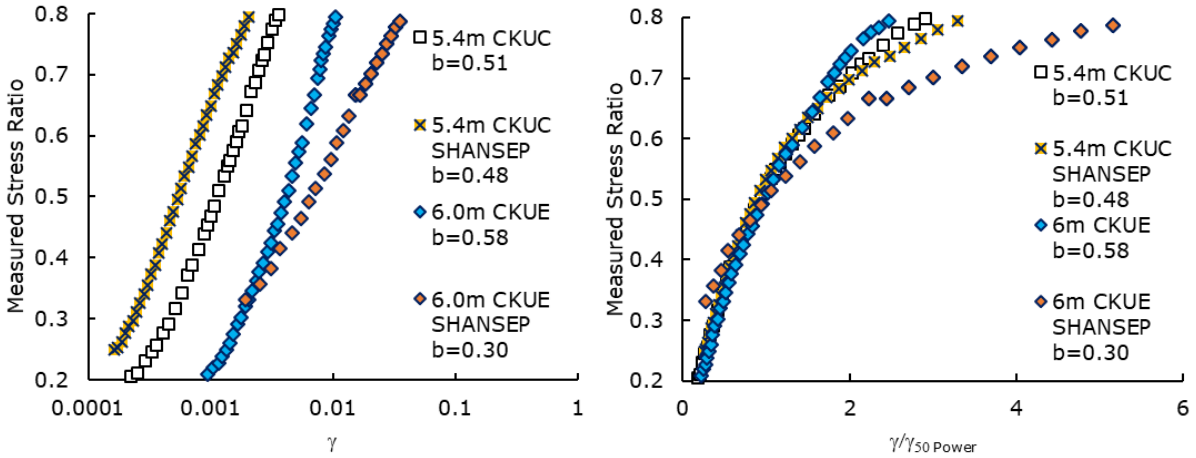

Figure 4- 32. Effect of SHANSEP procedure on the normalised stress-strain behaviour of 4 intact specimens of Bothkennar

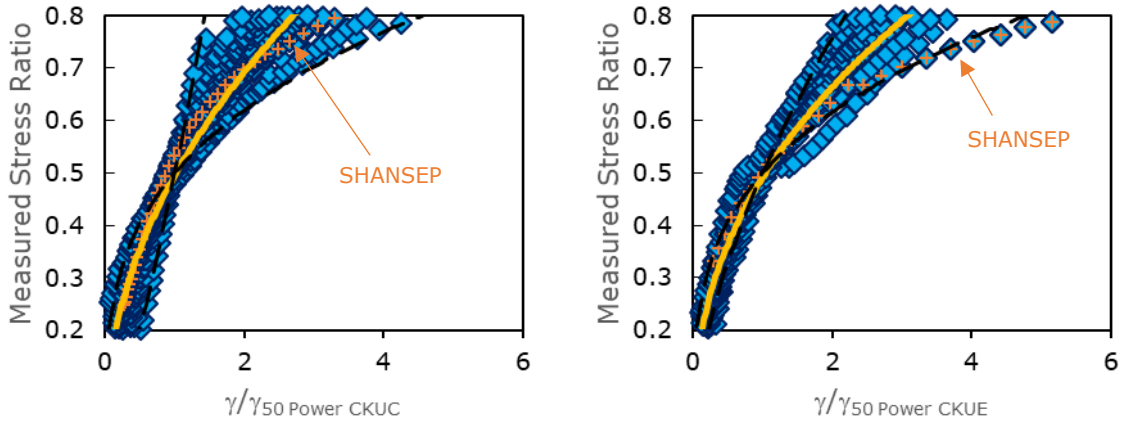

Figure 4- 33. Normalised stress-strain behaviour of all BTK/TXCU-34

Smith et al. (1992) describe the effect of consolidating samples using the SHANSEP procedure (under K_0 conditions to a normally consolidated state) as an "incomplete" destructuration of the soil matrix so that the Y3 yield surface is modified and the Y3 yield behaviour is transitional between the "sedimentary and intrinsic states". Both model parameters indicate that there is a shift in stress-strain behaviour when using SHANSEP consolidation that brings the soil to a transitional state. Intact specimens that were consolidated using the SHANSEP procedure show a reduction in $\gamma_{50\ Power\ CKUC}$ and increase in $\gamma_{50\ Power\ CKUE}$ compared to specimens that were sampled from the same depth and tested using the Recompression method – see Figure 4- 32. The reference strains measured from SHANSEP tests are well within the range measured from normally consolidated reconstituted soils. The *b*-values, however, are in the lower range of the same test data. In both CKUC and CKUE lower *b*-values indicate an increase

in non-linearity caused by the SHANSEP procedure, which is only slight in compression compared to the large change in extension (Figure 4- 32). This can also be seen in Figure 4- 33 where the normalised behaviour in extension is obviously more nonlinear compared to the other extension tests of BTK/TXCU-34 but in compression the normalised behaviour would perhaps not be considered unusual.

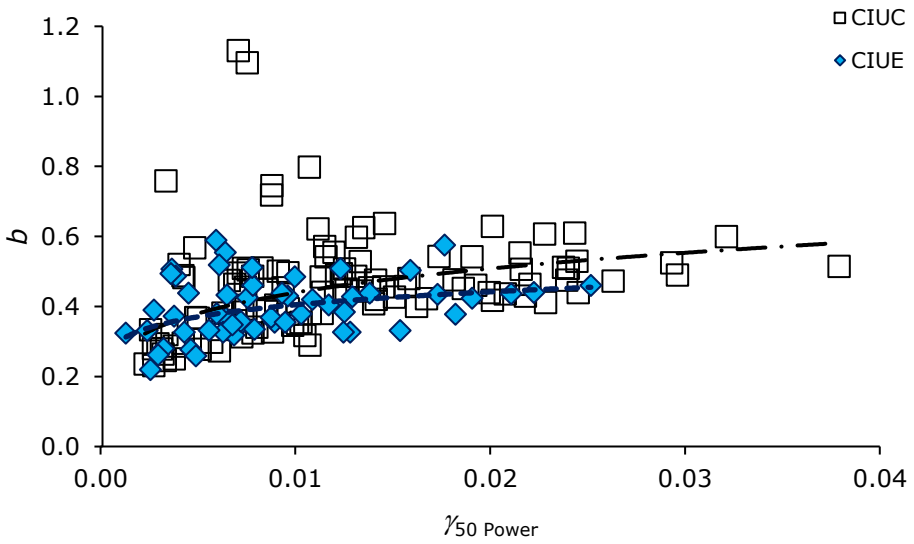

Figure 4- 34. Comparison of Power Law model parameters from triaxial tests consolidated under isotropic stress conditions

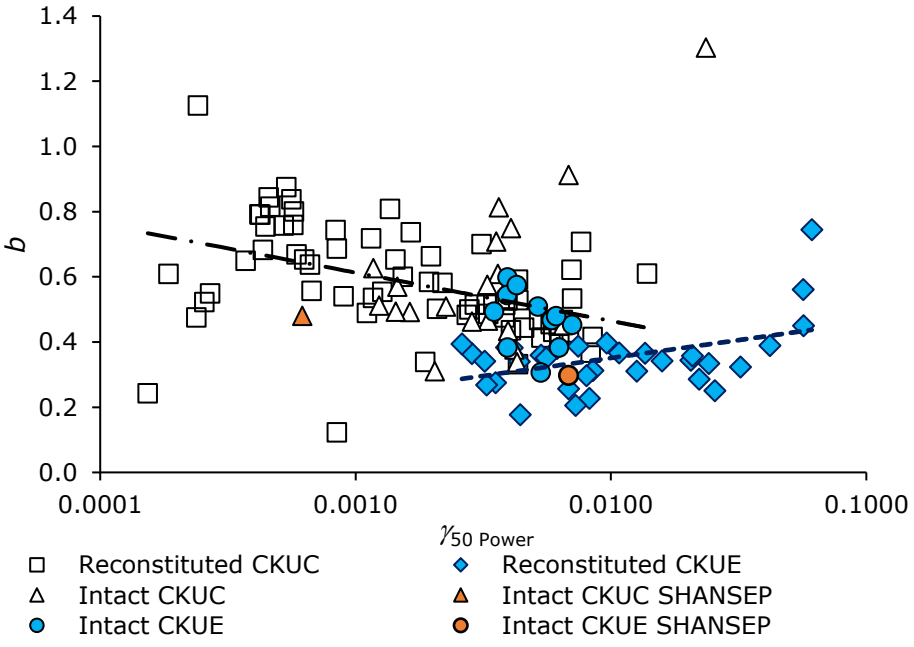

Figure 4- 35. Comparison of Power Law model parameters from triaxial tests consolidated under K_0 stress conditions

A comparison of $\gamma_{50\ Power}$ and b shown in Figures 4- 34 and 4- 35 demonstrates a shift in stress-strain behaviour between structured and destructured specimens. The parameters are weakly correlated in all 4 test modes on reconstituted soils (R^2 = 0.15 to 0.22). CKUC tests on intact Bothkennar clay with lower values of $\gamma_{50\ Power}$ are associated with more nonlinear behaviour (lower b-values) although the data is rather scattered, whereas in CKUC tests on reconstituted soil a lower $\gamma_{50\ Power}$ is often accompanied by less non-linearity (higher b-values). Opposite trends are indicated by the model parameters of CKUE tests. Intact test parameters and reconstituted test parameters of each test mode converge at the lower ranges of b. The SHANSEP test parameters are within or close to this convergence of behaviours and provides further evidence of the transitional nature of the SHANSEP test specimens.

4.3.9 Relationship between *b, OCR,* and point of maximum curvature (max_K)

Since the characterisation of triaxial stress-strain by the Power Law model has identified differences in structured and destructured soils that appear to be related to b, the parameter requires further investigation. The point of maximum curvature (max_K) of a stress-strain curve plotted in natural (linear) axes represents a "complete loss of stiffness" (Malandraki and Toll 1994). The point of maximum curvature from stress-strain data has been used by Miura et al. (1984) to identify yield in triaxial tests on sand under high confining stresses. The approach by Smith et al. (1992) in identifying the Y3 yield point from triaxial stress-strain plots appears to have been identifying a marked change in the test curve; but this is likely to have been only supplementary to the primary method of identifying a marked change in direction of effective stress path (the same authors probably produced 9 of the 34 triaxial tests on Bothkennar clay presented here).

Using the digitised or tabulated data points, the point of maximum curvature was calculated for every triaxial test in the two databases. The point marks the upper value of stress and strain from the identified increment of maximum curvature; hence, it is an upper estimate of the true point of max_K. This method is evidently approximate and precision of the estimate will vary according to the spacing of data points from the test. (Parameters for the triaxial tests published by Sheahan (1991) were obtained from tabulated data and have been highlighted in the plots). Because of this uncertainty, the parameters shown

in Figures 4- 36, 4- 37, 4- 38 and 4- 39 are highly scattered and no attempt was made to correlate the data. However, broad trends in the data provide a useful illustration of pre-failure yielding behaviour.

The parameter $\gamma_{maxK}/\gamma_{50\ Power}$ is defined by the ratio of strain at the point of maximum curvature and $\gamma_{50\ Power}$. When plotted against *b*, $\gamma_{maxK}/\gamma_{50\ Power}$ demonstrates a broadly positive trend in all CKUC and CKUE tests (Figures 4- 36 and 4- 37). If max_K represents a yield point, it implies that *b* characterises the onset of Y3 yielding and that the non-linearity of the soil deformation is directly related to this yield point. A plausible outcome of this assumption is that Y3 yielding often initiates at stresses lower than *S*=0.5.

It appears from Figures 4- 36 and 4- 37 that $\gamma_{maxK}/\gamma_{50\ Power}$ from intact tests are scattered within the lower to mid range of the reconstituted tests. However, when $\gamma_{maxK}/\gamma_{50\ Power}$ is plotted against *OCR* (apparent or applied), a larger discrepancy between intact and reconstituted soils is apparent for CKUC tests. If max_K represents approximately the onset of Y3, then it would appear that a possible reason for values of $\gamma_{50\ Power\ CKUC}$ in BTK/TXCU-34 being larger than the reconstituted parameters (see Figure 4- 28) is that by *S*=0.5 the onset of Y3 yielding has already taken place at a lower $\gamma_{maxK}/\gamma_{50\ Power}$. The resulting measurement of $\gamma_{50\ Power}$ is then a manifestation of irrecoverable "large-scale changes in particle packing" (as defined by Smith et al. 1992) at a more progressed stage of yielding behaviour. A possible

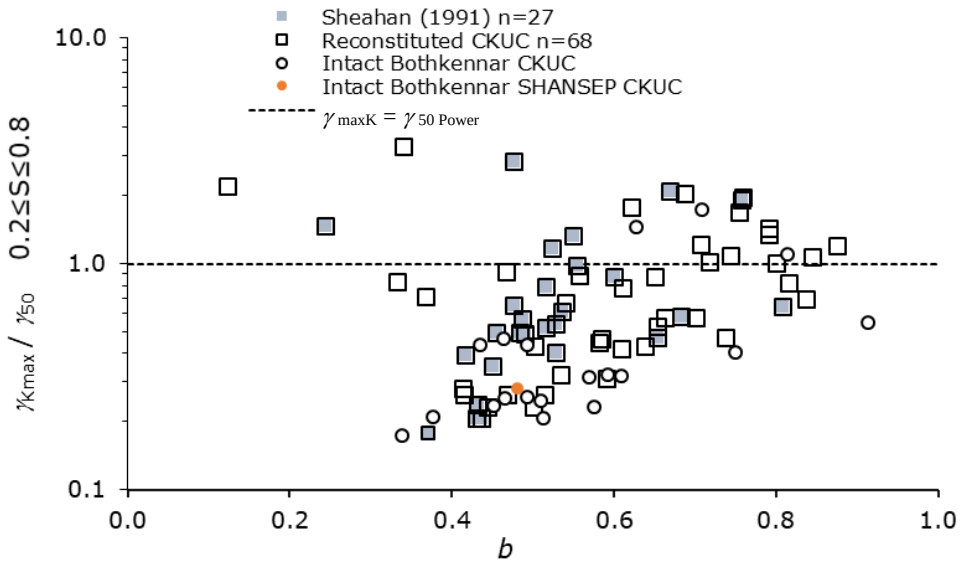

Figure 4- 36. Variation of the *point of maximum curvature* with *b* from CKUC triaxial tests

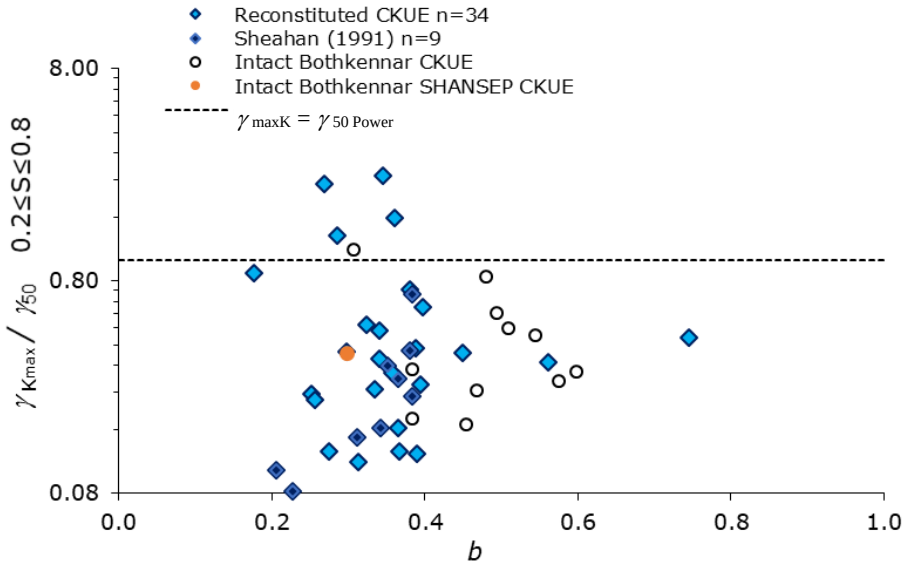

Figure 4- 37. Variation of the *point of maximum curvature* with *b* from CKUE triaxial tests

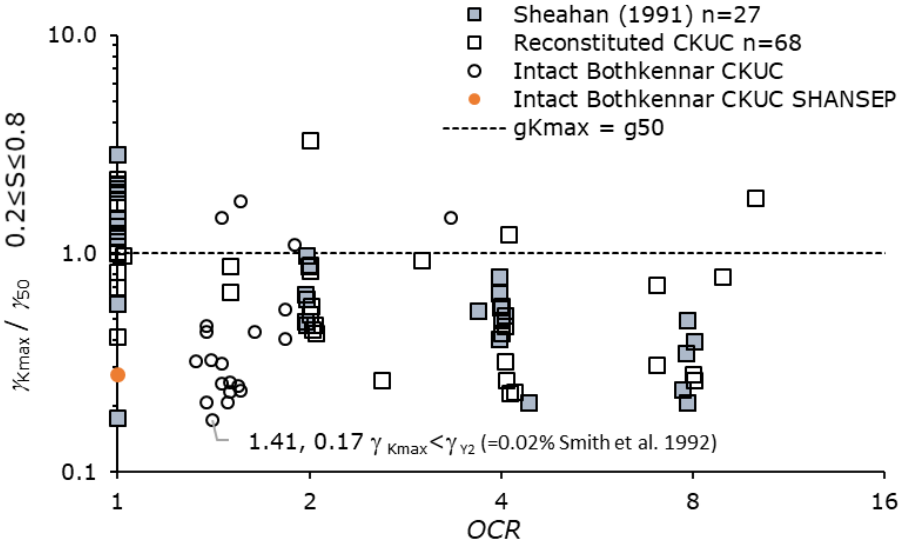

Figure 4- 38. Variation of the *point of maximum curvature* with *OCR* (applied or apparent) from CKUC triaxial tests

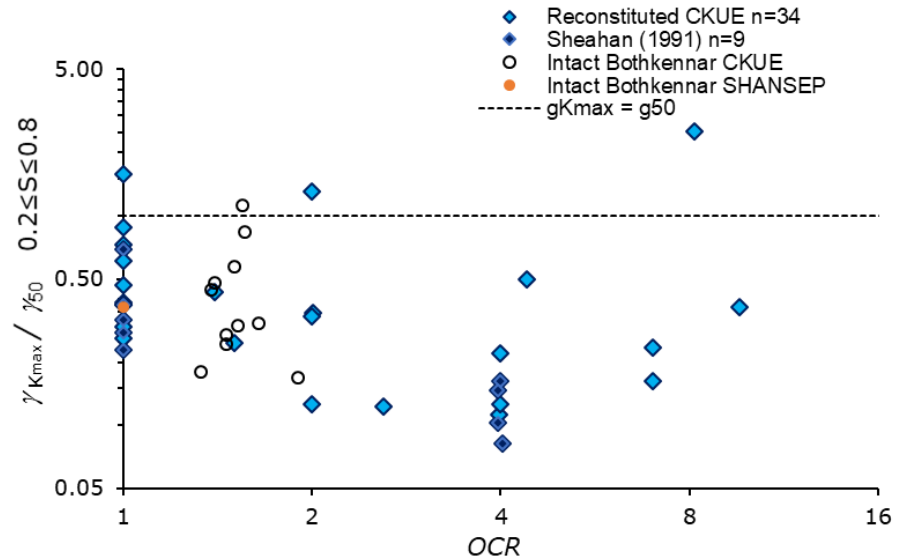

Figure 4- 39. Variation of the *point of maximum curvature* with *OCR* (applied or apparent) from CKUE triaxial tests

justification for such an assertion is that in all except one test (identified in Figure 4- 38), the strain measurements of γ_{maxK} from Recompression tests are greater than the recommended value of γ_{Y2}, where γ_{Y2} is the critical value of shear strain marking the Y2 yield surface of Bothkennar identified by Smith et al. 1992).

4.3.10 Influence of consolidation stress on Power Law model parameters

In the preceding sections a comparison between intact and reconstituted data was accomplished by choosing similar values of applied and apparent *OCR*. Since the same *OCR* value can be achieved after the soil has experienced different stress histories, this section examines the influence of consolidation stress on parameter variability. Casey et al. (2016) identified a positive correlation between undrained modulus of normally consolidated reconstituted specimens ($E_{u50\ CKUC\ NC}$) and effective stress level at the end of consolidation (0.1 MPa ≤ σ'_{v0} ≤ 100 MPa). However, when the data was reanalysed using the Power Law framework (Casey 2016), $\gamma_{50\ Power\ CKUC\ NC}$ showed no clear evidence of stress-dependency below effective stresses of 1 MPa. This suggests that the stress-dependency of $E_{u50\ CKUC\ NC}$ at σ'_{v0}<1 MPa is controlled by increasing shear stresses in the soil sample while the shear strains to mobilise *S*=50% in CKUC remain approximately the same (Casey 2016 recommended an average value of $\gamma_{50\ Power\ CKUC\ NC}$ = 0.0005).

Reconstituted soil tests and Recompression tests on intact samples differ in the range of effective consolidation stresses applied just before commencing the shear stage of a triaxial test. This is because higher effective stresses are needed to establish a normally consolidated condition after the reconstitution process is complete – typically 1.5 or 2 times the "sampling" pressure applied in the consolidometer. A similar increase in effective stresses from estimated in-situ stresses is applied during the SHANSEP test procedure. Figure 4- 40 shows the vertical effective stresses applied in the tests reported by SERC (1989).

Figures 4- 41 and 4- 42 show the variation in $\gamma_{50\ Power\ CKUC}$ and $\gamma_{50\ Power\ CKUE}$ with σ'_{v0} for both reconstituted and intact test databases. Range of *OCR* for each test mode is listed in Table 4- 7. Tests from the same publication are identified by symbols; dotted lines indicate the parameters from the same series of reconstituted tests with equal maximum consolidation pressures and increasing *OCR*. Coloured

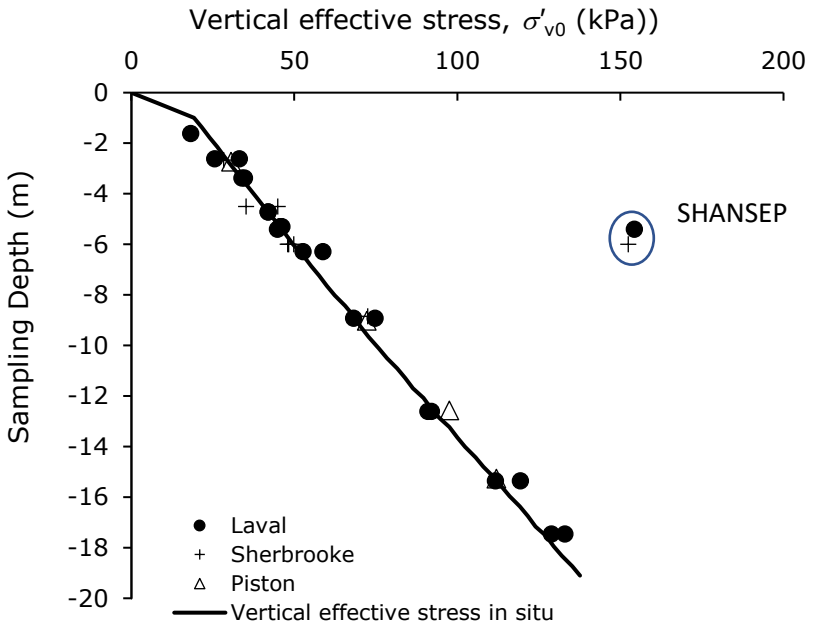

Figure 4- 40. Vertical effective stress in situ (digitised from Nash et al. 1992a) and applied to tests in BTK/TXCU-34

circles indicate tests with similar values of *OCR*. Test results from Abdulhadi (2009) – who studied the influence of consolidation stress level on stress-strain behaviour – is highlighted with a dashed line.

The dotted lines in Figure 4- 41 demonstrate a consistent trend of increasing $\gamma_{50\ \text{Power CKUC}}$ with decreasing σ'_{v0} (increasing *OCR*), that appears to be insensitive to the value of maximum consolidation pressure. There is large scatter of $\gamma_{50\ \text{Power}}$ from CKUC and CKUE tests on reconstituted soil tested at similar values of *OCR*, but little evidence of stress-dependency. Figure 4- 41 shows that where σ'_{v0}<1 MPa, the scatter is larger than the range in $\gamma_{50\ \text{Power CKUC}}$ observed by Casey (2016) as a result of one outlying value measured by Sheahan (1991) – also identified as an outlier in Figure 4- 19. Sheahan (1991) experimented with varying undrained shear strain rate which is a possible cause of CKUC parameter variation (see section 4.3.11). Figure 4- 41 suggests that one triaxial test measurement of $\gamma_{50\ \text{Power CKUC}}$ and *OCR* from a reconstituted test series (and applying the slope coefficient of Equation 4.3 in Table 4.5) may be a more accurate approach for estimating the other strain parameters in a test series than trying to establish a link between $\gamma_{50\ \text{Power CKUC}}$ and σ'_{v0}. Taking this approach would be more challenging for CKUE tests because the trend between $\gamma_{50\ \text{Power CKUC}}$ and *OCR* is more scattered within a single test series (Figure 4- 42) and on average (Equation 4.4 in Table 4.5).

Intact Bothkennar samples were reconsolidated following the Recompression procedure to a lower range of effective stresses than the reconstituted soils. The Recompression tests demonstrate more scatter in $\gamma_{50\ Power}$ than any dependence on effective stress. A comparison of SHANSEP and reconstituted test parameters shows that before shearing in compression, the intact specimen was consolidated to a vertical effective stress within the experimental stress range of reconstituted soils. At this stress level, the SHANSEP and reconstituted tests performed at *OCR*=1 show similar values of $\gamma_{50\ Power\ CKUC}$. CKUE tests on reconstituted soils were sheared at higher vertical effective stresses than the SHANSEP CKUE test and a comparison cannot be made. It is possible that the increase in σ'_{v0} within the first 3.5m (Figure 4- 40), and the associated reduction in apparent *OCR* (Figure 4- 25), produces a comparable but more inclined trend between $\gamma_{50\ Power}$ and σ'_{v0} in the Bothkennar clay than can be seen within the various test series on reconstituted soils. However, the deeper intact specimens show no apparent trend between $\gamma_{50\ Power}$ and σ'_{v0} in either CKUC or CKUE test modes.

It is well known that the undrained shear strength (c_u) varies with vertical effective stress (σ'_{v0}); the SHANSEP framework of strength characterisation is based upon a reliable correlation of the two parameters (Ladd et al. 1977, Mayne 1980). The database measurements of c_u are presented in Figures 4- 43 and 4- 44 as companion plots to Figures 4- 41 and 4- 42. As expected, a strong correlation exists between $c_{u\ NC}$ and σ'_{v0} for both CKUC tests (R^2 = 1.00) and CKUE tests (R^2 = 0.92). The best-fit correlations are described by power laws with exponents approximately equal to 1. A similar relationship is expected to exist between $E_{u\ 50\ CKUC}$ and σ'_{v0} since no stress-dependency of $\gamma_{50\ Power}$ could be identified. Reasons for the larger scatter of $\gamma_{50\ Power\ CKUE}$ require further investigation.

The ratio of regression coefficients between the two test modes indicates strength anisotropy in normally consolidated reconstituted soils $(c_{u\ NC}/\sigma'_{v0})_{CKUE} / (c_{u\ NC}/\sigma'_{v0})_{CKUC}$ = 0.39 and an average value of $c_{u\ NC}$ = 0.25. If a rough estimate of *OCR* is made from the extrapolated trend lines it would suggest the intact specimens to be lightly overconsolidated. The effect of SHANSEP versus Recompression procedures differs by test mode: $c_{u\ NC}/\sigma'_{v0\ CKUC}$ moves closer to the average reconstituted value whereas $c_{u\ NC}/\sigma'_{v0\ CKUE}$ increases.

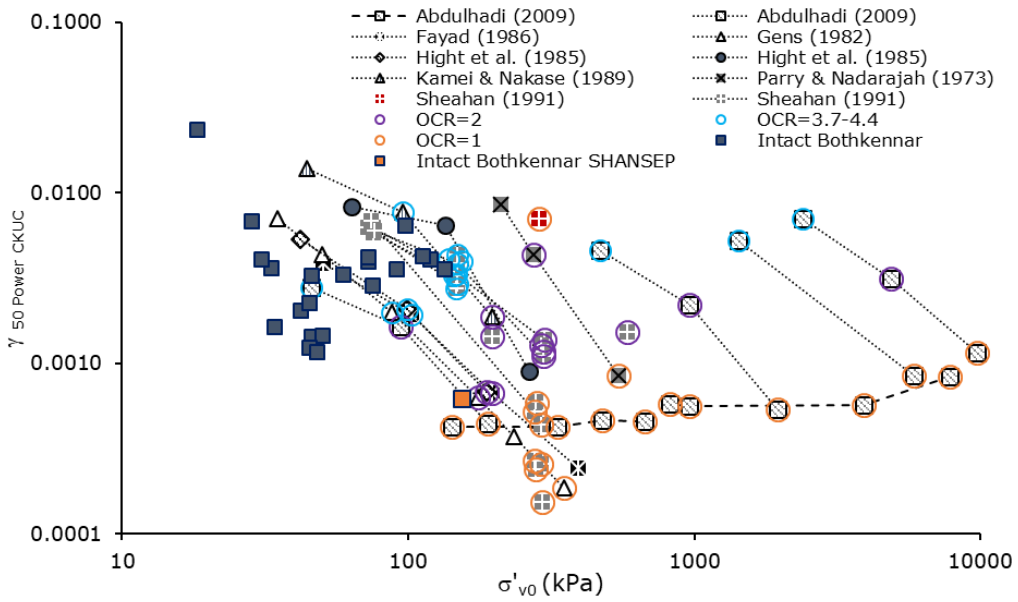

Figure 4- 41. Variation in $\gamma_{50\ Power\ CKUC}$ with present vertical effective consolidation stress σ'_{v0}

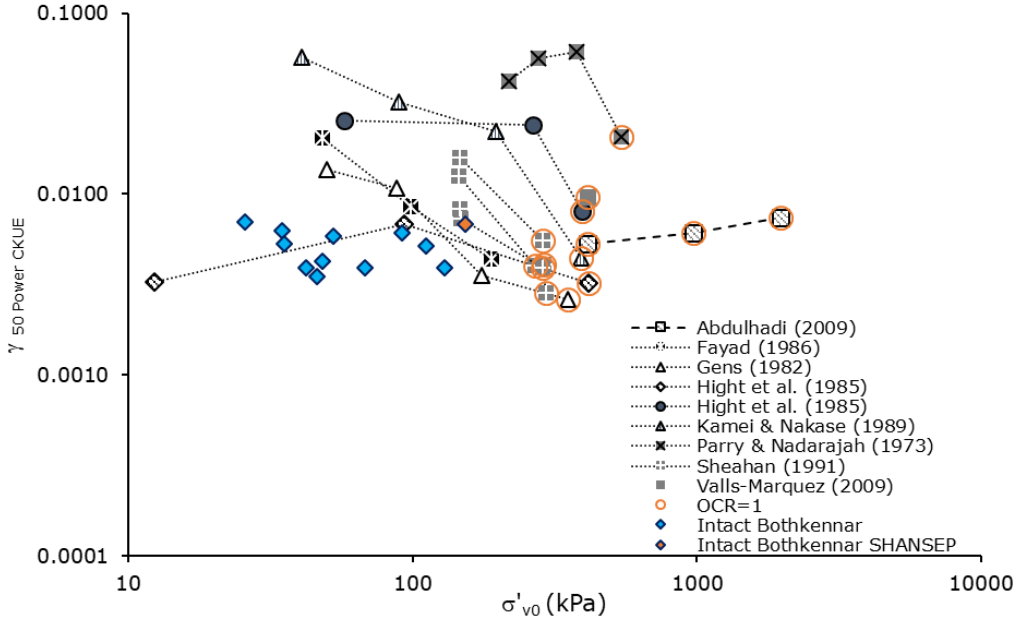

Figure 4- 42. Variation in $\gamma_{50\ Power\ CKUE}$ with present vertical effective consolidation stress σ'_{v0}

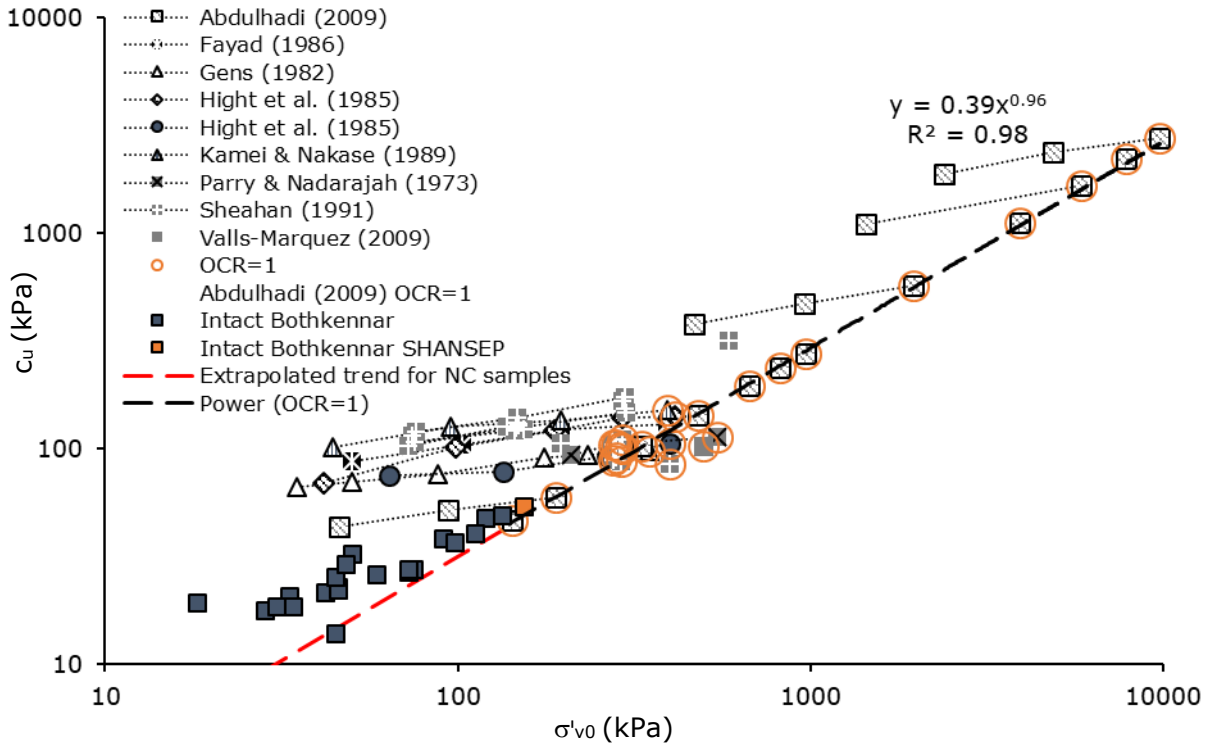

Figure 4- 43. Variation of undrained shear strength (c_u) with present vertical effective consolidation stress (σ'_{v0}) measured in CKUC triaxial tests

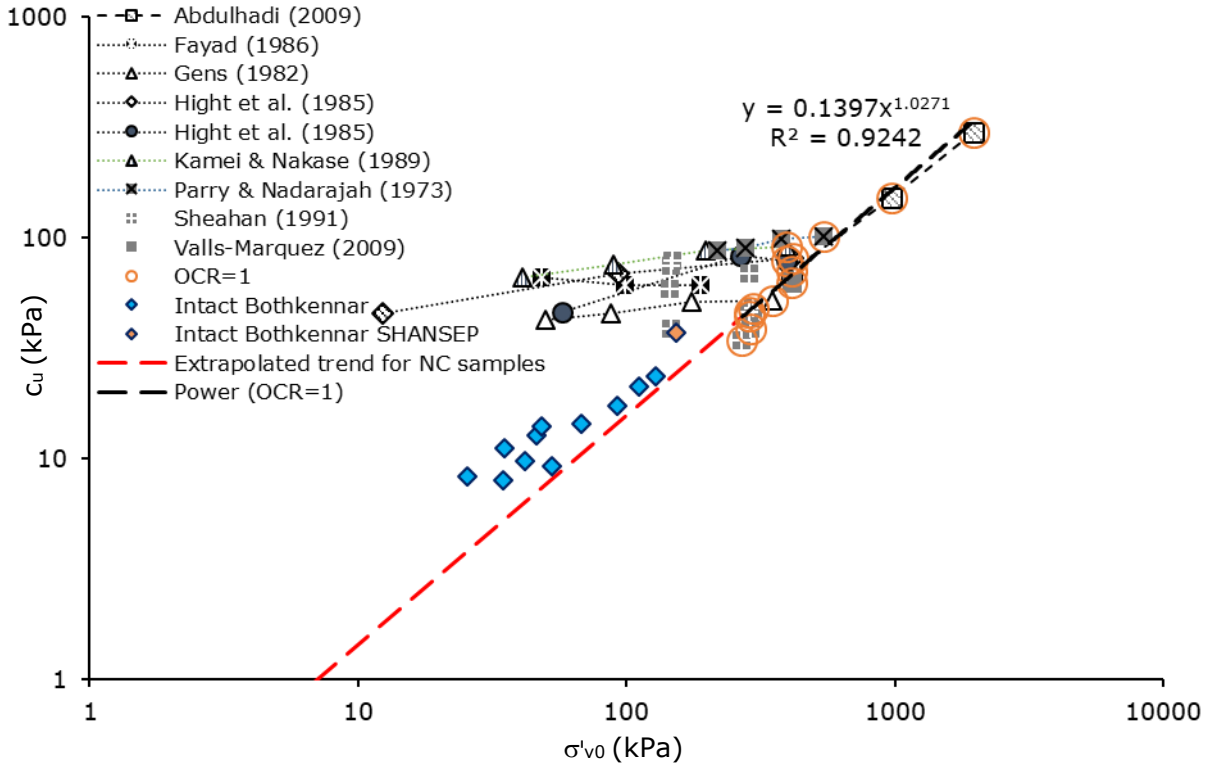

Figure 4- 44. Variation of undrained shear strength (c_u) with present vertical effective consolidation stress (σ'_{v0}) measured in CKUE triaxial tests

4.3.11 Influence of strain rate

To investigate the cause of variability shown by the normally consolidated parameters presented in Figures 4- 41 to 4- 44, the test data of specimens with *OCR*=1 are plotted against strain rate in Figures 4- 45 and 4- 46. For only 9 of the 34 tests on intact Bothkennar samples a strain rate was reported by SERC (1989) and the strain parameters from these tests are shown in Figure 4- 47.

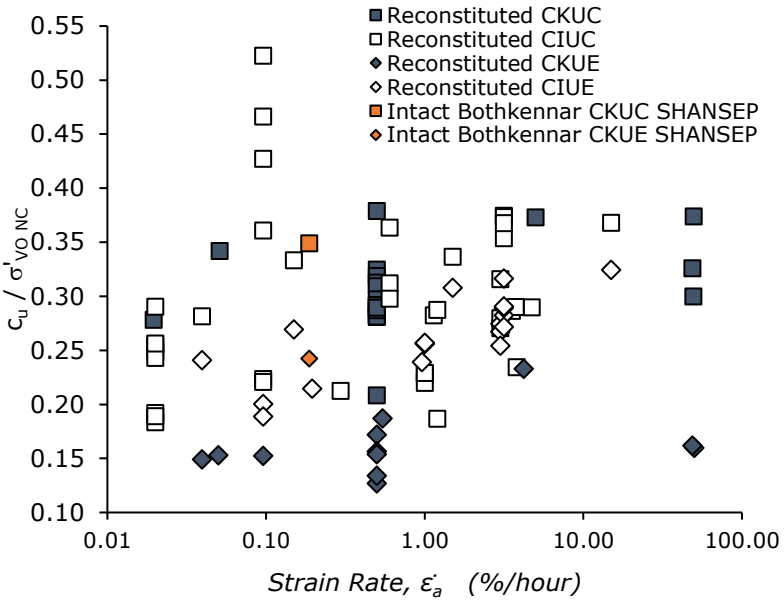

Figure 4- 45. Variation of normally consolidated strength ratio $c_u / \sigma'_{VO\ NC}$ with axial strain rate applied during undrained shear

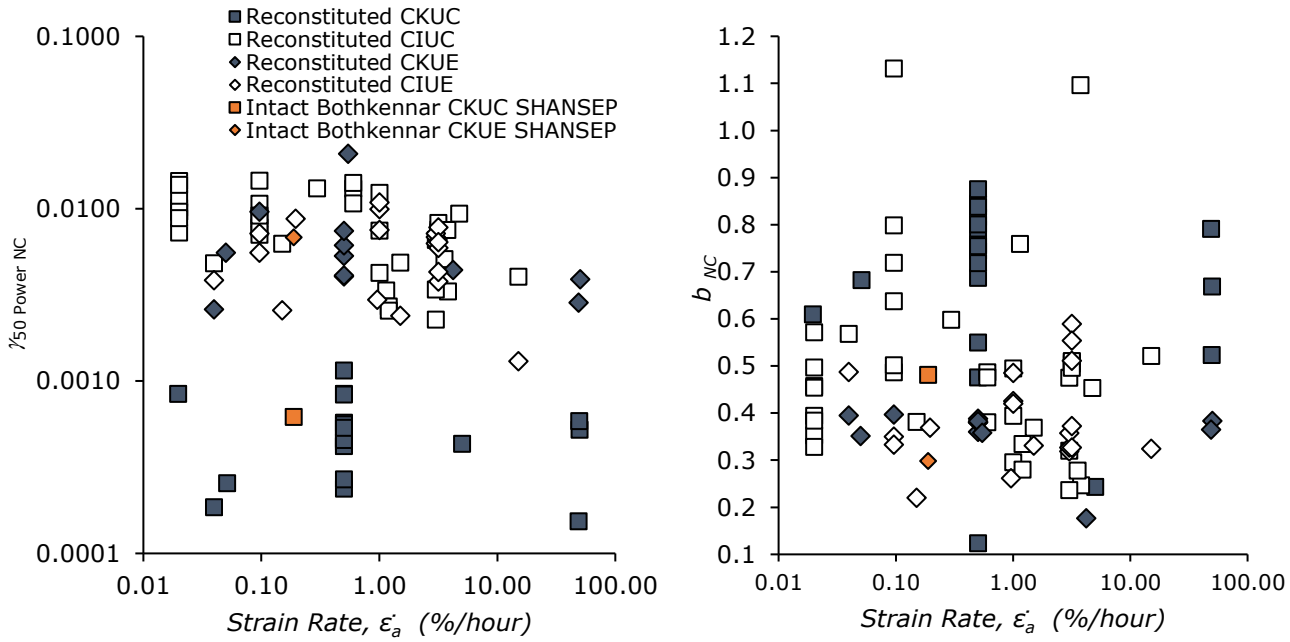

Figure 4- 46. Variation of $\gamma_{50\ Power\ NC}$ and b with axial strain rate applied during undrained shear

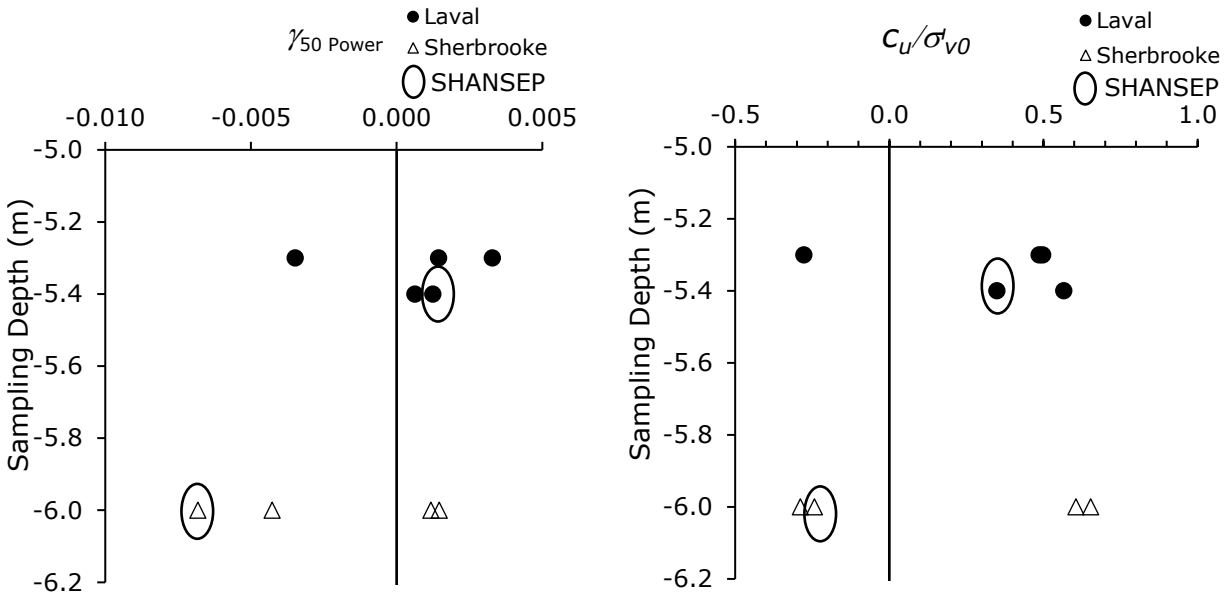

Specimens sampled from 5.3m were tested at $\dot{\varepsilon}_a$ =0.04%/hour. All others in the displayed depth range were tested at 0.19%/hour.

From 5.3 to 6.0 mbgl:

$\gamma_{50\ Power}$	Corresponding E_u
CKUC Min. = 0.0006	130.6 MPa
CKUC Max. = 0.0033	10.2 MPa
CKUE Min. = -0.0035	-5.50 MPa
CKUE Max. = -0.0068	-8.12 MPa

Figure 4- 47. Variation of $\gamma_{50\ Power}$ and c_u / σ'_{VO} with axial strain rate applied during undrained shear

Sheahan et al. (1996) demonstrated with an experimental programme of CKUC tests on reconstituted Boston Blue Clay that for normally and overconsolidated samples ($1 \leq OCR \leq 8$) an increase in undrained shear strength normalised by preconsolidation stress (c_u/σ'_{vc}) with strain rate was associated with suppressed shear-induced pore pressure and – in specimens only where OCR=1 or 2 – with a higher mobilised friction angle. (Note – the tests published by Sheahan et al. 1996 were included in the reconstituted database presented here using tabulated data from Sheahan's PhD thesis published in 1991 and represent 27 of 67 CKUC tests in RFG/TXCU-278). Normally consolidated specimens showed the greatest rate-dependency of 7 to 11.5% increase in c_u / $\sigma'_{VO\ NC}$ per log cycle $\dot{\varepsilon}_a$ (%/hour) (Sheahan et al. 1996). However, the same tests showed stress-strain curves that were rate-independent and unique to OCR when plotted using Mobilised Stress Ratio, $S = (\tau - \tau_0)/(c_u - \tau_0)$ (Sheahan et al. 1996).

The larger database of 20 reconstituted soils (excluding Hight et al. 1985 as strain rate information was unavailable) presented in Figures 4- 45 and 4- 46 shows that the strain rate effect on

c_u / $\sigma'_{VO\ NC}$ is not well represented by average trends in test data from a larger variety of soils and laboratories. Broadly the test data of each test mode in Figure 4- 45 do show an increase in c_u / $\sigma'_{VO\ NC}$ with strain rate except possibly those from CKUE tests. The scatter is highly variable particularly for CIUC tests. A decrease in $\gamma_{50\ Power\ NC}$ is observed at strain rates greater than 1%/hour but no trend is apparent for *b*-values with strain rate (Figure 4- 46). The scatter is large in all parameters and it is not possible to deduce reliable average modifier factors.

Smith et al. (1992) reported an increase of 5-7% in both c_u and "stiffness" with increased strain rate. Two strain rates were used in their experiments: $\dot{\varepsilon_a}$ =0.04%/hour and $\dot{\varepsilon_a}$ =0.19%/hour. The data plotted in Figure 4- 47 show an increase in c_u / $\sigma'_{VO\ CKUC}$ but no significant change in the CKUE tests. The strain parameter measured in compression indicates higher stiffness at S = 0.5 with higher strain rate but a larger change in $\gamma_{50\ Power}$ occurs within 0.1m with no change in strain rate. The accompanying increase in c_u between sampling depths of 5.4m-5.3m means that an over ten-fold increase in $E_{u\ 50\ Power}$ is found for samples tested over a depth interval of 0.1m. The reduction in $E_{u\ 50\ Power\ CKUE}$ observed from 5.3m to 6.0m appears to be the result of the destructuration process during consolidation using the SHANSEP procedure.

4.3.12 Influence of sampling disturbance

The effect of sampling disturbance on the Bothkennar clay was studied in detail by Clayton et al. (1992) by reconsolidating the samples under various stress paths and applying controlled cycles of strain. They showed that the variation of stiffness (normalised secant stiffness E_u/p'_0 at ε_a=0.1%) and peak stress (c_u) reduced progressively with larger strain amplitudes. In Figure 4- 48 and 4- 49 only five CKUC tests have magnitudes of $\gamma_{50\ Power}$ less than $\gamma = 1.5\varepsilon_a = 0.0015$ but from the few available tests there is no evidence that larger strain parameters were measured from Laval samples than from Sherbrooke samples. The other tests also do not show any obvious pattern of $\gamma_{50\ Power}$ with reducing sampling disturbance (in order of reducing sampling disturbance: Piston, Laval, Sherbrooke) but there is possibly an increase in *b* (Figure 4- 49). Differences in peak stress and stress-strain data were found in tests undertaken by City University and Imperial College to be explained by different procedures of

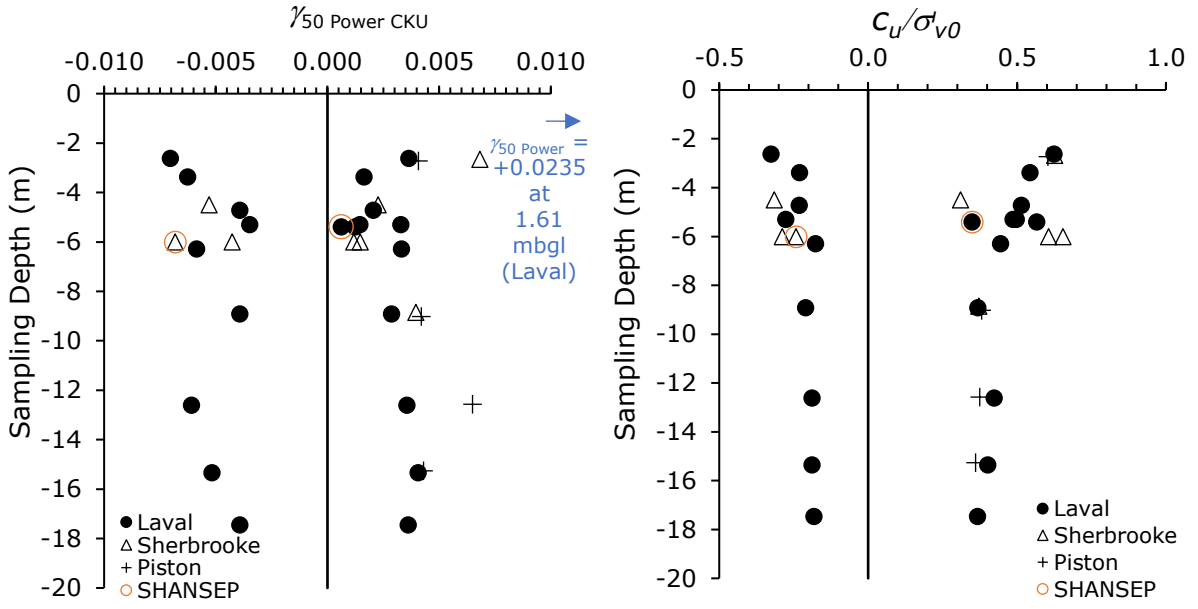

Figure 4- 48. Variation of $\gamma_{50\ Power}$ with sampling depth and sampling procedure (positive = triaxial compression; negative = triaxial extension)

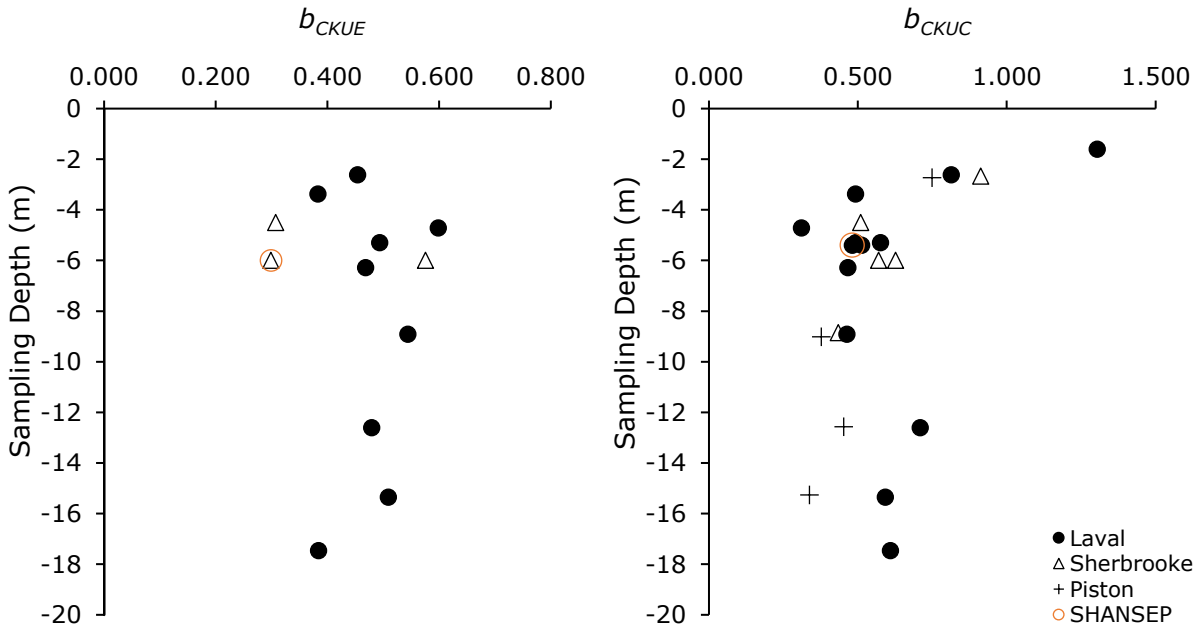

Figure 4- 49. Variation of *b* with sampling depth and sampling procedure

sampling and extrusion (Hight et al. 1992b). Consequently, reduced sampling disturbance has an observable effect on all of the parameters shown in Figure 4- 48: the Recompression test data shown between 5.3m and 6.0m in Figure 4- 48 (tests performed by Imperial College) have higher normalised peak strengths (c_u / σ'_{VO}), lower mobilised strains ($\gamma_{50\ Power}$), and higher *b*-values than the other test data.

Smith et al. (1992) showed that the Y3 yield surface of Sherbrooke tests was more extensive than the Y3 yield surface of Laval samples, and so this does not invalidate the idea proposed earlier that higher *b* values may be associated with an onset of Y3 yielding at higher values of $\gamma_{maxK}/\gamma_{50\ Power}$. With more test data on intact samples it may be possible to investigate the relationship of lower *b* values associated with more ductility and destructuration (demonstrated earlier with the limited number of SHANSEP tests on intact samples). Of course, this simplified characterisation of sampling disturbance effects on stress-strain would need to be clarified with an inspection of sample condition prior to testing (unavailable in the report) and an assessment of volumetric strains during reconsolidation stress paths (unavailable in the report for 25 of 34 tests) which may also vary according to specimen size and facies type (Hight et al. 1992b). The advantage of using an effective stress test database of reconstituted soils for characterising parameter variability is that the effect of sampling disturbance is not present.

4.3.13 Influence of plasticity

For engineers considering the use of published empirical correlations based on plasticity (or liquid limit, liquidity index, or other basic soil property measurement) for the selection of design parameters, a rational approach would be to consider test mode primarily before assessing the influence of plasticity. The following figures (4- 50 and 4- 51) have been plotted using this approach and the test

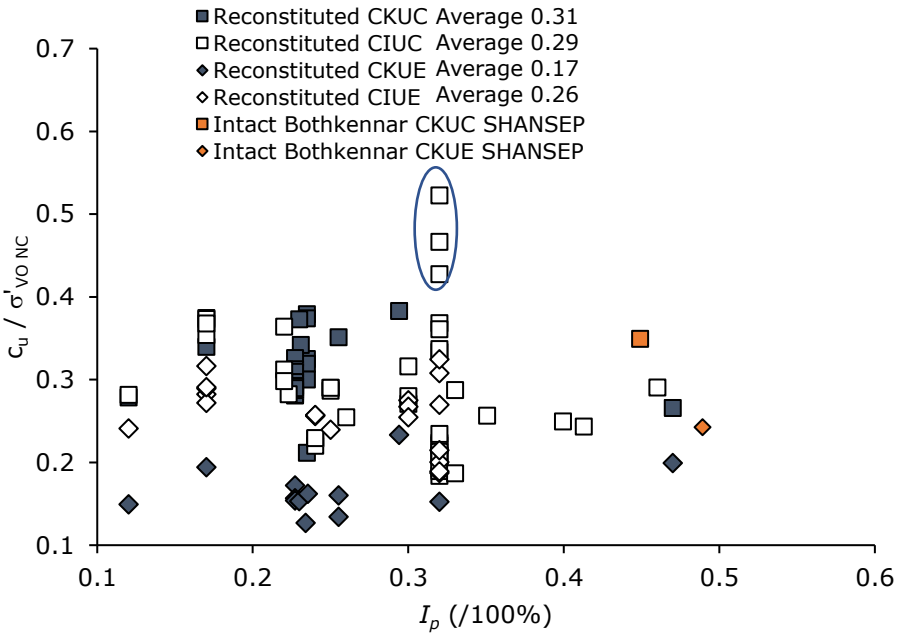

Figure 4- 50. Relationship between normalised undrained shear strength and plasticity index (I_P) for reconstituted soil samples normally consolidated under isotropic or K_0 conditions and sheared in undrained triaxial compression or extension (SHANSEP tests on intact Bothkennar clay included for comparison)

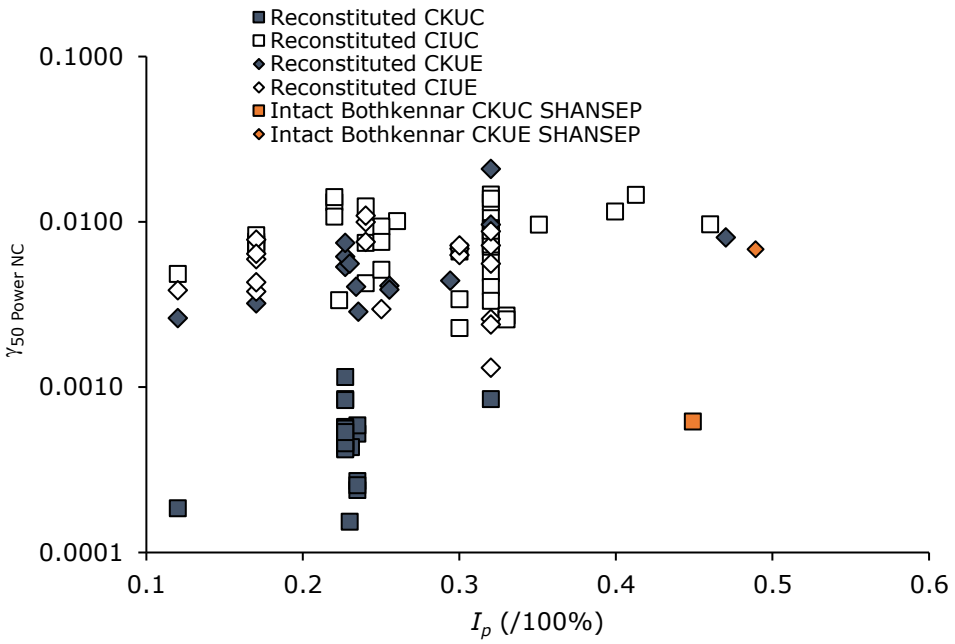

Figure 4- 51. Relationship between $\gamma_{50\ Power}$ and plasticity index (I_P) for reconstituted soil samples normally consolidated under isotropic or K_0 conditions and sheared in undrained triaxial compression or extension (SHANSEP tests on intact Bothkennar clay included for comparison)

modes demonstrate distinct bands (and means) of parameter values. However, the triaxial test measurements of $c_u / \sigma'_{VO\ NC}$ for reconstituted soils do not correlate with plasticity index (as it does for the field vane data of normally consolidated intact soils published by Skempton 1954, 1957). This is interesting because plasticity is a remolded soil property and it is unlikely to describe different types of structural modes and bonding between soil particles that result from depositional and geological aging/erosion processes (e.g., Won 2013). There is an apparent increase in both $\gamma_{50\ Power\ CKUE}$ and $c_u / \sigma'_{VO\ NC\ CKUE}$ with I_P but the sub-database of CKUE tests has the lowest number of data points.

The applied shear mode appears to influence $c_u / \sigma'_{VO\ NC}$ as the normalised compressive strengths generally exceed those measured in extension. Excluding apparent outliers (circled in Figure 4- 50), the overall range of undrained strength ratio varies between 0.13 and 0.38, which corresponds closely to the ranges obtained by Ladd (1991) and Jamiolkowski et al. (1985) from CKUC and CKUE tests on intact soft clay and silt samples which had been normally consolidated to a higher effective consolidation stress than the estimated in situ preconsolidation stress (i.e. following a SHANSEP consolidation procedure). CKUC test data from reconstituted samples and the intact sample shown in Figure 4- 50 match the expected range from the cited previous publications (0.27 to 0.38 and 0.25 to 0.37) excluding one value

from a kaolin specimen which appears to be unusually low. A mean value of $c_u / \sigma'_{VO\ NC\ CKUC}$ (0.31, excluding kaolin) closely corresponds to values calculated by Ladd (1991) and Jamiolkowski et al. (1985) to be 0.31 and 0.315. A tentative comparison with the triaxial compression test database presented by Chandler (1988) also indicates strong agreement of the mean; however, Chandler's data consists of specimens tested using either reconsolidation or SHANSEP procedures to obtain K_0-consolidated strength values and includes several 'corrected' results from isotropically consolidated samples.

The above comparison with previous studies gives some confidence in the test results presented in the normally consolidated database of CKU tests, although it would be valuable to compile a similar database of normally consolidated intact soil tests with measurements made following Recompression consolidation procedures both for CKU and CIU tests. A comparison with previous studies of overconsolidated soils was previously shown in Figure 4- 23. The difference in means calculated by test mode is useful here to identify the relative centres in distribution of the normally consolidated strength and strain parameters. It is observed in Figures 4- 50 and 4- 51 that the strength and strain anisotropy of normally consolidated reconstituted soils is more pronounced in CKU tests than CIU tests. Anisotropy is considered in further detail in section 4.4.

Figure 4- 52 shows that the plasticity and water content of the Bothkennar clay varies progressively with depth. Classification tests were reported for each of the triaxial test specimens (SERC 1989). Figure 4- 52 matches the profiles published from tests by Nash et al. (1992a) which also showed

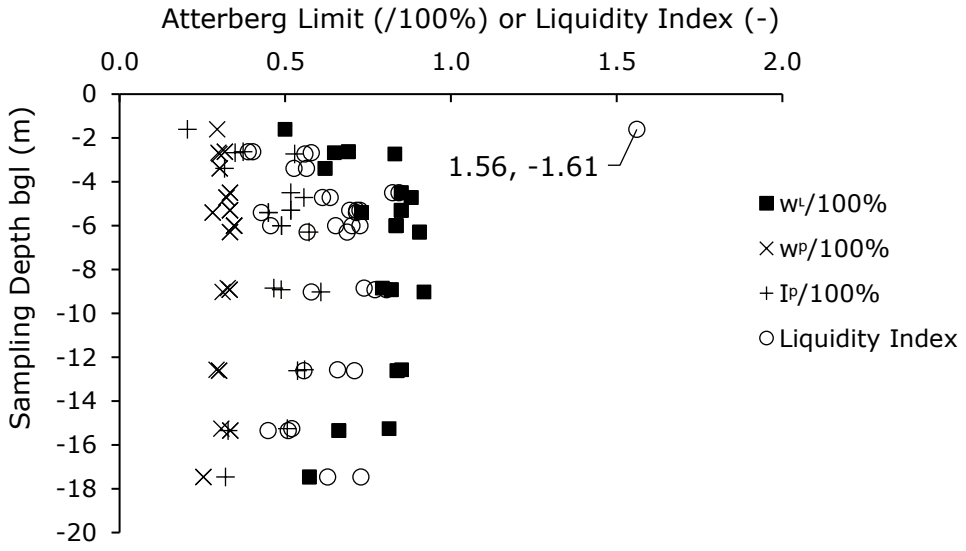

Figure 4- 52. Variation of classification test results reported for the triaxial test specimens in BTK/TXCU-34

reducing trend with depth. Hawkins et al. (1989) explained that the soft clay site at Bothkennar was selected for the research project funded by SERC because it was considered more uniform than other soft clay deposits in the UK. The depositional conditions are described as a "stable estuarine environment" (Nash et al. 1992a) at a water depth of 5 to 10m (Paul et al. 1992). The liquidity index test results in Figure 4- 52 show the considerable range in moisture content, which was found to be variable across the site, possibly linked to deposition conditions, and only weakly (positively) correlated with degree of mottling (Nash et al. 1992a). The upper 7-8m of the deposit are dominated by mottled facies with bedded layers occurring from approximately 5m and becoming more dominant between 8-20m below ground level (Paul et al. 1992). Weathering in the first 4m and mottling to 8m alters to some degree the sedimentation structures inherited from deposition, which may affect stiffness due to reduced particle bonding (Paul et al. 1992). Mottling is also associated with higher organic content (Paul et al. 1992); the same authors identified that w_L (and I_p) reduced by 10% after eliminating organic content by hydrogen peroxide treatment. A variation of 10% may explain to some degree the scatter of results shown in Figure 4- 14.

4.3.14 Multiple Linear Regression Analysis: influence of multiple experimental variables

It can be concluded from the previous sections that a significant relation exists between $\gamma_{50\ \mathrm{Power}}$ and *OCR* of reconstituted soils that is of similar form to the strength normalisation framework proposed by Ladd et al. (1977) and Mayne (1980). However, the evidence of greater scatter in Figure 4- 19 than Figure 4- 23 suggests that the variability of $\gamma_{50\ \mathrm{Power}}$ cannot be explained by *OCR* to the same extent as c_u / σ'_{VO}. A preliminary assessment of other possible explanatory variables including strain rate and plasticity index shows that any correlation with normally consolidated parameters ($c_u / \sigma'_{VO\ \mathrm{NC}}$, $\gamma_{50\ \mathrm{Power\ NC}}$, b_{NC}) is weak or absent. The expected correlation between $c_u / \sigma'_{VO\ \mathrm{NC\ CKUC}}$ and strain rate is very weak, which can only be explained by the larger variety of soil materials, specimen preparation procedures, testing procedures, and measurement interpretation procedures compared with those adopted by Sheahan et al. (1996) who used reconsituted samples of a single material (Boston Blue Clay) to demonstrate strain-rate dependency of $c_u / \sigma'_{VO\ \mathrm{CKUC\ NC}}$. Using plasticity index (I_p) as an indicator of material type did not suggest that a relationship existed with any of the normally consolidated parameters

($c_u / \sigma'_{VO\ NC}$, $\gamma_{50\ Power\ NC}$, $b_{\ NC}$). The model non-linearity parameter, b, may be representative of soil ductility and correlates weakly with the point of maximum curvature in the stress-strain curve expressed by the parameter $\gamma_{maxK}/\gamma_{50\ Power}$ in CKU tests. However, no correlation between $\gamma_{maxK}/\gamma_{50\ Power}$ and b was found in CIU tests.

Without further investigation, application of the simple correlations of the Power Law model parameters with *OCR* is arguably limited because of the uncertain effects of testing variations and material variability. Therefore, a multiple linear regression analysis was undertaken of the parameter database of reconstituted soils tests (including *OCR*=1) to investigate the following variables, in order: *OCR*, strain rate ($\dot{\varepsilon_a}$), liquid limit (w_L), and plastic limit (w_P). These four selected variables are independent (uncorrelated) so that the numerical results maintain accuracy. Additional single linear regressions between vertical effective consolidation stresses and the test variables were investigated. Table 4- 7 summarises the minima and maxima of all investigated variables by test mode. In the text, tested regression models are denoted as f(*variable 1, variable 2, variable 3, variable 4*).

Results of the multiple linear regression analysis are listed by dependent variable: c_u and c_u / σ'_{VO} (Table 4- 8), $\gamma_{50\ Power}$ (Table 4- 9), and b (Table 4- 10). Figures 4- 53, 4- 54, 4- 55, and 4- 56 illustrate the assessment of parameter variability based on the database correlations using predicted-measured plots and bandwidths of prediction error (Koutsoftas et al. 2017, Kootahi and Mayne 2017), using by example the CIUC test database. Factor errors (Equation 3.16) were calculated by the spread of 80% of the data points about the line of equality, hence representing the 10th and 90th percentiles of predicted data. Factor errors are a useful indicator of the added value of each regressor which is made visible by a contraction of the dotted lines towards the line of equality (see Figure 4- 54).

Figures 4- 53, 4- 54, 4- 55, and 4- 56 show that the peak strength parameters of CIUC tests are more sensitive than the deformation parameters to the selected explanatory variables. There is broad agreement with this outcome shown by the test data of the other test modes (Tables 4- 8, 4- 9, 4- 10). In all test modes, strain rate consistently reduces the factor error of predicted c_u / σ'_{VO} when *OCR* is included in the same regression model. Liquid limit has an effect only on c_u / σ'_{VO} measured in CIU tests; plastic limit offers no improvement to the model. It is interesting that the regression model of $b_{\ CIUE}$ decreases

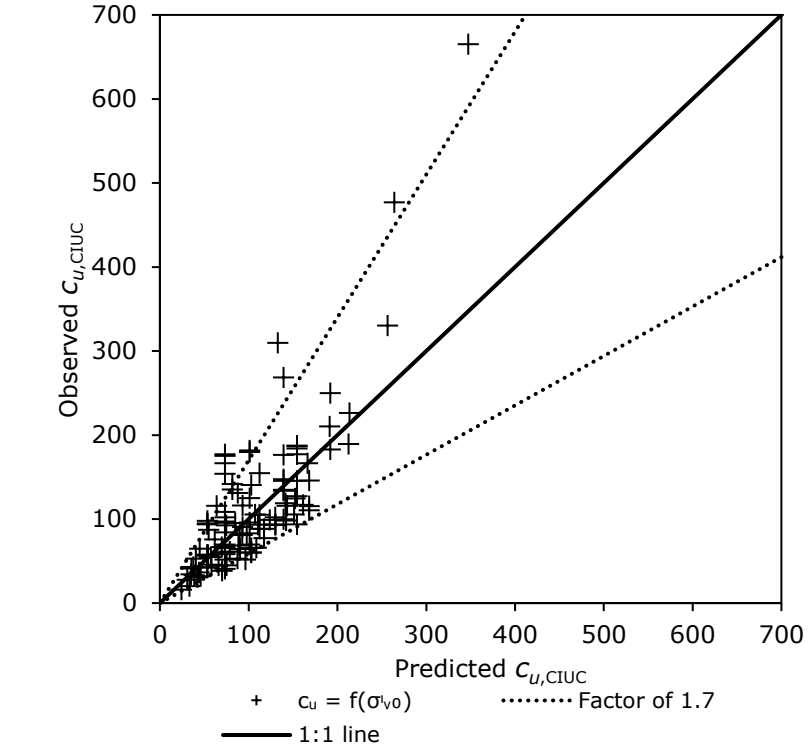

Figure 4- 53. Predicted-measured plots of $c_{u\ CIUC}$ (n=115 data points, RFG/TXCU-278) predicted using the best-fit single linear regression with σ'_{v0}

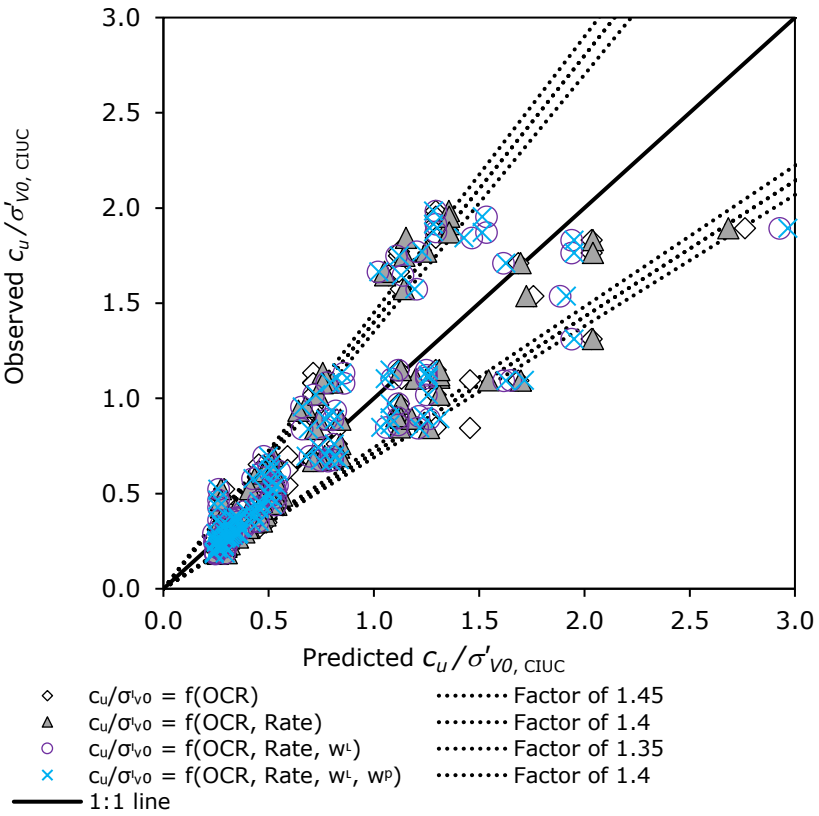

Figure 4- 54. Predicted-measured plots of $c_{u\ CIUC}/\sigma'_{v0}$ (n=115 data points, RFG/TXCU-278) predicted using best-fit single and multiple linear regression equations with the following variables: *OCR*, strain rate ($\dot{\varepsilon_a}$), w_L and w_P (see Table 4- 8)

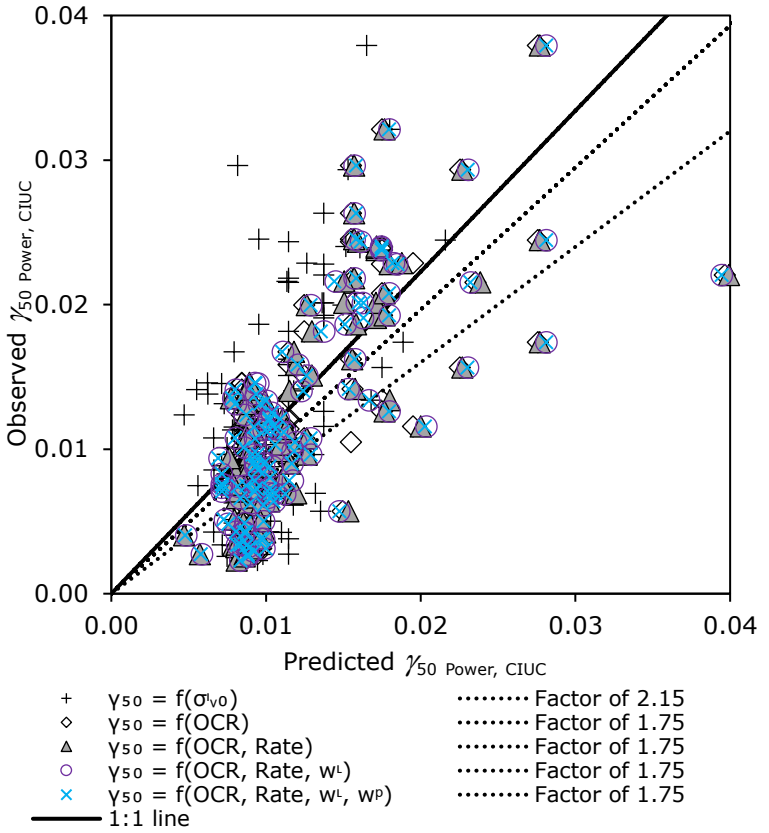

Figure 4- 55. Predicted-measured plots of $\gamma_{50\ Power,\ CIUC}$ (n=114 data points, RFG/TXCU-278) predicted using best-fit single and multiple linear regression equations with the following variables: σ'_{v0}, *OCR*, strain rate ($\dot{\varepsilon_a}$), w_L and w_P (see Table 4- 9)

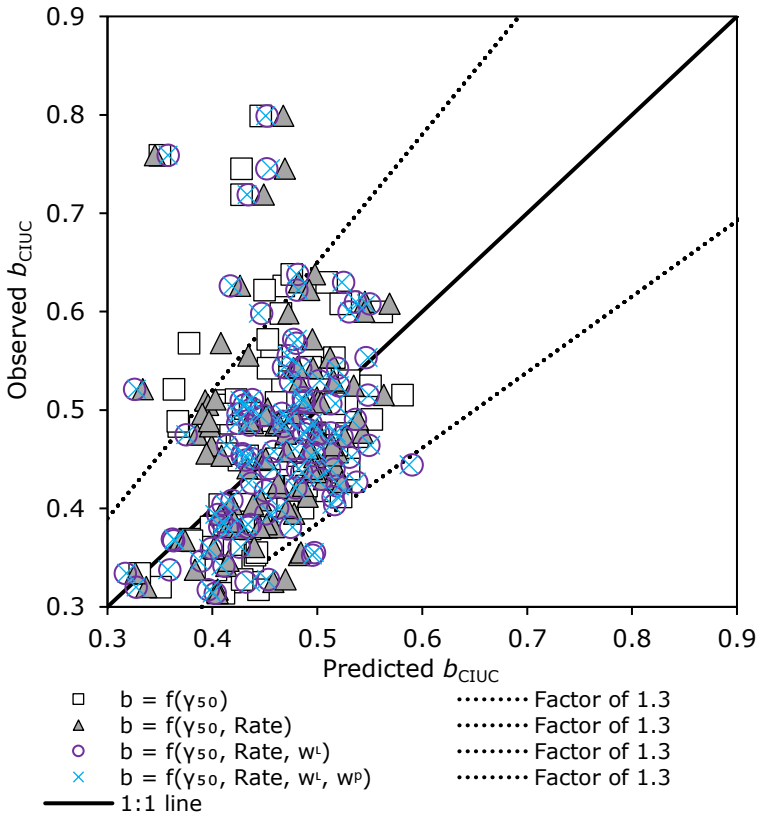

Figure 4- 56. Predicted-measured plots of b_{CIUC} (n=114 data points, RFG/TXCU-278) predicted using best-fit single and multiple linear regression equations with the following variables: $\gamma_{50\ Power,\ CIUC}$, strain rate ($\dot{\varepsilon_a}$), w_L and w_P (see Table 4- 10)

in bias, COV, and factor error by introducing more independent variables to the model (Table 4- 10) but this is not shown for the other test modes. It is concluded that for the purpose of developing practical correlations, b is insensitive to all variables except $\gamma_{50\ \mathrm{Power}}$ (the plotted data can be viewed in Figures 4- 34 and 4- 35). Only triaxial extension tests (not compression tests) demonstrate that $\gamma_{50\ \mathrm{Power}}$ is sensitive to strain rate, liquid limit and plastic limit in addition to *OCR* (Table 4- 9).

However, the low factor error of $\gamma_{50\ \mathrm{Power\ CIUE}}$ = f(*OCR*, *Strain rate*, w_L, w_P) is misleading; introducing w_P to the multiple linear regression model decreases factor error and simultaneously increases bias and COV. There is also a marked shift in the value of regression coefficients for *OCR*, *Strain rate* and w_L; holding all other independent variables constant, the proportionate change in $\gamma_{50\ \mathrm{Power\ CIUE}}$ caused by increasing the value of one independent variable from its minimum to maximum (Table 4- 7) is very different to the changes seen in the regression model excluding w_P. Using the same logic, the regression models for $\gamma_{50\ \mathrm{Power\ CKUC}}$ and $\gamma_{50\ \mathrm{Power\ CKUE}}$ show that strain rate becomes significant only when w_L and w_P are included and this implies that the multiple linear regression model is overfitting the data. This assertion is supported by a lack of agreement of CIUC and CIUE tests regarding the significance of multiple linear regressors as these tests would be expected to show more similar patterns in stress-strain behaviour than CKU tests. This is because the isotropically consolidated materials are expected to be less inherently anisotropic than CKU specimens and because no stress-induced anisotropy occurs during shear (i.e. $\tau_0 = 0$). For these reasons, it is concluded that the variance of $\gamma_{50\ \mathrm{Power}}$ for the tests in RFG/TXCU-278 is related primarily to *OCR* and the residual variation expressed by standard error and factor error of $\gamma_{50\ \mathrm{Power}}$ = f(*OCR*) cannot be explained by s*train rate*, w_L, or w_P.

Analysing the parameters of RFG/TXCU-278 in this way leads to an important observation: the influence of testing variations other than strain rate outweigh the influence of strain rate, w_L, and w_P in controlling the variability of c_u/σ'_{VO}, $\gamma_{50\ \mathrm{Power}}$, and b. Strain rate reduces the factor error of c_u/σ'_{VO} by a factor of 0.10 but the factor error remains between 1.15 and 1.4 after accounting for w_L and w_P. Since none of the independent variables demonstrate a consistent reduction in factor error of $\gamma_{50\ \mathrm{Power}}$, and of b, the factor errors of the single linear regressions are indicative of the parameter variability caused by variations in test method. Another explanation could be that the material strongly influences the

parameters and that w_L and w_P are not good indicators of variable material composition. However, w_L improved the regression models of c_u/σ'_{VO} in CIU test modes and so this implies that w_L is a reasonable indicator of soil composition (despite the evidence that $c_u/\sigma'_{VO\ \mathrm{CKU}}$ is insensitive to w_L which suggests that CKU strength variation in reconstituted soils is more closely linked to stress-induced anisotropy). Overall, the author judges the influence of testing variation and measurement uncertainty to be the dominant cause of parameter variability (expressed as factor error) about the identified transformation models of c_u/σ'_{VO} = f(*OCR*, *Strain rate*), $\gamma_{50\ \mathrm{Power}}$ = f(*OCR*) and b = f($\gamma_{50\ \mathrm{Power}}$).

4.3.15 Calculated uncertainty of using parameter transformation models to predict stress-strain

The previous section demonstrated a method to identify causes of parameter variability by comparing different transformation models. A similar approach is adopted in this section to quantify uncertainty of using parameter transformation models to predict stress-strain behaviour. The following parameter transformation models were adopted:

$$\gamma_{50\ \mathrm{Power\ CIUC}} = 0.039\sigma'^{-0.263}_{v0} \quad \text{and, mean } b_{\mathrm{CIUC}} = 0.46 \tag{4.10}$$

$$\gamma_{50\ \mathrm{Power\ CIUC}} = 0.0074+0.0010\,OCR \quad \text{and, mean } b_{\mathrm{CIUC}} = 0.46 \tag{4.11}$$

$$\gamma_{50\ \mathrm{Power\ CIUC}} = 0.0074+0.0010\,OCR \quad \text{and, } b_{\mathrm{CIUC}} = 1.153\gamma_{50\ \mathrm{Power\ CIUC}}^{0.209} \tag{4.12}$$

$$\gamma_{50\ \mathrm{Power\ CIUE}} = 0.022\sigma'^{-0.208}_{v0} \quad \text{and, mean } b_{\mathrm{CIUE}} = 0.40 \tag{4.13}$$

$$\gamma_{50\ \mathrm{Power\ CIUE}} = 0.0042+0.0013\,OCR \quad \text{and, mean } b_{\mathrm{CIUE}} = 0.40 \tag{4.14}$$

$$\gamma_{50\ \mathrm{Power\ CIUE}} = 0.0042+0.0013\,OCR \quad \text{and, } b_{\mathrm{CIUE}} = 0.724\gamma_{50\ \mathrm{Power\ CIUE}}^{0.127} \tag{4.15}$$

$$\gamma_{50\ \mathrm{Power\ CKUC}} = 0.012\sigma'^{-0.358}_{v0} \quad \text{and, mean } b_{\mathrm{CKUC}} = 0.58 \tag{4.16}$$

$$\gamma_{50\ \mathrm{Power\ CKUC}} = 0.00049\,OCR^{1.35} \quad \text{and, mean } b_{\mathrm{CKUC}} = 0.58 \tag{4.17}$$

$$\gamma_{50\ \mathrm{Power\ CKUC}} = 0.00049\,OCR^{1.35}$$

$$\text{and, } b_{\mathrm{CKUC}} = 0.168\text{-}0.149\log_{10}(\gamma_{50\ \mathrm{Power\ CKUC}}) \tag{4.18}$$

$$\gamma_{50\ \mathrm{Power\ CKUE}} = 0.026\sigma'^{-0.185}_{v0} \quad \text{and, mean } b_{\mathrm{CKUE}} = 0.35 \tag{4.19}$$

$$\gamma_{50\ \mathrm{Power\ CKUE}} = 0.0038\,OCR \quad \text{and, mean } b_{\mathrm{CKUE}} = 0.35 \tag{4.20}$$

$$\gamma_{50\ \mathrm{Power\ CKUE}} = 0.0038\,OCR$$

$$\text{and, } b_{\mathrm{CKUE}} = 0.571+0.110\log_{10}(\gamma_{50\ \mathrm{Power\ CKUE}}) \tag{4.21}$$

Equations 4.10 to 4.21 were used to predict all stress-strain data in RFG/TXCU-278 between $0.2 \leq S \leq 0.8$ (n = 5199 for all test modes combined, see Table 4- 1). Predicted data are plotted against the "measured" (digitised or tabulated) data in Figures 4- 57 to 4- 68. Three parameters are used to demonstrate the effect of transformation modelling error: S, γ and $G_{sec}/(c_u - \tau_0)$, where G_{sec} is the secant undrained shear modulus and $G_{sec}/(c_u - \tau_0)$ is referred to as normalised secant modulus. The following observations can be made from Figures 4- 57 to 4- 68.

Comparing the factor errors of $\gamma_{50\ Power} = f(\sigma'_{v0})$ with those of $\gamma_{50\ Power} = f(OCR)$ for each test mode demonstrates a consistent reduction in error of the predicted stress-strain data when OCR is included in the parameter transformation model in place of σ'_{v0}. This result is to be expected on the basis of stronger correlations existing between $\gamma_{50\ Power}$ and OCR than between $\gamma_{50\ Power}$ and σ'_{v0} (Table 4- 9). The results in Figures 4- 57 to 4- 68 provide no evidence that it is more beneficial (less uncertain) to use b-values estimated from $b = f(\gamma_{50\ Power})$ where $\gamma_{50\ Power} = f(OCR)$, than from the mean b-value of the test mode.

All parameter transformation models are biased i.e. the mean factor error calculated for the predicted data points using Equations 4.10 to 4.21 is not equal to unity. However, the degree of bias varies with the test mode and with the parameter being predicted by the model. It is also shown here that the definition of bias for large databases of stress-strain measurements is better described by the median. Lower bias would be expected with a higher number of data points (Ching and Phoon 2014b); this can be examined by comparing bias of CIUC test data with CIUE test data. The CIUC regression models (Equations 4.10, 4.11, and 4.12) are unexpectedly more biased when using the mean to calculate bias than predicting CIUE data (using Equations 4.13, 4.14, and 4.15). However, when the median is used to calculate bias of the predicted data, the predicted data of CIUC tests are less biased than CIUE tests. Calculating both the median and mean factor errors provides a better statistical summary of the centre of the distribution than calculating the mean alone. Bias is evidently inappropriate for summarising the spread in error of the predicted stress-strain data. The calculated median and 10th and 90th percentiles, also plotted in Figures 4- 57 to 4- 68, demonstrate a way of describing errors in predicted stress-strain data that reflects the skew and centre of the distribution.

It could be viewed as quite plausible that the reason for the need to use median instead of mean is a direct consequence of the model fitting error of the Power Law model on the individual test data points. However, in section 4.2 it was shown that the Power Law modelling error skews the data towards underpredicting S and overpredicting γ for test measurements taken between S=30-70% but the overall mean bias of the predicted database is approximately 1.0 (Table 4- 1). This is reproduced by part (d) of all Figures 4-57 to 4- 68 and the median bias is also included for comparison. In almost every part (d) of Figures 4-57 to 4- 68, the median and mean bias are close to 1.0 but the values do not agree. The use of median bias in (d) sub-figures indicates that the modelling error of the Power Law skews the prediction on average by up to 4% from the line of equality.

The use of $G_{sec}/(c_u - \tau_0)$ as a stress-strain parameter demonstrates the combined effect of transformation modelling error on predictions of S and γ. In all test modes, the use of transformation models results in a significant bias towards underpredicting secant modulus. CIU transformation models are less biased in predicting γ than CKU transformation models which tend to more significantly underestimate γ measured between $0.2 \leq S \leq 0.8$. The resulting bias of $G_{sec}/(c_u - \tau_0)_{\text{CKU}}$ indicates that on average the secant modulus is underestimated.

This analytical approach demonstrates that a factor error of up to 8 (overpredicted) and 3 (underpredicted) can result from using transformation models Equations 4.11, 4.14, 4.17, and 4.20 to predict normalised secant modulus measured during undrained triaxial stress-strain tests. Factor error is calculated from the 10^{th} and 90^{th} percentiles to encompass 80% of the data points. Calculated factor error varies with test mode with the largest error displayed by CKUE test data. By comparing the factor errors in parts (b) and (d) in all Figures 4-57 to 4- 68, it is possible to quantify the error range associated with using the parameter transformation models to estimate stress-strain behaviour. If the Power Law model parameters were to be used in designs for characterising stress-strain behaviour and the transformation models of Equations 4.11, 4.14, 4.17, and 4.20 were adopted to estimate variation of stress-strain behaviour with shear mode and *OCR*, then the design calculations may acknowledge that between 12% (CIUC) and 29% (CKUC) of the error associated with the transformation model is attributed to the model fitting error of the Power Law.

Table 4- 7. Minimum and maximum parameter values of the reconstituted test database by test mode

Test Mode	Min c_u	Max c_u	Min c_u/σ'_{v0}	Max c_u/σ'_{v0}	Min γ_{50} Power	Max γ_{50} Power	Min b	Max b	Min σ'_{vm}	Max σ'_{vm}	Min σ'_{v0}	Max σ'_{v0}	Min OCR	Max OCR	Min *Rate*	Max *Rate*	Min w_L	Max w_L	Min w_P	Max w_P
Units	kPa	kPa	-	-	-	-	-	-	kPa	kPa	kPa	kPa	-	-	%/hour	%/hour	/100%	/100%	/100%	/100%
CIUC	15.9	665.1	0.18	1.98	0.0023	0.0379	0.23	1.13	105.0	2900.0	9.0	2900.0	1.0	32.0	0.020	15.0	0.25	0.74	0.13	0.42
CIUE	32.4	745.4	0.19	1.66	0.0013	0.0252	0.22	0.59	125.0	2900.0	20.7	2900.0	1.0	12.0	0.039	15.0	0.25	0.72	0.13	0.40
CKUC	43.6	2742.2	0.21	2.30	0.00015	0.0138	0.12	1.13	142.0	9743.0	35.0	9743.0	1.0	10.0	0.005	53.8	0.25	0.72	0.13	0.40
CKUE	34.15	301.78	0.127	3.679	0.0026	0.0567	0.18	0.75	209.2	1961.0	12.3	1961.0	1.0	9.6	0.039	50.6	0.25	0.7	0.13	0.40

Table 4- 8. Multiple Linear Regression of c_u/σ'_{v0}

Test Mode	Regression model	R^2	S.E.	p-value	Data within error bounds:	± %Error	Factor Error	Bias	COV	Proportionate change in the independent variable, Y: max(X1)-min(X1)	max(X2)-min(X2)	max(X3)-min(X3)	max(X4)-min(X4)
CIUC n=115	$c_u = 0.854\sigma'^{0.764}_{vm}$	0.58	0.177	<0.001	81%	50	1.75	0.87	0.48	0.68	-	-	-
	$c_u = 8.80\sigma'^{0.461}_{v0}$	0.65	0.160	<0.001	81%	45	*1.7*	1.0	0.4	0.71	-	-	-
	$c_u = 0.109\sigma'_{vm} + 0.144\sigma'_{v0}$	0.86	32.39	<0.001	81%	51	1.6	0.98	0.24	0.47	0.64	-	-
	$c_u/\sigma'_{v0} = 0.288OCR^{0.653}$	0.86	0.114	<0.001	81%	45	*1.45*	0.88	0.17	0.95	-	-	-
	$c_u/\sigma'_{v0} = 0.298OCR^{0.639}Rate^{0.038}$	0.87	0.112	<0.001	80%	35	*1.4*	0.87	0.16	0.93	0.10	-	-
	$c_u/\sigma'_{v0} = 0.248OCR^{0.635}Rate^{0.036}w_L^{-0.309}$	0.88	0.105	<0.001	80%	35	*1.35*	0.87	0.15	0.93	0.10	-0.14	-
	$c_u/\sigma'_{v0} = 0.213OCR^{0.632}Rate^{0.040}w_L^{-0.085}w_P^{-0.224}$	0.88	0.105	<0.001	80%	35	*1.4*	0.85	0.15	0.92	0.11	-0.04	-0.11
CIUE n=55	$c_u = 0.617\sigma'^{0.822}_{vm}$	0.78	0.124	<0.001	80%	40	1.45	1.04	0.27	0.82	-	-	-
	$c_u = 8.843\sigma'^{0.456}_{v0}$	0.59	0.171	<0.001	80%	50	*1.65*	1.08	0.41	0.72	-	-	-
	$c_u = 0.109\sigma'_{vm} + 0.153\sigma'_{v0}$	0.96	22.35	<0.001	80%	35	1.4	1.15	0.22	0.42	0.62	-	-
CIUE n=55	$c_u/\sigma'_{v0} = 0.267OCR^{0.729}$	0.92	0.083	<0.001	80%	25	*1.30*	1.02	0.18	0.83	-	-	-
	$c_u/\sigma'_{v0} = 0.271OCR^{0.719}Rate^{0.053}$	0.94	0.074	<0.001	80%	25	*1.25*	1.01	0.16	0.82	0.15	-	-
	$c_u/\sigma'_{v0} = 0.252OCR^{0.717}Rate^{0.057}w_L^{-0.110}$	0.94	0.073	<0.001	80%	25	*1.2*	1.01	0.16	0.82	0.16	-0.05	-
	$c_u/\sigma'_{v0} = 0.191OCR^{0.715}Rate^{0.055}w_L^{0.301}w_P^{-0.413}$	0.94	0.072	<0.001	80%	25	*1.2*	1.01	0.15	0.82	0.15	0.15	-0.21
CKUC n=74	$c_u = 0.344\sigma'^{0.953}_{vm}$	0.95	0.094	<0.001	80%	30	1.35	0.92	0.24	0.97	-	-	-
	$c_u = 3.842\sigma'^{0.655}_{v0}$	0.76	0.20	<0.001	80%	60	*1.75*	1.13	0.43	0.89	-	-	-
	$c_u = 0.174\sigma'_{vm} + 0.111\sigma'_{v0}$	0.997	28.63	<0.001	80%	30	1.3	1.07	0.20	0.62	0.40	-	-
	$c_u/\sigma'_{v0} = 0.300OCR^{0.790}$	0.94	0.066	<0.001	80%	20	*1.2*	0.99	0.19	0.76	-	-	-
CKUC n=65	$c_u/\sigma'_{v0} = 0.305OCR^{0.786}Rate^{0.032}$	0.96	0.058	<0.001	80%	15	*1.15*	1.01	0.16	0.75	0.12	-	-
	$c_u/\sigma'_{v0} = 0.258OCR^{0.773}Rate^{0.038}w_L^{-0.224}$	0.96	0.054	<0.001	80%	15	*1.15*	1.01	0.16	0.74	0.15	-0.10	-
	$c_u/\sigma'_{v0} = 0.169OCR^{0.758}Rate^{0.031}w_L^{0.371}w_P^{-0.598}$	0.96	0.053	<0.001	80%	15	*1.15*	1.01	0.15	0.73	0.12	0.16	-0.28
CKUE n=34	$c_u = 0.252\sigma'^{0.924}_{vm}$	0.77	0.088	<0.001	79%	30	1.30	1.02	0.20	0.95	-	-	-
	$c_u = 19.0\sigma'^{0.241}_{v0}$	0.32	0.153	<0.001	79%	40	1.50	1.06	0.36	0.56	-	-	-
	$c_u = 0.141\sigma'_{vm} + 0.021\sigma'_{v0}$	0.98	13.5	<0.001	79%	25	1.30	1.06	0.20	0.92	0.15	-	-
	$c_u/\sigma'_{v0} = 0.165OCR^{0.952}$	0.94	0.087	<0.001	79%	25	1.30	1.02	0.20	0.80	-	-	-
CKUE n=28	$c_u/\sigma'_{v0} = 0.163OCR^{0.931}\ Rate^{0.025}$	0.95	0.076	<0.001	81%	25	1.25	1.01	0.18	0.83	0.07	-	-
	$c_u/\sigma'_{v0} = 0.189OCR^{0.948}Rate^{0.012}w_L^{0.210}$	0.95	0.074	<0.001	81%	20	1.25	1.01	0.17	0.84	0.03	0.09	-
	$c_u/\sigma'_{v0} = 0209\ OCR^{0.948}Rate^{0.014}w_L^{0.043}w_P^{0.156}$	0.95	0.075	<0.001	81%	20	1.25	1.01	0.17	0.84	0.04	0.02	0.07

Table 4- 9. Multiple Linear Regression of $\gamma_{50\ Power}$

										Proportionate change in the independent variable, Y			
Test Mode	Regression model	R^2	S.E.	*p*-value	Data within error bounds	± %Error	Factor Error	Bias	COV	max(X1)-min(X1)	max(X2)-min(X2)	max(X3)-min(X3)	max(X4)-min(X4)
CIUC *n*=114	$\gamma_{50\ Power} = 0.00147\sigma'^{0.314}_{vm}$	0.09	0.266	<0.01	81%	75	2.4	1.48	0.64	0.37	-	-	-
	$\gamma_{50\ Power} = 0.039\sigma'^{-0.263}_{v0}$	0.20	0.249	<0.001	81%	70	2.15	1.30	0.47	-0.54	-	-	-
	$\gamma_{50\ Power} = 0.0074+0.0010OCR$	0.51	0.005	<0.001	81%	60	1.75	1.03	0.40	0.88	-	-	-
	$\gamma_{50\ Power} = 0.0080+0.0010OCR -0.00028Rate$	0.53	0.005	<0.001	81%	55	1.75	1.02	0.39	0.87	-0.12	-	-
	$\gamma_{50\ Power} = 0.0054+0.0010OCR -0.00028Rate+0.0044w_L$	0.53	0.005	<0.001	81%	55	1.75	1.03	0.40	0.88	-0.12	0.06	-
	$\gamma_{50\ Power} = 0.0054+0.0010OCR -0.00029Rate-0.0032w_L+0.0024w_P$	0.53	0.005	<0.001	81%	55	1.75	1.04	0.40	0.88	-0.12	0.04	0.02
CIUE *n*=55	$\gamma_{50\ Power} = 0.00049\sigma'^{0.449}_{vm}$	0.21	0.247	<0.001	80%	70	1.95	1.17	0.60	0.48	-	-	-
	$\gamma_{50\ Power} = 0.022\sigma'^{-0.208}_{v0}$	0.11	0.262	<0.05	80%	70	2.30	1.17	0.56	-0.35	-	-	-
	$\gamma_{50\ Power} = 0.0042+0.0013OCR$	0.65	0.0032	<0.001	80%	55	1.70	1.00	0.39	0.60	-	-	-
	$\gamma_{50\ Power} = 0.0048+0.0013OCR -0.00024Rate$	0.68	0.0032	<0.001	80%	50	1.60	1.00	0.36	0.61	-0.15	-	-
	$\gamma_{50\ Power} = 0.0015+0.0013OCR -0.00026Rate+0.0063w_L$	0.70	0.0031	<0.001	80%	45	1.60	1.00	0.35	0.61	-0.16	0.12	-
	$\gamma_{50\ Power} = 0.0010+0.0014OCR -0.00003Rate-0.048w_L+0.103w_P$	0.86	0.0021	<0.001	80%	30	1.35	1.09	0.69	0.63	-0.02	-0.94	1.17
CKUC *n*=67	$\gamma_{50\ Power} = 0.00043\sigma'^{0.201}_{vm}$	0.03	0.498	<0.5	81%	200	4.0	1.76	1.04	0.19	-	-	-
	$\gamma_{50\ Power} = 0.012\sigma'^{-0.358}_{v0}$	0.16	0.464	<0.001	81%	150	4.0	1.64	1.04	-0.45	-	-	-
	$\gamma_{50\ Power} = 0.0009OCR$	0.65	0.0016	<0.001	81%	70	2.15	0.90	0.67	0.58	-	-	-
	$\gamma_{50\ Power} = 0.00049OCR^{1.35}$	0.79	0.234	<0.001	81%	60	2.0	1.16	0.65	0.69	-	-	-
CKUC *n*=62	$\gamma_{50\ Power} = 0.00053OCR^{1.30}Rate^{-0.032}$	0.72	0.273	<0.001	81%	60	2.15	1.28	1.13	0.66	-0.07	-	-
	$\gamma_{50\ Power} = 0.0022OCR^{1.38}Rate^{-0.081}\ w_L^{1.83}$	0.82	0.218	<0.001	81%	100	9.1	0.27	0.99	0.71	-0.17	0.43	-
	$\gamma_{50\ Power} = 0.0019OCR^{1.37}Rate^{-0.083}\ w_L^{1.99} w_P^{-0.155}$	0.82	0.219	<0.001	81%	50	1.80	1.17	0.91	0.70	-0.17	0.47	-0.04
CKUE *n*=30	$\gamma_{50\ Power} = 0.00018\sigma'^{0.661}_{vm}$	0.08	0.395	<0.5	79%	-	3.00	1.51	1.02	0.48	-	-	-
	$\gamma_{50\ Power} = 0.026\sigma'^{-0.185}_{v0}$	0.04	0.404	<0.5	79%	-	2.85	1.54	1.08	-0.31	-	-	-
	$\gamma_{50\ Power} = 0.0038OCR$	0.45	0.0086	<0.001	80%	90	2.10	1.38	0.83	0.61	-	-	-
	$\gamma_{50\ Power} = 0.0053OCR^{0.658}$	0.43	0.267	<0.001	80%	60	2.05	1.22	0.73	0.48	-	-	-
CKUE *n*=28	$\gamma_{50\ Power} = 0.0051OCR^{0.685}Rate^{0.0025}$	0.47	0.262	<0.001	80%	80	1.80	1.20	0.72	0.50	0.01	-	-
	$\gamma_{50\ Power} = 0.022OCR^{0.839}Rate^{-0.107}\ w_L^{1.93}$	0.81	0.160	<0.001	80%	40	1.60	1.06	0.37	0.62	-0.25	0.66	-
	$\gamma_{50\ Power} = 0.055OCR^{0.841}Rate^{-0.092}\ w_L^{0.653} w_P^{1.29}$	0.82	0.161	<0.001	80%	45	1.50	1.06	0.36	0.62	-0.21	0.22	0.47

Table 4- 10. Multiple Linear Regression of *b*

Test Mode	Regression model	R^2	S.E.	*p*-value	Data within error bounds	± %Error	Factor Error	Bias	COV	Proportionate change in the independent variable, Y: max(X1)-min(X1)	max(X2)-min(X2)	max(X3)-min(X3)	max(X4)-min(X4)
CIUC *n*=114	$b = 1.153\gamma_{50\ Power}^{0.209}$	0.22	0.110	<0.001	80%	25	1.3	0.97	0.33	0.37	-	-	-
	$b = 1.110\gamma_{50\ Power}^{0.203}Rate^{-0.028}$	0.25	0.108	<0.001	80%	25	1.3	0.98	0.34	0.36	-0.12	-	-
	$b = 1.60\gamma_{50\ Power}^{0.204}Rate^{-0.029}w_L^{-0.205}$	0.29	0.106	<0.001	80%	25%	1.3	0.98	0.33	0.36	-0.12	-0.14	-
	$b = 0.939\gamma_{50\ Power}^{0.203}Rate^{-0.028}w_L^{-0.156}\ w_P^{-0.049}$	0.29	0.106	<0.001	80%	25%	1.3	0.98	0.32	0.36	-0.12	-0.11	-0.04
CIUE *n*=55	$b = 0.724\gamma_{50\ Power}^{0.127}$	0.15	0.085	<0.01	80%	25	1.3	1.02	0.2	0.38	-	-	-
	$b = 0.723\gamma_{50\ Power}^{0.126}Rate^{0.004}$	0.15	0.086	<0.05	80%	25	1.3	1.02	0.2	0.38	0.02	-	-
	$b = 0.615\gamma_{50\ Power}^{0.149}Rate^{-0.016}w_L^{-0.395}$	0.47	0.068	<0.001	80%	25	1.25	1.01	0.15	0.45	0.10	-0.42	-
	$b = 0.726\gamma_{50\ Power}^{0.128}Rate^{0.018}w_L^{-0.786}\ w_P^{-0.398}$	0.49	0.068	<0.001	80%	20	1.2	1.01	0.15	0.38	0.11	-0.85	0.45
CKUC *n*=67	$b = 0.672-0.235\log_{10}(OCR)$	0.22	0.148	<0.001	81%	25	1.3	1.00	0.24	-0.24	-	-	-
	$b = 0.168-0.149\log_{10}(\gamma_{50\ Power})$	0.20	0.150	<0.001	81%	30	1.3	1.00	0.24	-0.46	-	-	-
CKUC *n*=62	$b = 0.177-0.147\log_{10}(\gamma_{50\ Power}) -0.011\log_{10}(Rate)$	0.19	0.155	<0.01	81%	30	1.30	1.00	0.24	-0.29	-0.04	-	-
	$b = 0.095-0.136\log_{10}(\gamma_{50\ Power}) -0.002\log_{10}(Rate)-0.320(w_L)$	0.22	0.154	<0.01	81%	30	1.35	1.00	0.25	-0.26	-0.01	-0.15	-
	$b = 0.323-0.125\log_{10}(\gamma_{50\ Power}) +0.006\log_{10}(Rate)-0.996(w_L) +0.655(w_P)$	0.23	0.154	<0.01	81%	30	1.30	1.00	0.24	-0.24	0.02	-0.46	0.32
CKUE *n*=34	$b = 0.571+0.110\log_{10}(\gamma_{50\ Power})$	0.20	0.091	<0.01	79%	30	1.30	1.00	0.24	0.26	-	-	-
CKUE *n*=28	$b = 0.383-0.023\log_{10}(\gamma_{50\ Power}) -0.022\log_{10}(Rate)$	0.14	0.061	<0.5	80%	25	1.30	1.00	0.18	0.11	-0.25	-	-
	$b = 0.390+0.015\log_{10}(\gamma_{50\ Power}) -0.026\log_{10}(Rate)+0.066(w_L)$	0.15	0.062	<0.5	80%	25	1.30	1.00	0.18	0.07	-0.29	0.11	-
	$b = 0.291+0.016\log_{10}(\gamma_{50\ Power}) -0.029\log_{10}(Rate)+0.384(w_L) -0.322(w_P)$	0.16	0.064	<0.5	80%	30	1.30	1.00	0.18	0.08	-0.33	0.65	-0.58

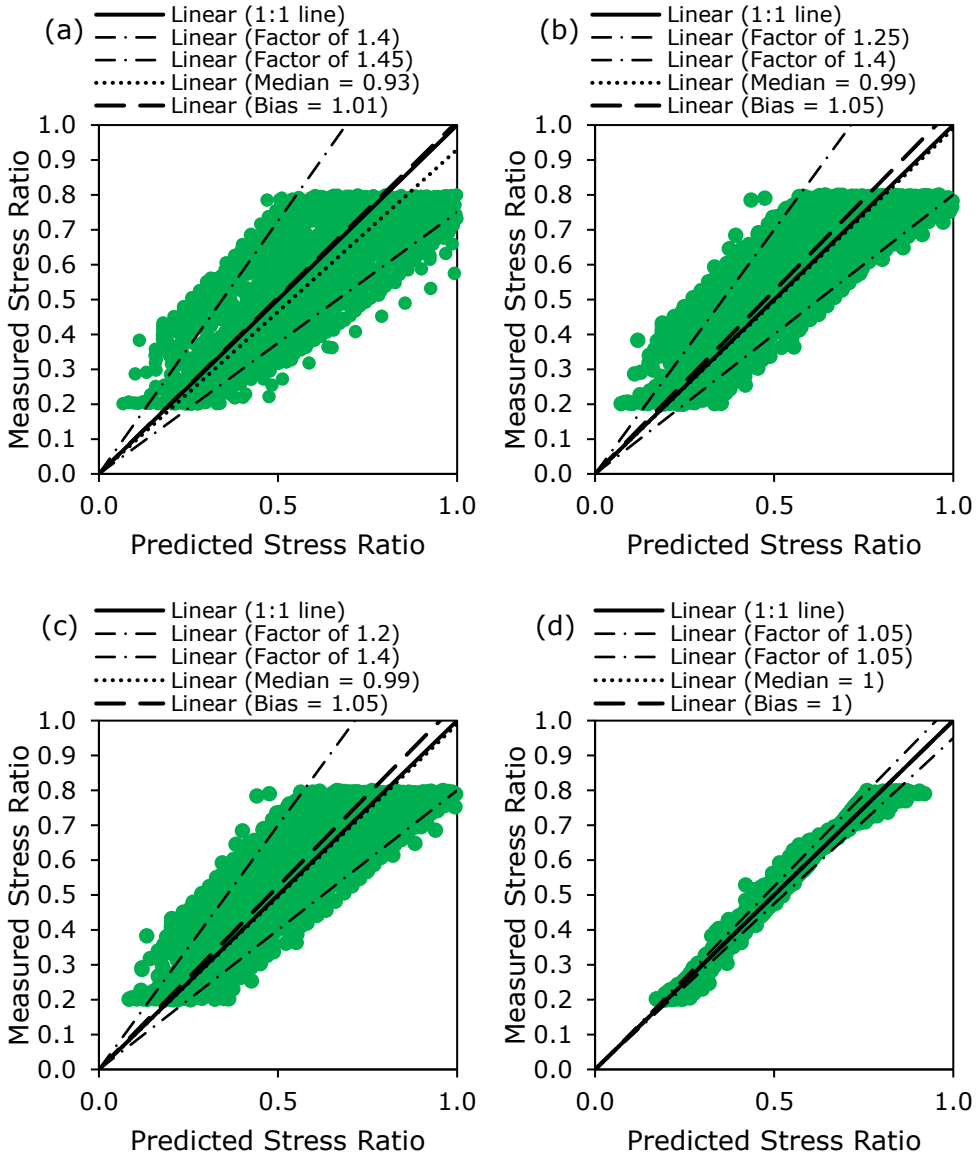

Figure 4- 57. Predicted-measured plots of Measured Stress Ratio (S) of *all stress-strain data* between 20%≤S≤80% (n=2069 data points) in the CIUC test database (RFG/TXCU-278), predicted using: (a) Equation 4.10 (b) Equation 4.11 (c) Equation 4.12 (d) model parameters $\gamma_{50\ Power}$ and b of every triaxial test

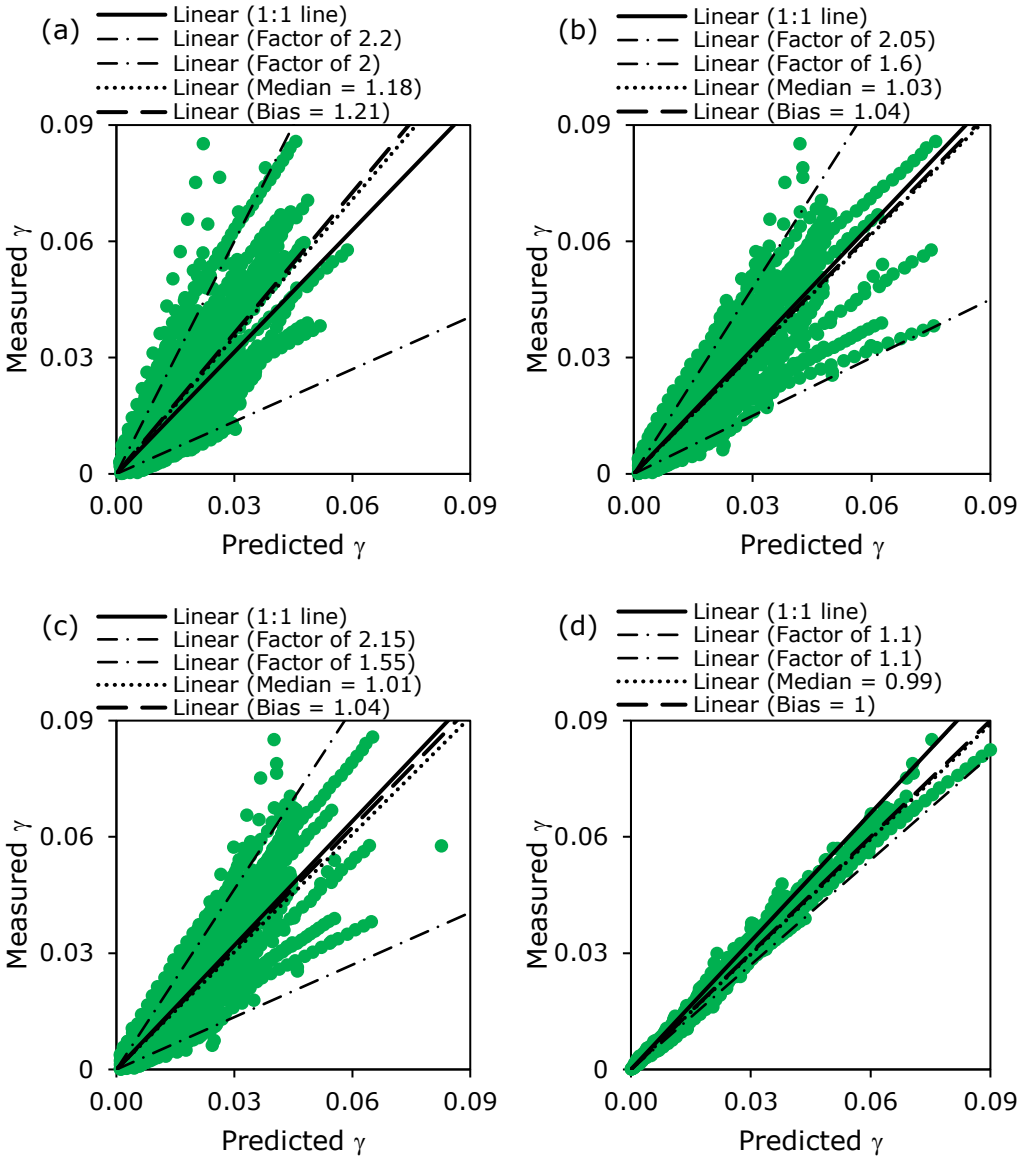

Figure 4- 58. Predicted-measured plots of γ (= 1.5ε_a) of *all stress-strain data* between 20%≤*S*≤80% (*n*=2069 data points) in the CIUC test database (RFG/TXCU-278), predicted using: (a) Equation 4.10 (b) Equation 4.11 (c) Equation 4.12 (d) model parameters $\gamma_{50\ \text{Power}}$ and *b* of every triaxial test

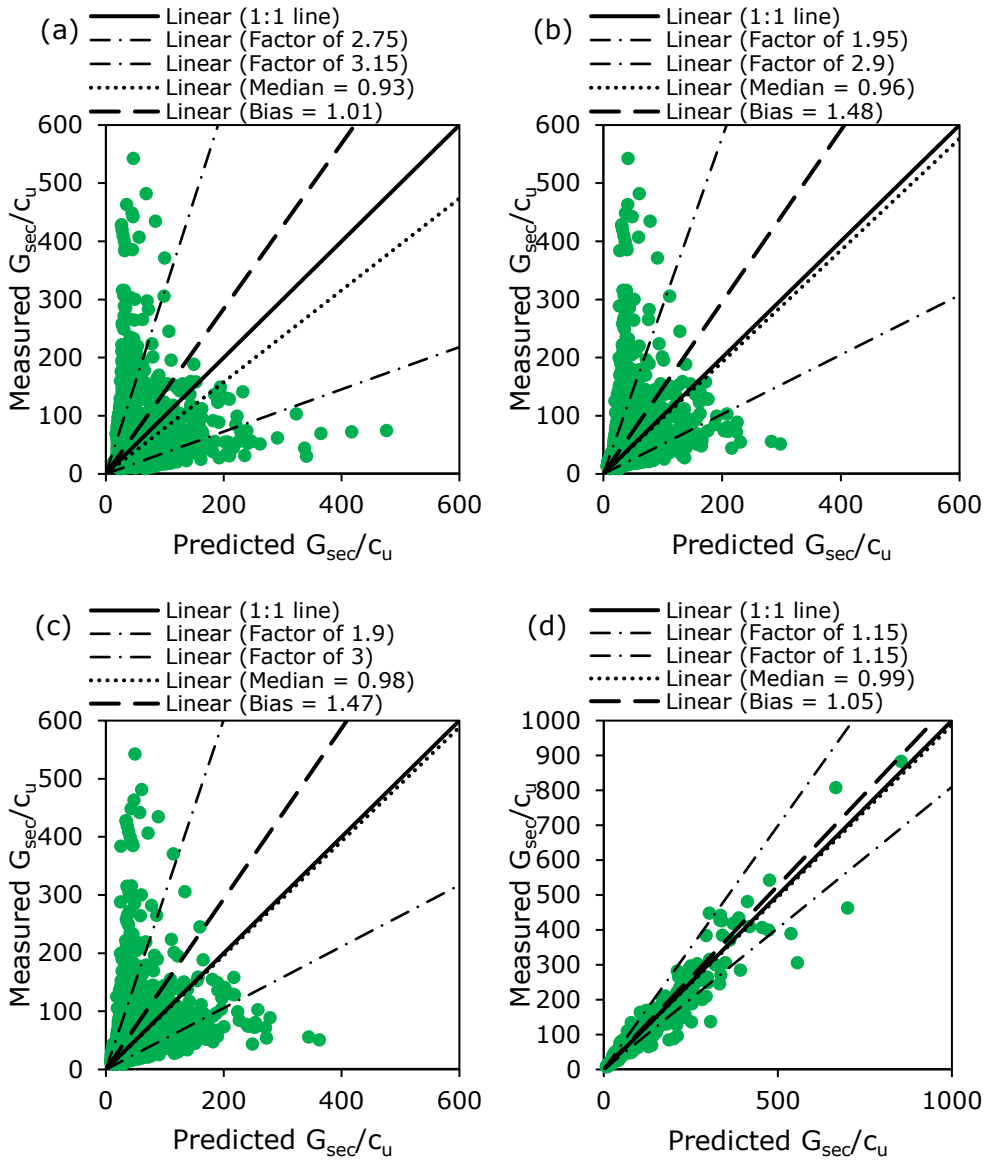

Figure 4- 59. Predicted-measured plots of G_{sec}/c_u (since τ_0=0) of *all stress-strain data* between 20%≤*S*≤80% (*n*=2069 data points) in the CIUC test database (RFG/TXCU-278), predicted using: (a) Equation 4.10 (b) Equation 4.11 (c) Equation 4.12 (d) model parameters $\gamma_{50\ Power}$ and *b* of every triaxial test

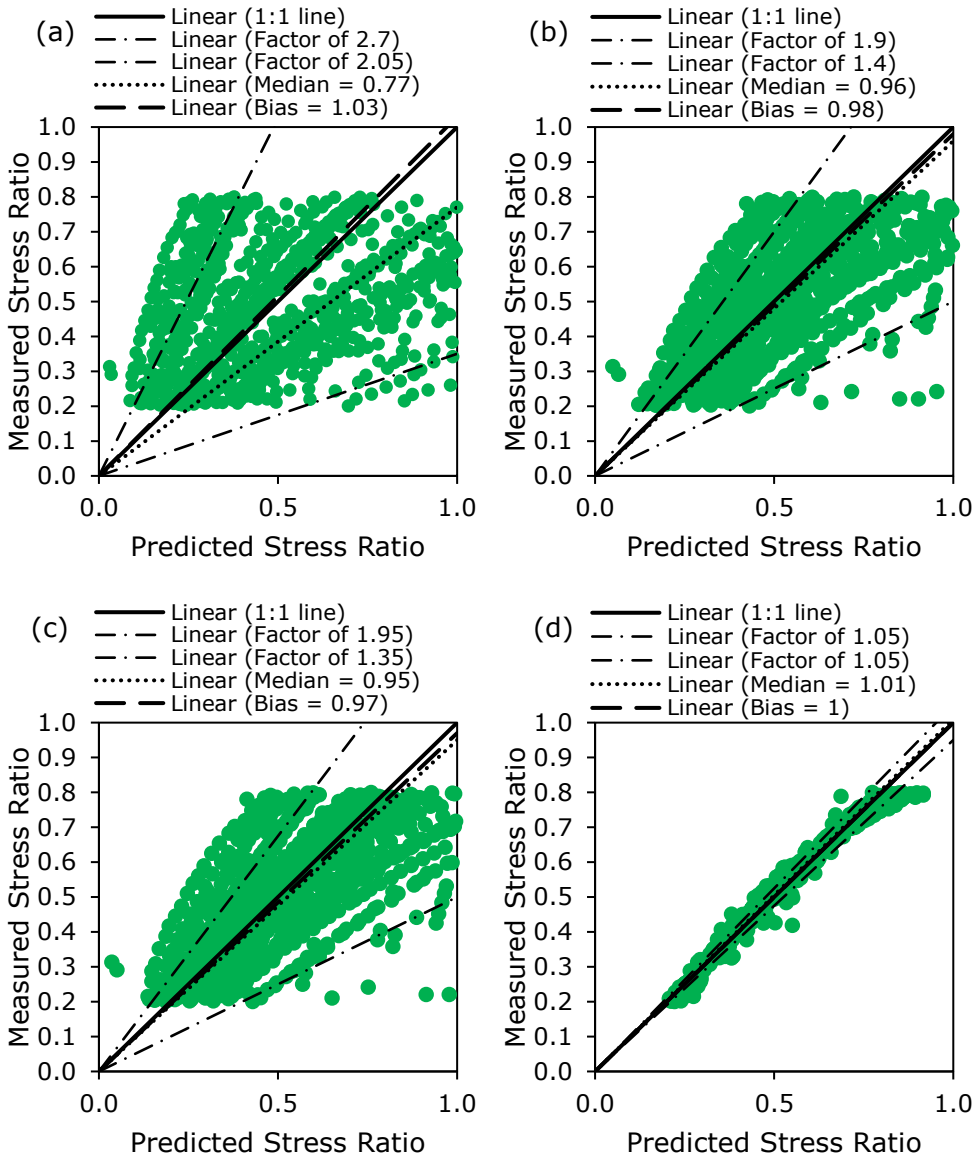

Figure 4- 60. Predicted-measured plots of Measured Stress Ratio (*S*) of *all stress-strain data* between 20%≤*S*≤80% (*n*=1049 data points) in the CKUC test database (RFG/TXCU-278), predicted using: (a) Equation 4.16 (b) Equation 4.17 (c) Equation 4.18 (d) model parameters $\gamma_{50\ Power}$ and *b* of every triaxial test

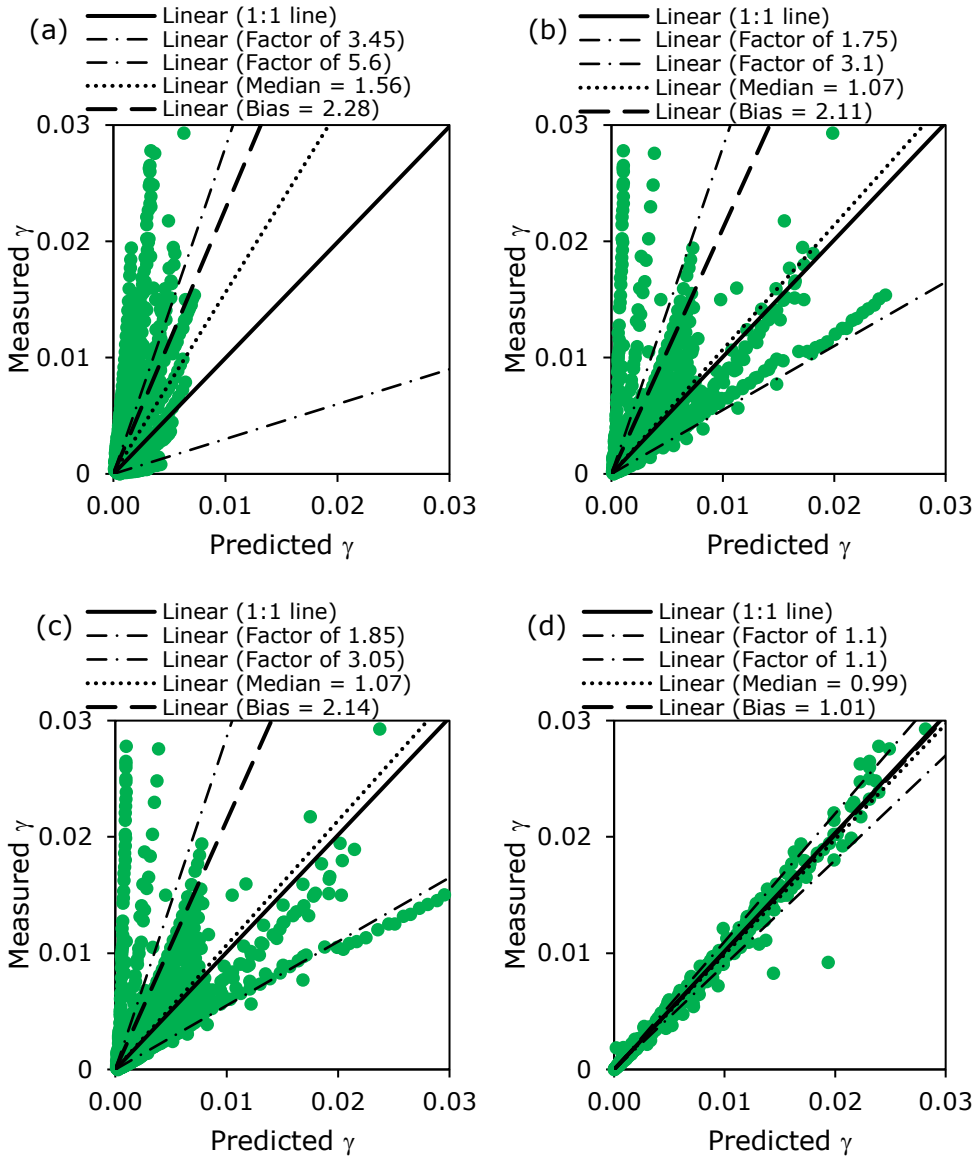

Figure 4- 61. Predicted-measured plots of γ (= 1.5ε_a) of *all stress-strain data* between 20%≤*S*≤80% (*n*=1049 data points) in the CKUC test database (RFG/TXCU-278), predicted using: (a) Equation 4.16 (b) Equation 4.17 (c) Equation 4.18 (d) model parameters $\gamma_{50\ Power}$ and *b* of every triaxial test

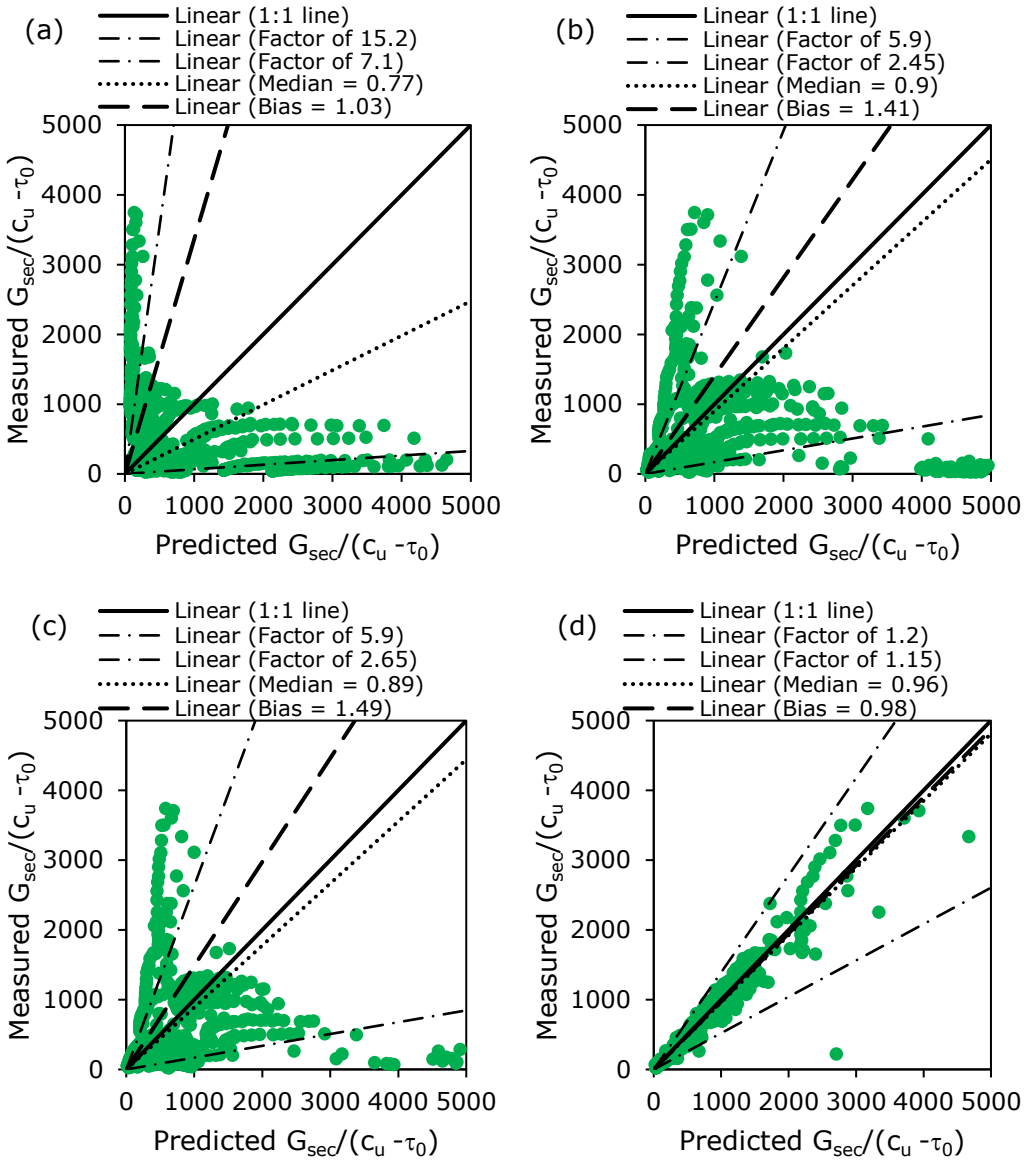

Figure 4- 62. Predicted-measured plots of $G_{sec}/(c_u\text{-}\tau_0)$ of *all stress-strain data* between 20%≤*S*≤80% (*n*=1049 data points) in the CKUC test database (RFG/TXCU-278), predicted using: (a) Equation 4.16 (b) Equation 4.17 (c) Equation 4.18 (d) model parameters $\gamma_{50\ Power}$ and *b* of every triaxial test

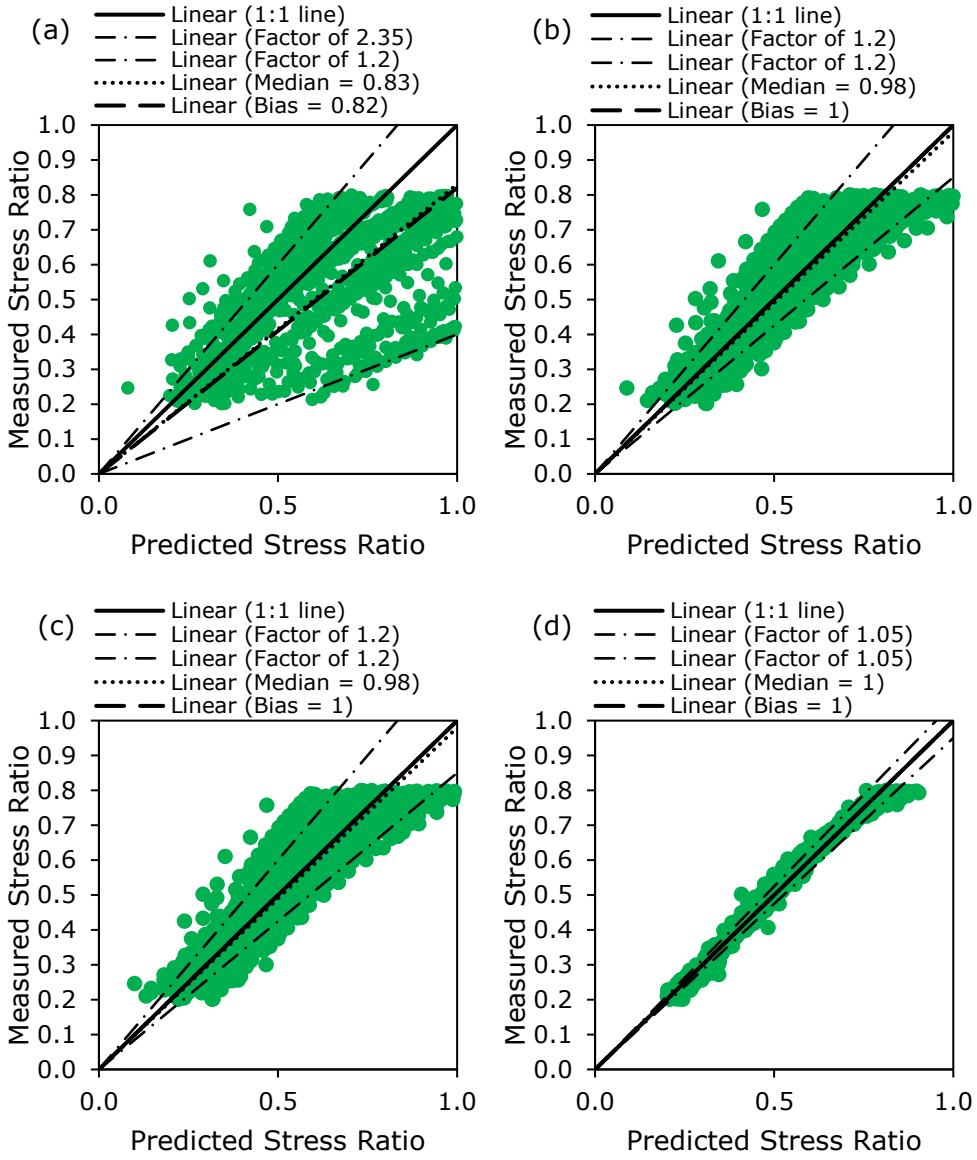

Figure 4- 63. Predicted-measured plots of Measured Stress Ratio (*S*) of *all stress-strain data* between 20%≤*S*≤80% (*n*=1217 data points) in the CIUE test database (RFG/TXCU-278), predicted using: (a) Equation 4.13 (b) Equation 4.14 (c) Equation 4.15 (d) model parameters $\gamma_{50\ Power}$ and *b* of every triaxial test

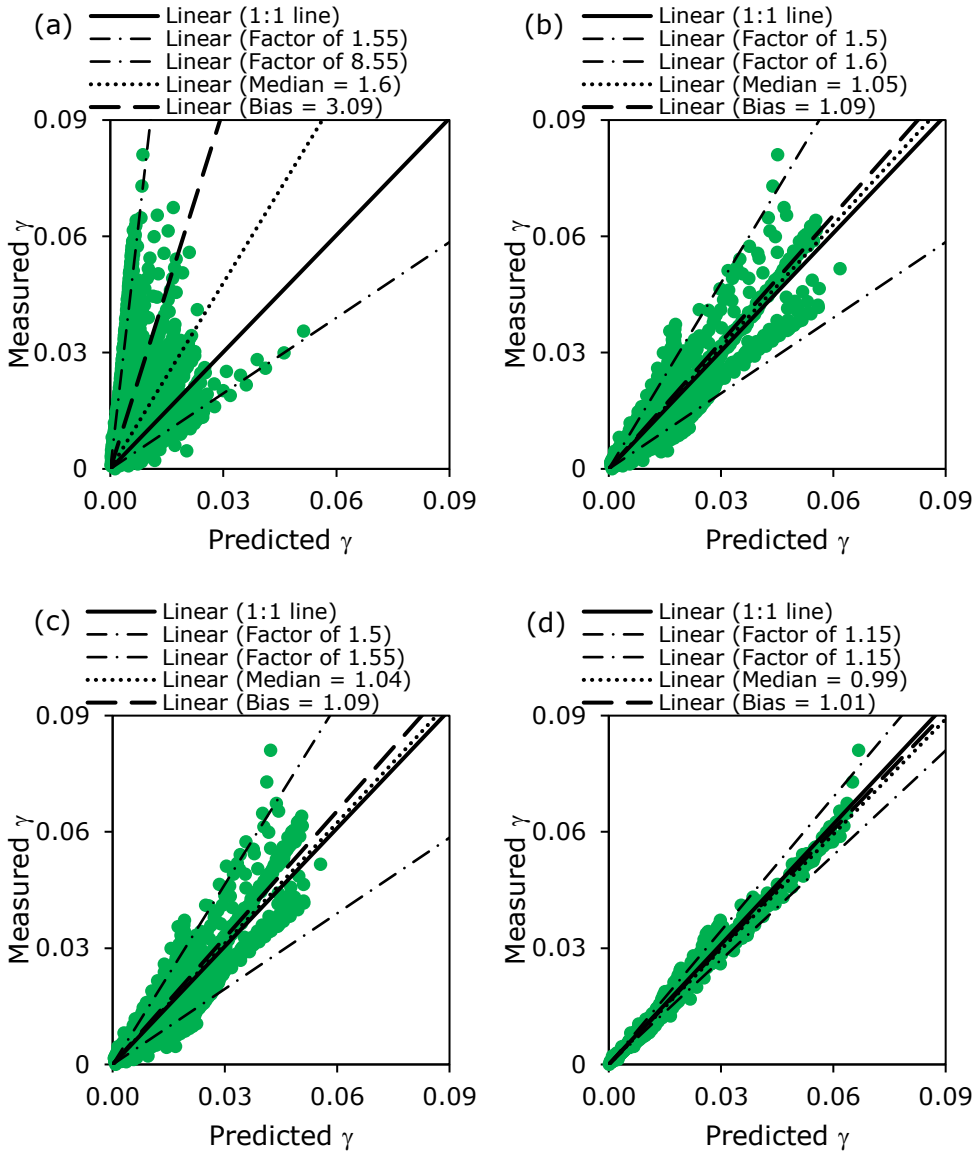

Figure 4- 64. Predicted-measured plots of γ (= $1.5\varepsilon_a$) of *all stress-strain data* between 20%≤*S*≤80% (*n*=1217 data points) in the CIUE test database (RFG/TXCU-278), predicted using: (a) Equation 4.13 (b) Equation 4.14 (c) Equation 4.15 (d) model parameters $\gamma_{50\ \text{Power}}$ and *b* of every triaxial test

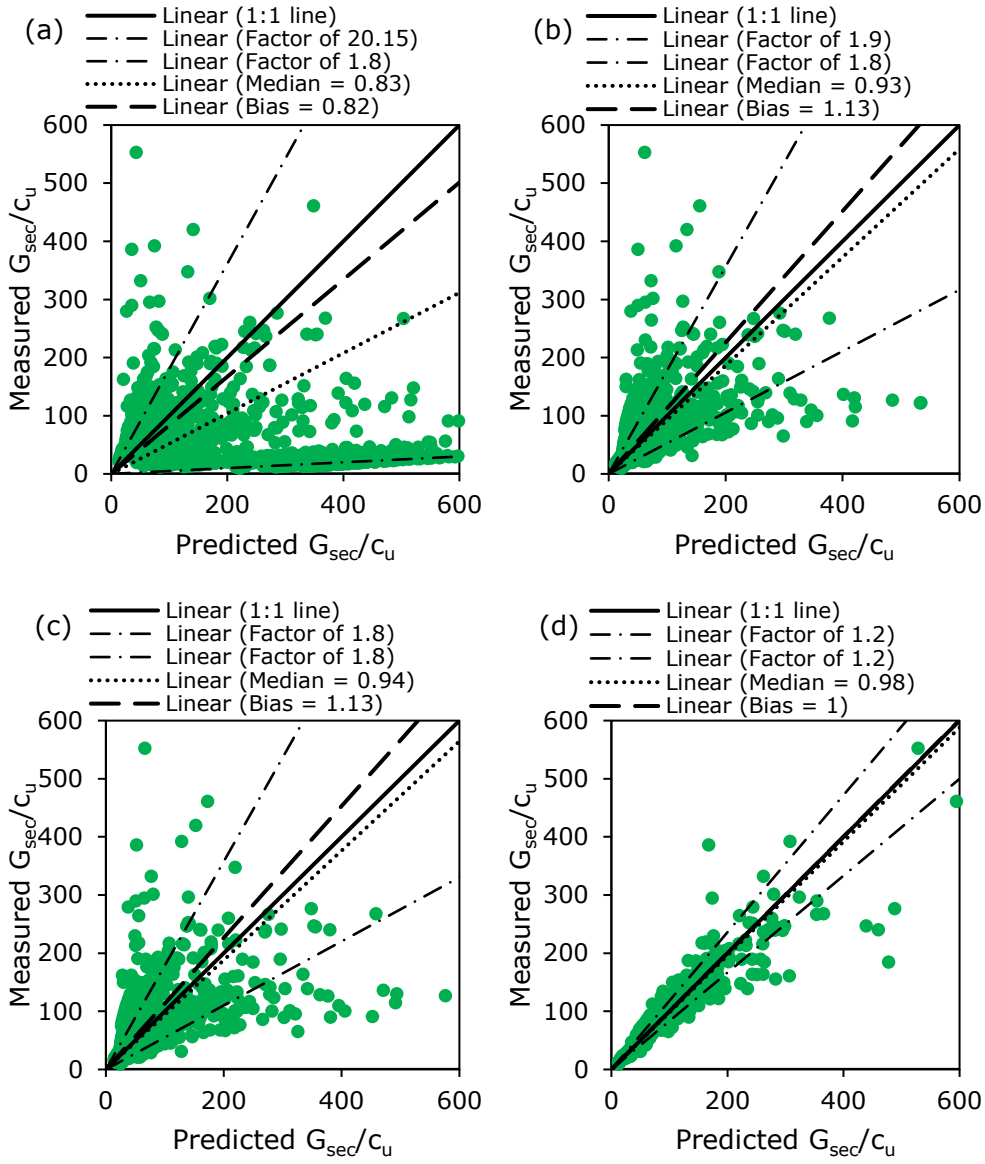

Figure 4- 65. Predicted-measured plots of G_{sec}/c_u (since τ_0=0) of *all stress-strain data* between 20%≤*S*≤80% (*n*=1217 data points) in the CIUE test database (RFG/TXCU-278), predicted using: (a) Equation 4.13 (b) Equation 4.14 (c) Equation 4.15 (d) model parameters $\gamma_{50\ Power}$ and *b* of every triaxial test

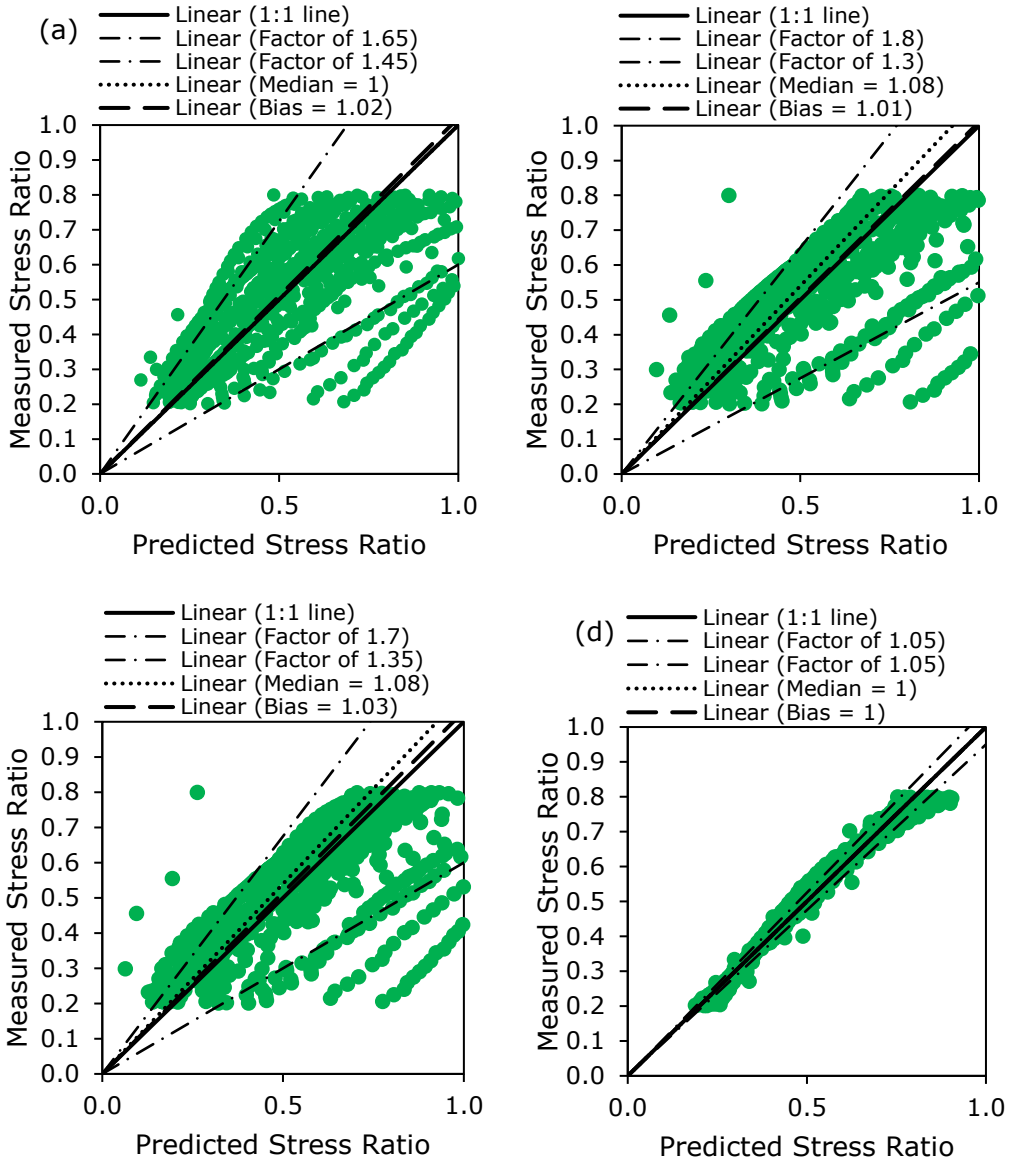

Figure 4- 66. Predicted-measured plots of Measured Stress Ratio (S) of *all stress-strain data* between 20%≤S≤80% (n=864 data points) in the CKUE test database (RFG/TXCU-278), predicted using: (a) Equation 4.19 (b) Equation 4.20 (c) Equation 4.21 (d) model parameters $\gamma_{50\ Power}$ and b of every triaxial test

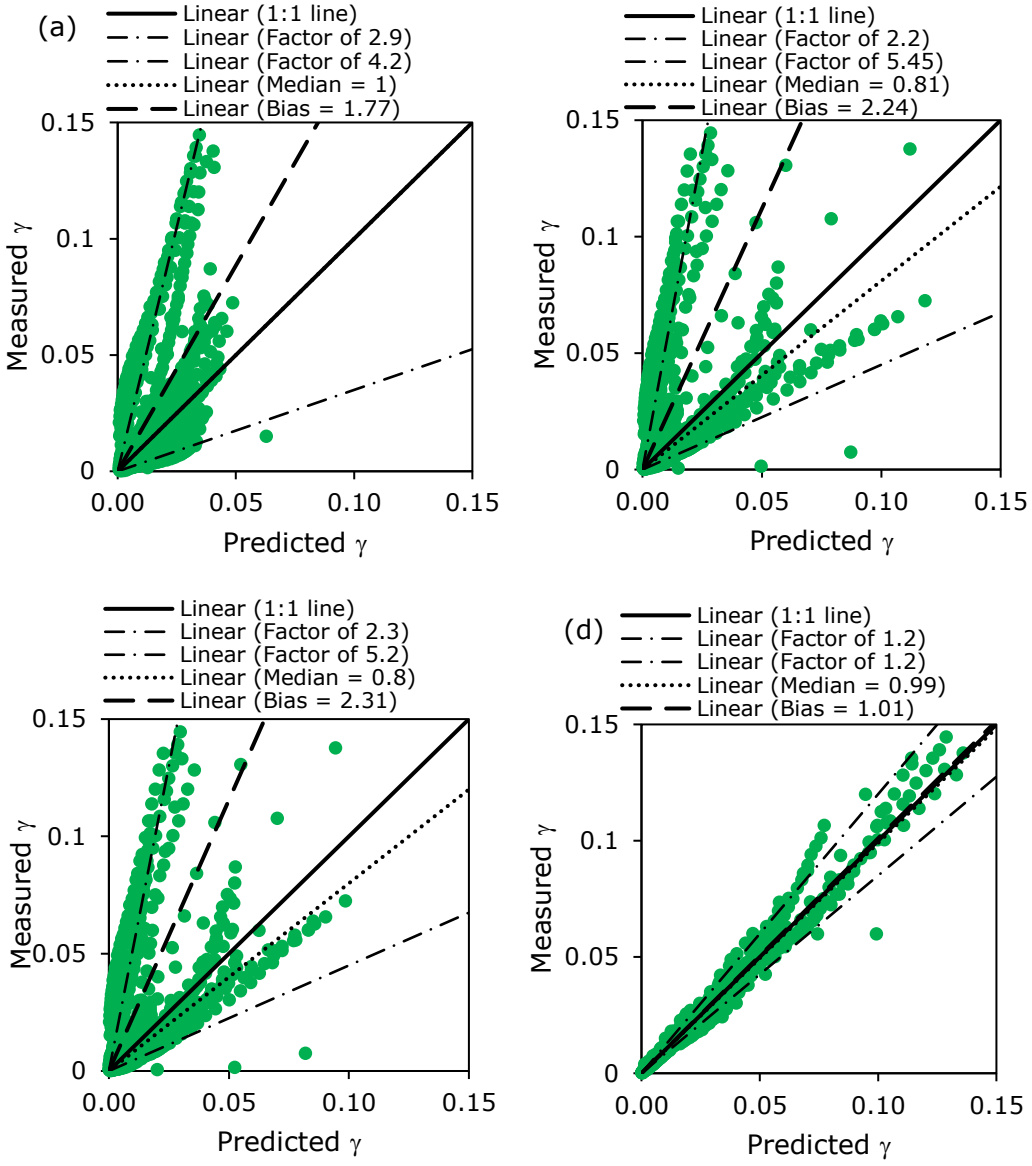

Figure 4- 67. Predicted-measured plots of γ (= $1.5\varepsilon_a$) of *all stress-strain data* between 20%≤*S*≤80% (*n*=864 data points) in the CKUE test database (RFG/TXCU-278), predicted using: (a) Equation 4.19 (b) Equation 4.20 (c) Equation 4.21 (d) model parameters $\gamma_{50\ \text{Power}}$ and *b* of every triaxial test

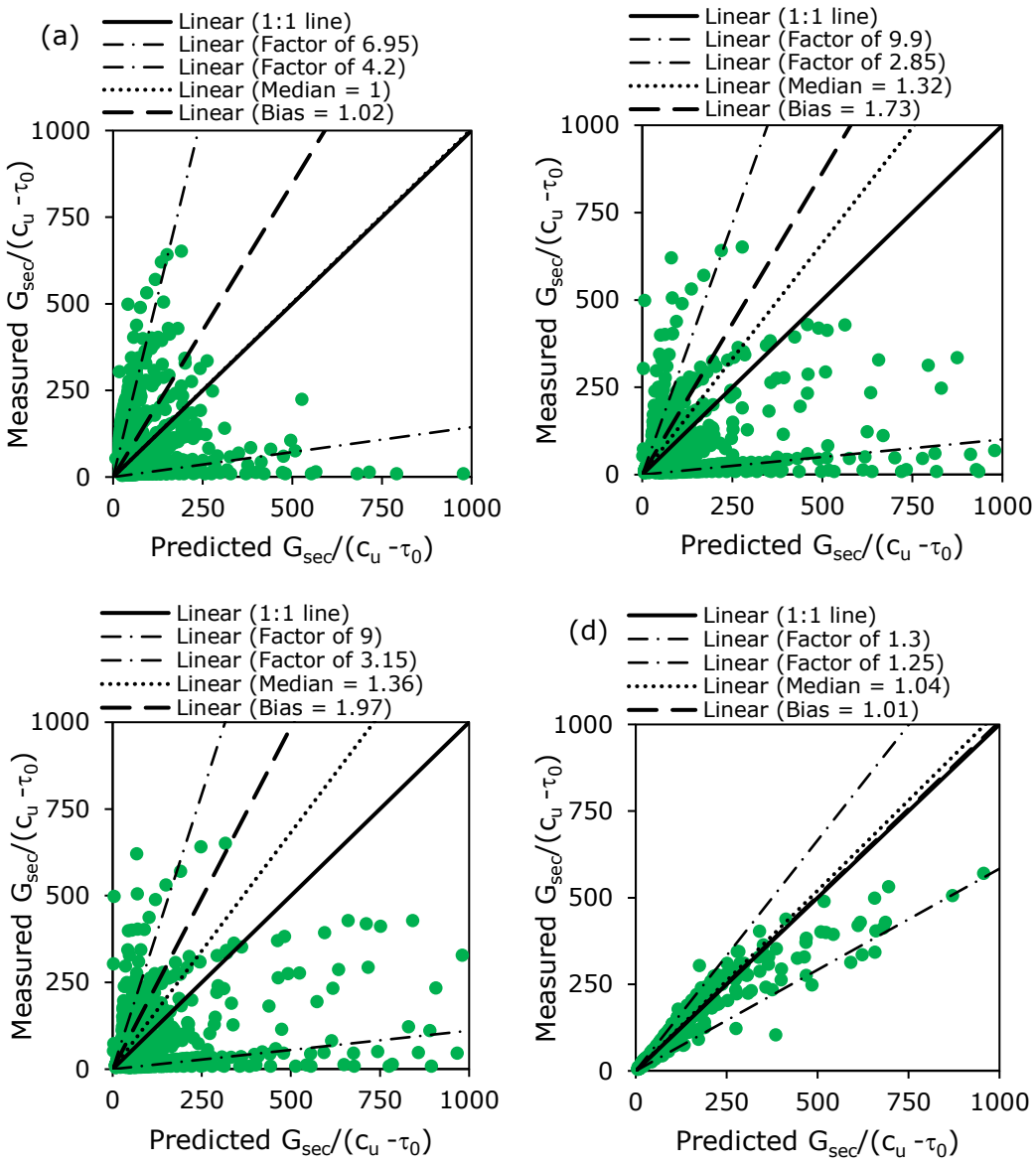

Figure 4- 68. Predicted-measured plots of $G_{sec}/(c_u-\tau_0)$ of *all stress-strain data* between 20%≤*S*≤80% (*n*=864 data points) in the CKUE test database (RFG/TXCU-278), predicted using: (a) Equation 4.19 (b) Equation 4.20 (c) Equation 4.21 (d) model parameters $\gamma_{50\ Power}$ and *b* of every triaxial test

4.4 Analysis of shear-mode anisotropy by comparison of compression and extension parameters

4.4.1 Comparing shear modes to estimate parameter variation

So far, the database analysis in this chapter has highlighted the importance of stress history (*OCR*) to explain the variation of the model parameters (c_u/σ'_{VO}, $\gamma_{50\ Power}$, and b) of reconstituted soils. When ground investigations are limited, a method to quantify the variation of the model parameters due to changing shear modes is valuable when evaluating the sensitivity of such parameters.

4.4.2 Research objective

(1) To assess the viability of using a comparison of compression and extension parameters to predict triaxial extension behaviour when test data is scarce

(2) To evaluate the parameter variability associated with shear mode compared with the parameter variability associated with stress history of the soil sample.

4.4.3 Comparing average trends in compression and extension parameters

One approach to assess strain anisotropy from triaxial tests is shown in Figures 4- 69 and 4- 70. Here the model parameters that represent shear strain γ at S=0.3, 0.5, and 0.7 are plotted against *OCR*. Best-fit linear regressions of $\gamma_{50\ Power}$ = f(*OCR*), previously reported in Table 4.9, are plotted together with linear regressions of the same form (all $R^2 > 0.4$) to describe the average variation of strains mobilised at S = 0.3 and 0.7. Between $0.3 \leq S \leq 0.7$, the average parameter variation with *OCR* in CIU tests indicates the strain behaviour to be isotropic. The CKU test parameters are distinctly anisotropic and the strain anisotropy varies with *OCR* – the largest difference in the average trends being apparent in the parameters relevant to normally consolidated soils. This approach is useful for an interpretation of the influence of *OCR* on strain anisotropy. However, where the *OCR* of a deposit is uncertain, a different approach would be needed. In the next section, practical correlations between compression and extension strain behaviours in triaxial compression and extension are developed for the tests in RFG/TXCU-278. Parameter anisotropy of the tests in BTK/TXCU-34 is also studied in the next section.

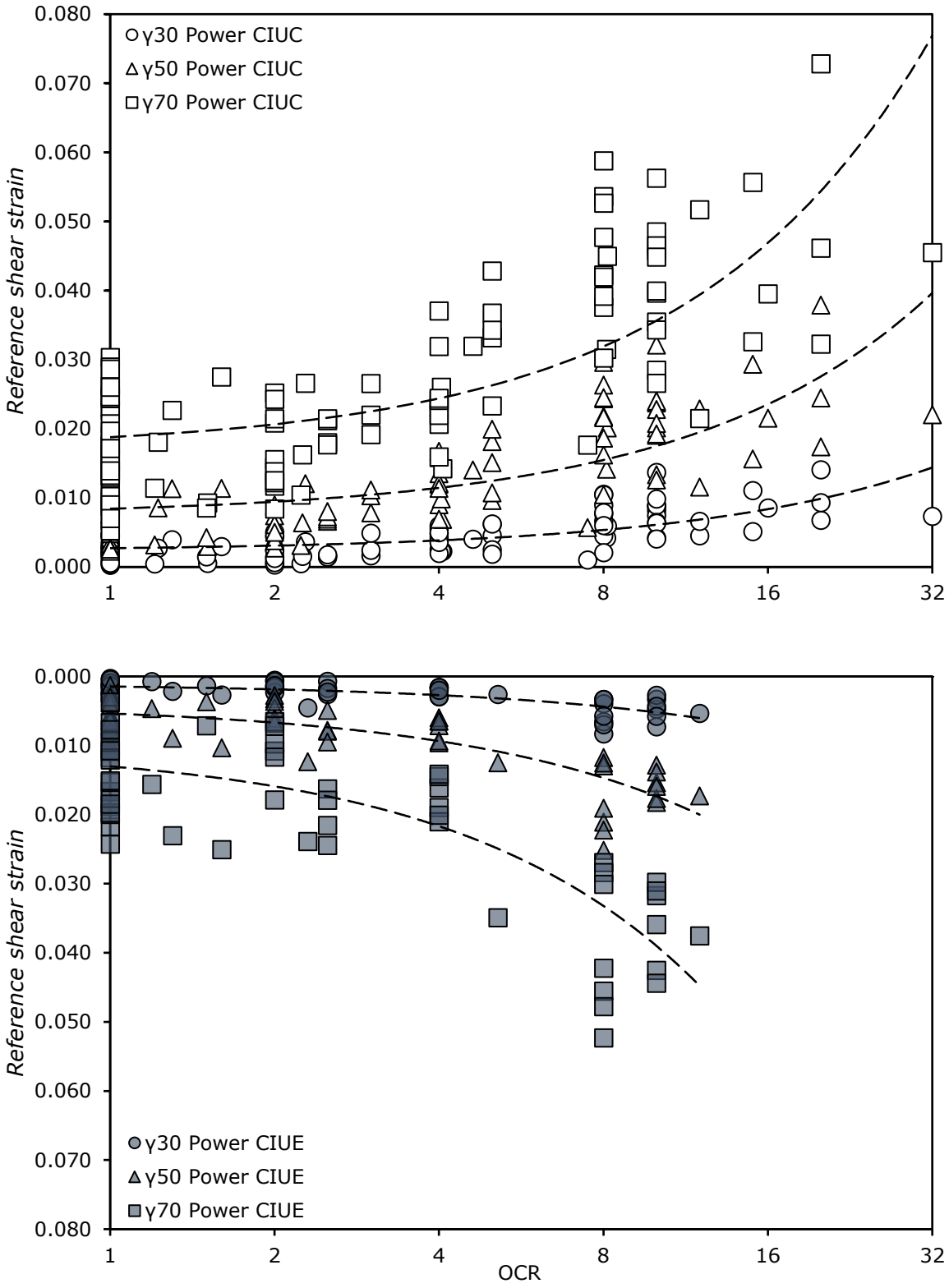

Figure 4- 69. Variation of $\gamma_{30\ Power}$, $\gamma_{50\ Power}$ and $\gamma_{70\ Power}$ with *OCR* for triaxial compression and extension tests consolidated under K_0 conditions prior to shear

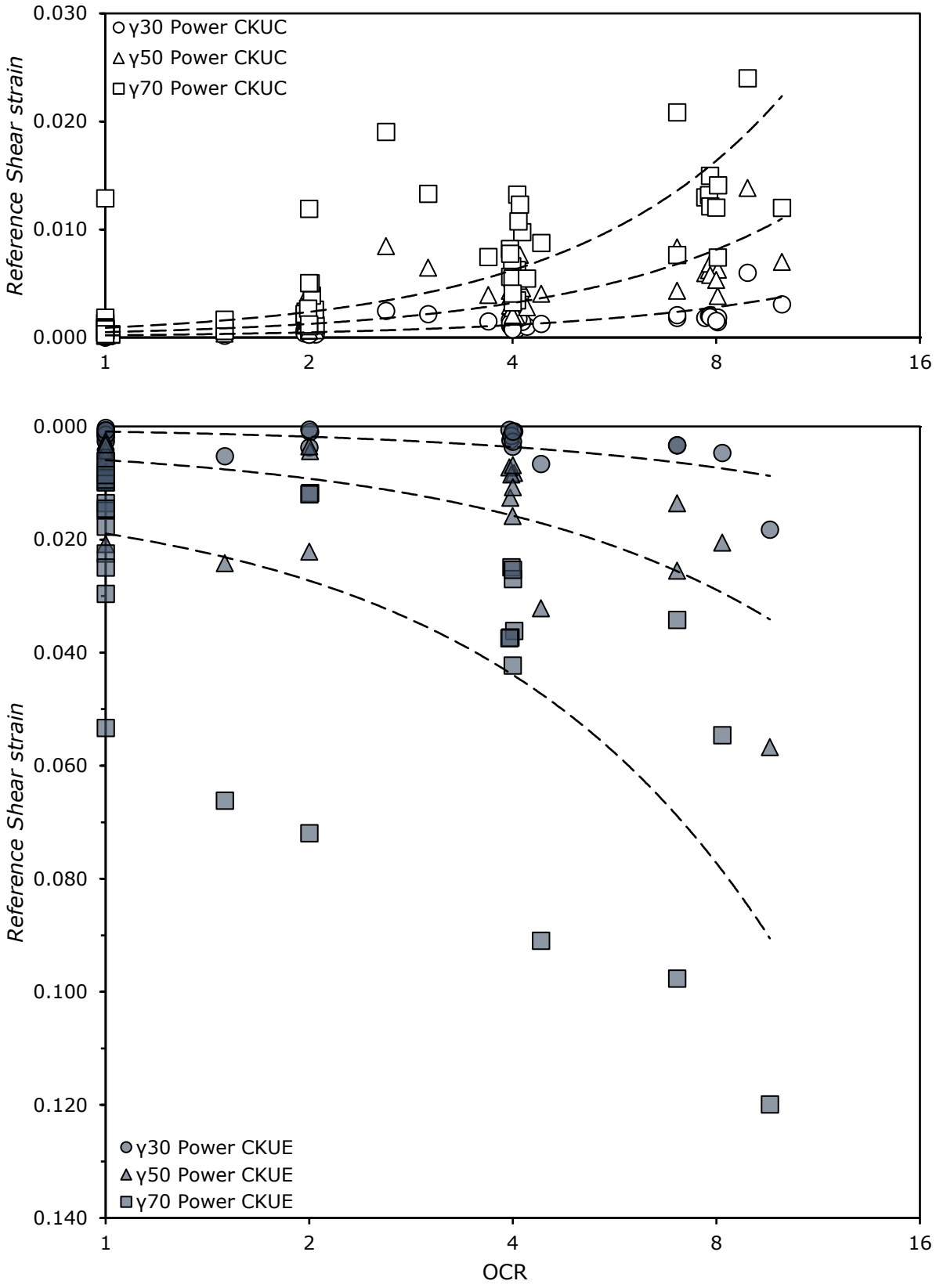

Figure 4- 70. Variation of $\gamma_{30\ Power}$, $\gamma_{50\ Power}$ and $\gamma_{70\ Power}$ with *OCR* for triaxial compression and extension tests consolidated under K_0 conditions prior to shear

4.4.4 Parameter transformation models from comparisons of compression and extension

In Figures 4- 71 to 4- 75, the strength and strain parameters obtained for each digitised test are presented by comparing extension and compression modes. Pairs of tests (i.e. extension and compression) were selected from the same publication and laboratory with identical *OCR* (±0.1) and undrained strain rate. Intact tests on Bothkennar clay undertaken by City University and Imperial College (reported by SERC 1989) are shown for comparison with RFG/TXCU-278. The database of strength parameters from triaxial tests reported by Mayne & Holtz (1985) is included in Figure 4- 71. Where correlations are significant between the parameters of each shear mode, the regression lines are plotted in Figures 4- 71 to 4- 75. Tables 4- 11 to 4- 14 include statistical summaries of the shear mode parameter transformation models.

Single linear regression analysis indicates that a significant relationship exists between c_u/σ'_{v0} in compression and in extension for isotropically-consolidated samples, with a high coefficient of determination and $p<0.001$ (see Figure 4- 71). K_0-consolidated specimens have greater strength anisotropy and less scatter (standard error). The intact soils show similar ranges in c_u/σ'_{v0} to the reconstituted soils and produce close best-fit lines between normalised compression and extension strengths whether tested from isotropic or K_0 stresses before shearing to failure. A comparison of predicted vs. measured data in Table 4- 14 shows the factor error of the regression to be ·/1.3 to 1.6 depending on consolidation type (CIU or CKU) and specimen type (reconstituted or intact). Peak strength measured in triaxial extension of the intact soils consolidated under K_0 stresses can be predicted with a factor error of ·/1.55 without the need to include *OCR* in the parameter transformation model.

Significant correlations also exist between the reference strains measured in extension and compression from isotropic or K_0 consolidated conditions on reconstituted soils; however, no correlations exist for the test data compiled in BTK/TXCU-34. Figures 4- 72 to 4- 74 show that the reference strains at all three stress ratios are less sensitive to shear mode if tested from an isotropic stress state. CIU strains become more isotropic as the stress ratio approaches peak stresses; the opposite effect is found for CKU strains. Considering only $\gamma_{50\,\mathrm{Power}}$ the slope regression coefficient for CKU tests is greater than five times the slope observed in the CIU test data. Reference strains mobilised at S=0.5 in

CKUE, in some cases, are one order of magnitude greater than the strains mobilised in CKUC – a similar difference can be observed between the regression coefficients in Equations 4.17 and 4.20. However, considerable scatter of the strain anisotropy warrants further investigation. No correlation to describe the shear mode effect was found for b^* or b (see Table 4- 7 for parameter ranges) although CKU tests show more disparity between compression and extension (see Figure 4- 74).

The factor errors (reported in Tables 4- 11 to 4-14) demonstrate that $\gamma_{70\ \text{Power Compression}}$ can be used to predict $\gamma_{70\ \text{Power Extension}}$ with greater accuracy than using $\gamma_{50\ \text{Power}}$ or $\gamma_{30\ \text{Power}}$ to predict their corresponding reference strains. Using Table 4- 17 a designer could justify the likely variation of reference strain $\gamma_{70\ \text{Power}}$ with shear mode from a single triaxial compression test on fine-grained soil with no prior information about the material or in-situ conditions. For the reconstituted soils in RFG/TXCU-278, the factor error of the data points of $\gamma_{70\ \text{Power}}$ about the regression line is ·/1.4 to 1.6 (dependent on CIU or CKU test conditions) whereas the error increases to ·/2.2 if $\gamma_{50\ \text{Power}}$ is used. The reported factor errors indicate the combined effects of variable material composition and procedures used in the triaxial tests of RFG/TXCU-278 on strain anisotropy. Factor errors can be incorporated into parameter sensitivity analyses to simulate the possible range in mobilised strains.

Using the suggested approach for strain anisotropy may only be appropriate for soils where behaviour is not dominated by their structure, however. No correlations between reference strains exist for intact Bothkennar clay specimens at any stress ratio, and it may be more appropriate to describe $K_\gamma = \gamma_{S(\%)\ \text{Power Extension}} / \gamma_{S(\%)\ \text{Power Compression}}$ by an average. At S=30%, K_γ of Bothkennar clay is closer to unity than at other stress ratios and about one-half of the reconstituted soils are more anisotropic than the Bothkennar clay. At S= 50% and 70%, on average K_γ increases (and all >1) and reference strains of the reconstituted soils are more anisotropic than the intact soil in nearly all tests. It is interesting to note that the strains of the intact soils and of the reconstituted soils are similar at S=30% and that divergence becomes more pronounced as stress ratio increases. Greater deformations generally occur pre-failure in reconstituted soils tested in CKUE. Strain anisotropy of the intact soil specimens appears to be also governed by higher measurements of $\gamma_{50\ \text{Power CKUC}}$ than expected for reconstituted soils of the same *OCR* (taking as before *YSR* = apparent *OCR* for the tests on Bothkennar clay); see Figures 4- 28 and 4- 29.

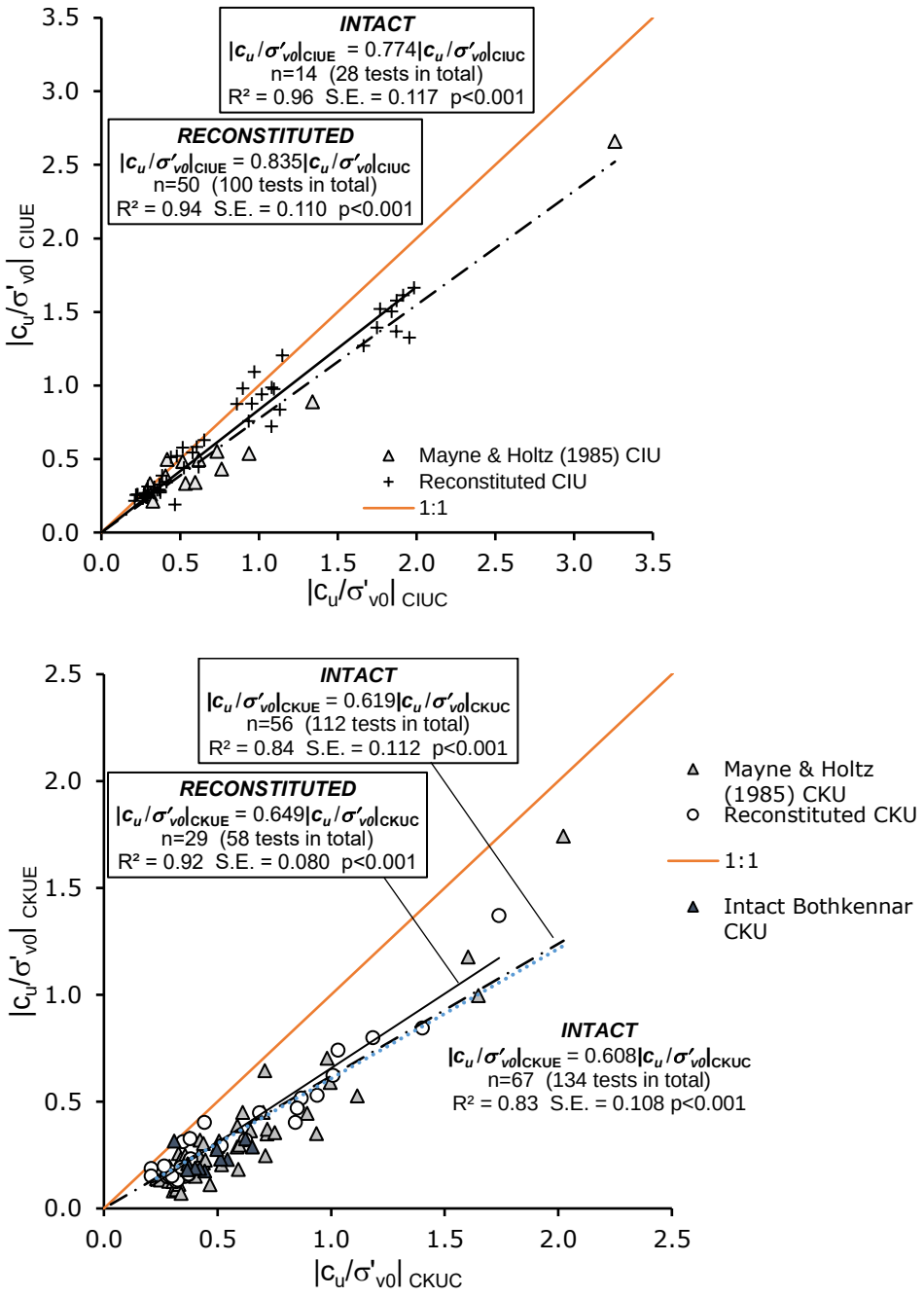

Figure 4- 71. Comparison of c_u/σ'_{v0} from triaxial extension and compression tests on two similarly reconstituted specimens, or two intact specimens from the same sample depth, tested at the same laboratory and with identical strain rate: (a) CIU tests (b) CKU tests

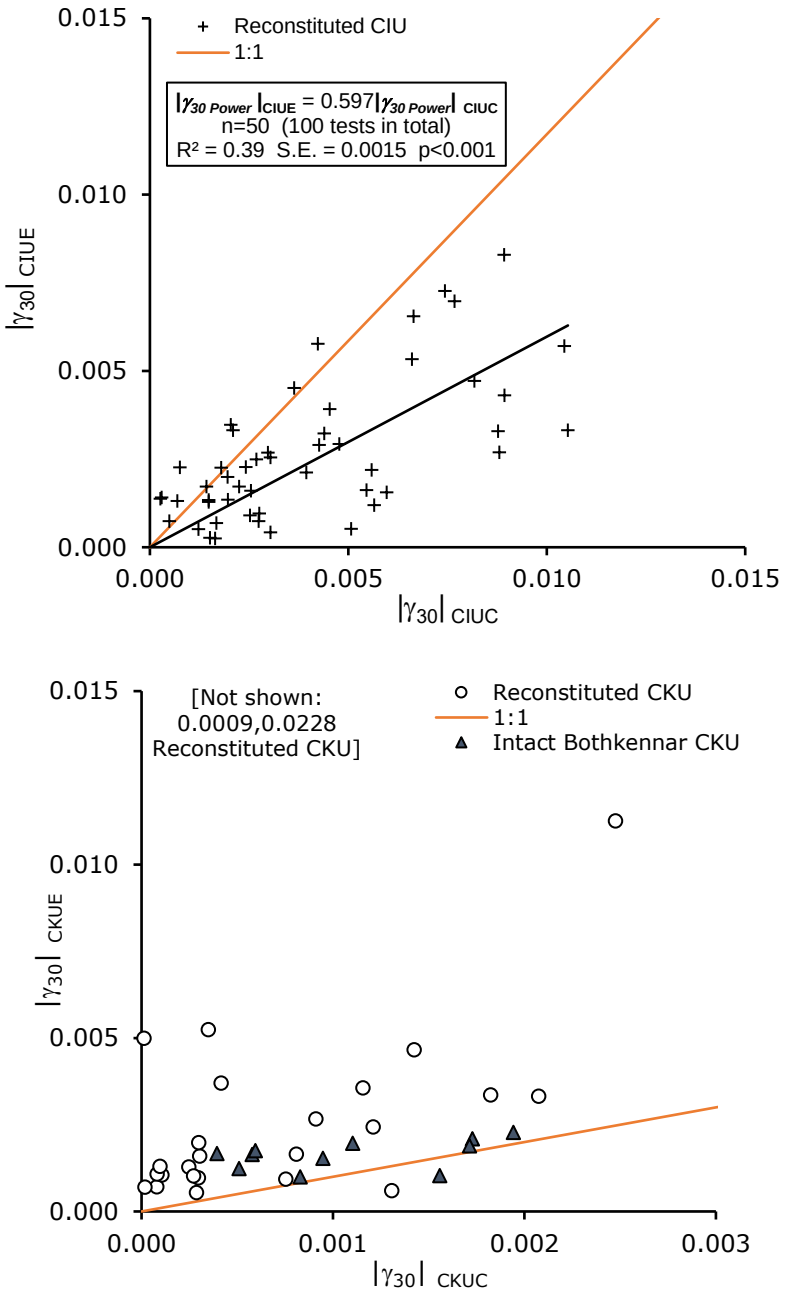

Figure 4- 72. Comparison of $\gamma_{30\ CIU}$ and $\gamma_{30\ CKU}$ from triaxial extension and compression tests on two similarly reconstituted specimens, or two intact specimens from the same sample depth, tested at the same laboratory and with identical strain rate: (a) CIU tests and (b) CKU tests

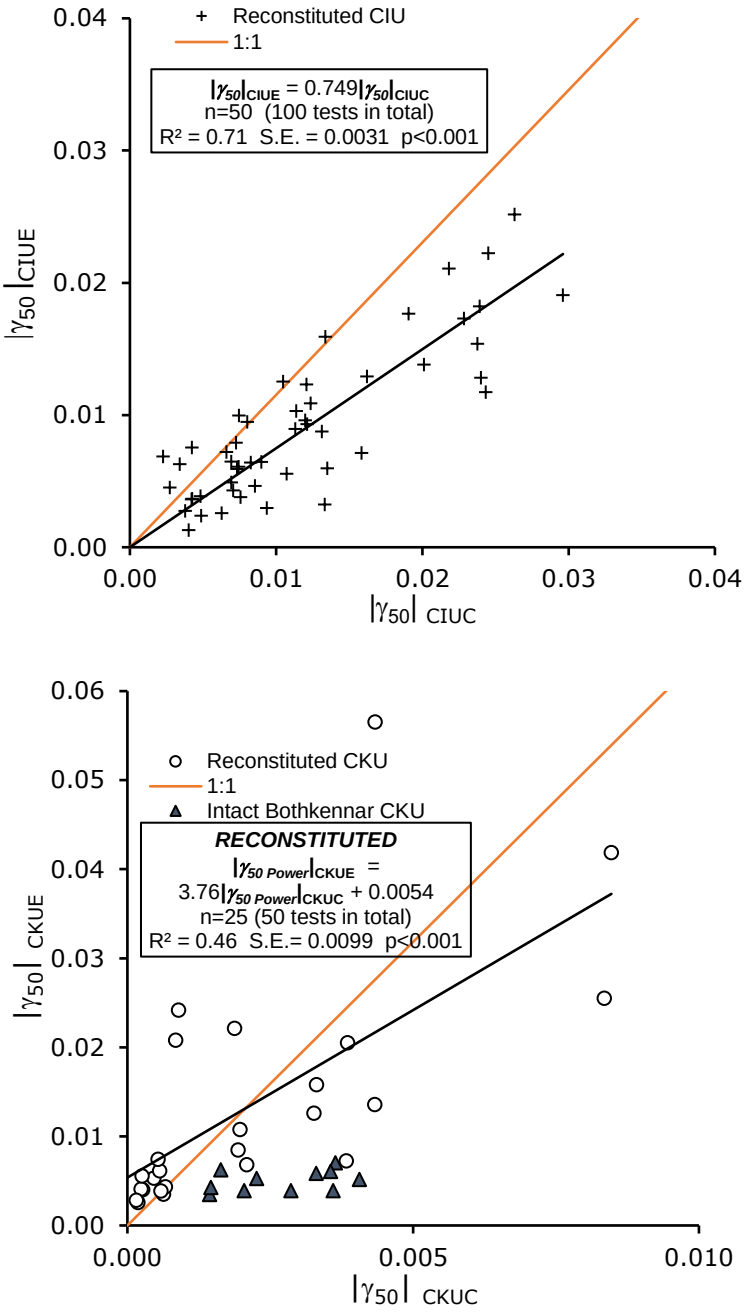

Figure 4- 73. Comparison of $\gamma_{50\ CIU}$ and $\gamma_{50\ CKU}$ from triaxial extension and compression tests on two similarly reconstituted specimens, or two intact specimens from the same sample depth, tested at the same laboratory and with identical strain rate: (a) CIU tests and (b) CKU tests

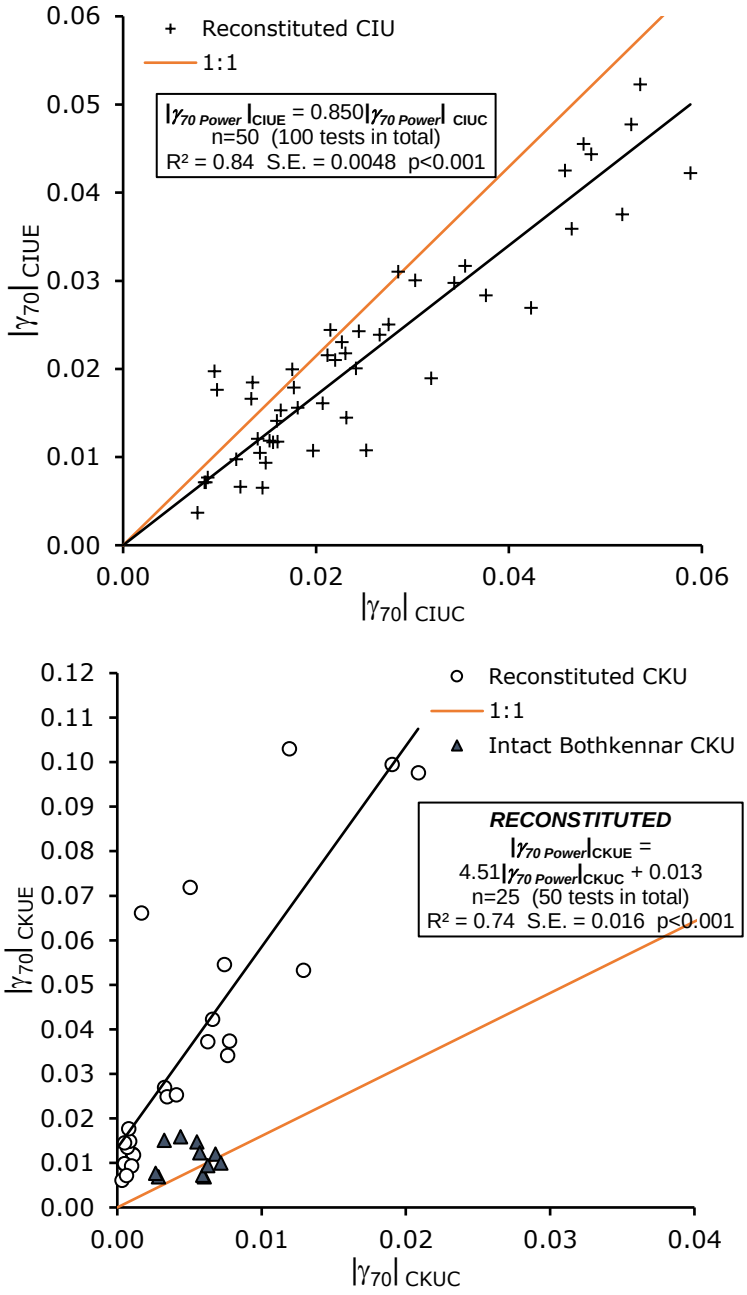

Figure 4- 74. Comparison of $\gamma_{70\ CIU}$ and $\gamma_{70\ CKU}$ from triaxial extension and compression tests on two similarly reconstituted specimens, or two intact specimens from the same sample depth, tested at the same laboratory and with identical strain rate: (a) CIU tests and (b) CKU tests

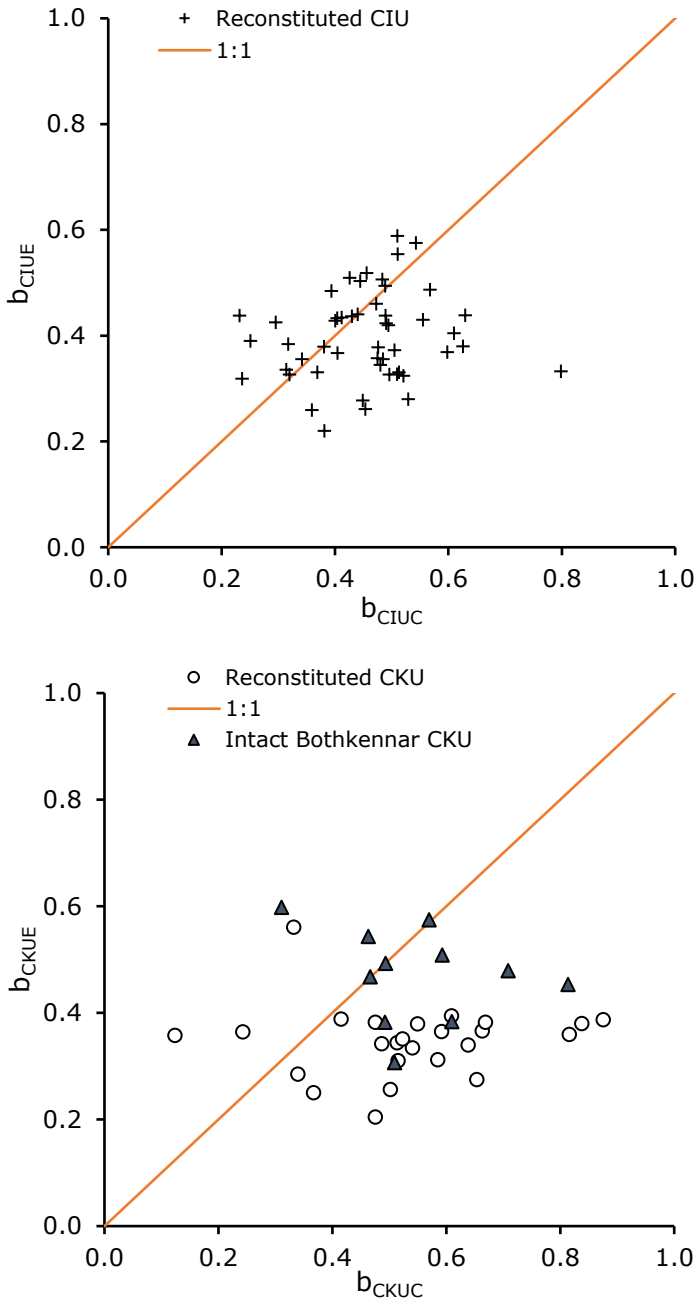

Figure 4- 75. Comparison of *b*-values from triaxial extension and compression tests on two similarly reconstituted specimens, or two intact specimens from the same sample depth, tested at the same laboratory and with identical strain rate: (a) CIU tests (b) CKU tests

Table 4- 11. Single Linear Regression of $\gamma_{30\ Power\ Extension}$ with $\gamma_{30\ Power\ Compression}$

Sample type	Database Reference	*OCR*	CIU, CKU or CAU	$K_{\gamma 30} = (\gamma_{30\ Power})_E / (\gamma_{30\ Power})_C$	n	R^2	S.E.	p-value	Data within error bounds	± %Error	Factor Error	Bias	COV
Reconstituted	RFG/TXCU-278	1-7	CKU	No correlation; mean=7.5 excluding $K_{\gamma 30}$ = 370	25	-	-	-	-	-	-	-	-
Intact	BTK/TXCU-34	1.3-1.9	CKU	No correlation; mean=1.93	11		-	-	-	-	-	-	-
Reconstituted	RFG/TXCU-278	1-12	CIU	0.597	50	0.39	0.0015	<0.001	80%	-	2.7	1.59	1.04

Table 4- 12. Single Linear Regression of $\gamma_{50\ Power\ Extension}$ with $\gamma_{50\ Power\ Compression}$

Sample type	Database Reference	*OCR*	CIU, CKU or CAU	$K_{\gamma 50} = (\gamma_{50\ Power})_E / (\gamma_{50\ Power})_C$	n	R^2	S.E.	p-value	Data within error bounds	± %Error	Factor Error	Bias	COV
Reconstituted	RFG/TXCU-278	1-7	CKU	See Fig. 4- 72	25	0.46	0.0099	<0.001	80%	80	2.2	0.97	0.70
Intact	BTK/TXCU-34	1.3-1.9	CKU	No correlation; mean=2.06	11	-	-	-	-	-	-	-	-
Reconstituted	RFG/TXCU-278	1-12	CIU	0.749	50	0.71	0.0031	<0.001	80%	60	1.7	1.15	0.53

Table 4- 13. Single Linear Regression of $\gamma_{70\ Power\ Extension}$ with $\gamma_{70\ Power\ Compression}$

Sample type	Database Reference	*OCR*	CIU, CKU or CAU	$K_{\gamma 70} = (\gamma_{70\ Power})_E / (\gamma_{70\ Power})_C$	n	R^2	S.E.	p-value	Data within error bounds	± %Error	Factor Error	Bias	COV
Reconstituted	RFG/TXCU-278	1-7	CKU	See Fig. 4- 73	25	0.74	0.016	<0.001	80%	50	1.6	0.97	0.59
Intact	BTK/TXCU-34	1.3-1.9	CKU	No correlation; mean=2.32	-	-	-	-	-	-	-	-	-
Reconstituted	RFG/TXCU-278	1-12	CIU	0.850	50	0.84	0.0048	<0.001	80%	35	1.4	1.05	0.33

Table 4- 14. Single Linear Regression of c_u/σ'_{v0} Extension with c_u/σ'_{v0} Compression

Sample type	Database Reference	*OCR*	CIU or CKU	$K_s = (c_u/\sigma'_{v0})_E / c_u/\sigma'_{v0})_C$	n	R^2	S.E.	p-value	Data within error bounds	± %Error	Factor Error	Bias	COV
Reconstituted	RFG/TXCU-278	1-7	CKU	0.649	29	0.92	0.080	<0.001	83%	35	1.40	0.95	0.24
Intact	Mayne & Holtz 1985	1-20	CKU	0.619	56	0.84	0.112	<0.001	82%	30	1.60	0.88	0.29
Intact	Mayne & Holtz 1985 and BTK/TXCU-34	1-20	CKU	0.608	67	0.83	0.108	<0.001	81%	40	1.55	0.89	0.30
Reconstituted	RFG/TXCU-278	1-12	CIU	0.835	50	0.94	0.110	<0.001	82%	30	1.30	1.07	0.17
Intact	Mayne & Holtz 1985	1-20	CIU	0.774	14	0.96	0.117	<0.001	79%	30	1.40	1.01	0.25

4.5 Recommended correlations to describe parameter variability of reconstituted soils

This chapter demonstrates a method of quantifying parameter variability using a simple calculation of factor errors about an average regression line. The database analysis of RFG/TXCU-278 in the preceding sections of the chapter has facilitated the development of the following correlations, which describe the average variation of the undrained strength and strain parameters of reconstituted soils per test mode with *OCR*:

$$\gamma_{50\ \text{Power CIUC}} = 0.0074 + 0.0010\,OCR \tag{4.11}$$

(n = 114, R^2 = 0.51, *S.E.* = 0.0051, p < 0.001, Factor Error = 1.75 with 80% of the data)

$$\gamma_{50\ \text{Power CIUE}} = 0.0042 + 0.0013\,OCR \tag{4.14}$$

(n = 55, R^2 = 0.65, *S.E.* = 0.0033, p < 0.001, Factor Error = 1.70 with 80% of the data)

$$\log_{10}(\gamma_{50\ \text{Power CKUC}}) = 1.35\log_{10}(OCR) - 3.31 \tag{4.17}$$

(n = 67, R^2 = 0.79, *S.E.* = 0.234, p < 0.001, Factor Error = 2.0 with 80% of the data)

$$\gamma_{50\ \text{Power CKUE}} = 0.0038\,OCR \tag{4.20}$$

(n = 30, R^2 = 0.45, *S.E.* = 0.0086, p < 0.001, Factor Error = 2.10 with 80% of the data)

$$\log_{10}\left(\frac{c_u}{\sigma'_{v0}}\right)_{\text{CIUC}} = 0.653\log_{10}(OCR) - 0.541 \tag{4.22}$$

(n = 115, R^2 = 0.86, *S.E.* = 0.114, p < 0.001, Factor Error = 1.45 with 80% of the data)

$$\log_{10}\left(\frac{c_u}{\sigma'_{v0}}\right)_{\text{CIUE}} = 0.729\log_{10}(OCR) - 0.574 \tag{4.23}$$

(n = 55, R^2 = 0.92, *S.E.* = 0.083, p < 0.001, Factor Error = 1.30 with 80% of the data)

$$\log_{10}\left(\frac{c_u}{\sigma'_{v0}}\right)_{\text{CKUC}} = 0.790\log_{10}(OCR) - 0.522 \tag{4.24}$$

(n = 74, R^2 = 0.94, *S.E.* = 0.066, p < 0.001, Factor Error = 1.20 with 80% of the data)

$$\log_{10}\left(\frac{c_u}{\sigma'_{v0}}\right)_{\text{CKUE}} = 0.952\log_{10}(OCR) - 0.782 \tag{4.25}$$

(n = 34, R^2 = 0.94, *S.E.* = 0.087, p < 0.001, Factor Error = 1.30 with 80% of the data)

Axial strain rate ($\dot{\varepsilon}_a$ in %/hour) improves the estimate of c_u/σ'_{v0} by a reduction in factor error of 11 to 28%:

$$\log_{10}\left(\frac{c_u}{\sigma'_{v0}}\right)_{\text{CIUC}} = 0.639\log_{10}(OCR) - 0.038\log_{10}(\dot{\varepsilon}_a) - 0.526 \quad (4.26)$$

(n = 115, R^2 = 0.87, *S.E.* = 0.112, p < 0.001, Factor Error = 1.40 with 80% of the data)

$$\log_{10}\left(\frac{c_u}{\sigma'_{v0}}\right)_{\text{CIUE}} = 0.719\log_{10}(OCR) - 0.053\log_{10}(\dot{\varepsilon}_a) - 0.567 \quad (4.27)$$

(n = 55, R^2 = 0.94, *S.E.* = 0.074, p < 0.001, Factor Error = 1.25 with 80% of the data)

$$\log_{10}\left(\frac{c_u}{\sigma'_{v0}}\right)_{\text{CKUC}} = 0.786\log_{10}(OCR) - 0.032\log_{10}(\dot{\varepsilon}_a) - 0.516 \quad (4.28)$$

(n = 65, R^2 = 0.96, *S.E.* = 0.058, p < 0.001, Factor Error = 1.15 with 80% of the data)

$$\log_{10}\left(\frac{c_u}{\sigma'_{v0}}\right)_{\text{CKUE}} = 0.931\log_{10}(OCR) - 0.025\log_{10}(\dot{\varepsilon}_a) - 0.788 \quad (4.28)$$

(n = 28, R^2 = 0.95, *S.E.* = 0.076, p < 0.001, Factor Error = 1.25 with 80% of the data)

Parameter variability can also be described by shear mode:

$$\gamma_{50\ \text{Power CIUE}} = 0.749\gamma_{50\ \text{Power CIUC}} \quad (4.29)$$

(n = 50, R^2 = 0.71, *S.E.* = 0.0031, p < 0.001, Factor Error = 1.7 with 80% of the data)

$$\gamma_{50\ \text{Power CKUE}} = 3.76\gamma_{50\ \text{Power CKUC}} + 0.0054 \quad (4.30)$$

(n = 25, R^2 = 0.46, *S.E.* = 0.0099, p < 0.001, Factor Error = 2.2 with 80% of the data)

$$\left(\frac{c_u}{\sigma'_{v0}}\right)_{\text{CIUE}} = 0.835\left(\frac{c_u}{\sigma'_{v0}}\right)_{\text{CIUC}} \quad (4.31)$$

(n = 50, R^2 = 0.94, *S.E.* = 0.110, p < 0.001, Factor Error = 1.30 with 80% of the data)

$$\left(\frac{c_u}{\sigma'_{v0}}\right)_{\text{CKUE}} = 0.649\left(\frac{c_u}{\sigma'_{v0}}\right)_{\text{CKUC}} \quad (4.32)$$

(n = 29, R^2 = 0.92, *S.E.* = 0.080, p < 0.001, Factor Error = 1.40 with 80% of the data)

However, the nonlinearity parameter *b* does not correlate with *OCR* or shear mode. The variability of *b* is therefore described using mean ± standard deviation:

$$\text{mean } b_{CIUC} = 0.459 \pm 0.143$$

$$\text{mean } b_{CIUE} = 0.399 \pm 0.082$$

$$\text{mean } b_{CKUC} = 0.581 \pm 0.167$$

$$\text{mean } b_{CKUE} = 0.350 \pm 0.100$$

4.6 Discussion

The evidence presented in this study suggests that the variability of $\gamma_{50\ Power}$ cannot be explained by *OCR* and shear-mode anisotropy to the same extent as c_u/σ'_{v0}. However, knowledge of *OCR* is significant as it can indicate the magnitude of $\gamma_{50\ Power}$ of a reconstituted soil to within a factor error of ·/1.7 to 2.1, dependent on the test mode considered (and 80% of the data points as defined by Equation 3.19). Comparing this with the calculated factor errors for c_u/σ'_{v0} of the same tests shows that peak stresses can be predicted with less than $^3/_5$ the error using *OCR* as the single independent variable – hence confirming that strain data are more varied than undrained strength data. It is possible that the strain data have been affected more by the digitisation process although steps were taken to minimise inconsistencies of the digitisation of each stress-strain curve. It is more likely that the strain measurement system and boundary conditions of the sample employed for each test has a stronger influence on the data variability. External strain measurements were predominantly used by the cited publication authors (see Table 3- 6) which are known to be sensitive to seating and bedding errors, non-uniform sample deformations, and compliance of the apparatus (e.g., Jardine et al. 1984).

With the experimental strain rates in the database varying by about 3 log cycles in each test mode (Table 4- 7), 30% of the variation in measured c_u may be expected due to variation in axial strain rate (Kulhawy and Mayne 1990). However, when axial strain rate is included with *OCR* as an independent variable in the multiple linear regression model of c_u/σ'_{v0}, an increase in c_u/σ'_{v0} of 7 to 15% is associated with increasing the strain rate by approximately 3 log cycles. Any association of strain rate

with the deformation parameters $\gamma_{50\ Power}$ and b is either very weak or absent (Table 4- 8 and 4- 9). For CIUC and CIUE tests, c_u/σ'_{v0} can be estimated with less error from the derived transformation models if w_L is available in addition to *OCR* and strain rate but the added information of w_L does not reduce the error in the estimation of $\gamma_{50\ Power}$ and b. The comparison here is interesting because it suggests that while c_u varies strongly with stress history (σ'_{v0} and *OCR*), strain rate, and possibly composition (indicated by w_L), when tested for association with the same variables the nonlinear deformation of a reconstituted sample is influenced only by the *OCR*. Moreover, the degree of non-linearity (b) is highly uncertain; significant correlations exist only between b and $\gamma_{50\ Power}$. Unlike the experimental results presented by Vardanega et al. (2012), no correlations were found between b and *OCR* for RFG/TXCU-278.

The above suggests that the normalisation procedure, using the parameter S, removes the effects of strain rate and composition (indicated by w_L) on $\gamma_{50\ Power}$ while *OCR* remains a dominant influence; or alternatively, the strong association between *OCR* and c_u is similarly present between *OCR* and $\gamma_{50\ Power}$ but the variability due to measurement uncertainty (Figure 3 -1) has a greater effect on $\gamma_{50\ Power}$ - which could potentially mask the effects of strain rate and w_L. A further explanation is that $\gamma_{50\ Power}$ is sensitive to other variables that were not tested in this study, which may be representative of differences in water content, fabric and mineralogy. However, it is likely that the significant variability shown by the non-linearity parameter, b, and its lack of significant association with *OCR* or other variables, is indicative of the variability due to measurement uncertainty of strains between $20\% \leq S \leq 80\%$.

When considering the possible anisotropy of stress-strain behaviour in design problems, a variety of soil tests can be employed to assess the effect of shear mode on c_u variation (e.g., Kulhawy and Mayne 1990, Low et al. 2011, Ratananikom et al. 2015). Here the same approach was taken to assess the effect of shear mode on γ, demonstrating that reference strains are more sensitive to shear-mode anisotropy than peak stresses and the effect is less predictable (more uncertain). At a stress ratio of 0.5, shear-mode anisotropy of strain is influenced strongly by consolidation mode: for K_0 consolidated samples, the ratio K_γ can vary by up to an order of magnitude for the same *OCR*. Estimation of K_γ with *OCR* is therefore highly uncertain, and a better approach may be adopted by undertaking one compression test to predict the corresponding strain in extension and accepting an error of ·/1.6 to 2.2

(at S=0.7 or 0.5) without concerning *OCR*. The factor error increases when the values of K_γ in Table 4- 12 and 4- 13 are applied to the Bothkennar clay tests of BTK/TXCU-34, overpredicting all values of $\gamma_{50\ \text{Power CKUE}}$ and $\gamma_{70\ \text{Power CKUE}}$ respectively by a factor of 3 and 3.4 on average (the factor varies between 1.8 and 5.8). Whilst conservative, if such an error is unacceptable, any serviceability designs reliant on K_0 stress paths and knowledge of deformations in triaxial extension would require CKUE tests.

The detailed analysis of BTK/TXCU-34 and RFG/TXCU-278 in sections 4.3 and 4.4 identified distinct differences in stress-strain behaviour between the two databases of soil tests and a designer should exercise caution before applying correlations developed from reconstituted materials to natural fine-grained deposits. A comparison of reconstituted parameters and intact parameters could however be valuable, as demonstrated by the framework of Burland (1990) concerning the compressibility of natural clays. In this chapter it was shown that for a given *OCR* (taken as equal to *YSR*), on average, reconstituted triaxial specimens (consolidated one-dimensionally to higher stresses than the intact Bothkennar specimens) deform less at S=50% (lower $\gamma_{50\ \text{Power CKUC}}$) and more nonlinearly (lower b_{CKUC}) in undrained compression than intact Bothkennar clay specimens. In triaxial extension, reconstituted soils deform about the same or more (greater $\gamma_{50\ \text{Power CKUE}}$) than intact Bothkennar clay and the stress-strain curves tend to be more nonlinear (lower b_{CKUE}). When tested using SHANSEP procedures, the Bothkennar clay is partly destructured and both model parameters indicate that there is a shift in stress-strain behaviour that brings the soil to a transitional state (Figure 4- 35): destructuration of a soil may then be indicated by lower *b* values. However, weathering and higher *OCR* towards ground level seem to be associated with higher *b* values in the Bothkennar clay (Figure 4- 22).

If the measurement uncertainty of the parameters is now taken to be represented by the standard deviation of b_{CKUC} = ±0.17 (Figure 4- 21) and the factor error of $\gamma_{50\ \text{Power CKUC}}$ associated with $\gamma_{50\ \text{Power CKUC}}$ = f(*OCR*) = ·/2.0 (Table 4- 9), then it can be concluded that the increases in b_{CKUC} and $\gamma_{50\ \text{Power CKUC}}$ with decreasing depth in the shallowest 4m of clay exceed the expected variance due to measurement uncertainty, hence permitting more confidence in the identified variation with depth.

The advantage of using a simple curve-fitting method to approximate stress-strain data with Model 2 is that only 4 parameters (τ_0, c_u, $\gamma_{50\,\mathrm{Power}}$, and b) are needed to simulate stress-strain behaviour between $20\% \leq S \leq 80\%$. This is a significant range of nonlinear soil behaviour and foundation performance. For procedures of settlement prediction which rely upon the assumption of similarity between the load-settlement relationship and the experimental stress-strain curve (e.g. Skempton 1951, Bolton et al. 1990, Osman and Bolton 2005, Klar and Klein 2014), such a range represents a factor of safety on undrained collapse of 5 to 1.25. Models with fewer parameters typically require fewer tests; in this case only one triaxial test is needed, which means that parameter distributions can be developed for variability analyses to examine possible causes of variation. A simple model such as Model 2 can also be calibrated with any geotechnical test that measures constant volume deformations with deviator stress – on the condition that the test shears the soil to peak failure. This chapter has demonstrated that the test mode is significant: c_u, $\gamma_{50\,\mathrm{Power}}$, and b, or indeed the parameters for any other stress-strain model of choice, must always be reported with the relevant test mode (i.e. CKUC, CIUC, CKUE, CIUE, UU, FV, plate load test, pile load test, pressuremeter test and so on).

There is a trade-off between model simplicity and simulation complexity: simplifying the model means that fewer facets of behaviour can be simulated. An example of this trade-off was demonstrated in section 4.2 by comparing Model 1 with Models 2 and 3; excluding a non-linearity parameter resulted in significant modelling error and bias. Despite its advantage of simplicity, the chosen model (Model 2) is limited by the stress range to which it has been calibrated ($20\% \leq S \leq 80\%$) and by the required normalisation procedure: the modelled portion of the stress-strain curve is always defined relative to the peak yield stress (c_u). As a result, other yield points are missed or obscured: the point of maximum curvature may fall outside the modelled range of stress ratio; Y1 (the elastic yield point) will always fall below S=0.2; Y2, the condition at which plastic strains accumulate (Smith et al. 1992), may or may not occur at stresses lower than S=0.2. Hence, if the numerical model of soil behaviour adopted for design requires a more nuanced knowledge of yield surfaces, or within a specified range of strain, then Model 2 is simply inadequate. Model 2 is further limited by the curve fitting procedure which requires a minimum of 3 data points between $20\% \leq S \leq 80\%$. The representation of

stress-strain non-linearity would undoubtedly improve with a higher number of data points. For RFG/TXCU-278, this number varies between 3 and 200 and may explain some of the variability of *b*.

A similar compromise must be achieved between test simplicity (cost) and information about the soil. For instance, UU tests are popular due to their speed and low cost, but without pore pressure measurements no information can be obtained about the effective stresses before and during shear. More complex constitutive models necessitate more sophisticated tests, and hence greater investment in the ground investigation phase of the project. However, this chapter has demonstrated using a large database of reconstituted soil tests that a CU triaxial test is affected by parameter uncertainty and the degree of uncertainty varies with test mode and available information. For a given *OCR*, the variability (possibly resulting from measurement uncertainty) of $\gamma_{50\ Power\ CKUE}$, expressed by a factor error of ·/2.1, exceeds the variability of $\gamma_{50\ Power}$ measured from CKUC, CIUC and CIUE tests (in order of reducing error, see Table 4- 9 and section 4.5). When *OCR* is unknown, but a single compression test is available, the variability of strain anisotropy allows $\gamma_{50\ Power\ CKUE}$ to be estimated to an accuracy of ·/2.2; hence the reduction in uncertainty achieved by measurement of *OCR* versus the measurement of $\gamma_{50\ Power\ CKUC}$ (and the cost of the tests required) is only 8%. Using the information in this chapter and/or following the demonstrated method with another database of soil tests, it would be possible to justify the procurement of additional testing where the uncertainty associated with parameter estimates from empirical correlations is unacceptable for the design.

The end of this chapter concludes Part (1) of the thesis. A key conclusion of Part (1) is that the variability of c_u/σ'_{v0} and $\gamma_{50\ Power}$ measured in the new database of reconstituted soil tests could not be explained by including additional predictors in a multiple regression model (using strain rate, liquid limit, and plastic limit in addition to *OCR*), implying that measurement uncertainty outweighs the influence of these variables on parameter variability. In Part (2), this hypothesis is tested: chapters 5 and 6 describe the methods and results of a laboratory investigation that examines parameter variation due to testing procedure and measurement interpretation using two soils. The new experimental data also provide opportunity to test the predictive capability of the empirical transformation models correlating CIU parameters with *OCR* and anisotropy, as proposed in Part (1). Furthermore, a direct

comparison of the stress-strain measurements on specimens from the same experimental programme would provide a more rigorous examination of the effects of reconstituted and intact states on the measured parameters. Since few experimental data were previously available for CIU tests on Bothkennar clay, and since published triaxial extension data are generally less available than triaxial compression data, the new CIUC and CIUE tests add to the present knowledge of stress-strain behaviour variations with stress history and anisotropy.

5. Developing an experimental strategy to investigate stress-strain variability using two soils

Parts of this chapter have been included in the following publication:

Beesley M.E.W., Vardanega P.J., and Ibraim, E., 2019. "Developing an experimental strategy to investigate stress-strain models using kaolin*"*. In: *Recent Advancements on Expansive Soils*, *GeoMEast 2018*, Springer, Cham, Switzerland: 99-118.

5.1 Introduction

To interrogate and validate the results of the triaxial test database analysis (presented in Chapter 4), an independent set of new experimental data was obtained from a laboratory programme of triaxial compression and extension tests. This chapter describes the selection of suitable test materials, apparatus and procedures used in the experiments.

5.2 Selection of experimental materials

Materials for the laboratory test programme were selected to deliver the following objectives:

(1) Using one reconstituted soil, to undertake a new series of CU triaxial compression and extension tests on samples consolidated at different overconsolidation ratios (*OCR*), for comparison with the results of the database analysis presented in Chapter 4.

(2) To investigate the sensitivity of parameters to different CU triaxial test procedures (used to consolidate and shear the specimen).

(3) Using the same test procedures (i.e. reconstitution, consolidation, and undrained shear), to investigate the sensitivity of parameters to two different reconstituted soils.

(4) Using the same soil and test procedures (i.e. reconstitution, consolidation, and undrained shear), to investigate the sensitivity of parameters to reconstituted and intact material states.

Objective (1) makes it possible to evaluate variations in stress-strain behaviour and the resulting parameters (c_u/σ'_{v0}, $\gamma_{50\ \mathrm{Power}}$, and b) so that the prediction limits of the database analysis can be tested. Adopting the parameter uncertainty framework proposed in Chapter 3 (Table 3- 1), objective (2) seeks to quantify parameter uncertainty associated with items 2b, 3b and 4 using a series of controlled experiments on a single material. Hence, one of the conclusions in Chapter 4 may be challenged: parameter variability (of c_u/σ'_{v0}, $\gamma_{50\ \mathrm{Power}}$, and b) that could not be explained by empirical MLR predictions (using *OCR*, strain rate, liquid limit, and plastic limit) was attributed to measurement uncertainty. Finally, objectives (3) and (4) facilitate an assessment of soil constituents and destructuration effects on the model parameters (c_u/σ'_{v0}, $\gamma_{50\ \mathrm{Power}}$, and b).

Two fine-grained materials were used for the experimental investigation: Kaolin (reconstituted) and Bothkennar (undisturbed and reconstituted).

5.2.1 Reconstituted Kaolin

To address objectives (1) and (2) i.e. to investigate the sensitivity of c_u/σ'_{v0}, $\gamma_{50\ \mathrm{Power}}$, and b to *OCR*, shear mode, and different test procedures, a large quantity of uniform fine-grained samples was required. Kaolin was selected as the primary test material as it has: (i) a uniform grade available in large quantities; and (ii) a relatively fast consolidation rate for fine-grained material. Uniform grading of dry powdered kaolin can be achieved by quarrying and processing china clay. One Speswhite Kaolin batch from a single supplier (Imerys) was used. Kaolin has been used extensively by experimental researchers to investigate mechanical behaviour of fine-grained soil due to the relatively short time required to complete consolidation for a plastic soil. For this reason, a significant proportion (88 tests) of RFG/TXCU-278 was compiled from experiments using kaolin samples. With an appropriate method of making uniform laboratory samples, kaolin may be a useful 'benchmark' experimental material to which reconstituted samples from natural deposits can be compared (i.e. objective 3).

5.2.2 Undisturbed and Reconstituted Bothkennar clay

The second material, Bothkennar clay, was available from an intact block sample that was used in a previous experimental investigation by Sukolrat (2007). In 1984, researchers at Bristol University (Hawkins et al. 1989) initiated a nationwide search for a soft clay test site. Nash et al. (1992a) undertook a detailed ground investigation of the Bothkennar Test Site in Scotland, United Kingdom, as partners in a multi-institutional research consortium commissioned by the Science and Engineering Research Council (SERC). Characterisation of the Bothkennar soil deposit involved the analyses of extensive in-situ, laboratory, and field tests which were published primarily in Volume 42 of the journal '*Geotechnique*' in June 1992 (and reported by SERC 1989). Such a superior deposit characterisation is an advantage in the context of this research which aims to quantify the variability of parameters deduced from test measurements. Further samples of Bothkennar clay were taken from the site in 1997 (Sukolrat 2007). Fortunately, at the outset of the project, some of the natural block samples from the second ground investigation were still available in the Geomechanics Laboratory at Bristol University. To limit waste material and in view of programme constraints, a block of Bothkennar clay was used in this study which had been trimmed and resealed by Sukolrat (2007).

5.2.3 Geology of Bothkennar

Bothkennar is a postglacial deposit formed by estuarine conditions in the Forth valley. It is likely to have been deposited around 10 000 BP under water levels between 5 to 20m (Nash et al. 1992a, Paul et al. 1992). The clay bed appears to have been lightly overconsolidated by a combination of erosion during the fall in sea level, fluctuations in groundwater (Nash et al. 1992a), and ageing effects (Hight et al 1992a). It is a plastic clayey silt (Hight et al. 1992a), with unusually high UU measurements of undrained shear strength for a low *OCR* fine-grained material (Nash et al. 1992a). High organic content was found to increase liquid limit and plasticity index (Paul et al. 1992). The stress-strain-strength behaviour of the soil is likely to be affected by the presence of organic material and silt. Variation in c_u measurements has been attributed to the soil's natural variability in structure (Hight et al 1992a). Hight et al. (1992b) observed that the clay had a sensitive structure demonstrated by differences in yield stresses between disturbed specimens.

5.3 Experimental procedures

Development of the final triaxial experimental procedure was an iterative process; the author's experimental strategy was to develop testing conditions that would:

(1) be consistent with sample reconstitution and consolidation methods used by the authors of the database publications,

(2) be consistent with routine triaxial test practices employed by commercial laboratories,

(3) facilitate an assessment of undrained stress-strain behaviour using techniques suitable for the chosen material, and

(4) facilitate an assessment of parameter measurement uncertainty.

Two procedures (a) and (b) were developed to examine potential differences in material behaviour (Kaolin) related to reconstitution and consolidation methods. New designs for a triaxial extension cap and axial LVDT connection system were required to shear the specimens in triaxial extension and to accommodate problems with sample tilt. Different load caps were also tested in triaxial compression to evaluate the effect on stress-strain measurements and associated model parameters. These developments are explained in further detail in the following sections.

5.3.1 Laboratory infrastructure

5.3.1.1 Pressure supply

The geomechanics laboratory at the University of Bristol operates the pressure systems of the laboratory workstations via a continuous source of dry compressed air. An Atlas Copco GA5 oil-injected rotary screw compressor produces the compressed air. The compressed air is regulated to mitigate pressure variations from 8 Bar using a manostat pressure regulator and an automated back-up compressor.

5.3.1.2 Power supply

Data acquisition and pressure control systems require a reliable power source, particularly for longer testing regimes applicable to CU tests on fine-grained soil specimens. In the event of a power mains system failure, the geomechanics laboratory is equipped with an uninterrupted power supply

(UPS) system that provides a limited (approximately 20 minutes) emergency power supply. This was particularly useful during construction work for the Queen's Building extension as it twice prevented test failures due to unforeseen power cuts.

5.3.1.3 De-aired water supply

Cell and back pressures used in triaxial experiments are operated in the geomechanics laboratory using saturated hydraulic systems i.e. a network of drains and a water supply. The water must be de-aired to prevent erroneous volume change measurements. This is achieved by a centralised vacuum pump of Venturi design which connects to all the laboratory work stations.

5.3.2 Experimental apparatus

When selecting experimental apparatus, a compromise was needed regarding whether the equipment was suitable to test soft clay specimens, could be reproduced in routine commercial testing facilities, and was available for the programme duration.

5.3.2.1 Conventional triaxial apparatus (CIU tests)

The conventional triaxial cell was chosen for consolidated undrained (CU) tests; a schematic representation of the setup is shown in Figure 5- 1 (reproduced with permission from Bialowas 2017, Figure 3.5). The tests reported in this study were undertaken using the same triaxial system as Bialowas (2017), with some modifications to the load caps and LVDT specimen attachment as noted above.

The CU triaxial apparatus includes the following components:

(1) A hydrostatic cell pressure system comprising:
   a. A triaxial cell filled with fluid (de-aired water) to apply pressures,
   b. Air compressor and air/water (W/A) interface connected to the cell by drains,
   c. Pressure transducer to monitor pressure changes in the cell,

(2) A drainage/back pressure system comprising:
   a. A rubber membrane to seal the specimen against ingress of cell fluid,
   b. Back pressure (BP) control system to vary hydraulic pressure in the specimen, here facilitated by an air compressor and air/water (W/A) interface,

c. Pressure transducers at the top and base drain connections,

d. Volume gauge (VG) to monitor water flowing into/out of the specimen

e. Drains connecting the specimen to the air/water interfaces and pore pressure transducers,

f. Porous stones (and filter papers) between the specimen and the drains to prevent material eroding from the specimen,

(3) A load frame to apply axial load to the specimen during shear,

(4) An internal load cell to measure changes in axial load,

(5) An axial displacement measurement system, here using a linear displacement transducer (LDS) to measure external displacement of the triaxial cell and internal linear variable displacement transducers (LVDTs) to measure local axial displacement of the specimen.

The conventional triaxial testing system as described is typically used for isotropically consolidated triaxial shear tests. This is because the axial load on a sample is controlled by a simple load frame and therefore it is difficult to control $K = \sigma'_h/\sigma'_v$ with reasonable precision.

5.3.2.2 Conventional triaxial apparatus (UU tests)

In addition, unconsolidated undrained (UU) tests were performed as companion tests to the CU programme. Although not typical in practice, the UU tests were undertaken with pore pressure measurements (at the base of the specimen) to establish stress path behaviour. This was achieved simply by creating a closed drainage line connection to the base of the specimen and inserting a pressure transducer into the drainage line. The UU triaxial apparatus is almost identical to the CU triaxial apparatus and includes the following components from section 5.3.1.1: 1a, 1b, 1c, 2a, c (base only), e, f (base only), 3, 4, 5 (LDS only).

5.3.2.3 Conventional oedometer apparatus (CK tests)

To provide a comparison with isotropic compressibility parameters from CU triaxial tests, one-dimensional compression behaviour of the reconstituted soils was investigated using two types of oedometer apparatus. The conventional fixed ring oedometer, is used widely in practice (Clayton et al.

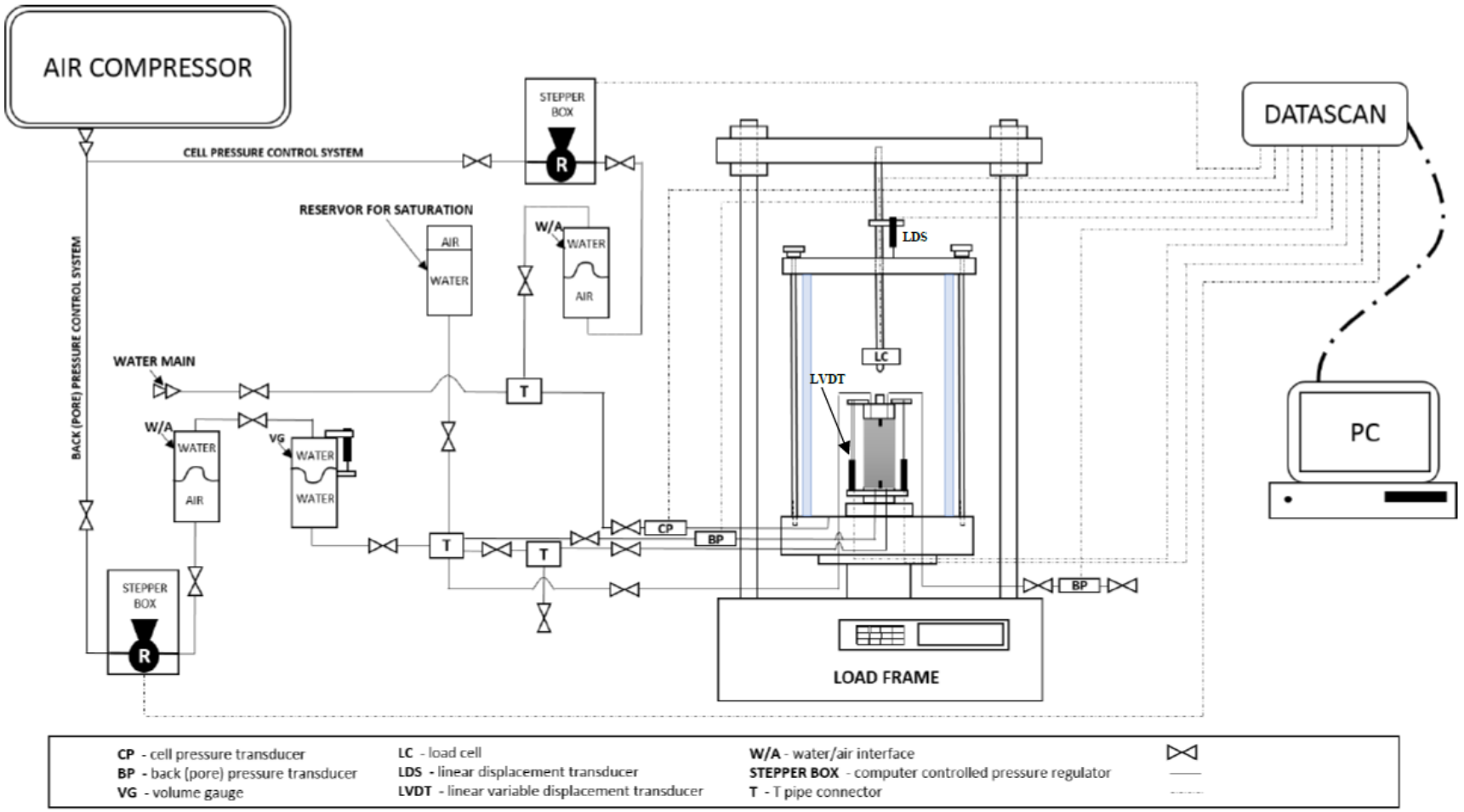

Figure 5- 1. Diagram of the conventional triaxial testing system used for CU tests (reproduced with permission from Bialowas 2017)

1995). The conventional fixed ring oedometer apparatus at Bristol University was used previously by Nash et al. (1992b) to study one-dimensional behaviour of intact Bothkennar samples with the incremental load (IL) method. The load is applied by adding dead weights at the end of a lever arm (of known length), which transmits the load to the top cap via the loading yoke (for reference see Clayton et al. 1995, Figure 8.19). However, a second loading system designed by Bialowas (2017) was also used in this experimental investigation, which applies load by utilising a hydraulic stress-controlled triaxial frame.

Both oedometer apparatuses include the following components:

(1) A fixed rigid ring to confine the specimen thereby preventing lateral deformation,

(2) porous stones at the base and top of the specimen to provide vertical double drainage,

(3) a cell submersed in water open to atmospheric pressure,

(4) loading frame that applies vertical load to the specimen top cap,

(5) linear displacement gauge or transducer to measure changes in specimen height.

5.3.2.4 Consolidometer apparatus

In this study, a tall floating ring consolidometer was used to create individual reconstituted soil specimens suitable for testing in the CU and UU triaxial apparatus. Similar devices were used by Pennington (1999), Sukolrat (2007) and Bialowas (2017) for their experimental investigations at Bristol University. With regard to the studies that contributed experimental data to RFG/TXCU-278, 92 triaxial tests were performed on specimens reconstituted individually by the use of tall consolidometers (Parry & Nadarajah 1974, Conn 1988, Abdulhadi 2004, Gasparre 2005, Sachan & Penumadu 2007, Abdulhadi 2009, Valls-Marquez 2009, Kamal 2012); 15 test specimens were formed by pressing the soil directly into a rigid mould (Parry 1956, 1960, Atkinson & Little 1988); 41 test specimens were prepared from a slurry with no other information provided about the method (Loudon 1967, Hight et al. 1985, Vardanega et al. 2012); the majority (131 triaxial tests) were reconstituted using a large diameter consolidation tank developed to produce multiple specimens.

Batch consolidometers are suitable for reconstituting samples under low normal stresses and where a longer consolidation time may be offset by producing multiple samples at once. Moreover,

batch samples are less adversely affected by side friction development along the consolidometer walls. For this project, the programme duration did not allow enough time to develop and evaluate a new batch consolidometer device. Instead, following the recommendations of Pennington (1999), Sukolrat (2007) and Bialowas (2017), tall consolidometers (Figure 5- 2) were used to prepare individual test specimens with 38mm and 50mm diameters. The effect of side-wall friction is evaluated in section 5.3.3.

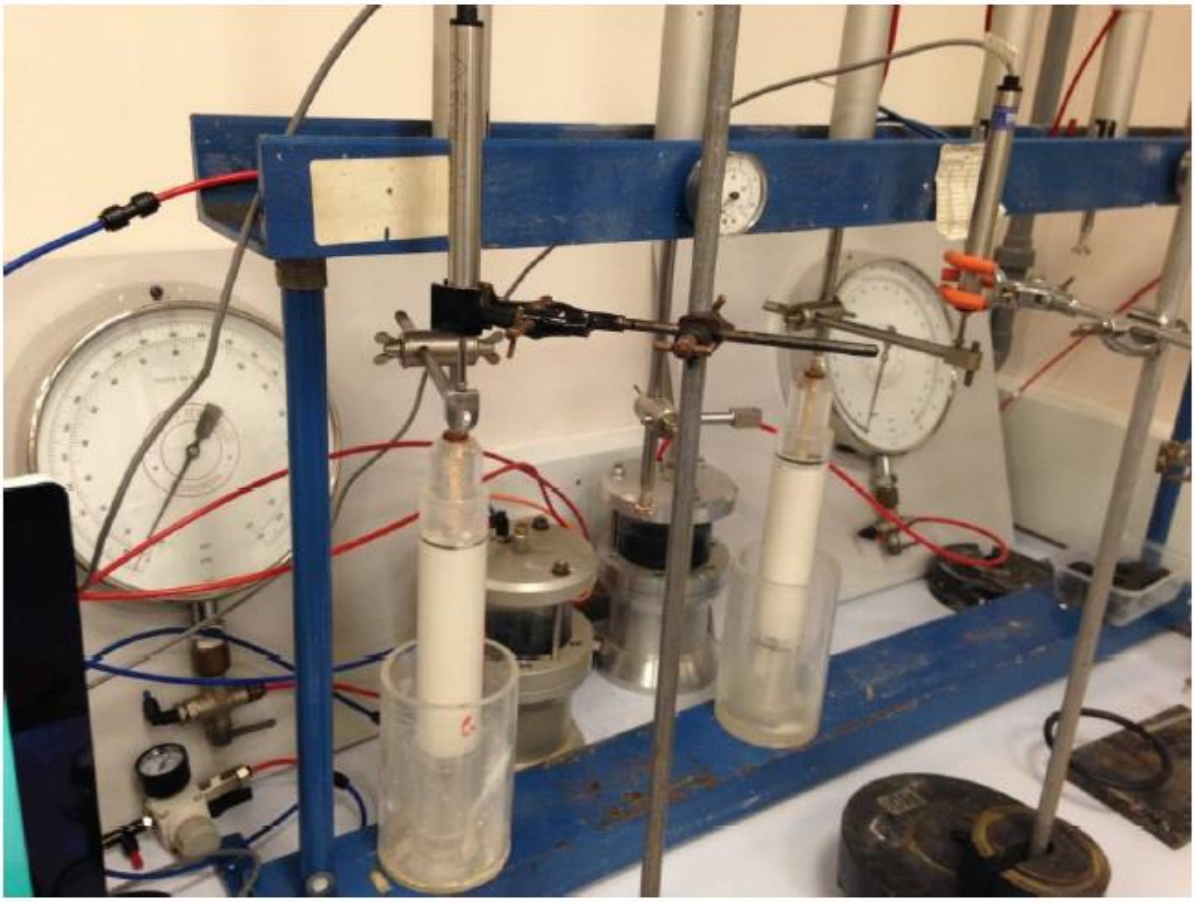

Figure 5- 2. Consolidometers (38mm internal diameter) set up before applying vertical stress to Kaolin slurries

5.3.3 Sampling procedure

5.3.3.1 Reconstituted Kaolin samples

The sampling procedure for reconstituted kaolin triaxial samples was developed from the method described by Bialowas (2017). For all triaxial and oedometer tests, powdered kaolin was initially oven-dried for approximately 12 hours which was subsequently cooled for 3 to 4 hours. This was followed by ten minutes of hand mixing to form a slurry at a water content of $1.95w_L$ (using deaired

deionized water) before curing overnight. Air bubbles were removed from the cured slurry by applying vacuum and vibrations (using a mini shaking table) typically over a period of 2 hours.

For oedometer samples, the de-aired slurry was poured directly into the oedometer ring. For the triaxial samples, the de-aired slurry was then poured into a consolidometer with an internal diameter of 50mm or 38mm (the latter was used for only two UU tests, see Table 5- 3). Compression of the slurry was achieved by applying three increments of vertical pressure to reach a maximum sampling consolidation pressure. Maximum applied pressure varied according to Procedure (a) and Procedure (b) (see section 5.3.4.6). A 24-hour interval was needed for the slurry to consolidate under a single load increment with a further 48 hours following the final increment (i.e. 5 days total duration in the consolidometer). However, to successfully consolidate the slurry it was necessary to continuously monitor settlements and to break shaft friction regularly by displacing the floating ring. Vertical settlements were monitored using a single LDS (Figure 5- 2) to determine the end of each primary consolidation cycle. In two tests ('CIUC-1-b-200' and 'CIUC-1-b-404') the specimens were further 'swelled' to *OCR*=2 in the consolidometer prior to extrusion; although negligible height change was observed during the swelling stage, which was likely to be the result of large shaft friction mobilised in the tall consolidometer. The extruded sample height was designed to be 100mm for CU triaxial tests. All UU specimens were trimmed to size.

5.3.3.2 Reconstituted Bothkennar samples

Identical consolidometers were used to reconstitute the Bothkennar and Kaolin samples. Since Bothkennar clay has a lower saturated hydraulic conductivity than Kaolin, a greater time was required to reach the end of a primary consolidation cycle - approximately 72 hours compared to 24 hours. A further 72 hours followed the final consolidation stage at a constant maximum stress of 100kPa (i.e. 12 days total duration in the consolidometer).

The only remaining differences in sampling procedure between the two reconstituted soils arose from preparing the slurry, described as follows. Trimmings from the samples of darker coloured intact material (see 5.3.3.4) were grated and tested for moisture content (moisture content specimens were untreated and oven dried over 2 days). Deaired deionized water was added to the gratings to form a

slurry at a water content of $1.95w_L$. This was followed by ten minutes of hand mixing and twenty minutes of mechanical mixing before curing overnight. As for the kaolin slurries, air bubbles were removed by placing the slurry mix into a vacuum chamber before pouring into the consolidometer.

5.3.3.3 Evaluation of repeatability using reconstitution procedures

Shaft friction along the consolidometer tube can affect the compression measurement data significantly. Sukolrat (2007) performed oedometer tests on a reconstituted Bothkennar clay sample trimmed down after extrusion from a 75mm consolidometer: yield stress measurements indicated that 35% to 55% of the applied vertical pressure (100kPa) had been lost due to friction. He also observed that frictional losses and moisture content increased from the top to base of sample.

A floating ring consolidometer was used to reduce the effect of shaft friction by regularly displacing the ring. This was found to be more effective with the 50mm-diameter consolidometer and so only a limited number of tests were performed using 38mm tubes. To evaluate repeatability of the reconstitution technique, in Figure 5- 3 the measurement data are plotted from 22 reconstituted samples immediately after extrusion. All data points refer to samples reconstituted using the 50mm consolidometer apparatus except where highlighted. For procedure (a), lower applied stresses were used during consolidation of the slurries (see section 5.3.4.6). Generally an extruded height of 96-106mm and up to 0.17 variation in void ratio could be achieved by the same reconstitution procedure.

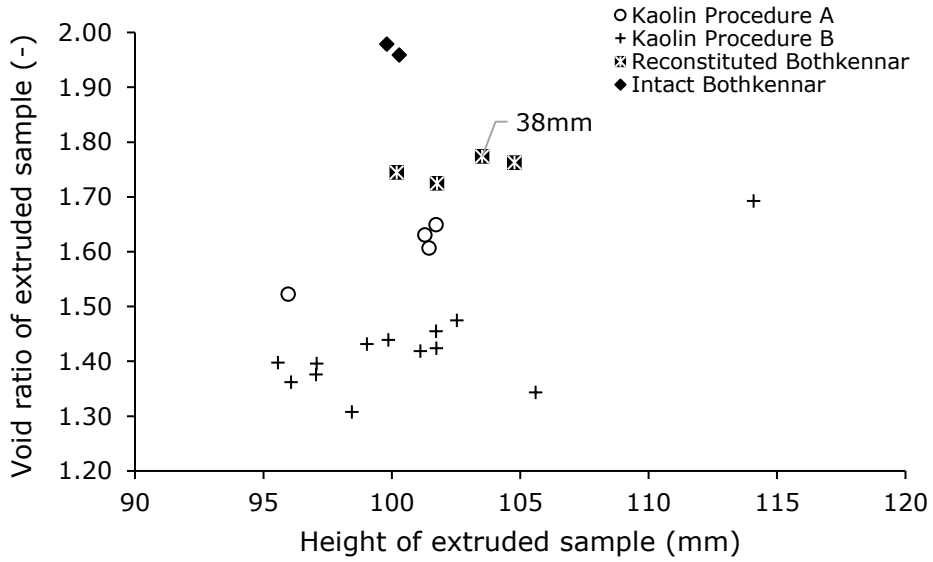

Figure 5- 3. Reconstituted sample height and void ratio measured immediately after extrusion from the consolidometer. Trimmed intact Bothkennar specimens also plotted for reference.

To assess the effect of friction losses on stress history, two Kaolin samples that had been reconstituted in the 50mm consolidometer were trimmed (to 38 x 76 mm cylinder) and set up in the UU triaxial apparatus with a saturated base drainage line connected to a pore pressure transducer. Applying a confining stress under undrained conditions, the change in pore pressure indicated initial effective stresses of 50.3 and 59.5 kPa. These measurements indicate that 50% to 58% of the applied vertical pressure (120kPa) had been lost due to friction and agree with earlier observations by Sukolrat (2007) of consolidometer wall friction effects.

5.3.3.4 Intact Bothkennar samples

The samples of Bothkennar clay used in this experimental study were originally extracted from the site in 1997 using Sherbrooke samplers (Sukolrat 2007). All triaxial specimens were trimmed from a single block sampled at a depth of 5.4m. The block of material had been coated in three layers of wax and cling film and stored in a cool room under temperature control. After previous investigations by Sukolrat (2007), the cylindrical block had been cut down to a smaller wedge (Figure 5- 4) which was suitable to test two intact cylindrical triaxial specimens with 50mm diameter and 100mm height.

The natural clay sample was observed to be in good visual condition, despite having been stored for an extended time and trimmed to extract experimental specimens for a previous study. Figure 5- 5 shows that once the outer oxidised layers were removed, the inner material was proven to be a dark fine-grained material with some areas of paler mottling, as described by previous researchers to be distinctive of the Bothkennar clay. Moisture contents of the trimmings were slightly lower in the outer brown material (67.7% and 67.9%) compared to the inner darker material (70.8% and 71.6%). Using a piano wire and lathe, the wedge was carefully trimmed to the required dimensions. One triaxial specimen was set up immediately in the triaxial cell. The other was carefully waxed and wrapped in cling film before testing could commence, for storage over a further fortnight.

5.3.4 CU Triaxial test procedure

The general procedure for CIU tests is described in detail in Appendix 5.1. The steps taken to saturate the back-pressure system and mitigate possible leaks are included for information, since such procedures were critical to ensure the success of each test. During the setup of triaxial samples in the

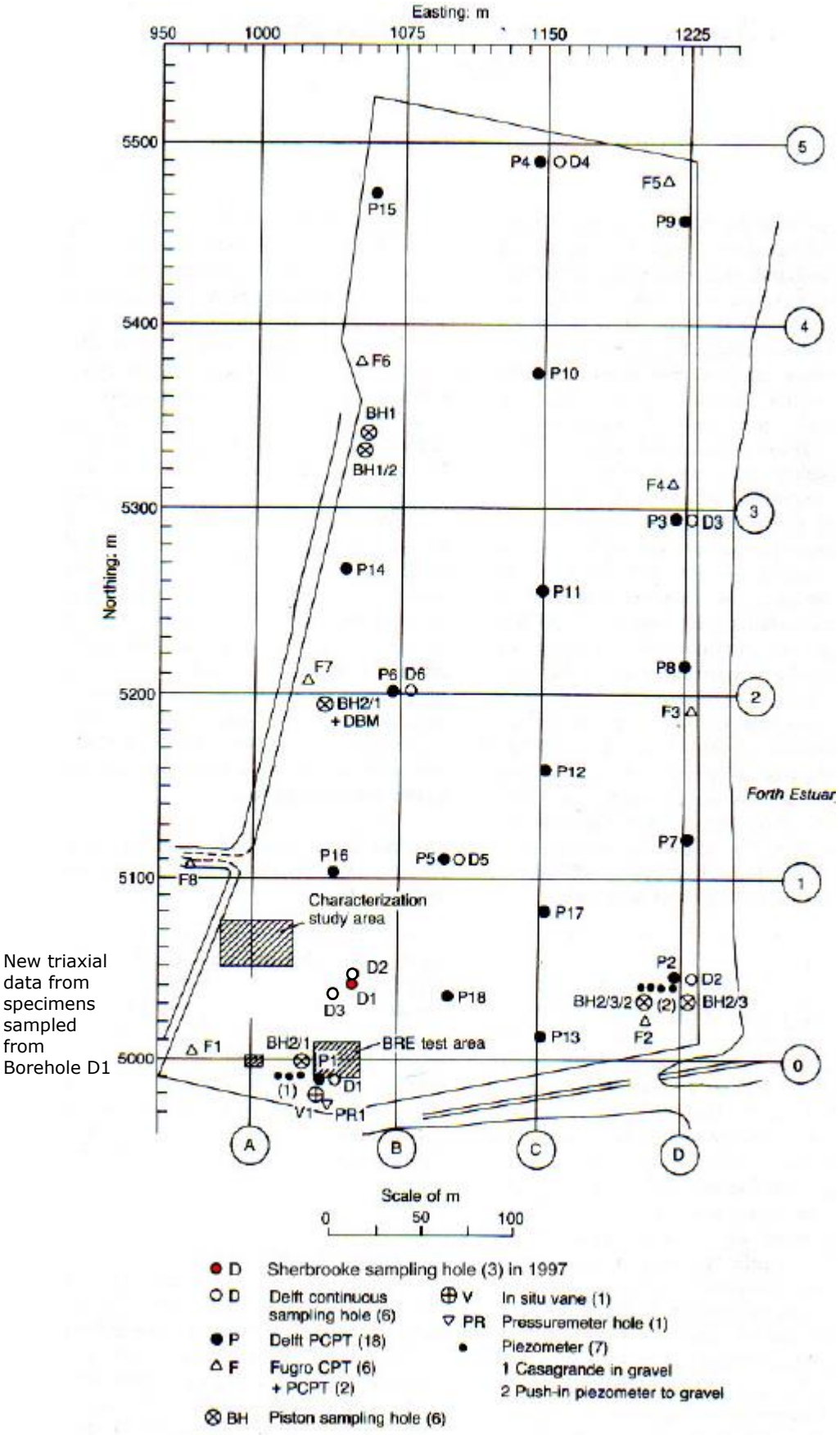

New triaxial data from specimens sampled from Borehole D1

Figure 5- 4. Location of borehole D1: origin of Bothkennar samples investigated in this study (modified from Hight et al. 1992a and Sukolrat 2007) © ICE Publishing

Figure 5- 5. Preparation of intact Bothkennar triaxial specimens by trimming with a piano wire and lathe

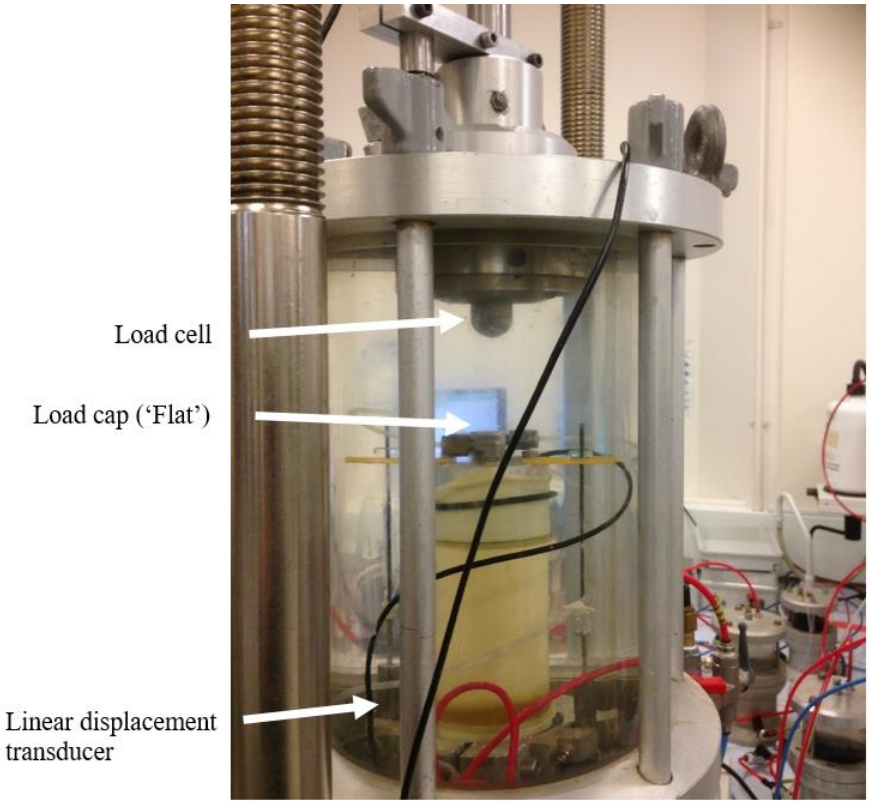

Figure 5- 6. Compression test setup of kaolin inside conventional isotropic triaxial cell (Linear displacement transducers are attached to the base and top caps with a lightweight connection system)

apparatus, two linear voltage displacement transducers (LVDTs) were attached to the top and base caps (Figure 5- 6) to measure axial strain during consolidation and shear. An advantage of this method was that it enabled reliable monitoring of the change in distance between the bender elements embedded in the caps. For brevity, the bender test results are not discussed in this study. Owing to the low strength of the reconstituted clay samples, mid-height LVDTs attached directly to the middle section of the sample were judged to be inappropriate. The local strain measurements will be affected by any bedding of the caps; however, for fine-grained materials, the bedding error is likely to be low (Sarsby et al. 1980).

5.3.4.1 Selection of saturation pressure

An uncertain effect on p' occurred during the reconstitution and extrusion of Kaolin CIU samples, which was indicated by apparently inconsistent measurements of residual pore pressure under zero confining stress. Therefore, different trial values of effective stress were applied to saturate samples

in the preliminary tests. To achieve saturation, the cell and back pressures were raised simultaneously at a rate of 25 to 50kPa/hour. The changes in void ratio and axial strain during the saturation period are included in Table 5- 2 with the measured B values (Skempton 1954b defines the B value).

5.3.4.2 Selection of consolidation testing rate

To minimise the accumulation of excess pore pressures, a continuous consolidation rate was selected by performing one isotropic consolidation test ('CI- 1') under a series of effective (total) stress increments: 20 (20), 40 (20), 60 (20), 100 (40), and 200 (100) kPa. Table 5- 1 lists values for t_{100} obtained using the hand-drawn procedure of tangents to the 'primary' and 'secondary' consolidation data, assuming a linear initial relationship between volume change and √*time* (Bishop & Henkel 1962):

Table 5- 1. t_{100} parameters from a series of isotropic consolidation curves on a single Kaolin specimen

p' (kPa)	20	40	60	100
t_{100} (min)	68	80.1	78	62

Taking t_{100} = 80.1 minutes and using equations 6.1, 6.2 and 6.3 assuming double drainage, c_v (0.409mm^2/s) and degree of excess pore dissipation per hour (85.4%) is calculated:

$$c_v = \frac{\pi h^2}{4t_{100}} \qquad (6.1)$$

$$t = \frac{T_v h^2}{c_v} \qquad (6.2)$$

$$\bar{U} = 1 - \frac{2}{3} exp\left(\frac{1}{4} - 3T_v\right) \qquad \text{for } T_v > 1/12 \qquad (6.3)$$

Where, c_v = coefficient of consolidation; h = drainage path length, and drainage takes place at both ends with no radial boundary drainage; t_{100} = time intercept of two intersecting tangent lines representing the initial linear relationship of volume change with √*time* and 100% consolidation (Bishop & Henkel 1962); T_v = time factor; $\bar{U}$ = degree of consolidation.

8kPa/hour was selected to achieve a compromise between reasonable speed and limiting excess pore pressure accumulation. With limited Bothkennar clay available for initial investigations, a consolidation rate of 1kPa/hour was selected in accordance with the procedure recommended by Sukolrat (2007).

5.3.4.3 Procedures (a) and (b) for reconstitution and consolidation of Kaolin

To investigate the effects of testing variation, triaxial samples were reconstituted and consolidated according to one of the two following procedures. Sample reconstitution was achieved in the consolidometer under a maximum applied vertical stress of (a) σ'_v = 60kPa, or (b) σ'_v = 120kPa. Saturation pressures varied from (a) 5 to 20kPa, or (b) 35 to 60kPa. Isotropic consolidation was controlled using continuous loading rates of (a) 8kPa/hour, or (b) 5kPa/hour. Identifiers (a) and (b) are included as part of each test reference, shown in Table 5- 2.

5.3.4.4 Undrained shear

All samples were sheared undrained using a conventional displacement-controlled load frame. Selection of strain rate was based on the isotropic compressibility parameter c_v and a 'significant strain' level in accordance with the British Standard BS 1377 Part 8 (BSI 1990). For this research, with the focus on moderate stress range (corresponding to $0.2 \leq \tau_{mob}/c_u \leq 0.8$), a conservative (low) strain value was chosen corresponding to τ_{mob}/c_u = 0.2 using kaolin test data compiled in RFG/TXCU-278. Strain rates of 0.002%/min and 0.0013%/min were adopted respectively for Kaolin and Bothkennar samples.

5.3.4.5 Mitigating sample tilt

Preliminary tests demonstrated that triaxial samples developed varying degrees of tilt during isotropic consolidation. This led to two potential concerns: (1) misalignment of the LVDTs, resulting in loss of local strain data and, more pertinently, in the restraint on sample deformation if the LVDT rods became stuck; (2) misalignment of the load cap connection prior to shear. Although lack of alignment due to specimen tilting is not uncommon (Baldi et al. 1988), tilt causes eccentricity of the axial load applied to the specimen or specimen disturbance if alignment is forced. To alleviate some of the effects of (1) and (2), the sampling procedure (b) was developed to produce samples with a lower initial void ratio, with the aim of reducing volumetric compression before undrained shear. To reduce

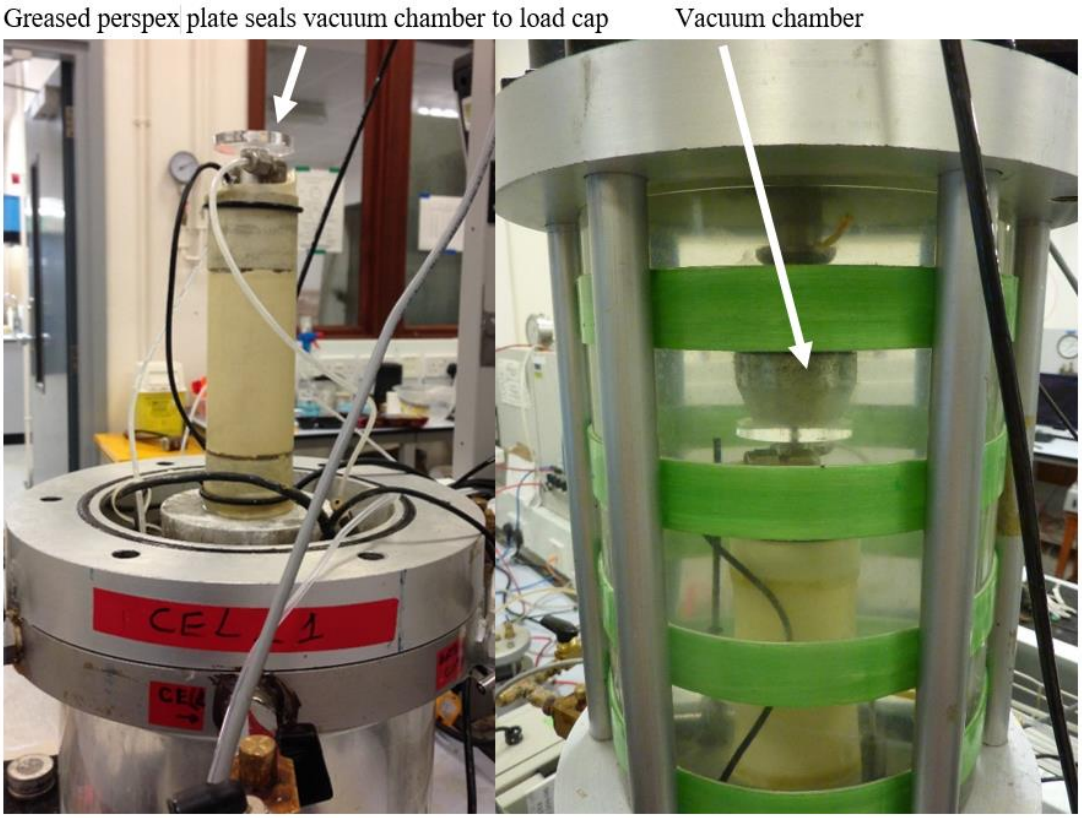

Figure 5- 7. Extension test setup of Kaolin sample CIUE-8-a-52 inside conventional isotropic triaxial cell with extension cap "Vacuum-1"

the risk of interference between the LVDTs and sample deformation during the test, the original LVDT connection system was replaced with smooth, lightweight components and a wider range of movement. Newly installed 3D printers at the University of Bristol were ideally suited to the design and manufacture of lightweight components.

5.3.4.6 Load cap connections – triaxial compression

'Flat' load cap connections were used for most triaxial compression tests and a photograph of this connection type is shown in Figure 5- 6. A concave surface was manufactured into the top cap for 'CIUC-2-b-200' to observe the difference in behaviour when the load cap was forced into vertical axial alignment at the initiation of undrained shear (results shown in Chapter 6).

5.3.4.7 Load cap connections – triaxial extension

To undertake extension tests in the conventional triaxial cell, two cap designs using vacuum chambers were investigated: 'Vacuum-1' consists of a rigid vacuum chamber fixed to the internal load cell, which

connects to a smooth Perspex plate on the top cap via vacuum seal (see Figure 5- 7); the second iteration of this component is the rotationally flexible extension cap ('Vacuum-2'), that was designed to accommodate up to 12 degrees of tilt. Figure 5- 8 shows a Kaolin sample during extension shear using Vacuum-2.

Since the triaxial cells were equipped with internal load cells and external tie bars, the connection between the specimen top cap and loading ram needed to be made after the cell had been fully assembled. It was not feasible to make the connection earlier in the test, e.g. before consolidation, because a conventional loading frame is not suited to controlling axial stresses in the specimen during consolidation. Instead, connections were achieved at the start of undrained shear. Figure 5- 9 shows deviator stress, axial displacement and axial strain measured during a connection of Vacuum-1 and Vacuum-2 on two overconsolidated samples of Kaolin (*OCR*=8). In both connection procedures, the loading ram was lowered to contact the top cap initially with a seating load of 6-9kPa, followed by application of vacuum pressure. Vacuum was achieved by a pipe connected between the vacuum chamber and a valve that could be opened to atmospheric pressure, causing a negative difference with confining cell pressure (250kPa).

Comparing plots shown in Figure 5- 9 (a) and Figure 5- 9 (b), a vacuum seal was achieved with a smaller seating load and smaller axial displacement (and strain) between top and base caps using Vacuum-2. Axial displacement is caused by compliance of all apparatus between the fixed loading frame and base platen; this includes loading ram, load cell, extension cap attached to the load cell, Perspex plate attached to the top cap, top platen, membrane, o-rings and porous stones. An axial displacement of 0.14mm, and 0.14% axial strain of the specimen, causes an initial deviator extension stress of about - 19kPa (Figure 5- 9 (b)) which will vary with stiffness of the soil specimen. Clearly this type of extension cap (Vacuum-1 and Vacuum-2) is unsuitable for small-strain shear measurements if the connection is made at the start of shear. However, connections with Vacuum-2 were judged to be appropriate for the purpose of studying moderate stresses and strains mobilised in the range of $0.2 \leq \tau_{mob}/c_u \leq 0.8$. Using Vacuum-2, specimen disturbance prior to extension shear was limited to a compression strain during contact alignment of the order 0.01% axial strain.

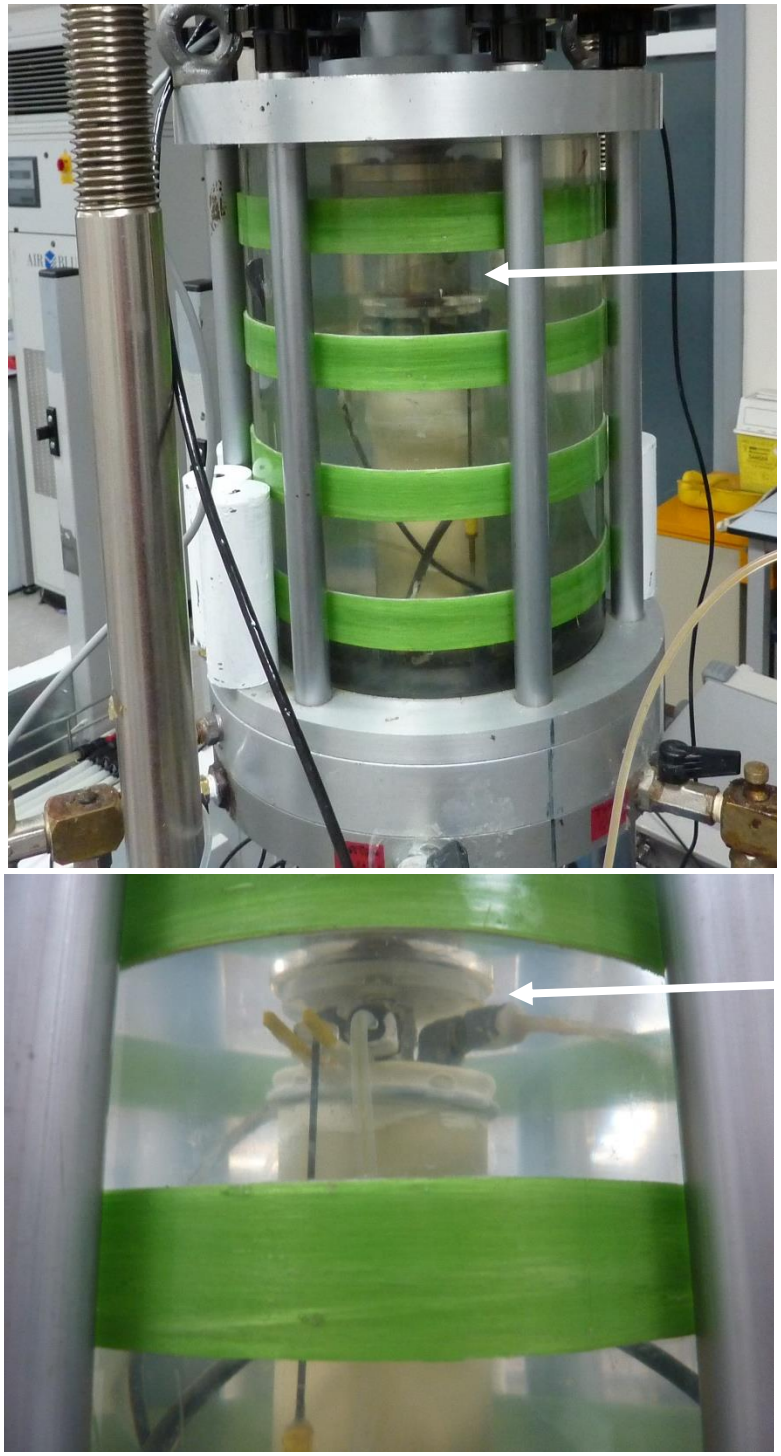

Figure 5- 8. Extension test setup of Kaolin sample inside conventional isotropic triaxial cell with extension cap "Vacuum-2"

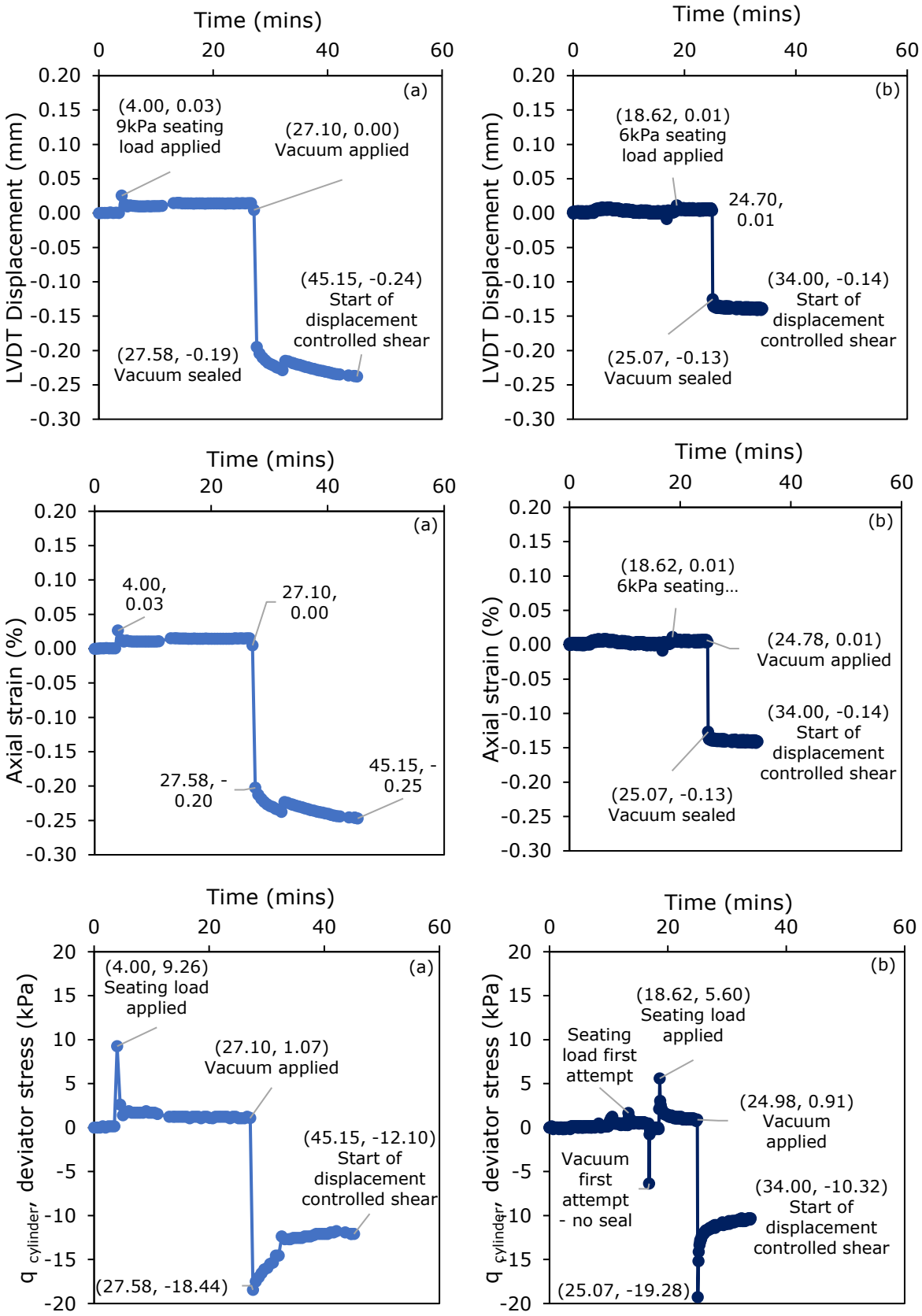

Figure 5- 9. Displacement and deviator stress measurements during connection between the loading ram and specimen top cap using (a) Vacuum-1 (b) Vacuum-2

5.3.5 UU Triaxial test procedure

Unconsolidated undrained tests are popular in practice because of the short time needed to complete a test. Up to 2% axial strain per minute may be used to shear the sample (Head 1982, p290) and no saturation or consolidation stages are required. BS 1377-7:1990 (BSI 1990) does not stipulate the need for pore pressure measurement as the purpose of a standard test is to measure only shear strength in terms of total stresses. For this study, a comparison of effective stress path and stress-strain behaviour in undrained triaxial compression between CIU and UU tests required the installation of a pore pressure measurement system (described in section 5.3.2.2). The standard procedure outlined by BS 1377-7:1990 (BSI 1990) was modified to facilitate the measurement of effective stress in the sample (p'_0) before and during undrained shear. Approximately one extra hour was needed before commencing undrained shear, in order to saturate the drainage line and pressure transducer and to allow sufficient time for the pore pressure to stabilise under the selected confining cell pressure. Further details on the tests are provided in Table 5.3; the complete procedure is included in Appendix 5.2.

5.3.6 Oedometer test procedure

Oedometer tests are routinely used to assess the consolidation characteristics of fine-grained, soils with low saturated hydraulic conductivity. During the test, soil compresses and swells one-dimensionally under lateral confinement and vertical displacement of the soil sample is monitored with time. In IL tests loads are applied incrementally: during compression, load is transferred from the initial excess pore water pressure to the soil skeleton, which results in increased effective stress; during a swelling stage, increments of loads are removed which causes negative excess pore water pressure and, with dissipation, a reduction in effective stress. The procedure adopted for the new IL oedometer tests on Kaolin and the reported IL tests on Bothkennar (Sukolrat 2007 and Nash et al. 1992b) was to apply load increments every 24 hours and to follow the procedure outlined by BS1377-5:1990 (BSI 1990). Table 5.4 lists details of the oedometer tests. The IL test procedure is outlined in Appendix 5.3.

5.4 Accuracy of sensors and control system

For monotonic triaxial tests with stress-controlled consolidation, the following sources of error are relevant to assessing the accuracy of measured quantities.

5.4.1 Calibration

Electronic transducers were calibrated against three types of reference equipment: for load and pressure, reference masses were applied through rotating hydraulic pistons (Budenberg S/N 21096/380); for displacement, a 10 μm Micrometer mounted in a one-dimensional guiding frame was used; to calibrate volume change, water passing through the chamber was measured using a 0.01g balance.

In addition, to keep a constant load on the power supply and thereby minimising the variation of transducer energisation voltage, during calibration (and subsequent tests) the same transducers were plugged into the unit (following the recommendation of Pennington 1999). The energisation voltage was monitored during the tests and transducer readings were 'corrected' to the energisation voltage recorded during calibration. To mitigate the possible effect of long-term drift in the transducers, during the two-year programme the calibrations of all transducers were undertaken annually.

5.4.2 Stability

The stability of a sensor is described by the change in output over time. Stability is determined by the manufacturer's design and as a result may be more or less sensitive to environmental fluctuations.

5.4.3 Control

TRIAX, a BBC Basic control programme developed by Durham University (Toll 1993) was used to control back and cell pressures and, indirectly, volume change through the back pressure system. A deviation limit of 0.1kPa was used for all pressure channels.

5.4.4 Resolution

Resolutions are specified by the manufacturer and describe the smallest unit of detectable change in measurement.

5.4.5 Combined uncertainty of measured quantities

To assess the combined effects of the calibration correction, stability, resolution, and – where relevant – control system, in Figure 5-10 the recorded change in readings from a mean value is plotted over a 10-hour period. To plot the region that encompasses 99% of the data points, percentiles at 0.005

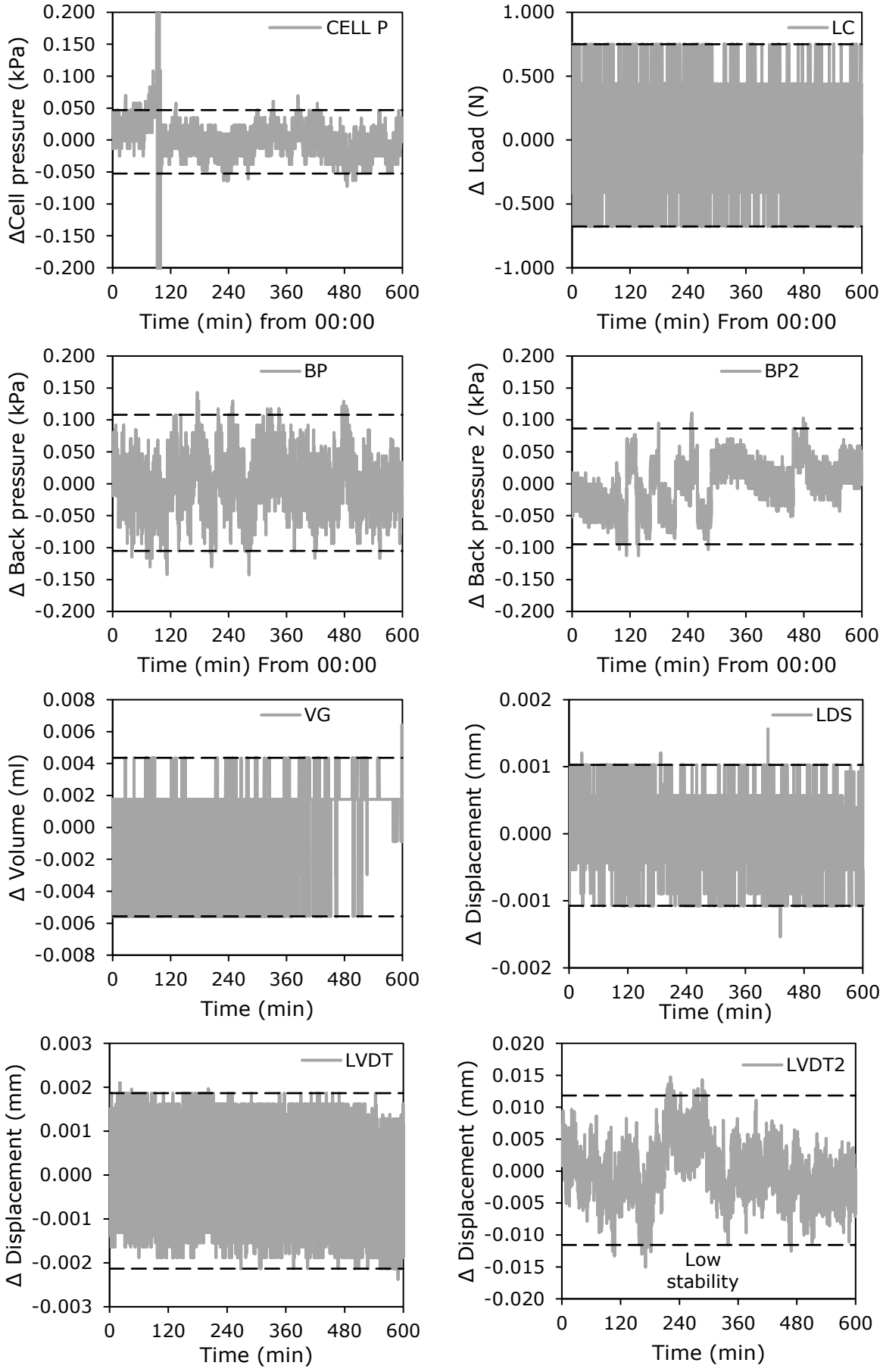

Figure 5- 10. Assessment of sensor accuracy; dashed lines indicate refer to a region that encompasses 99% of the data points

and 0.995 were calculated. It should be noted that readings were taken at 10 second intervals. Error bandwidths are reported with the maxima and minima in Table 5- 5.

5.5 Data calculations and parameter approximations

Volumetric strain, ε_v, was calculated from measurements obtained with the volume gauge using:

$$\varepsilon_v = \frac{\Delta V}{V_0} \tag{5.1}$$

Where, V_0 = initial volume. Owing to compliance of the volume gauge during saturation, the initial volume at the start of consolidation was calculated using final dry masses and final water contents and measurements of volume change during consolidation.

Axial strain, ε_a, was calculated from measurements provided by internal LVDTs, which monitored changes in height throughout the triaxial test procedure. If the limits of travel on the local transducer arm were exceeded during shear, external displacements were adopted for strain measurements where local strains were unavailable.

$$\varepsilon_a = \frac{\Delta H}{H_0} \tag{5.2}$$

Where, H_0 = initial height.

Shear strain, γ, during undrained triaxial extension was calculated using the equation recommended by Lam and Tatsuoka (1988):

$$\gamma = \varepsilon_1 - \varepsilon_3 = \frac{1}{2}(\varepsilon_v - 3\varepsilon_3) = \frac{3}{2}(-\varepsilon_3) = \frac{3}{2}(-\varepsilon_a) \tag{5.3}$$

Shear strain, γ, during undrained triaxial compression was calculated using the equation recommended by Lade (2016):

$$\gamma = \frac{3}{2}(\varepsilon_1) = \frac{3}{2}(\varepsilon_a) \tag{5.4}$$

Axial stresses were calculated from load measurements according to Equation 5.5:

$$\sigma_a = \sigma_3 + \frac{F}{A} \tag{5.5}$$

Where, σ_3 = applied cell pressure, F = value of the load measurement, and A = present cross-sectional area of the sample.

Stress acting on the cross-sectional area of the specimen is dependent on the shape of specimen deformation. Frictional ends (between the platens and specimen) were used to minimise errors of axial strain measurement and to evaluate the effect of nonuniform deformations on stress-strain parameters. Equations 5.6 and 5.7 were used to calculate cross-sectional area by respectively assuming right-hand cylinder and parabolic bulging/necking deformations:

$$A_{cylinder} = A_0 \left(\frac{1}{1 - \varepsilon_a}\right) \tag{5.6}$$

Where, A_0 = initial area at the start of undrained shear, calculated from calculated volume and measured height at the end of consolidation.

$$A_{parabolic} = A_{cylinder}\left(2 - \sqrt{[1 - \varepsilon_a]}\right) \tag{5.7}$$

Assessment of membrane restraint was conducted according to the method of Lade (2016): the order of magnitude of estimated stress contribution using this method is between 1 and 5%. However, the original values of stress are presented in this report without correcting for membrane restraint.

To calculate the power law model parameters, for consistency the model parameters were derived using the same procedure that was used for the database tests presented in Chapter 4: by applying either Equation 3.4 or 3.5 as appropriate to the test data and then using the fitted equation to calculate them (i.e., $\gamma_{50\ \text{Power CIUC}}$ and b_{CIUC}, $\gamma_{50\ \text{Power CIUE}}$ and b_{CIUE}, or $\gamma_{50\ \text{Power UU}}$ and b_{UU}).

Undrained shear strength, c_u, was determined from the maximum point of deviator stress. The same procedure was used to derive c_u for the database tests presented in Chapter 4.

5.6 Laboratory test programme

In total, 13 CIU triaxial tests on Kaolin samples and 3 CIU triaxial tests on Bothkennar samples (1 reconstituted and 2 intact) are presented. In addition, 2 UU triaxial tests on Kaolin samples and 4 UU triaxial tests on Bothkennar samples (2 reconstituted and 2 intact) are presented for comparison with the CIU test results. Three oedometer tests were undertaken on Kaolin samples. Tables 5.2, 5.3, and 5.4 report the details of all experiments and the results are presented in Chapter 6.

The test reference denotes the distinguishing features of each test: Material _ Test Mode _ OCR _ Procedure _ Applied Stress. Applied stress is p'_0 for CIU tests while for UU tests, which were undertaken with no control of effective stresses, the applied stress is p_0. Reconstituted samples have known (applied) *OCR* values; *OCR* of 1.5 for the intact specimens is an estimated value using the sampling depth of 5.4m and yield stress ratio profile recommended by Hight et al. (1992a) from IL tests performed by Nash et al. (1992b). Procedures (a) and (b) for CIU tests on Kaolin are described in Section 5.3.4. A single procedure was used for CIU tests on Bothkennar. A single procedure (see section 5.3.5) was followed for UU tests.

Table 5- 2. CIU triaxial test details – sample reconstitution, isotropic consolidation, and undrained shear

Triaxial Test:	KAO2-CI_1	KAO2-CIUC-1-a-395	KAO2-CIUC-2-a-208	KAO2-CIUC-8-a-51	KAO2-CIUE-8-a-52	KAO2-CIUC-1-b-200	KAO2-CIUC-1-b-403	KAO2-CIUC-2-b-200 (C)	KAO2-CIUC-2-b-200	KAO2-CIUC-8-b-50	KAO2-CIUE-1-b-200	KAO2-CIUE-1-b-400	KAO2-CIUE-2-b-200	KAO2-CIUE-8-b-50	NBOT-CIUC-1.5-29	NBOT-CIUE-1.5-28	RBOT-CIUC-1.5-99	RBOT-CIUE-1.5-99
Test Number	1	6	7	9	13	21	22	23	37	26	35	27	28	34	31	32	38	36
Material	Kaolin B2	Kaolin B2	Kaolin B2	Kaolin B2	Kaolin B2	Kaolin B2	Kaolin B2	Kaolin B2	Kaolin B2	Kaolin B2	Kaolin B2	Kaolin B2	Kaolin B2	Kaolin B2	Intact Bothkennar	Intact Bothkennar	Reconstituted Bothkennar	Reconstituted Bothkennar
Consolidometer / specimen diameter (mm)	50	50	50	50	50	50	50	50	50	50	50	50	50	50	50	50	50	50
Slurry height H_p (mm)	N/A	171.03	172.36	170.35	166.69	175.76	201.05	n/a	183.3	184.4	n/a	180.54	183.57	182.97	N/R	N/R	191.80	173.4
Max. applied stress in sampling device (kPa)	60	60	60	60	60	120	120	120	120	120	120	120	120	120	N/R	N/R	100	100
Extruded w_x (%)	66.0	63.1	59.8	64.1	62.5	54.2	52.7	54.3	62.7	53.51	55.41	54.73	54.26	56.88	71.07	72.28	63.89	64.63
Extruded H_x (mm)	N/A	101.28	95.97	101.72	101.45	95.57	96.08	97.08	114.08	97.05	99.87	101.74	101.11	102.53	100.29	99.80	101.76	100.20
Extruded e_x (mm)	1.643*	1.631	1.523	1.649	1.607	1.398	1.362	1.396	1.693	1.377	1.44	1.424	1.419	1.475	1.959	1.979	1.725	1.745
Saturation																		
Duration (days)	2.18	1.06	1.20	2.15	1.24	0.75	1.01	1.13	1.27	2.07	1.03	0.61	0.89	1.04	1.09	2.06	1.14	1.28
p'_{sat} (kPa)	6	4	20	7.5	5	35	34	60	59.66	66.53	59.34	59.55	65.96	60	20.12	20.83	60.15	51.31
Δe SAT	0.012	0.069	-0.068	0.089	0.290	-0.012	0.014	-0.038	-0.277	-0.024	0.004	0.011	0.002	-0.030	-0.012	-0.017	-0.118	-0.018
ε_a SAT (%)	1.410*	-0.053	-0.010	-0.005	-0.187	-0.203	0.313	2.137[a]	3.440	1.503	0.631	0.864	0.163	1.172	0.167	0.180	1.144	0.530
B value	0.947	0.949	0.952	0.959	0.971	0.958	0.947	0.914	0.93	0.849	0.890	0.925	0.900	0.935	0.924	0.860	0.960	0.970
Consolidation																		
Loading type	Discrete	8kPa/h	8kPa/h	8kPa/h	8kPa/h	5kPa/h	5kPa/h	5kPa/h	5kPa/h	5kPa/h	5kPa/h	5kPa/h	5kPa/h	5kPa/h	1kPa/h	1kPa/h	1kPa/h	1kPa/h
Increments	6	1	3	2	2	4	7	11	11	14	4	7	11	11	1	1	9	9
Duration (days)	10.21	5.89	3.45	2.95	2.76	8.08	4.88	4.69	4.61	5.09	7.67	5.10	4.73	5.76	7.04	7.61	10.67	13.80
Swelling																		
Duration (days)	0	0	1.10	4.01	6.13	0	0	10.08	2.93		0	0	3.04	6.15	0	0	10.04	5.75
Preshear held stress[b]																		
Duration (days)	3.01	0.73	0.05	2.19	4.30	6.19	1.23	7.42	1.09	0.21	6.22	1.75	1.15	1.19	5.10	7.28	5.73	1.38
Δe PRE	-0.004*	-.014	0.000	+.006	-.047	-.007	-.008	+.005	+.002	+.008	-.016	-.010	+.002	+.019	-.002	-.014	+.011	+0.001
e_m	1.142*	1.195	1.158	1.155	1.274	1.236	1.109	1.142	1.170	1.146	1.282	1.161	1.144	1.126	1.944	1.944	1.403	1.500
e_0	1.142*	1.195	1.180	1.254	1.271	1.236	1.109	1.159	1.189	1.220	1.282	1.161	1.171	1.260	1.944	1.944	1.414	1.504
p'_m (kPa)	395.69	395.16	401.80	399.35	399.85	200.41	403.15	399.87	401.33	401.29	200.30	402.40	399.36	399.47			149.28	149.83
p'_0 (kPa)	395.47	395.16	208.04	51.30	51.73	200.12	403.15	200.08	200.46	50.17	200.30	402.40	202.04	49.26	29.18	28.05	99.07	99.26
OCR	1.0	1.0	1.9	7.8	7.7	1.0	1.0	2.0	2.0	8.0	1.0	1.0	2.0	8.1	1.5 [c]	1.5 [c]	1.5	1.5
Shear mode	Excluded	UC	UC	UC	UE Vacuum-1	UC	UC Vacuum-2	UC	UC	UC	UE Vacuum-2	UE Vacuum-2	UE Vacuum-2	UE Vacuum-2	UC	UE Vacuum-2	UC	UE Vacuum-2
Load cap		Flat	Flat	Flat		Flat		Concave	Flat	Flat					Flat		Flat	
Filter strips		Yes	Yes	Yes	No	No	No	No	No	No	No	No	No	No	No	No	No	No

Notes: Kaolin samples were sheared with an axial displacement rate of 0.002mm/minute. Bothkennar samples were sheared at 0.0013mm/minute.
[a] The sample came into contact with the load cell during setup
[b] Duration of effective stress held prior to shear; this is included in the consolidation or swelling durations
[c] Estimated *OCR*
*Estimated values assuming an extruded sample height of 100mm
N/A not available
N/R not relevant

Table 5- 3. UU triaxial test details – sample reconstitution, pore pressure measurement, and undrained shear

Triaxial Test:	RBOT-UU-1-249	RBOT-UU-1-143	KAO2-UU-1-249	KAO2-UU-1-143	NBOT-UU-1.5-249	NBOT-UU-1.5-143
Test Number	41	42	43	44	45	46
Material	Reconstituted Bothkennar	Reconstituted Bothkennar	Kaolin B2	Kaolin B2	Intact Bothkennar	Intact Bothkennar
Consolidometer Diameter (mm)	38	38	50	50	38	38
Slurry height H_p (mm)	140	173.49	188.7	186.9	N/R	N/R
Max. applied stress in sampling device (kPa)	174	100	120	120	N/R	N/R
Extruded w_x (%)	56.26	68.23	51.67	50.31		
Extruded H_x (mm)	91.62	103.52	105.60	98.45		
Extruded e_x (mm)	1.463	1.774	1.343	1.308	1.881	1.887
Trimmed to length (mm)	75.0	75.0	75.0	75.0	75.65	63.82
Preshear conditions						
p_o applied (kPa)	249	143	249	143	249	143
Δu_o measured (kPa)	191.3	102.9	189.5	92.7	207.6	106.5
Duration to measure Δu_o (minutes)	30	45	60	43	103	152
p'_o measured (kPa)	57.7	40.1	59.5	50.3	41.4	36.5
OCR	1	1	1	1	1.5 *	1.5 *
Shear mode	UC	UC	UC	UC	UC	UC
Load cap	Concave	Flat	Flat	Flat	Flat	Flat
Filter strips	No	No	No	No	No	No
Axial displacement rate (mm/min)	0.75	0.75	0.75	0.75	0.75	0.64

* estimated *OCR*
N/R Not relevant

Table 5- 4. Oedometer test details (Kaolin only)

Oedometer Test	Batch No.	w_x %	σ'_{vm} kPa	σ'_{v0} kPa	No. Increments	Loading Type	Duration Consolidation days	Duration Swelling days	Duration Total days
KAO1-O-1.35	1	90.0	400	20	9	Discrete	6	3	9
KAO1-O-1.50	1	99.2	400	20	9	Discrete	6	3	9
KAO2-O-2.10	2	138.2	2000	100	20	Discrete	8	6	14

Table 5- 5. Calibration and precision of transducers

Channel Description	Sensor	Units	Calibration Factor (unit/Vdc)	Maximum precision error	99% precision error
Power supply	PS	Vdc	N/R	N/R	N/R
Load cell	LC	N	445187.5	1.429	1.427
Cell pressure	CP	kPa	-19371.25	2.592	0.283
Back pressure	BP	kPa	-19545.5	0.297	0.213
Volume gauge	VG	ml	21.056	0.225	0.181
External displacement transducer	LDS	mm	768.93	0.017	0.010
Back pressure	BP2	kPa	-13642.8	0.0031	0.0021
Internal strain transducer	LVDT	mm	0.7516	0.0045	0.0040
Internal strain transducer 2	LVDT2	mm	71.069	0.030	0.023

N/R = not relevant

6. Experimental results: material behaviour and parameter assessment of Kaolin and Bothkennar in the moderate stress range

Parts of this chapter have been included in the following publication:

Beesley M.E.W., Vardanega P.J., and Ibraim, E., 2019. "Developing an experimental strategy to investigate stress-strain models using kaolin*". Recent Advancements on Expansive Soils*, GeoMEast 2018, Springer, Cham, Switzerland: 99-118.

6.1 Material behaviour of Kaolin and Bothkennar

6.1.1 Research objectives:

(1) To investigate the variation of triaxial compression and extension stress-strain behaviour using routine testing apparatus widely available in industry (i.e. conventional triaxial cells).

(2) To evaluate the sources of measurement uncertainty influencing parameter variability identified by the database analysis in Chapter 4.

6.1.2 Classification of Kaolin and Bothkennar samples

Kaolin was provided by the supplier in two batches. Table 1 shows the mean and range of measured Atterberg limits and specific gravity for each batch of Kaolin. Liquid limit (w_L) was measured using the fall cone penetrometer and the thread-rolling test was used to measure plastic limit (w_P) as per the requirements given in BSI (1990). Specific gravity (G_s) was measured using the standard pyknometer method, following the procedure specified in BSI (1990). In total 6 liquid limit and 6 plastic limit tests were performed for Kaolin, corresponding respectively to values of mean ± standard deviation = 66.6 ± 0.6 and 35.1 ± 2.5.

Table 6- 1. Classification test results (assumed only if no test data available)

Soil	Relevant tests	w_L (%) Mean	*n*	Range	w_P (%) Mean	*n*	Range	G_S Mean	*n*	Range
KAOLIN (Batch 1)	Procedure A Oedometer	66.8	4	0.2	35.1	2	0.5	Not measured		
KAOLIN (Batch 2)	Procedure B	66.3	2	1.6	35.1	4	7.1	2.60	2	0.01
BOTHKENNAR	All	77.3	1	-	38.5	2	2.1	2.70 assumed by Sukolrat (2007)		

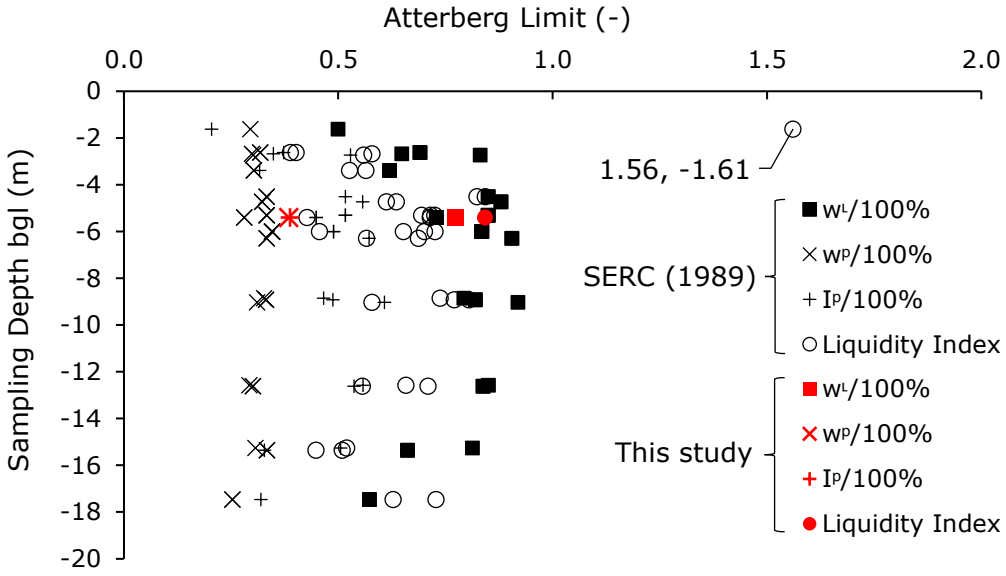

Figure 6- 1. Measurements of Atterberg Limits and moisture contents reported by SERC (1989) and performed by the author, plotted with sampling depth

Fewer limit tests were performed on the trimmings of Bothkennar clay (Table 6- 1); results are compared with those reported by SERC (1989) in Figure 6- 1. The w_L and w_P measurements are respectively in the lower and upper range of measurements reported by SERC (1989) and, correspondingly, the liquidity index is high but not outside the previously reported range. It is likely that the limit tests performed by the author overestimate the true plasticity of the soil because of the presence of organic material (the Bothkennar specimens were untreated before undertaking limit tests).

Particle size distributions of Kaolin (Batch 2) and Bothkennar are shown in Figure 6- 2. Measurements of grain size were obtained by laser diffraction using the Mastersizer 3000 (Malvern Instruments 2019). Following the Unified Soil Classification system, the results show that both materials are dominated by the presence of silt-sized particles. Kaolin has a greater clay content than Bothkennar; 27-32% of the Kaolin specimen is finer than 0.002mm and the remaining 70% is silt. 95% of the Bothkennar soil specimen classified as silt and it has a very small clay fraction of 1.5-2.5%.

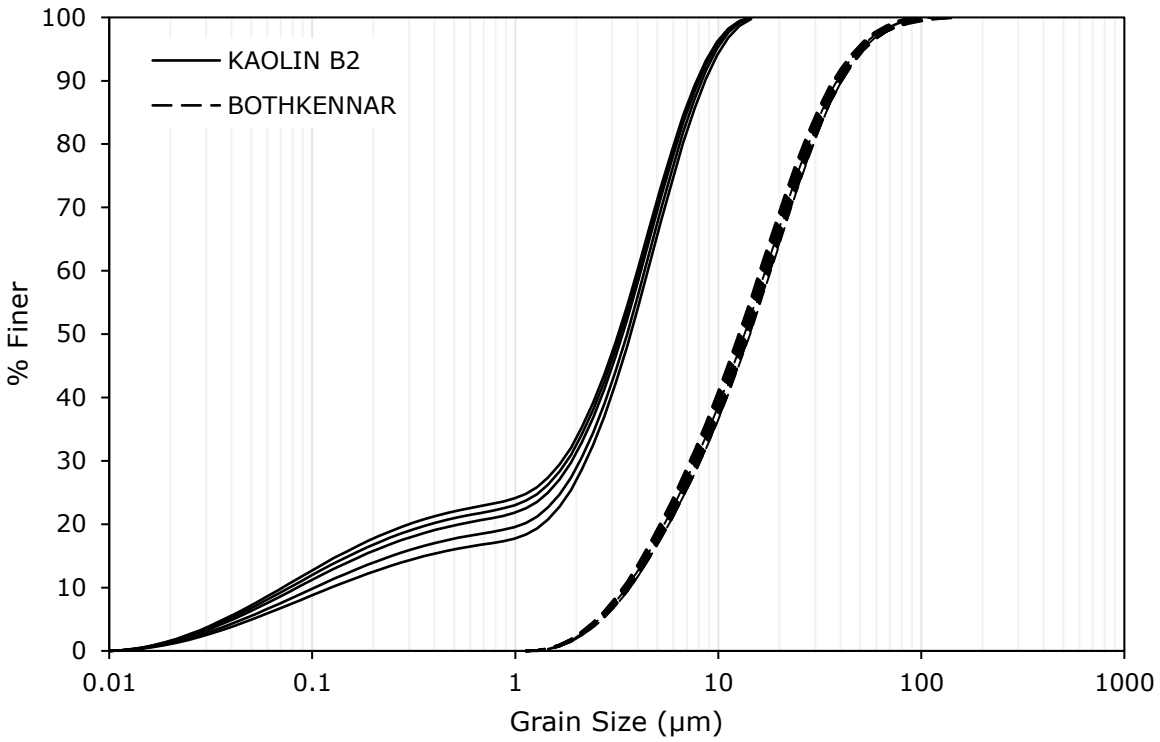

Figure 6- 2. PSD curves for 5 Kaolin specimens (B2 = Batch 2) and 10 Bothkennar specimens measured by laser diffraction using Mastersizer 3000 (Malvern Instruments 2019)

6.1.3 Compressibility of reconstituted Kaolin under K_0 conditions

Figure 6- 3 shows the one-dimensional compression behaviour of kaolin slurry represented in semi-logarithmic form. The samples tested at higher initial water contents exhibit a slightly upward concave shape that is indicated by differences in gradient between the dashed and full lines (values of slope coefficient λ are provided in Table 6- 2). Since the samples were compressed in the oedometer cell directly from a slurry, no 'preconsolidation' stress is observed. For vertical effective stresses greater than 10kPa, Hong et al. (2010) identified upward concave shapes in the compression curves of reconstituted fine-grained soil slurries and increasing compressibility with higher mixing water content. Table 6- 2 shows that close values of λ (0.235 to 0.247) were measured for the Kaolin slurries over a stress range greater than 60kPa with high R^2 and *RD* values, where *RD* is relative deviation (as defined in Waters and Vardanega 2009). Although the number of swelling lines is limited, the test data suggest that K_0-swelling behaviour (indicated by κ) is related to the maximum applied consolidation stress.

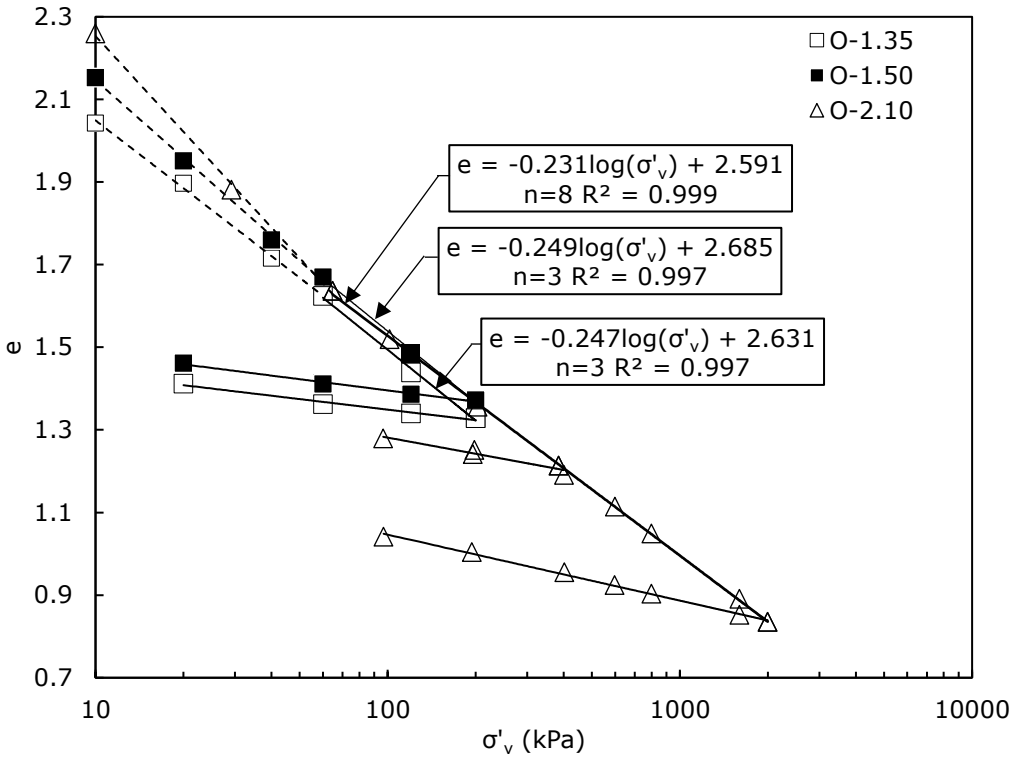

Figure 6- 3. Semi-logarithmic K_0-consolidation (oedometer) curves of reconstituted kaolin mixed at different initial water content

Table 6- 2. Calculated compressibility parameters

Test ID	Stress range kPa	*n*	*λ*	*R²*	*RD*	*λ**	*R²*	*RD*	Stress range kPa	*n*	*κ*	*R²*	*RD*	*κ **	*R²*	*RD*
K_0 consolidation (oedometer)																
O-1.35	10-60	4	0.237	.998	4.6	0.084	.997	5.9								
	60-200	3	0.247	.997	5.8	0.100	.998	4.2	200-20	4	0.037	.981	13.6	0.016	.983	13.2
O-1.50	10-60	4	0.272	.998	4.7	0.094	.999	2.8								
	60-200	3	0.249	.997	5.7	0.099	.998	4.1	200-20	4	0.039	.989	10.6	0.016	.990	10.1
O-2.10	10-60	3	0.339	.998	4.0	0.114	.999	1.0	100/400	5	0.057	.935	25.6	0.025	.932	26.0
	60-2000	8	0.231	.999	1.7	0.105	.998	4.6	2000-100	7	0.070	.997	5.7	0.036	.995	7.1

The normal compression curves were normalised using Equation 5.1 (Burland 1990):

$$I_v = \frac{e - e^*_{100}}{e^*_{100} - e^*_{1000}} \quad (6.1)$$

Where, I_v = void index; e = void ratio at an applied vertical effective stress (σ'_v); e^*_{100} = void ratio at σ'_v = 100kPa; e^*_{1000} = void ratio at σ'_v = 100kPa.

e^*_{1000} was found by fitting a linear regression through the normal compression data of O-2.10 using natural e and $\log_{10}(\sigma'_v)$ to determine C_c^* (note that the slope coefficient λ using $\ln(\sigma'_v)$ is shown in Figure 6- 3). Since only one of the three oedometer tests included stress increments up to 1000kPa, the approach taken here was to use the fitted values of e^*_{1000} and C_c^* to determine e^*_{100}. All void ratio measurements from O-1.35, O-1.50 and O-2.10 were normalised using the parameter values for Kaolin shown in Table 6- 3. The results are plotted with the ICL curve (shown by the dashed line) recommended by Burland (1990) in Figure 6- 4. The ICL curve is a good fit to the void index measurements during normal compression.

Although there was unfortunately not enough material available in the remainder of the block sample to undertake oedometer tests on Bothkennar, many oedometer test data were reported by Sukolrat (2007). The parameters in Table 6- 3 were identified from a data plot reported by Sukolrat (2007) showing the results of reconstituted Bothkennar samples (from a sampling depth of 5.4m) prepared from slurries mixed at a water content equal to $1.9w_L$ and compressed in the oedometer cell under incremental loads following BS1377-5:1990 (BSI 1990). The same procedures were used by the author to prepare the Bothkennar slurry and to perform oedometer tests on Kaolin samples. For these reasons, the parameters selected in Table 6- 3 to represent intrinsic one-dimensional compressibility of the Bothkennar soil are justified.

Table 6- 3. Parameter values adopted to determine the intrinsic compression lines of Kaolin and Bothkennar

Kaolin	$C_c^* = 0.532$	$e^*_{1000} = 0.976$	$e^*_{100} = 1.508$
Bothkennar	$C_c^* = 0.690$ (from Sukolrat 2007)	$e^*_{1000} = 0.780$ to 0.892	$e^*_{100} = 1.470$ to 1.582

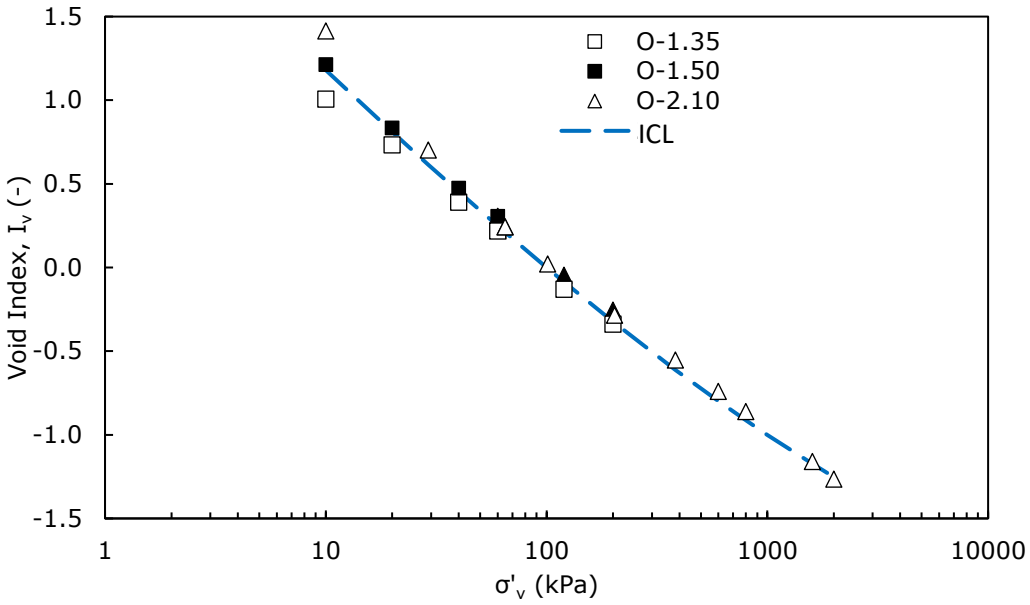

Figure 6- 4. Variation of void index (I_v) with vertical effective stress for reconstituted kaolin samples mixed at different initial water contents

6.1.4 Compressibility of reconstituted Kaolin and Bothkennar under isotropic conditions

Figures 6- 5 and 6- 6 show the compression data of triaxial samples undergoing isotropic consolidation plotted in semi-logarithmic form. A pronounced curve is exhibited in each test, which indicates that every sample had swelled during saturation to a lower effective stress than it had previously experienced. As expected, the apparent preconsolidation stresses observed in Figures 6- 5 and 6- 6 are somewhat lower than the stresses applied in the consolidometer: a maximum consolidation stress of 60kPa and 120kPa was used in procedures (a) and (b) respectively. Using measurements of pore pressure under an isotropic confining stress, it was shown in Chapter 5 (section 5.3.3.3) that 50-58% of the applied stress in the 50mm consolidometer had not been experienced by the kaolin sample. With similar consolidometer procedures, Sukolrat (2007) demonstrated a loss in applied stress of 35-55% in reconstituted Bothkennar samples on account of consolidometer side friction. By comparing curvatures of the compression test data in Figures 6- 5 and 6- 6, it is possible to distinguish samples which had been preconsolidated at higher stresses in the consolidometer i.e. procedure (b).

The results displayed in Figures 6- 5 and 6- 6 suggest that the reconstitution, saturation and consolidation procedures have a strong effect on the compressibility characteristics of kaolin

undergoing isotropic compression. None of the tests converge to a unique normal consolidation line in the stress range studied. The lack of convergence in tests performed using procedure (a) (Figure 6- 5) may be due to differences in swelling that occurred during the test setup and saturation stages; evidence for this is indicated by an increase in void ratio in the samples from their extruded states (at extrusion e = 1.52 to 1.65). For stresses greater than 200kPa, values of λ obtained by linear regression for the four tests performed using procedure (a) varies from 0.164 to 0.258 and increases with the value of void ratio measured at the end of saturation. The normal compression curves of tests performed using procedure (b) are relatively less variable; the smaller range of λ (0.124 to 0.208) is caused by an initially denser Kaolin sample (at extrusion e = 1.31 to 1.47) and less swelling before the start of isotropic consolidation.

There appears to be no clear trend in swelling behaviour of the overconsolidated samples (*OCR*=2 and 8). Values of κ vary from 0.019 to 0.054 and all samples underwent considerable height change. No discernible difference can be observed between the results of test procedures (a) and (b). However, 'CIUE-8-a-52' appears to continue to consolidate (or leak) at the end of the unloading stage.

ICL curves have been identified from oedometer test data and Table 6- 3 to represent the normal compression lines of the two reconstituted soils. Although convergence is not fully realised, there is a tendency towards convergence between the experimental data of Kaolin samples and the intrinsic curve at stresses greater than 250kPa, particularly for samples tested with procedure (b). In Figure 6- 7, the ICL curve determined for Bothkennar is plotted with isotropic compression test data, using upper and lower bound values of e^*_{1000} (Table 6- 3). Since the void ratios measured at the end of normal isotropic compression are closer in value to the upper bound curve, e^*_{1000} = 0.892 was chosen to represent the normal compression line of Bothkennar.

The normal compression curves of the reconstituted Bothkennar samples have a concave downward shape and a marked change in void ratio was measured during the period of sustained loading at the maximum consolidation stress. Although the normal compression curves of a reconstituted silt have been identified as concave downward by Georgiannou et al. (2018), it is unlikely in this case that

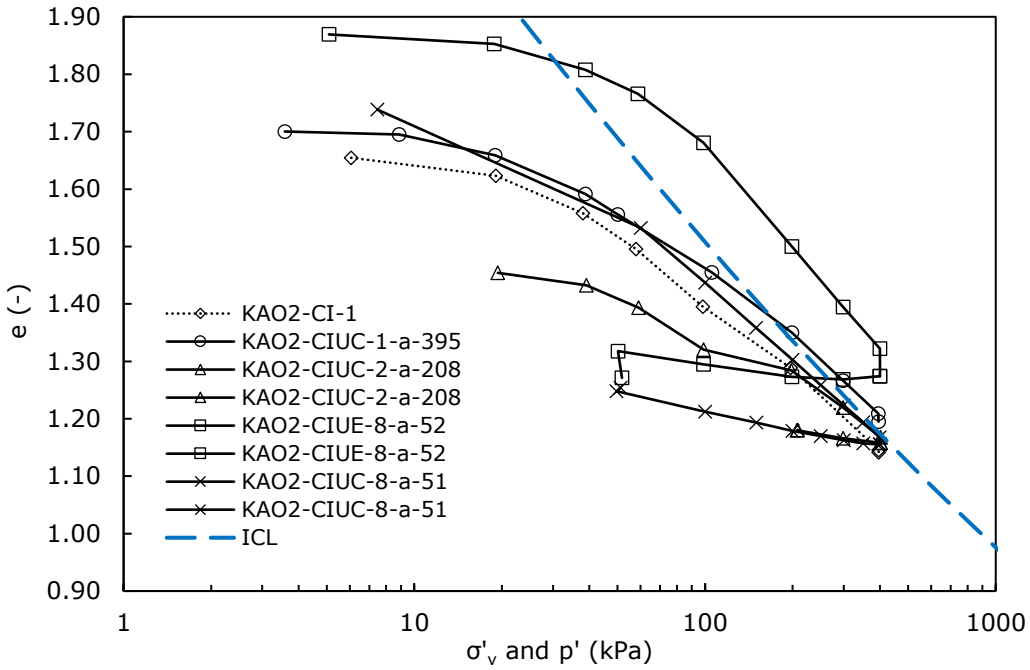

Figure 6- 5. Semi-logarithmic isotropic-consolidation curves of reconstituted kaolin at different initial water content using procedure (a)

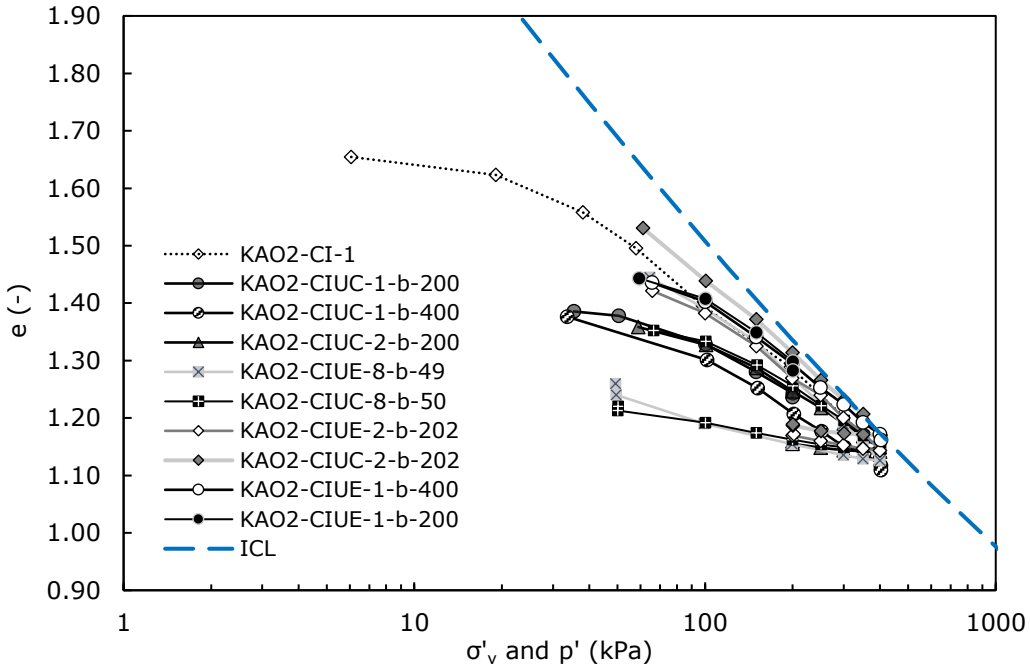

Figure 6- 6. Semi-logarithmic isotropic-consolidation curves of reconstituted kaolin at different initial water content using procedure (b)

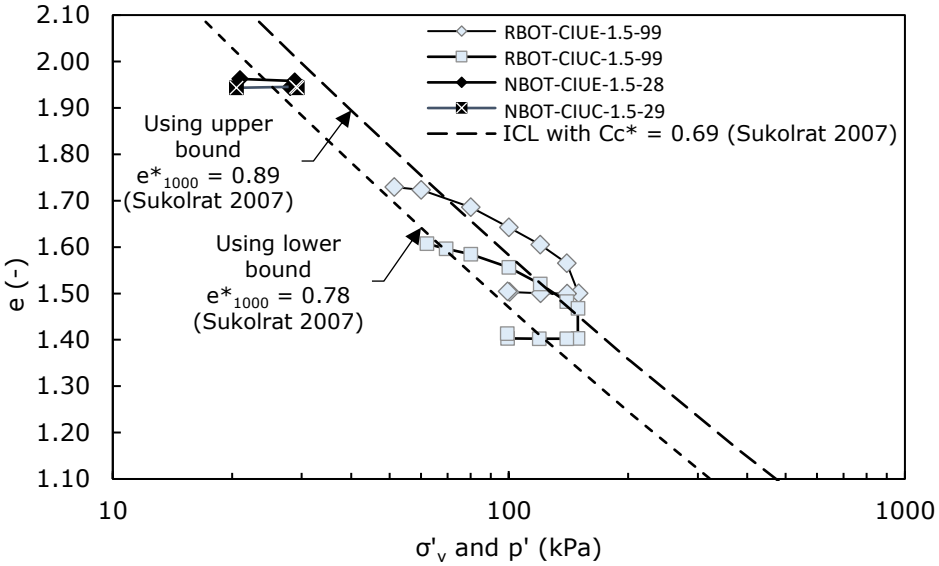

Figure 6- 7. Semi-logarithmic isotropic-consolidation curves of reconstituted Bothkennar and intact Bothkennar (during recompression)

the same apparent behaviour is linked to a similar mechanism. Georgiannou et al. (2018) and Sukolrat (2007) both used standard oedometer cells to measure normal compression behaviours of reconstituted slurries, but Sukolrat (2007) reported no evidence of a concave downward shape in the compression data of reconstituted Bothkennar between $10 \leq \sigma'_v \leq 1000$kPa. It is likely that the curvature shown by the triaxial specimens undergoing isotropic consolidation is related to the accumulation of excess pore pressures. An applied stress rate of 1kPa/hour was used for Bothkennar – considerably slower than the rate used for Kaolin (5kPa/hour). The samples were fully drained before commencing the unloading stage to *OCR*=1.5. A small increase in void ratio (Δe = 0.004 and 0.011) in the Bothkennar samples occurred during the swelling stage.

6.1.5 Shearing behaviour of reconstituted Kaolin

Figures 6- 8 to 6- 12 present the behaviour of triaxial samples during strain-controlled undrained shear. By observation during the shearing stage, little bulging or necking occurred in all CIU tests on Kaolin. These data were therefore analysed using the assumption of right cylinder deformation (Bishop and Henkel 1957); UU tests were observed to bulge more obviously and the parabolic shape assumption (Equation 5.7) was used to compute the stress data shown. The test parameters are reported in Table 6- 4 and Table 6- 5. Local strain measurements were used for the full range of the LVDT

transducers (at least 0-0.5% axial strain) in the stress-strain analysis for every test; one exception being 'KAO2-CIUE-2-b-200' which required the use of external strain measurements with correction for apparatus compliance.

The effective stress paths of the kaolin samples, shown in Figure 6- 8, follow patterns that are reasonably consistent with isotropically-consolidated samples at different values of *OCR* (see for example Wroth & Loudon 1967 and Sachan & Penumadu 2007 for similar studies). The normalised excess pore pressures generated in the normally consolidated samples (Figure 6- 9) exceed those measured in the lightly overconsolidated (*OCR*=2) samples, resulting in a more pronounced curve in effective stress path prior to peak failure. Similar normalised excess pore pressures developed within the low strength UU samples as the CIU samples normally consolidated to 200 and 400kPa. Stress paths for pairs of samples consolidated to the same *OCR* using procedure (a) or (b) and sheared using the same principle stress control system (for example KAO2-CIUC-1-a-395, KAO2-CIUC-1-b-403, and KAO2-CIUC-2-a-208, KAO2-CIUC-2-b-200, and KAO2-CIUC-8-a-51, KAO2-CIUC-8-b-50) are close in shape although some differences are observed in mean effective stress and peak deviator stress. The effective stress behaviour of the overconsolidated (*OCR*=8) samples correspond with the development of negative excess pore pressures; although the two samples sheared in extension show more tendency to dilate than the compression tests.

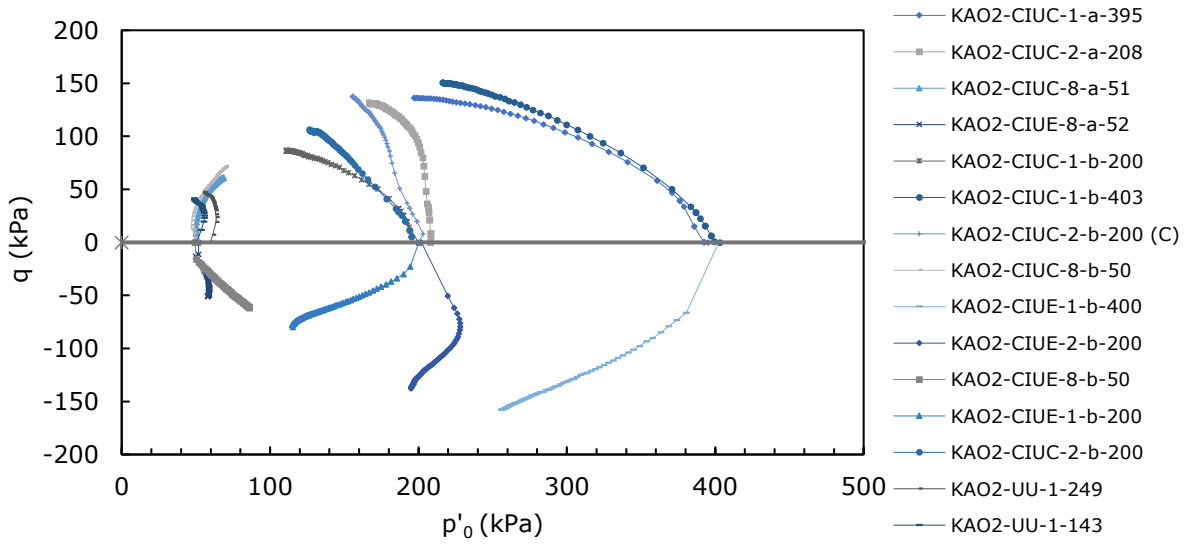

Figure 6- 8. Effective stress paths for CIU and UU triaxial tests on reconstituted Kaolin

Table 6- 4. Measured parameters of CIU triaxial tests

Triaxial Test:	KAO2-CIUC-1-a-395	KAO2-CIUC-2-a-208	KAO2-CIUC-8-a-51	KAO2-CIUE-8-a-52	KAO2-CIUC-1-b-200	KAO2-CIUC-1-b-403	KAO2-CIUC-2-b-200	KAO2-CIUC-2-b-200 (C)	KAO2-CIUC-8-b-50	KAO2-CIUE-1-b-400	KAO2-CIUE-2-b-200	KAO2-CIUE-8-b-50	KAO2-CIUE-1-b-200	NBOT-CIUC-1.5-29	NBOT-CIUE-1.5-28	RBOT-CIUE-1.5-99	RBOT-CIUC-1.5-99
λ	0.206	0.164	0.195	0.258	0.124	0.127	0.201	0.141	0.149	0.178	0.181	0.208	0.170	-	-	0.223	0.428
κ	-	0.034	0.045	0.023	-	-	0.024	0.019	0.034	-	0.038	0.054	-	-	-	0.010	0.061
Λ	-	0.793	0.769	0.911	-	-	0.881	0.865	0.769	-	0.769	0.738	-	-	-	0.957	0.858
p'_0 (kPa)	395.16	208.04	51.3	51.73	200.12	403.15	200.46	200.08	50.17	402.40	202.04	49.26	200.30	29.18	28.05	99.26	99.07
p'_e	370.60	395.87	285.91	265.31	309.46	540.94	380.36	434.17	331.69	429.64	411.07	278.97	252.34	27.52	27.46	122.13	165.86
OCR	1.0	1.9	7.8	7.7	1.0	1.0	2.0	2.0	8.0	1.0	2.0	8.1	1.0	1.5	1.5	1.5	1.5
Right cylinder																	
c_u (kPa)	68.25	65.9	30.62	-25.49	43.63	75.41	53.26	69.12	36.10	-78.98	-68.87	-30.80	-39.84	29.48	-20.28	Peak not reached	46.43
c_u/p'_0	0.17	0.32	0.60	-0.49	0.22	0.19	0.27	0.35	0.72	-0.20	-0.34	-0.63	-0.20	1.01	-0.72	-	0.47
p'_{peak} (kPa)	197.14	166.89	68.76	57.89	111	216.18	126.53	155.57	70.01	255.77	194.87	86.03	115.40	33.65	32.69	-	69.72
M_{peak}	0.69	0.79	0.89	-0.88	0.79	0.70	0.84	0.89	1.03	-0.62	-0.71	-0.72	-0.69	1.75	-1.24	-	1.33
$\varepsilon_{a\ peak}$ (%)	4.97	6.16	7.58	-9.24	6.05	5.63	7.329	10.49	7.06	-10.60	-12.50	-8.67	-12.34	1.28	-7.34	-	3.46
$q_f/\ p'_e$	0.37	0.33	0.21	-0.19	0.28	0.28	0.28	0.32	0.22	-0.37	-0.34	-0.22	-0.32	2.14	-1.48	-	0.56
$p_f/\ p'_e$	0.53	0.42	0.24	0.22	0.36	0.40	0.33	0.36	0.21	0.60	0.47	0.31	0.46	1.22	1.19	-	0.42
$\gamma_{50\ Power}$	0.0034	0.0051	0.0123	0.0162	0.0026	0.0053	0.0047	0.0060	0.0159	0.0116	0.0066	0.0206	0.0108	0.0048	0.0044	-	0.0027
b	0.358	0.358	0.417	0.486	0.273	0.425	0.325	0.329	0.398	0.355	0.236	0.405	0.289	0.730	0.348	-	0.476

Table 6- 5. Measured parameters of UU triaxial tests

Triaxial Test ID:	RBOT-UU-1-249	RBOT-UU-1-143	KAO2-UU-1-249	KAO2-UU-1-143	NBOT-UU-1.5-249	NBOT-UU-1.5-143
Parabolic bulging or necking						
c_u (kPa)	36.74	19.07	23.85	20.67	39.77	39.65
c_u/p'_0	0.63	0.48	0.40	0.41	0.96	1.09
p'_{peak} (kPa)	55.22	39.73	55.25	48.81	50.68	50.05
M_{peak}	1.33	0.96	0.86	0.85	1.57	1.58
$\varepsilon_{a\ peak}$ (%)	4.36	8.67	3.68	3.43	2.05	2.04
$q_f/\ p'_e$	0.52	0.78	0.25	0.18	2.34	2.38
$p_f/\ p'_e$	0.39	0.81	0.29	0.22	1.49	1.50
$\gamma_{50\ Power}$	0.0025	0.0044	0.0024	0.0023	0.0024	0.0041
b	0.500	0.645	0.509	0.585	0.745	1.140

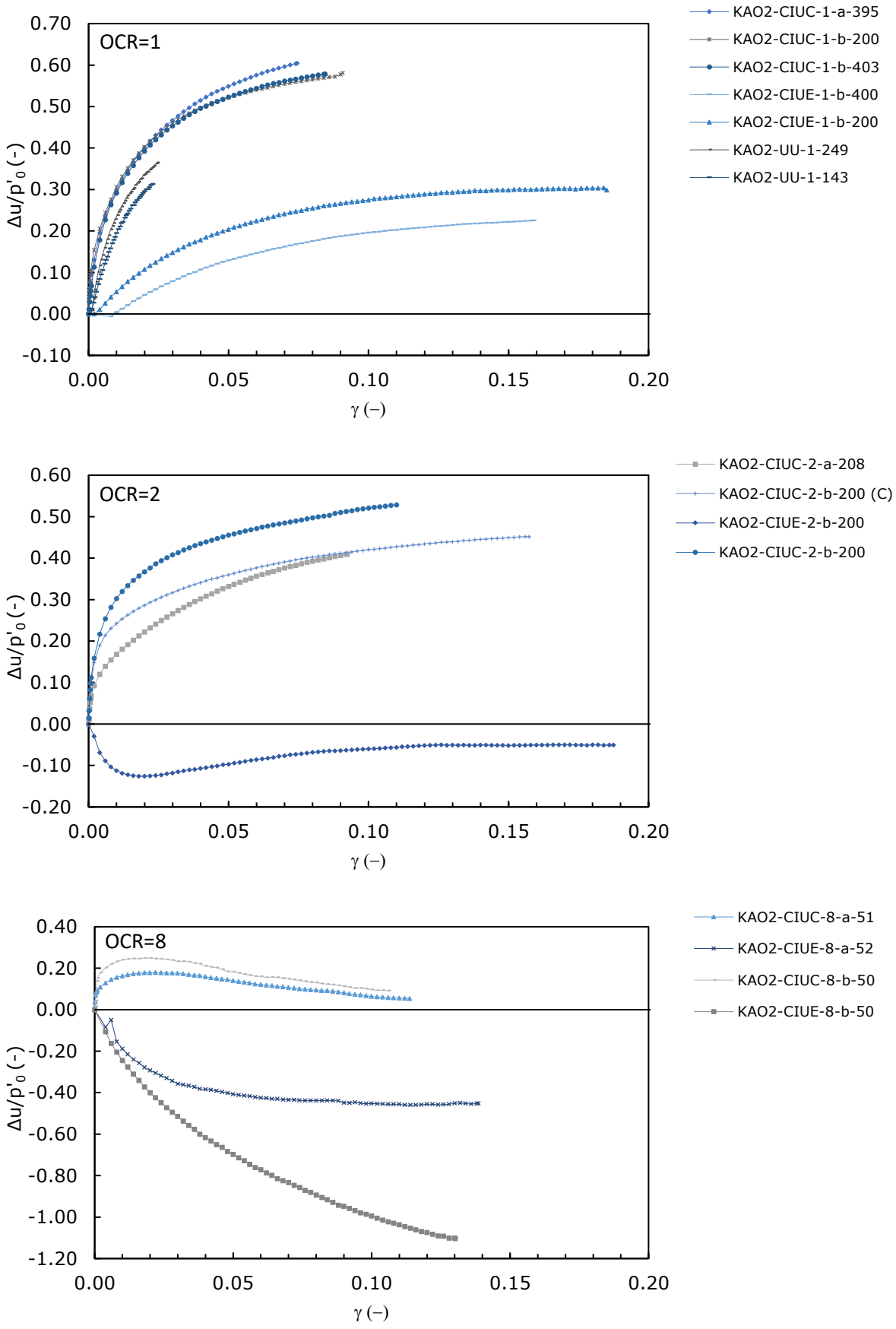

Figure 6- 9. Excess pore pressure-strain curves for CIU and UU triaxial tests on reconstituted Kaolin – comparison of tests by p'_0 normalisation

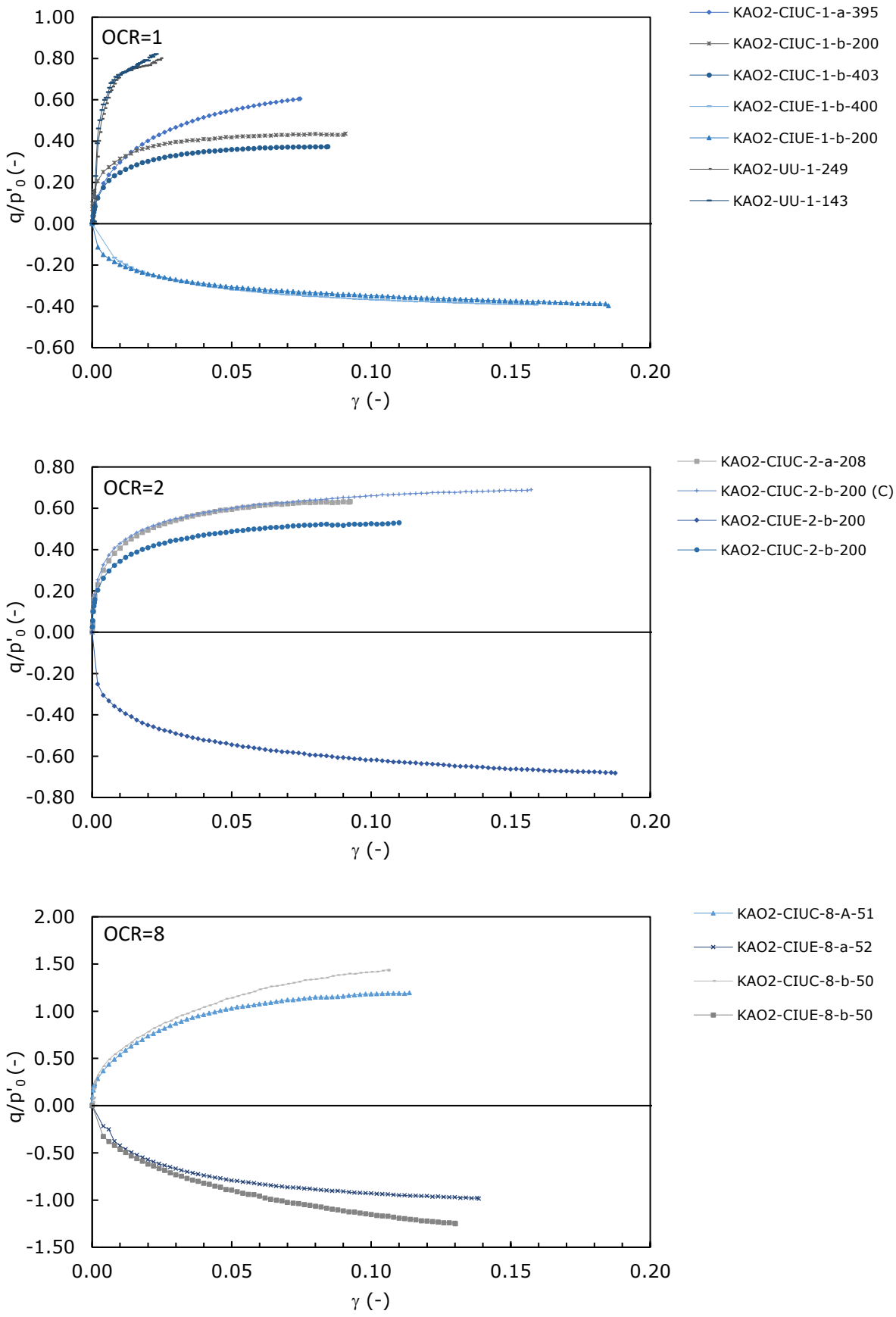

Figure 6- 10. Stress-strain curves for CIU and UU triaxial tests on reconstituted Kaolin – comparison of tests by p'_0 normalisation (assumed cylinder deformation)

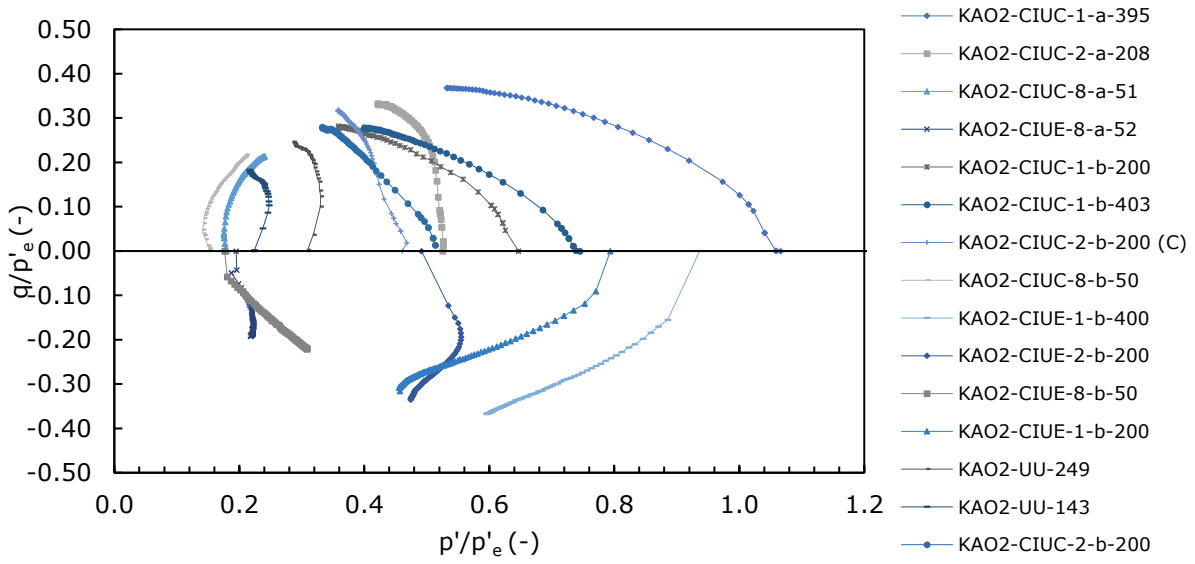

Figure 6- 11. Effective stress paths for CIU and UU triaxial tests on reconstituted Kaolin – comparison of tests by p'_e normalisation (assumed cylinder deformation)

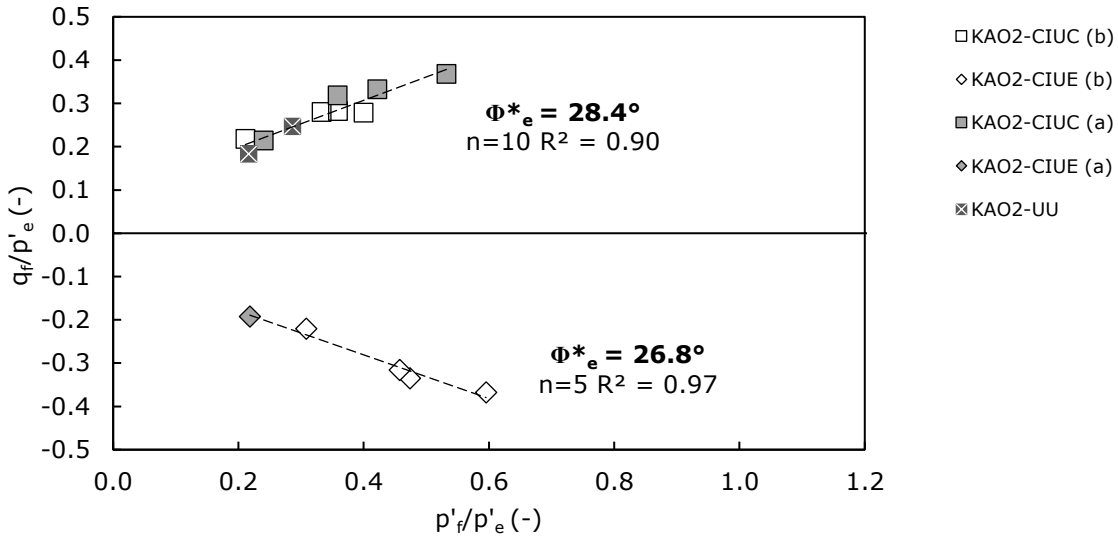

Figure 6- 12. Peak stresses for CIU and UU triaxial tests on reconstituted Kaolin tested with procedures (a) and (b) – comparison of tests by p'_e normalisation (assumed cylinder deformation)

The data in Figure 6- 10 illustrate the effect of overconsolidation and shear mode on the stress-strain behaviour and peak undrained shear strength. As expected, higher values of normalised deviator stress are reached at higher values of *OCR*. Additionally, the increments in normalised deviator stress measured up to $\gamma = 0.02$ are very similar for samples consolidated to the same *OCR* using procedure (a) or (b) and sheared using the same principle stress control system. If KAO2-CIUC-2-b-200 (C) is

considered anomalous (due to substantial bedding which occurred at the start of shear), the measured shear strain at failure increases with *OCR*. Similar results were shown by Parry & Nadarajah (1973).

The triaxial compression and extension curves are presented in normalised form in Figure 6-11. To normalise the data, the equivalent normal stress (p'_e) on the ICL was determined corresponding to the peak (which is equal to pre-shear) specific volume of the sample. The resulting Hvorslev strength envelopes are plotted in Figure 6- 12. $\Phi^*_{e\ COMPRESSION} = 28.4°$ was obtained by a close fit of all CIUC and UU compression tests (n=10 R^2=0.90); $\Phi^*_{e\ EXTENSION} = 26.8°$ for triaxial CIUE tests.

6.1.6 Shearing behaviour of reconstituted and intact Bothkennar

Figures 6- 13 to 6- 17 present the undrained triaxial compression and extension data measured for reconstituted and intact specimens of Bothkennar. The assumption of right-hand cylinder deformation was used for the computation of deviator stresses as only slight bulging was observed in CIU tests. Like the Kaolin samples, more obvious bulging took place during UU tests and for these tests the parabolic shape deformation is assumed. The intact stress-strain data show a more brittle response and higher peak undrained strength than the reconstituted specimens (Figure 6- 13). The intact specimen tested under CIUC conditions initially tends to dilate (negative pore pressures) at the start of undrained shear and the CIUE test is initially contractive. The companion tests on reconstituted specimens show initially a tendency to dilate but contractive behaviour dominates overall (Figure 6- 14 and 6- 15). A tendency to dilate may be expected for the high silt content of Bothkennar.

The normalised peak stresses are plotted in Figure 6- 17. Although test data are limited, strength envelopes have been tentatively drawn using CIUC and UU tests. The reconstituted (intrinsic) strength envelope does not coincide with the intact strength envelope, which suggests that the presence of naturally derived soil structure influences the stress-strain-strength behaviour. This result agrees with the earlier finding by Sukolrat (2007) who demonstrated - by a comparison of intact and reconstituted Bothkennar specimens tested in one-dimensional compression (oedometer) - that an enhanced intact soil structure influenced the normal compression data.

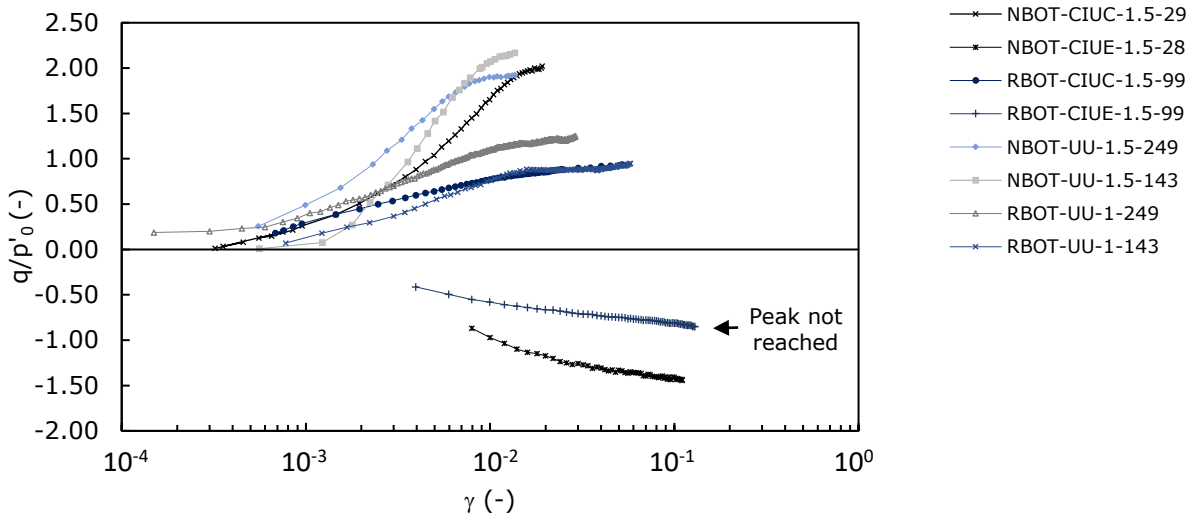

Figure 6- 13. Stress-strain curves for CIU and UU triaxial tests on reconstituted and intact Bothkennar – comparison of tests by p'_0 normalisation

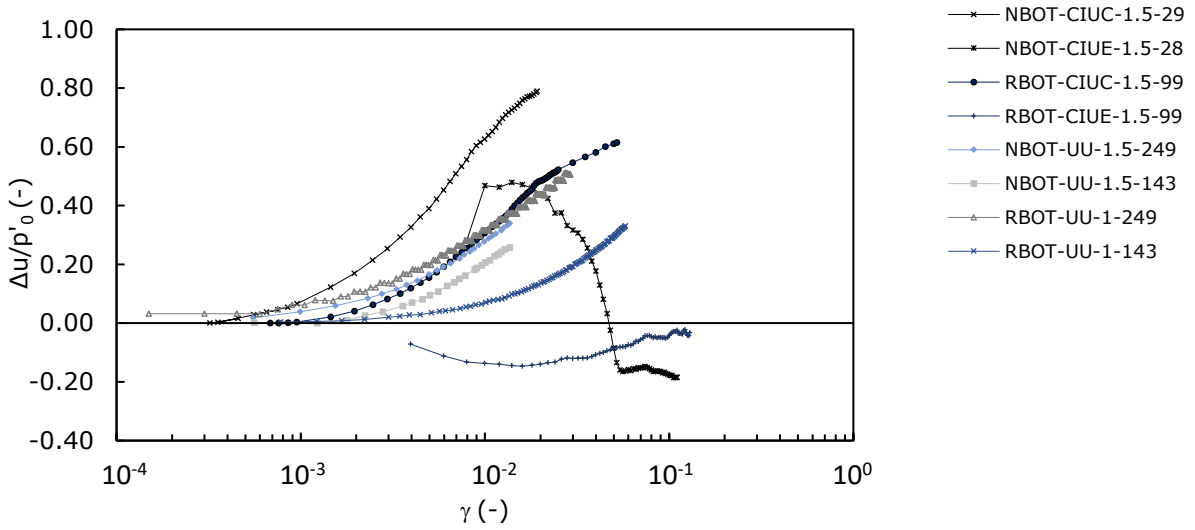

Figure 6- 14. Excess pore pressure-strain curves for CIU and UU triaxial tests on reconstituted and intact Bothkennar – comparison of tests by p'_0 normalisation

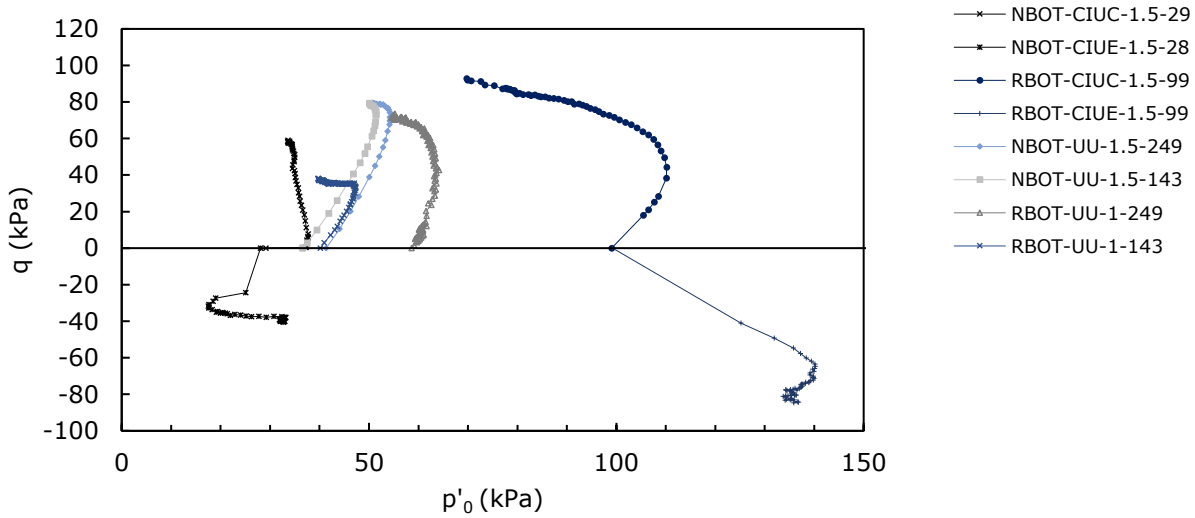

Figure 6- 15. Effective stress paths for CIU and UU triaxial tests on reconstituted and intact Bothkennar

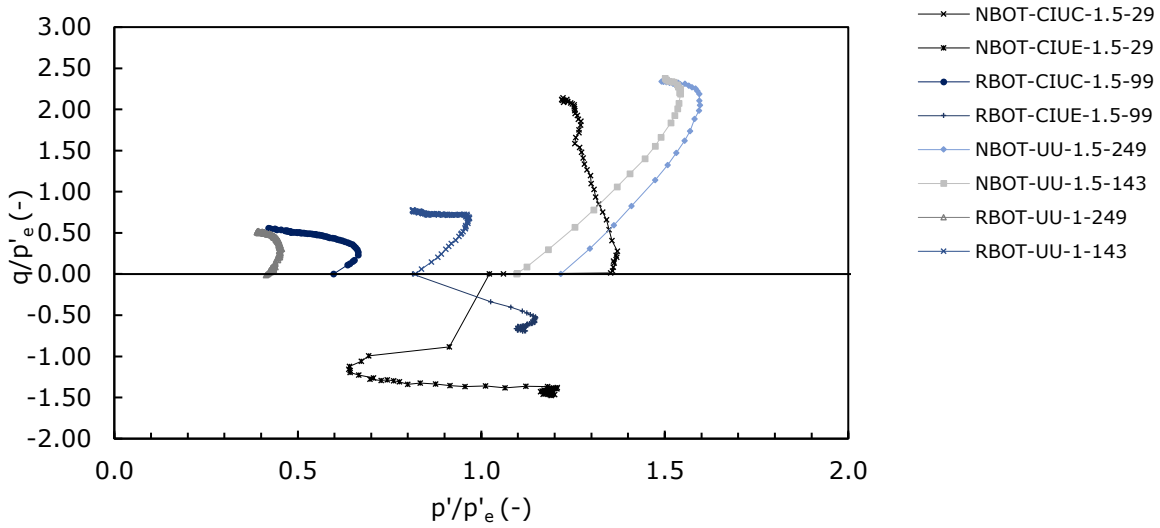

Figure 6- 16. Effective stress paths for CIU and UU triaxial tests on reconstituted and intact Bothkennar – comparison of tests by p'_e normalisation

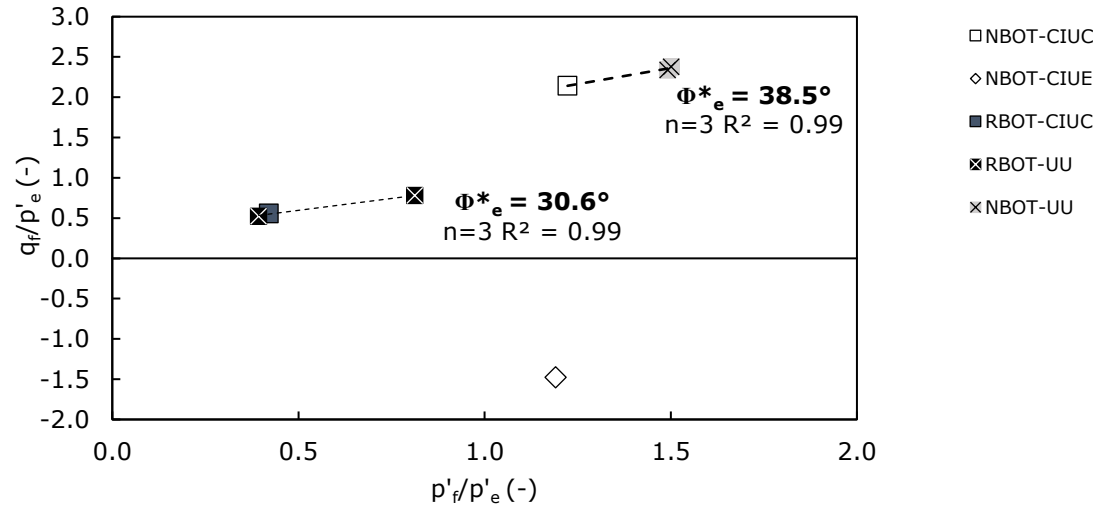

Figure 6- 17. Peak stresses for CIU and UU triaxial tests on reconstituted and intact Bothkennar – comparison of tests by p'_e normalisation (assumed cylinder deformation)

6.2 Influence of *OCR* and shear mode on parameter variability

6.2.1 Variation of c_u/σ'_{v0}, $\gamma_{50\ Power}$ and b with *OCR*

In Figures 6- 18 and 6- 19, the deformation parameter $\gamma_{50\ Power}$ for each test is presented to examine the effect of overconsolidation on measured shear strain. The results indicate that mobilised shear strain in Kaolin increases with *OCR* for both test modes, which agrees with the positive trends found earlier in Chapter 4 (Equations 4.1 and 4.2). A slope coefficient of Γ=0.0015 (fitted to n=8 data

points for 8 CIUC tests) is greater than the average slope of Γ=0.0010 found for CIUC data in RFG/TXCU-278. On average the CIUE test results demonstrate a change in $\gamma_{50\ \text{Power CIUE}}$ with *OCR* that matches Equation 4.2 (Γ=0.0013) although the strain magnitudes are almost double. Figure 6- 20 shows a comparison of the new experimental parameters with the data presented in chapter 4. Values of $\gamma_{50\ \text{Power CIUC}}$ and $\gamma_{50\ \text{Power CIUE}}$ are respectively in the lower and upper ranges of the sub-databases. Parameters measured from intact and reconstituted Bothkennar tests are also shown: all plot within the lower range of RFG/TXCU-278. No parameter is reported for RBOT-CIUE-1.5-99 because peak stress was not reached.

The nonlinearity parameter, *b*, is plotted with *OCR* in Figures 6- 21 and 6- 22. Unlike the CIUC test data published by Vardanega et al. (2012), no correlation exists between *b* and *OCR* for CIUC tests which may be due to a greater degree of scatter in values at *OCR*=1. Further tests at *OCR*>8 would facilitate a better comparison with the data reported by Vardanega et al. (2012). For Kaolin, *b* values in extension are similar to (or slightly less than) the values in compression with a difference of up to 0.1. Limited data are available for the Bothkennar but the intact specimens demonstrate more ductile behaviour in extension (lower *b*) than compression. The data suggest that a disparity exists between reconstituted Kaolin and Bothkennar, with the latter being described with significantly higher *b* values (0.48 to 1.14 observed in compression tests). Comparison with RFG/TXCU-278 in Figure 6- 22 indicates that the new *b* parameters for Kaolin are within the lower, more ductile, range of behaviour observed in CIUC and CIUE tests on reconstituted soils.

Figure 6- 23 shows that the normalised undrained shear strength (taken as the maximum value of deviator stress normalised by $\sigma'_{v0} = p'_0$) of CIUC and CIUE tests increases with *OCR*. Following the frameworks proposed by Ladd et al. (1977) and Mayne (1980) which were corroborated with the data in RFG/TXCU-278 in chapter 4, the parameter Λ_{CIUC} obtained by regression of all CIUC tests is 0.591 (for $(c_u/\sigma'_{v0})_{NC}$=0.197, *n*=8 and R^2=0.95). Note that Λ_{CIUC} was previously reported as 0.60 for a selection of preliminary tests by Beesley et al. (2019) (with $(c_u/\sigma'_{v0})_{NC}$=0.19, *n*=6 and R^2=0.92). A smaller rate of change with *OCR* is apparent for CIUE tests (Λ_{CIUE} = 0.488 and $(c_u/\sigma'_{v0})_{NC}$=0.208, *n*=5 and R^2=0.98).

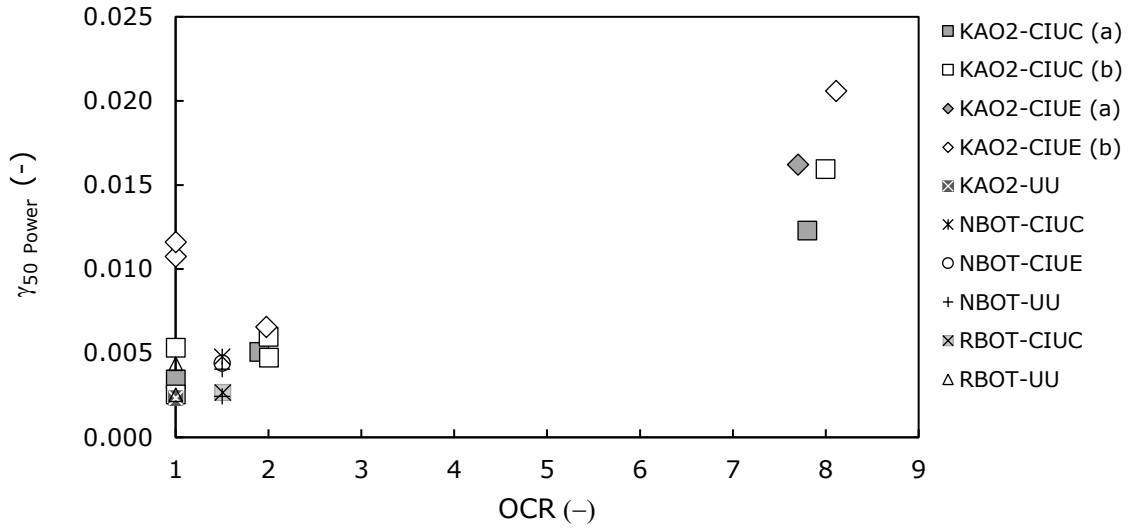

Figure 6- 18. Variation of deformation parameter $\gamma_{50\ Power}$ with *OCR*

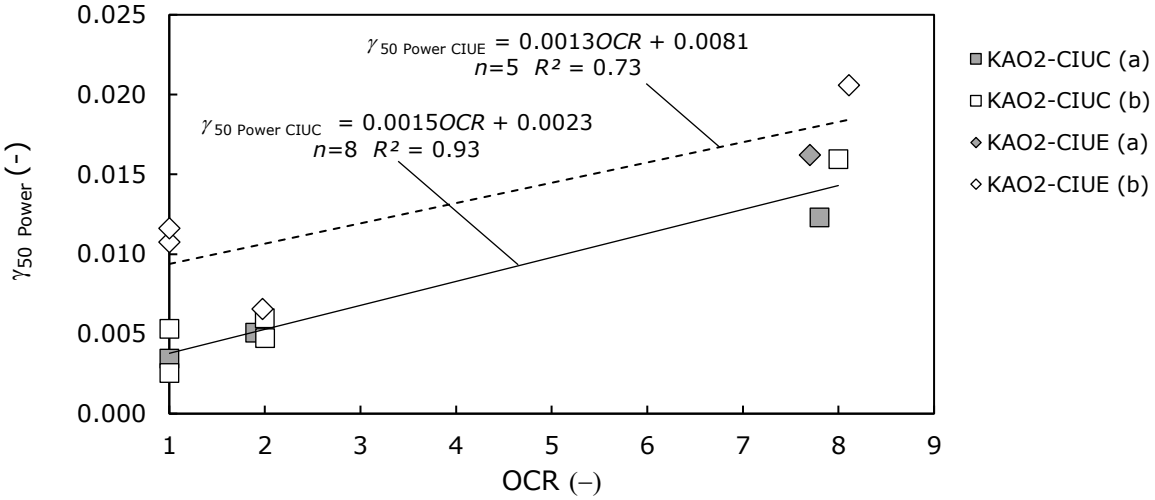

Figure 6- 19. Correlations between *OCR* and $\gamma_{50\ Power}$ by shear mode for Kaolin

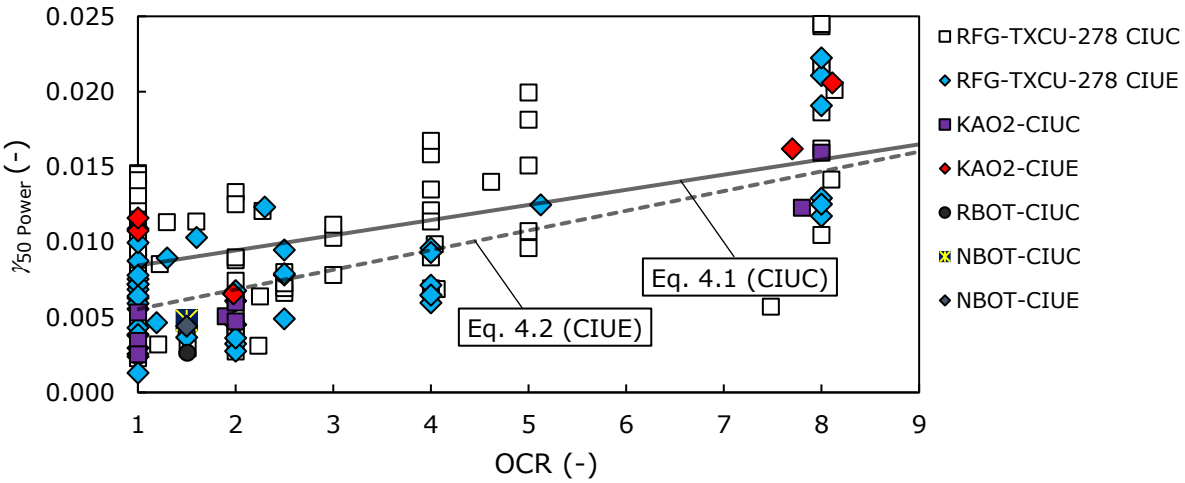

Figure 6- 20. Comparison of $\gamma_{50\ Power}$ from the author's CIU tests with values from database RFG/TXCU-278

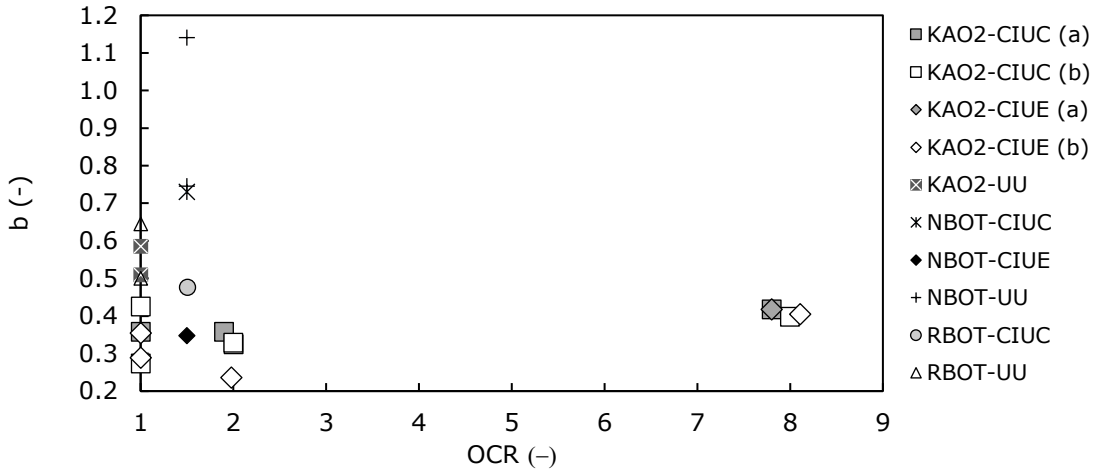

Figure 6- 21. Variation of deformation parameter *b* with *OCR*

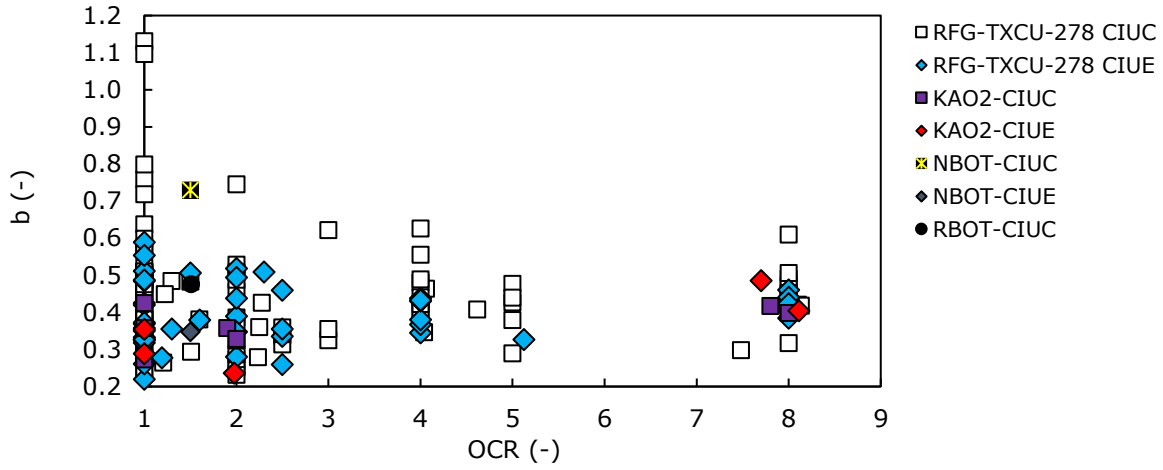

Figure 6- 22. Comparison of deformation parameter *b* from the author's CIU tests with values from database RFG/TXCU-278

Since an intact database of CIUC and CIUE stress-strain data is not available, the deformation parameters for the intact Bothkennar samples have been compared in Figures 6- 20 and 6- 22 with reconstituted test data. Reconstituting the sample and consolidating to the same assessed *OCR* (=1.5), at a higher consolidation stress (σ'_{v0}=99 in contrast to 29), results in lower values of e_0, $\gamma_{50\ \text{Power CIUC}}$ and b_{CIUC} (see also Figure 6- 30). In Figure 6- 25, the values of c_u/σ'_{v0} are compared with data reported by Mayne and Holtz (1985) and Mayne (1988) that were derived from a large database of CIU triaxial tests on intact samples. The peak strengths measured for intact Bothkennar in this study are in the upper range of the previously reported trends. Nash et al. (1992a) and Hight et al. (1992a) attributed their reported measurements of unusually high peak undrained shear strength to ageing of the soil deposit.

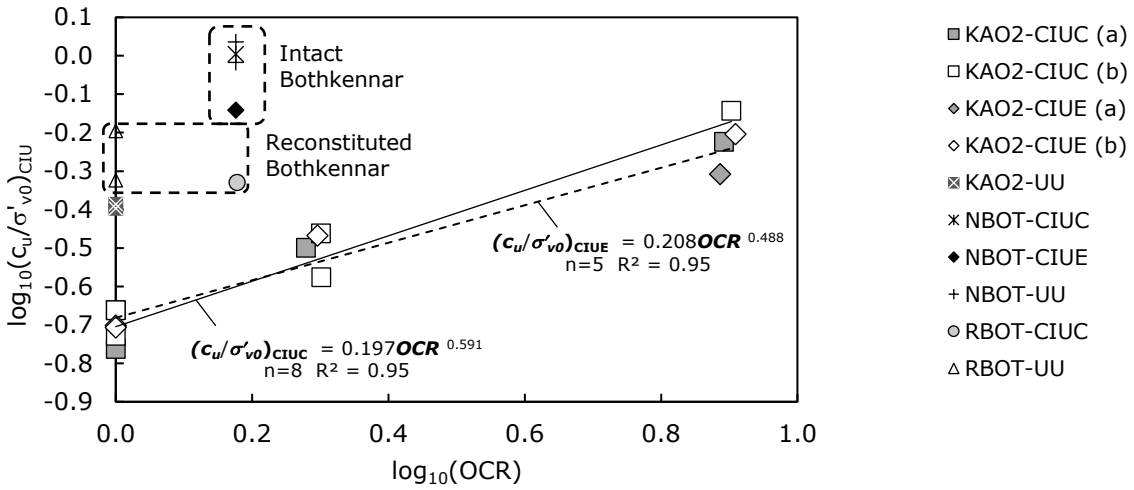

Figure 6- 23. Relationship between normalised undrained shear strength $(c_u/\sigma'_{v0})_{CIU}$ and *OCR* for Kaolin tests by shear mode, following the frameworks of Ladd et al. (1977) and Mayne (1980); UU tests and Bothkennar tests are plotted for reference

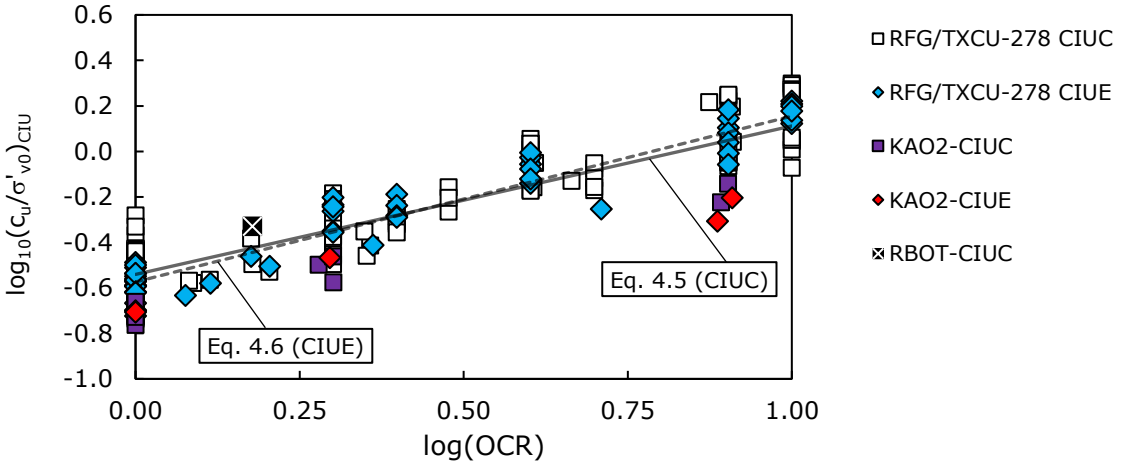

Figure 6- 24. Comparison of normalised undrained shear strength $(c_u/\sigma'_{v0})_{CIU}$ from the author's CIU tests on reconstituted Kaolin and Bothkennar with values from database RFG/TXCU-278

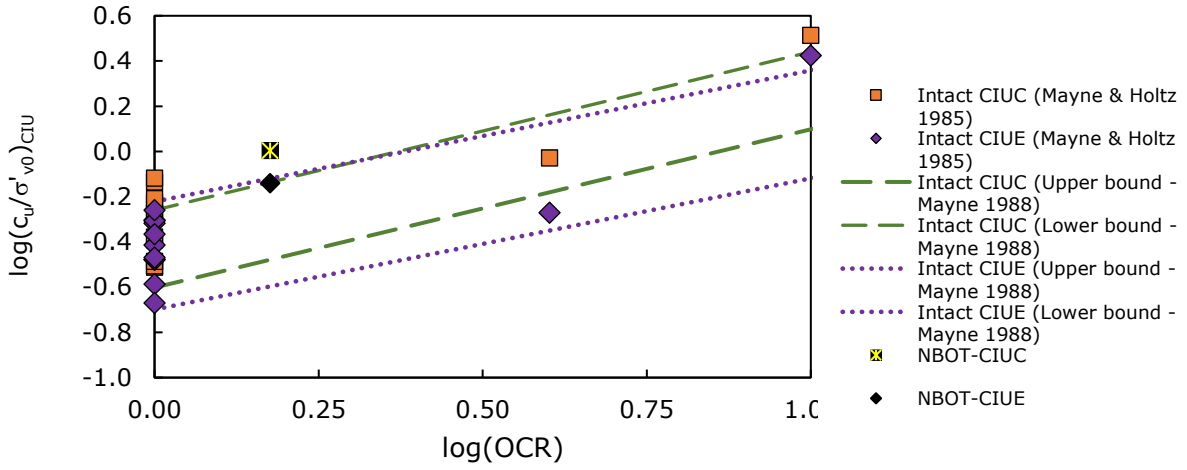

Figure 6- 25. Comparison of normalised undrained shear strength $(c_u/\sigma'_{v0})_{CIU}$ from the author's CIU tests on intact Bothkennar with values from Mayne & Holtz (1985) and the database published by Mayne (1988)

6.2.2 Influence of shear mode

Variations in nonlinear behaviour with shear mode can be examined by comparing Figures 6- 26 and 6- 27. The influence of *OCR* on mobilised strain is dominant at higher values of stress ratio (τ_{mob}/c_u>0.5) in lightly overconsolidated samples of Kaolin; when tested at *OCR*=8, the Kaolin deforms more throughout the moderate stress range in both shear modes. Triaxial extension tests indicate more ductile behaviour than compression tests for both soils (Figure 6- 27 and 6- 28). The more brittle response observed in the UU tests is likely to be explained by the higher strain rate (1%/min compared to 0.002%/min) and – in the case of reconstituted specimens – differences in fabric, since the soil samples were not subjected to isotropic compression following extrusion from the consolidometer.

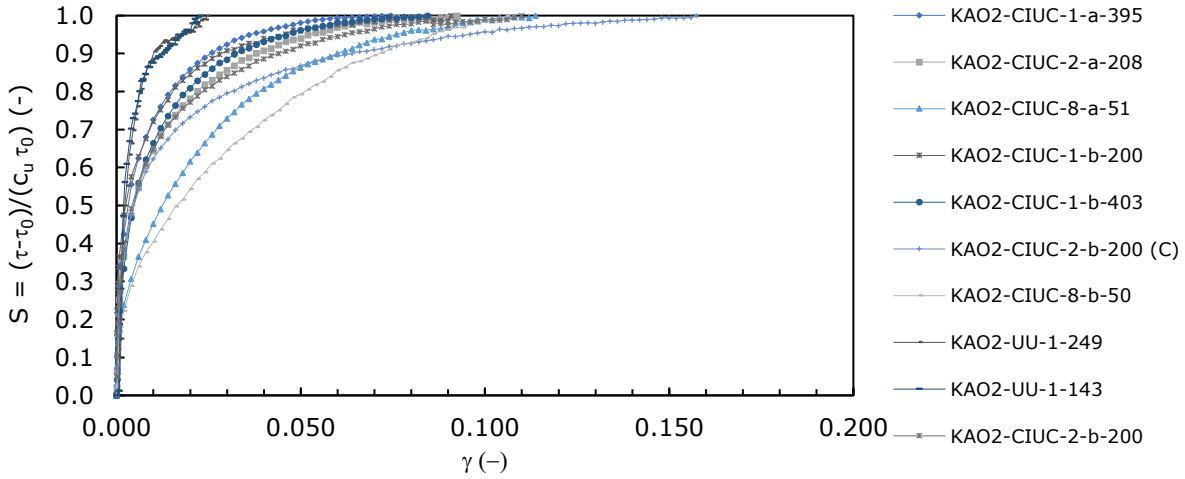

Figure 6- 26. Stress-strain curves for CIUC and UU triaxial tests on Kaolin – comparison of tests by c_u normalisation

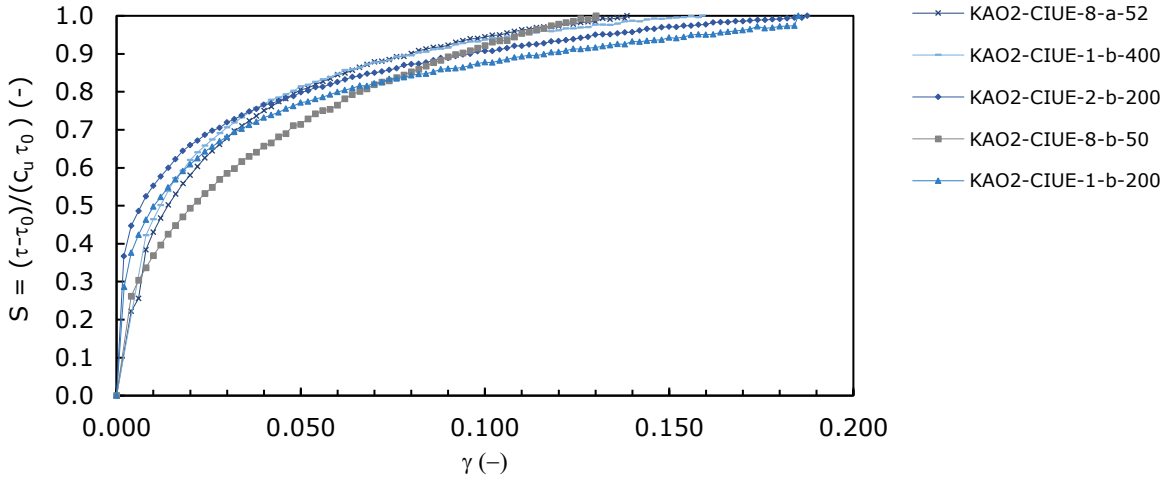

Figure 6- 27. Stress-strain curves for CIUE triaxial tests on Kaolin – comparison of tests by c_u normalisation

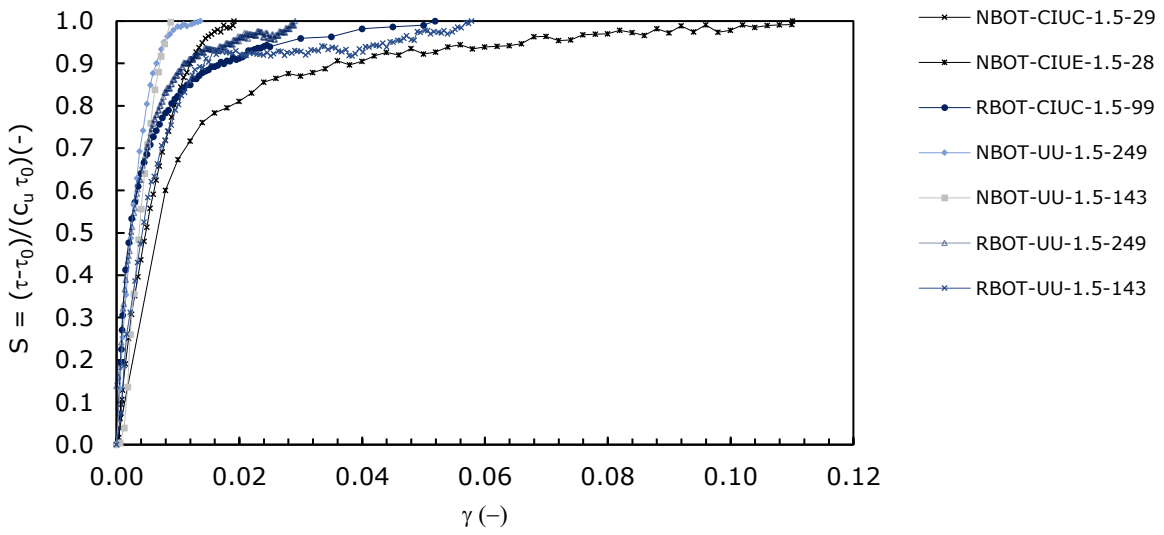

Figure 6- 28. Stress-strain curves for CIU and UU triaxial tests on reconstituted and intact Bothkennar – comparison of tests by c_u normalisation

6.3 Influence of test procedure on parameter variability

6.3.1 Effects of consolidation procedure on parameters

Table 6- 6 summarises the two investigated test procedures (a) and (b). The results suggest that the compressibility of reconstituted Kaolin is sensitive to the adopted procedure. Referring to measurements of void ratio on extrusion of the reconstituted samples and during isotropic consolidation, reported in Table 6- 4 and Figures 5- 3, 6- 5 and 6- 6, procedure (a) produced low-strength reconstituted samples with higher values of extruded void ratio and more apparent swelling during saturation. As a result, isotropic compressibility was variable (λ mean = 0.206 and SD = 0.039, n = 4) and significant volume change occurred when loading was paused, indicating that the loading rate was too high for the material to dissipate excess pore pressures. With procedure (b), the aim to produce less variable isotropic compression curves was achieved (λ mean = 0.164 and SD = 0.031, n = 9).

Table 6- 6. Summary of differences in test procedures (a) and (b)

	Reconstitution 3 single increments of one-dimensional consolidation stress	**Saturation** Continuous stress-controlled increase in back pressure	**Consolidation** Continuous stress-controlled isotropic consolidation rate
Procedure (a)	Maximum σ'_v = 60kPa	p'_{sat} = 4 to 20kPa	Rate = 8kPa/h
Procedure (b)	Maximum σ'_v = 120kPa	p'_{sat} = 34 to 65kPa	Rate = 5kPa/h

Figures 6- 5 and 6- 6 suggest that values of λ are sensitive to initial void ratio for isotropic samples. A smaller range in λ is observed for the oedometer tests when compared to isotropic data (Figure 6- 3), given the same range in initial void ratio. The rate of isotropic consolidation appears to have relatively little influence on measured compressibility parameters. However, the combined effects of variable shaft friction in the consolidometer and swelling during the sample setup and saturation stages led to increases in void ratio at the start of isotropic compression, and associated increases in λ.

To assess the influence of consolidation procedure on shear strains, $\gamma_{50\ Power}$ is plotted with *OCR* in Figure 6- 29 and the marker colours indicate whether the measurements relate to test procedures (a) or (b). The gradient (Γ) is influenced by the procedure adopted (a or b) – a smaller rate of change is associated with procedure (a) which resulted in higher values of e_0 but lower values of $\gamma_{50\ Power\ CIUC}$. The most obvious differences in $\gamma_{50\ Power}$ can be observed for the samples tested at *OCR*=8. For a given test mode, *OCR*, and consolidation stress, $\gamma_{50\ Power}$ varies by –7% to +55% and *b* varies by -17% to +19%

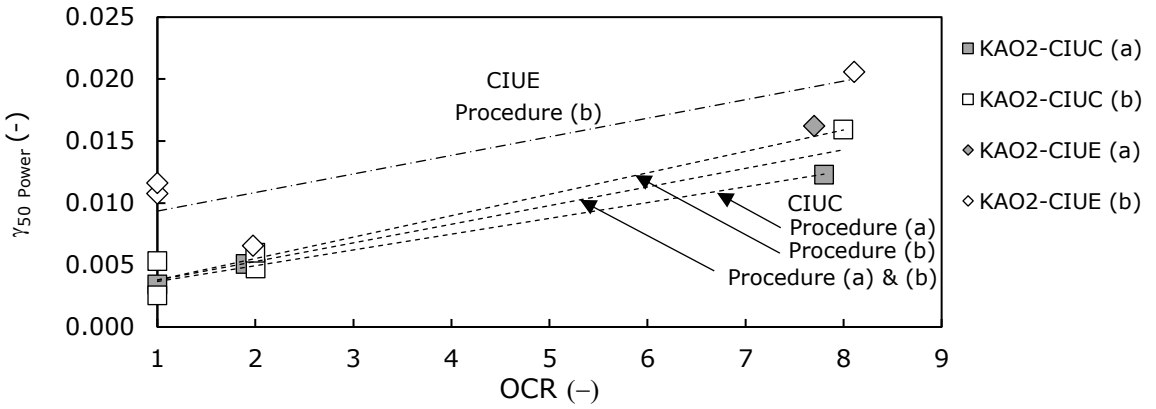

Figure 6- 29. Relationships between deformation parameter $\gamma_{50\ Power}$ and *OCR* for kaolin described by gradient Γ

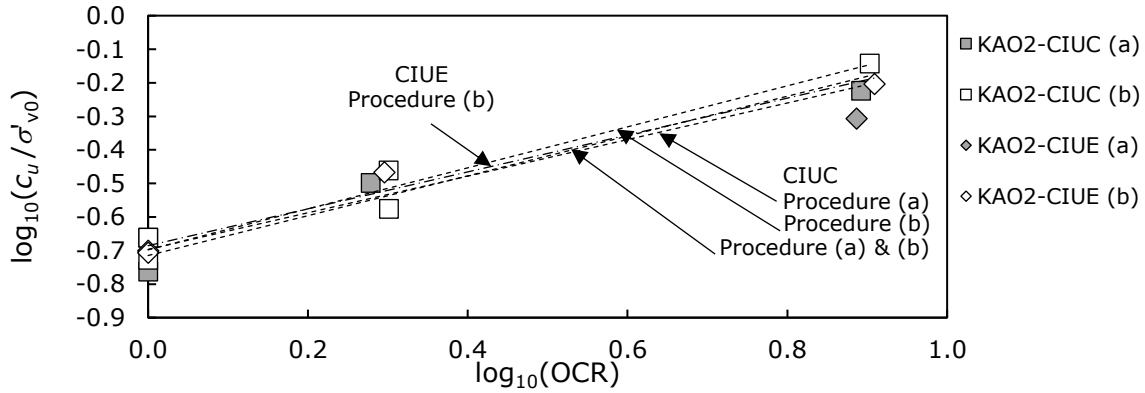

Figure 6- 30. Relationships between (c_u / σ'_{v0}) and *OCR* for kaolin described by gradient Λ

between procedure (a) and procedure (b). The same tests are plotted in Figure 6- 30 using c_u/σ'_{v0} and *OCR*. Comparing the trend lines with those in Figure 6- 29, the results show that procedure (a) produced lower values of $\gamma_{50\ Power}$ and c_u/σ'_{v0} compared with procedure (b). However, Λ is less sensitive to a change in procedure than Γ.

6.3.2 Effects of shearing procedure on parameters

The differences in procedure adopted during undrained shear of a test mode were minimised to understand the effects of consolidation procedure (a) and (b) on parameter variability. All samples were tested at the same strain rate; moreover, identical cells and load caps were used for each test mode - with the exception of two tests KAO2-CIUE-8-a-52 and KAO2-CIUC-2-b-200 (C). Examination of the stress paths and normalised stress-strain curves of Kaolin indicates that the large strain behaviour of KAO2-CIUC-2-b-200 (C) was significantly affected by bedding at the start of shear. A 'concave' load cap was used, which caused sudden displacement and changes in measured load when axial alignment was forced in the early stages of undrained shearing. Of the three CIUC tests performed at *OCR*=2, KAO2-CIUC-2-b-200 (C) demonstrated the largest value of $\gamma_{50\ Power}$. Despite this, the spread of $\gamma_{50\ Power}$ at *OCR*=2 is narrow compared to the results of tests performed at *OCR*=1 and *OCR*=8 using the same 'flat' compression load cap (Figure 6- 29).

As described in chapter 3, the use of a rotationally flexible extension cap caused an initial displacement during connection of the order of 0.13 to 0.4mm, which is dependent on the stiffness of the sample. It is likely that this initial rapid extension of the specimen affected the subsequent stress-strain behaviour. Importantly, a consequence of connecting the load cell to the specimen after consolidation was that the initial part of the undrained stress-strain curve was not measured. For stiffer samples, this presents a problem when considering the moderate stress range: the axial displacement that occurred during connection to the intact Bothkennar sample mobilised 60% of the subsequent peak stress (Figure 6- 31). The modelled stress strain curve is then an extrapolation to estimate $\gamma_{50\ Power}$ and *b*. Clearly the parameters obtained from extrapolated data are highly questionable. It would be valuable to repeat the test (NBOT-CIUE-1.5-28) with a modified version of the extension cap or using an improved procedure that allows the connection to be made with less displacement.

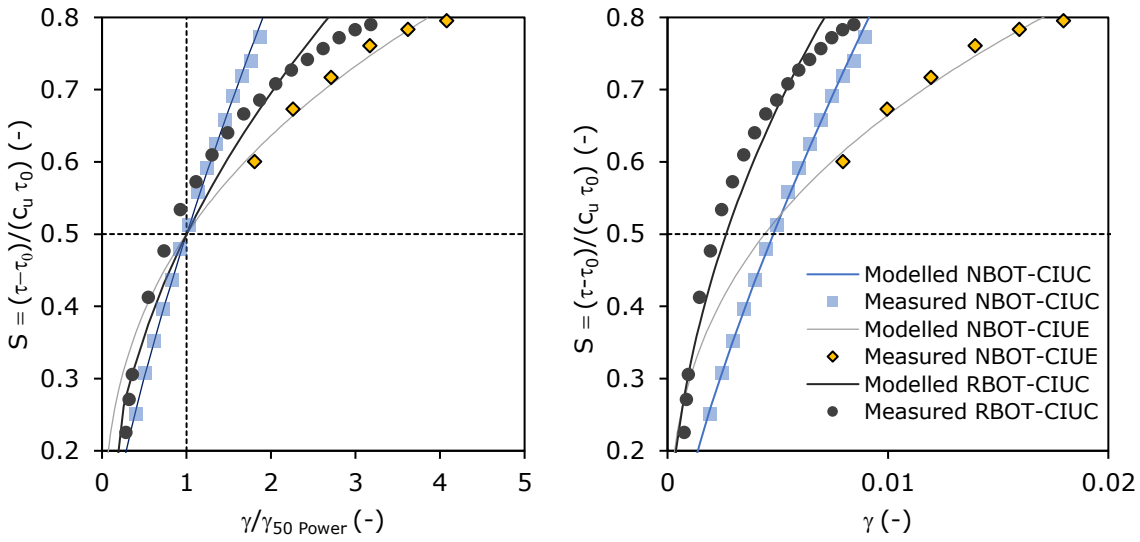

Figure 6- 31. Measured and modelled stress-strain curves for intact and reconstituted Bothkennar

6.4 Influence of data interpretation on parameter variability

6.4.1 Assumed deformation shape of triaxial specimen

During undrained shear of a triaxial sample, the deformation shape is commonly assumed to be either cylindrical or parabolic, due to the variable influence of frictional end restraint. Figure 6- 32 shows a comparison of parameters (c_u/σ'_{v0}, $\gamma_{50\ Power}$ and b) for each triaxial test deduced using the assumption of cylindrical or parabolic sample shape. (It should be noted here that the preliminary results reported in Beesley et al. 2019 used a greater number of data points per curve fitting – see section 6.4.2). In compression tests, the parabolic assumption estimates up to 5% reduction in strength compared to employing the assumption of right cylinder; up to -13% and ±6% are observed respectively in $\gamma_{50\ Power}$ and b. In triaxial extension, the strength increases up to 6% when using the assumption of parabolic necking compared with the value calculated assuming cylindrical deformation; for the same tests $\gamma_{50\ Power}$ increases by up to 28% and b decreases by up to 5%. These results confirm that the strength and deformation parameters, notably $\gamma_{50\ Power}$, are affected by the assumed shape and resulting stress (ratio) of the sample during shear and this source of variability in triaxial stress-strain measurements from commercial laboratories may have a significant influence on design calculations.

Table 6- 7. Comparison of model parameters using the assumption of right cylinder and reducing the number of fitted data points (*n*)

Triaxial Test	*n*	*b*	$\gamma_{50\ Power}$	*n*	*b*	$\gamma_{50\ Power}$	*n*	*b*	$\gamma_{50\ Power}$
KAO2-CIUC-1-a-395	957	0.335	0.0032	11	0.358	0.0034	3	0.360	0.0034
KAO2-CIUC-1-b-200	2477	0.263	0.0025	14	0.273	0.0026	3	0.269	0.0025
KAO2-CIUC-1-b-403	3592	0.406	0.0051	10	0.425	0.0053	3	0.402	0.0052
KAO2-CIUC-2-a-208	1311	0.341	0.0049	14	0.358	0.0051	3	0.354	0.0051
KAO2-CIUC-2-b-200 (C)	5546	0.293	0.0053	18	0.329	0.0060	3	0.325	0.0061
KAO2-CIUC-8-a-51	2510	0.416	0.0123	19	0.417	0.0123	3	0.424	0.0124
KAO2-CIUE-8-a-52	2797	0.413	0.0146	23	0.486	0.0162	3	0.415	0.0148

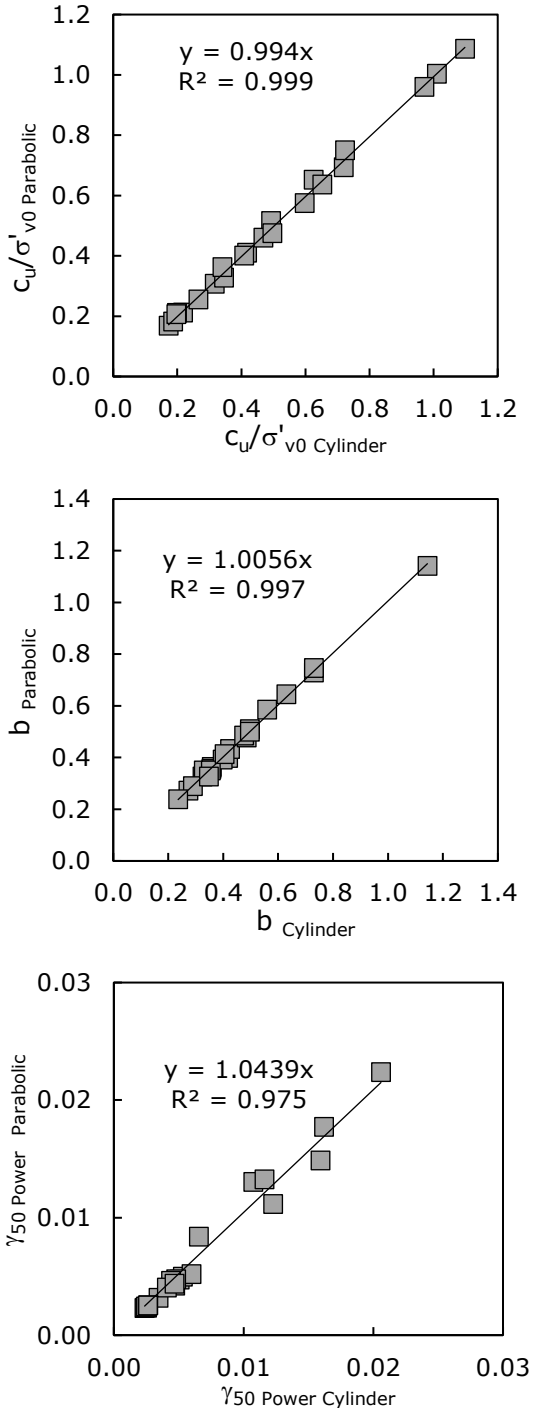

Figure 6- 32. Comparison of CIU parameters using the assumptions of right cylinder and bulging/necking in parabolic shape

6.4.2 Number of data points between *S*=0.2 and 0.8

The model parameters reported by Beesley et al. (2019) used the original measurements of stress-strain without filtering the data; the parameters are reported in the first column of Table 6- 7. In the second and third columns, parameters are reported for reduced numbers of data points. The second column represents the data reported in this chapter. For a given test, $\gamma_{50\ \mathrm{Power}}$ varies by 0% to +16% and *b* varies by -1% to +18% as *n* reduces.

6.5 Validation of transformation models from RFG/TXCU-278

In Figure 6- 33(a), the strain parameters measured by the author's CIU tests are compared with the estimated values using Equations 4.11 and 4.14 where *OCR* is the single independent variable. In Figure 6- 33(b), the normalised strength parameters measured by the same tests are compared with the estimated values using Equations 4.22 and 4.23 where *OCR* is the single independent variable and Equations 4.26 and 4.27 where *OCR* and strain rate ($\dot{\varepsilon}_a$) are multiple independent variables.

Equation 4.11 overpredicts the measured CIUC strains and Equation 4.14 underpredicts the measured CIUE strains - with the largest errors at *OCR*=1. Consequently, with a single experimental programme on Kaolin, the lower and upper error bounds of the transformation models for two test modes are tested: 50% of the new data fall outside the region encompassing 80% of the data of RFG/TXCU-278 (indicated by the dashed lines). The sample of reconstituted Bothkennar clay also deformed less in compression than the lower bound estimate. Since a significant correlation exists between the new test parameters and *OCR* in both test modes (Figure 6- 19), the error in the prediction made using the transformation models is caused by the model coefficients ($\gamma_{50\ \mathrm{Power}}$ at *OCR*=1 and I) and any differences in measurement due to testing procedure between RFG/TXCU-278 and the new test data. A likely explanation is that local strain measurements and a new type of extension cap were used.

However, Figure 6- 33(b) shows that including strain rate in the transformation model adjusts the overpredicted values of c_u/σ'_{v0} so that nearly all data points lie between the factor error bounds of 1.4 and 1.25 respectively in CIUC and CIUE. It is possible that a relationship with strain rate exists for

strain measurements as well as peak stress measurements, and a transformation model with multiple independent variables would adjust the coefficients ($\gamma_{50\ Power}$ at OCR=1 and I) accordingly. However, no relationship was found for the tests in RFG/TXCU-278. Given the scatter in $\gamma_{50\ Power}$ observed in the new CIUC and CIUE data, the variability due to testing procedure does appear to have a greater effect on $\gamma_{50\ Power}$ than on c_u/σ'_{v0}. This could be a reasonable explanation for the lack of correlation between $\gamma_{50\ Power}$ and strain rate in RFG/TXCU-278.

In Figure 6- 34, the measured values of $\gamma_{50\ Power\ CIUE}$ and $(c_u/\sigma'_{v0})_{\ CIUE}$ are compared with the values estimated by Equations 4.29 and 4.31. The plots demonstrate that the measured strength anisotropy (expressed by the parameter K_s) is close to the expected ratio of 0.835 with a measured range of 0.825 to 1.049; for the same tests, the measured strain anisotropy (expressed by the parameter K_γ) deviates substantially from the expected ratio of 0.749 with a measured range of 1.292 to 4.220. Having first checked the results in Figure 6- 33, this result is unsurprising - with $\gamma_{50\ Power\ CIUC}$ and $\gamma_{50\ Power\ CIUE}$ measurements respectively being lower and higher than expected from the database analysis. However, the peak stresses are valid (indeed, the measurements validate the Equations 4.22, 4.23, 4.26 and 4.27), which implies that the measurements of strain are more influenced by procedure than strength.

6.5.1 Validated uncertainty estimation of parameter transformation models

At the end of chapter 4 it was suggested that the variability of parameters c_u/σ'_{v0} and $\gamma_{50\ Power}$ of the triaxial tests in RFG/TXCU-278, which could not be explained by the variables *OCR*, strain rate, liquid limit, and plastic limit, could be attributed to measurement uncertainty. This hypothesis can be tested using the information in Figure 6- 33 and Figure 6- 35. It has already been shown that a correlation with *OCR* does exist with the new measurements of $\gamma_{50\ Power}$ for Kaolin, but the regression coefficients differ to the best-fit coefficients in Equations 4.11 and 4.14 which causes a factor error of up to 2.45 in CIUC and up to 2.10 in CIUE, with 50% of the values within the expected bounds (Figure 6- 33). Figure 6- 35 shows only the tests for which the same loading caps and shearing procedures were used for the test mode, i.e. the 'Flat' load cap for CIUC and 'Vacuum-2' for CIUE tests. Referring to Figure 6- 29 and Figure 6- 30, the following regression equations for the Kaolin tests are adopted:

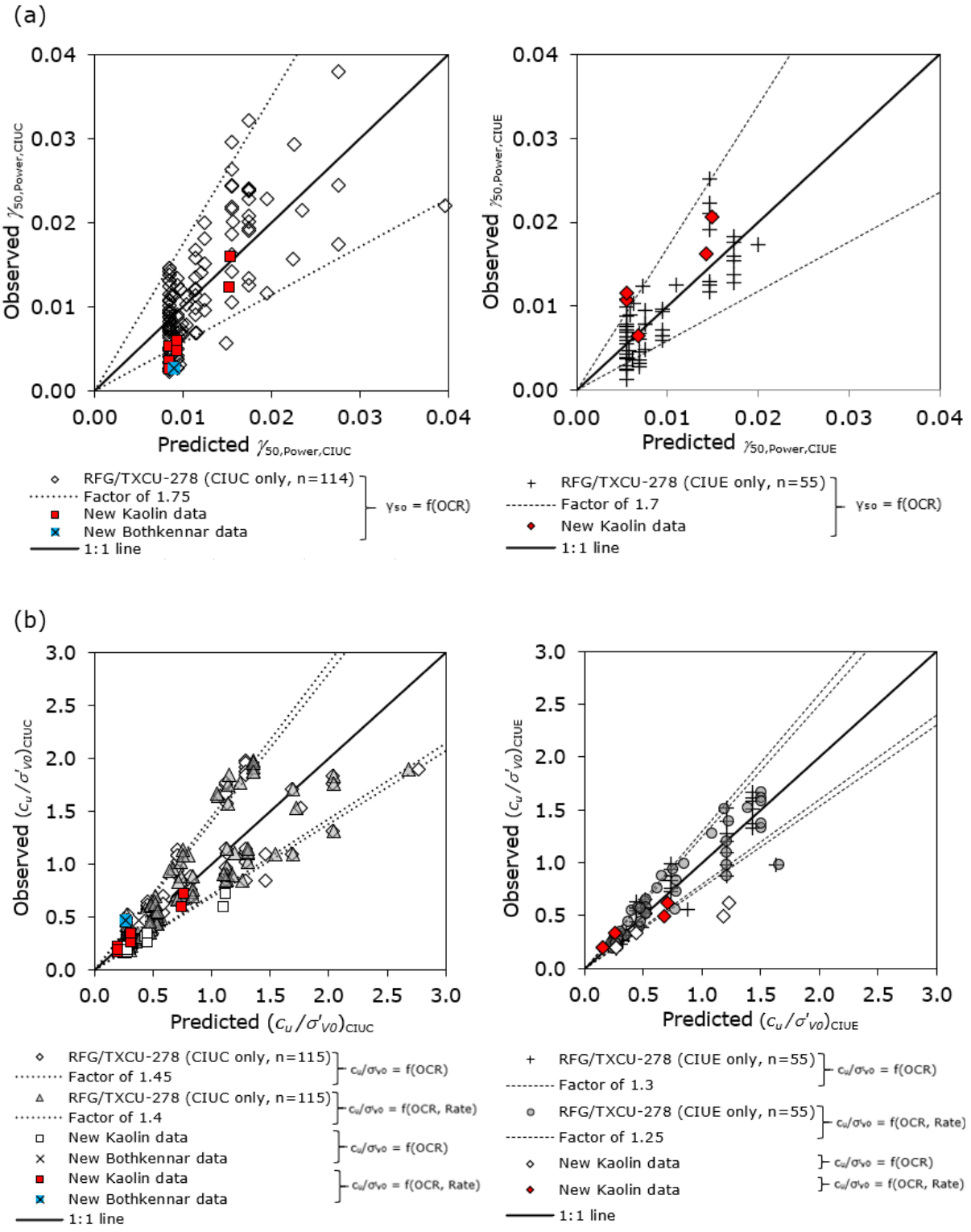

Figure 6- 33 (a) Predicted-measured plots of $\gamma_{50\ Power\ CIUC}$ and $\gamma_{50\ Power\ CIUE}$ predicted using Equations 4.11 and 4.14; **(b)** Predicted-measured plots of $(c_u/\sigma'_{v0})_{CIUC}$ and $(c_u/\sigma'_{v0})_{CIUE}$ predicted using Equations 4.22, 4.23, 4.26 and 4.27

(a)

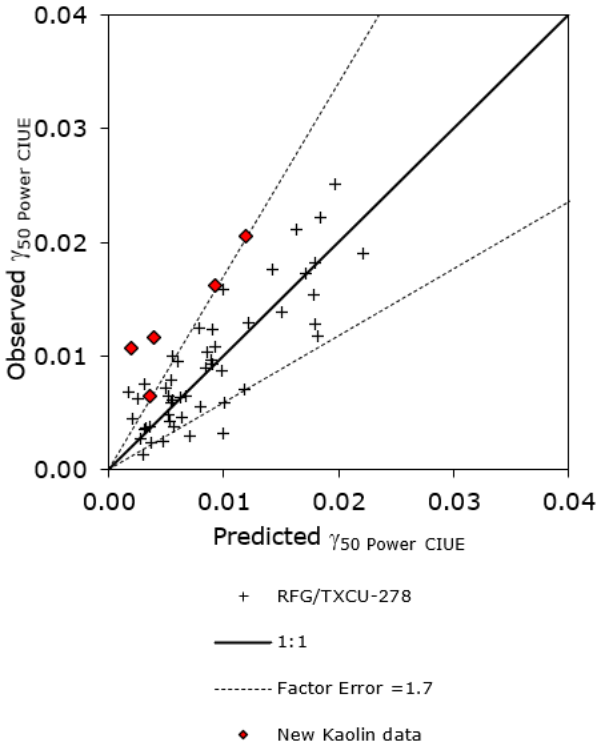

(b)

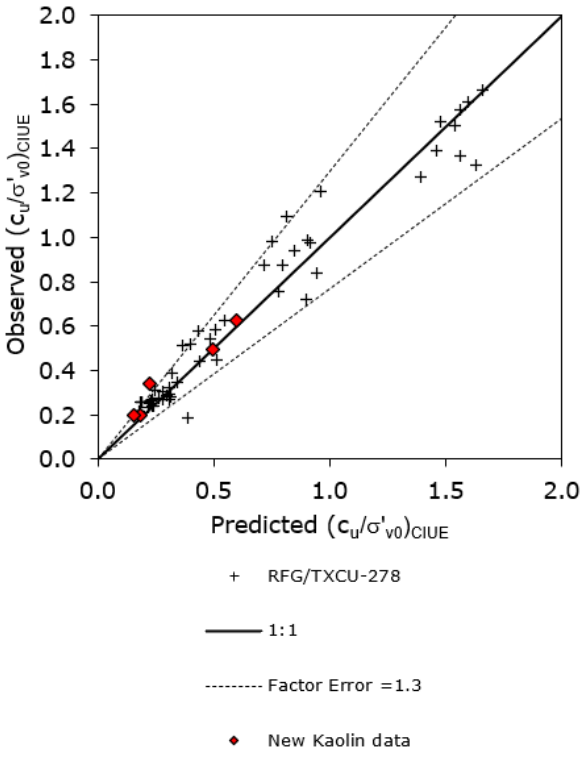

Figure 6- 34 (a) Predicted-measured plots of $\gamma_{50\ Power\ CIUE}$ predicted using Equation 4.29; **(b)** Predicted-measured plots of $(c_u/\sigma'_{v0})_{CIUE}$ predicted using Equation 4.31

$$\gamma_{50\ \text{Power CIUC}} = 0.0021 + 0.0015\,OCR \tag{6.2}$$

including Procedure (a) and (b) tests

(n = 7, R^2 = 0.94, *S.E.* = 0.0014, $p < 0.001$)

$$\gamma_{50\ \text{Power CIUE}} = 0.0079 + 0.0015\,OCR \tag{6.3}$$

including only Procedure (b) tests

(n = 4, R^2 = 0.76, *S.E.* = 0.0036, $p > 0.1$)

$$\log_{10}\left(\frac{c_u}{\sigma'_{v0}}\right)_{\text{CIUC}} = 0.593\log_{10}(OCR) - 0.715 \tag{6.4}$$

including Procedure (a) and (b) tests

(n = 7, R^2 = 0.97, *S.E.* = 0.049, $p < 0.001$)

$$\log_{10}\left(\frac{c_u}{\sigma'_{v0}}\right)_{\text{CIUE}} = 0.550\log_{10}(OCR) - 0.686 \tag{6.5}$$

including only Procedure (b) tests

(n = 4, R^2 = 0.98, *S.E.* = 0.045, $p > 0.1$)

Equations 6.2 and 6.4 are significant correlations ($p < 0.001$) whereas Equations 6.3 and 6.5 fail the test of significance. The scatter in measured $\gamma_{50\ \text{Power CIUE}}$ and $(c_u/\sigma'_{v0})_{\text{CIUE}}$ questions the validity of the assumed relationships with *OCR*. Hence, more CIUE tests would be needed to confirm or modify this relationship for the same Kaolin using the same procedures. Nonetheless, Equations 6.3 and 6.5 are adopted here to demonstrate the uncertainty estimation of the parameter transformation models from RFG/TXCU-278 (Equations 4.14, 4.23 and 4.27). Likewise Equations 6.2 and 6.4 are used here to demonstrate the uncertainty estimation of Equations 4.11, 4.22 and 4.26.

In Figure 6- 35(a), the measured strain parameters are compared with the estimated values using Equations 6.2 and 6.3 where *OCR* is the single independent variable. In Figure 6- 35(b), the normalised strength parameters measured by the same tests are compared with the estimated values using Equations 6.4 and 6.5 where *OCR* is the single independent variable. Consequently, the parameter variability due to the material's stress history is removed. It should be noted that this does not necessarily mean the associated effect of strain history (which may be variable due to limitations of the test equipment and procedures) has been removed. In Figure 6- 35, and referring also to Figure 3- 1, the observed parameter

variability of measured $\gamma_{50\ \text{Power CIUC}}$ is then explained by a combination of the following factors (1) to (4) while $(c_u/\sigma'_{v0})_{\text{CIUC}}$, which is unaffected by (4), is explained by a combination of (1) to (3). The observed parameter variability of $\gamma_{50\ \text{Power CIUE}}$ is then explained by (2), (3) and (4); the observed parameter variability of $(c_u/\sigma'_{v0})_{\text{CIUE}}$ is explained by (2) and (3).

(1) Intended variations due to test procedures (a) or (b)

(2) Measurement uncertainty due to test procedure and boundary conditions

(3) Unintended material variability of the samples due to the imperfect processes of artificial sedimentation and consolidation

(4) Parameter model error due to the imperfect process of curve-fitting

Comparing the data plotted in Figures 6- 33 and 6- 35, the factor errors of the strain parameter transformation models (Equation 4.14 for CIUC parameters with factor error of 1.75 and Equation 4.11 for CIUE parammeters with factor error of 1.70) are influenced more by the inaccuracy of using average regression coefficients (particularly $\gamma_{50\ \text{Power}}$ at OCR=1) instead of a suitable relationship for the material than the variability due to test procedure and measurement uncertainty. However, the latter remains significant, since if a more accurate estimate of $\gamma_{50\ \text{Power NC}}$ and Γ is made (i.e. Equations 6.2 and 6.3), the factor errors vary up to 1.49 (CIUC) and 1.66 (CIUE).

6.5.2 Validated uncertainty estimation of using parameter transformation models to predict stress-strain

The best estimate of model parameter b is the mean value for a test mode. Following the method demonstrated in chapter 4, the effect of using best estimate values of $\gamma_{50\ \text{Power}}$ and b to predict stress-strain in the moderate stress region is examined in Figure 6- 36 and Figure 6- 37. Due to the overprediction of γ and underprediction of S, G_{sec}/c_u is conservatively low for the CIUC tests on reconstituted Kaolin and Bothkennar by up to a factor of 7 (for 80% of the data). Conversely the CIUE tests are estimated to be stiffer than the measurements by up to a factor of 3.95 (for 80% of the data). Any empirical estimates of parameters that characterise nonlinear stress-strain behaviour should acknowledge such an error in the design calculations.

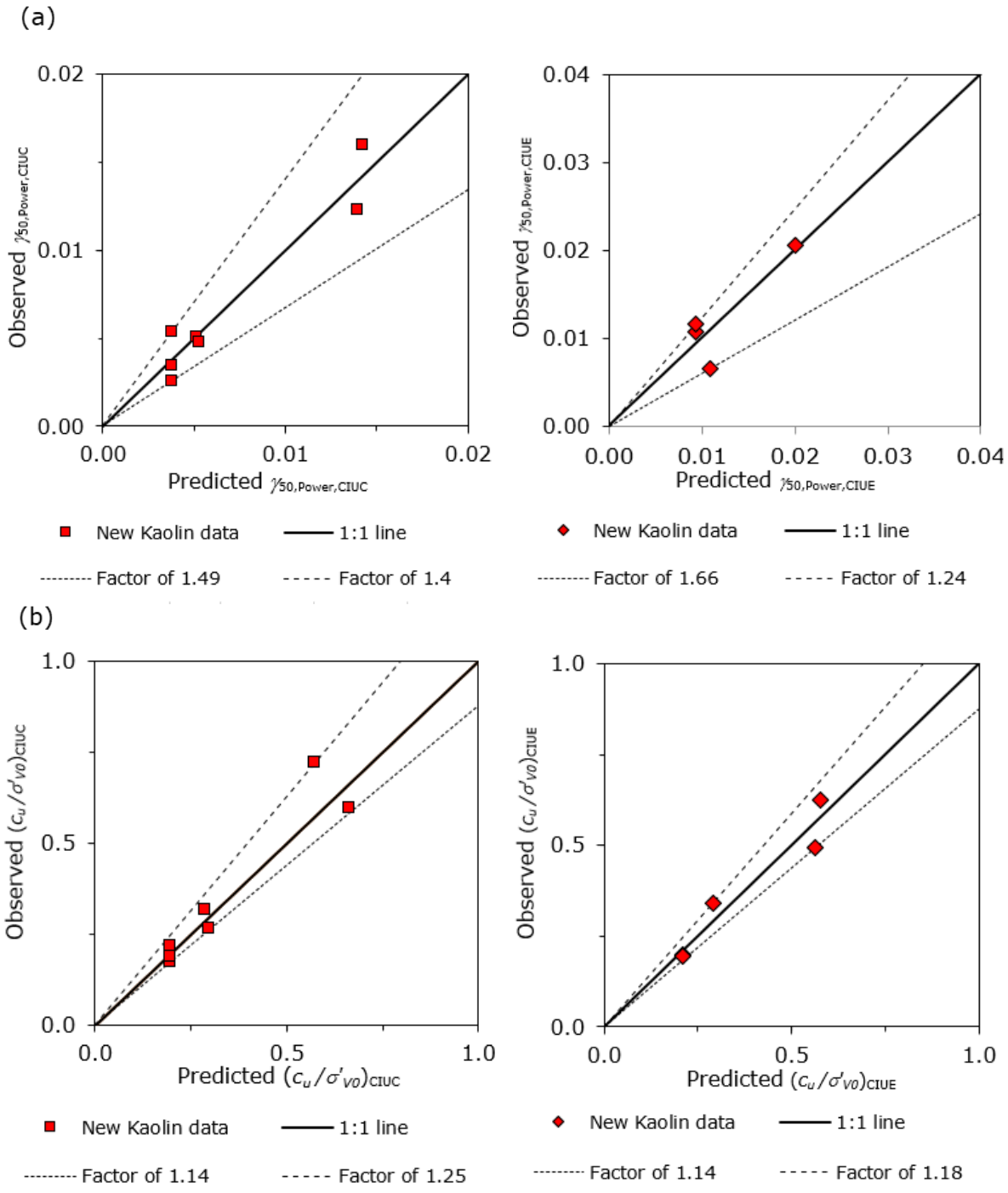

Figure 6- 35 (a) Predicted-measured plots of $\gamma_{50\ Power\ CIUC}$ and $\gamma_{50\ Power\ CIUE}$ predicted using Equations 6.2 and 6.3; **(b)** Predicted-measured plots of $(c_u/\sigma'_{v0})_{CIUC}$ and $(c_u/\sigma'_{v0})_{CIUE}$ predicted using Equations 6.4 and 6.5

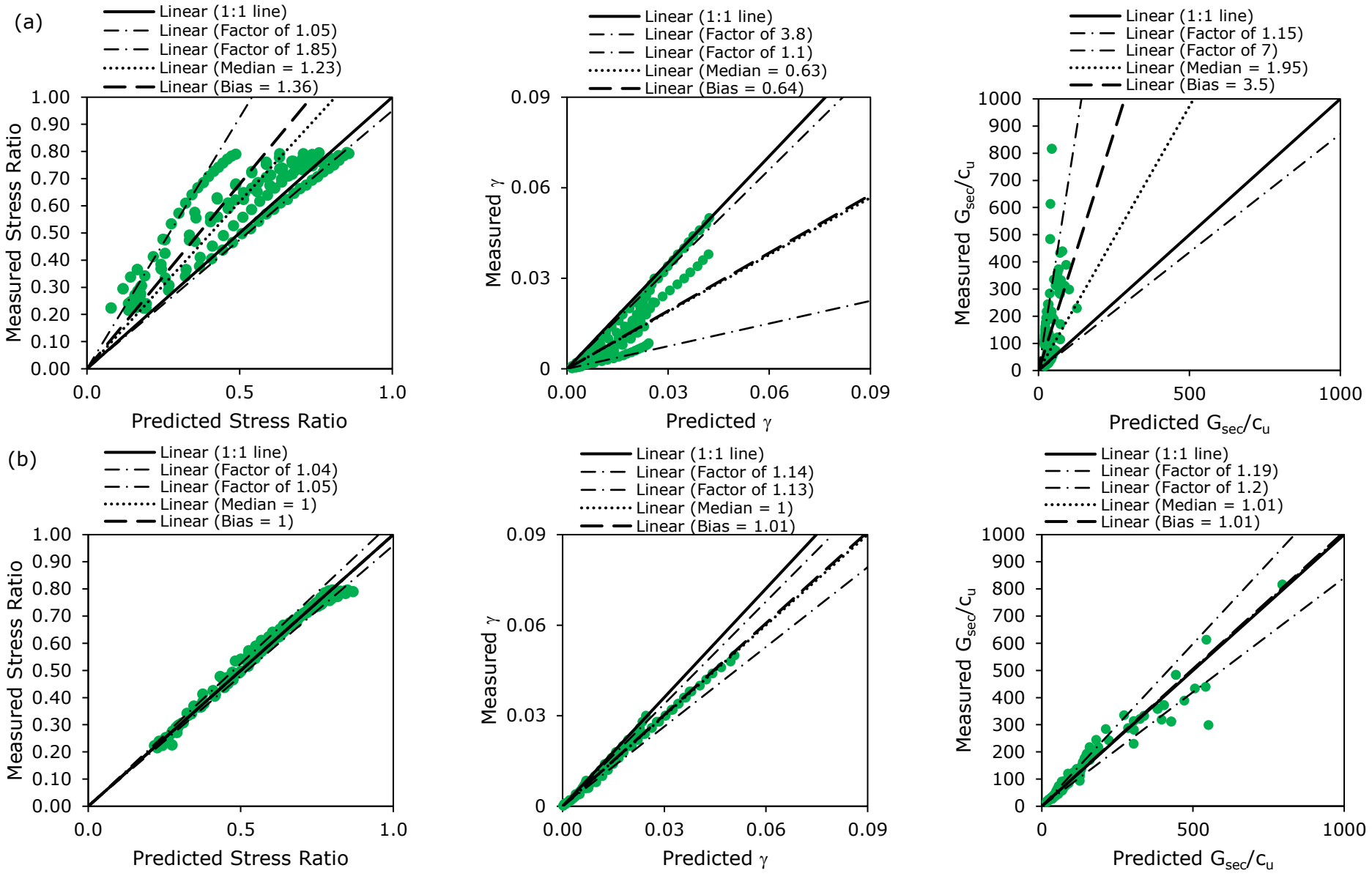

Figure 6- 36. Predicted-measured plots of *all new reconstituted Kaolin and Bothkennar stress-strain data* between 20%≤*S*≤80% tested in CIUC (*n*=144 data points) predicted using: (a) Equation 4.11 (b) model parameters $\gamma_{50\ Power}$ and *b* of every triaxial test

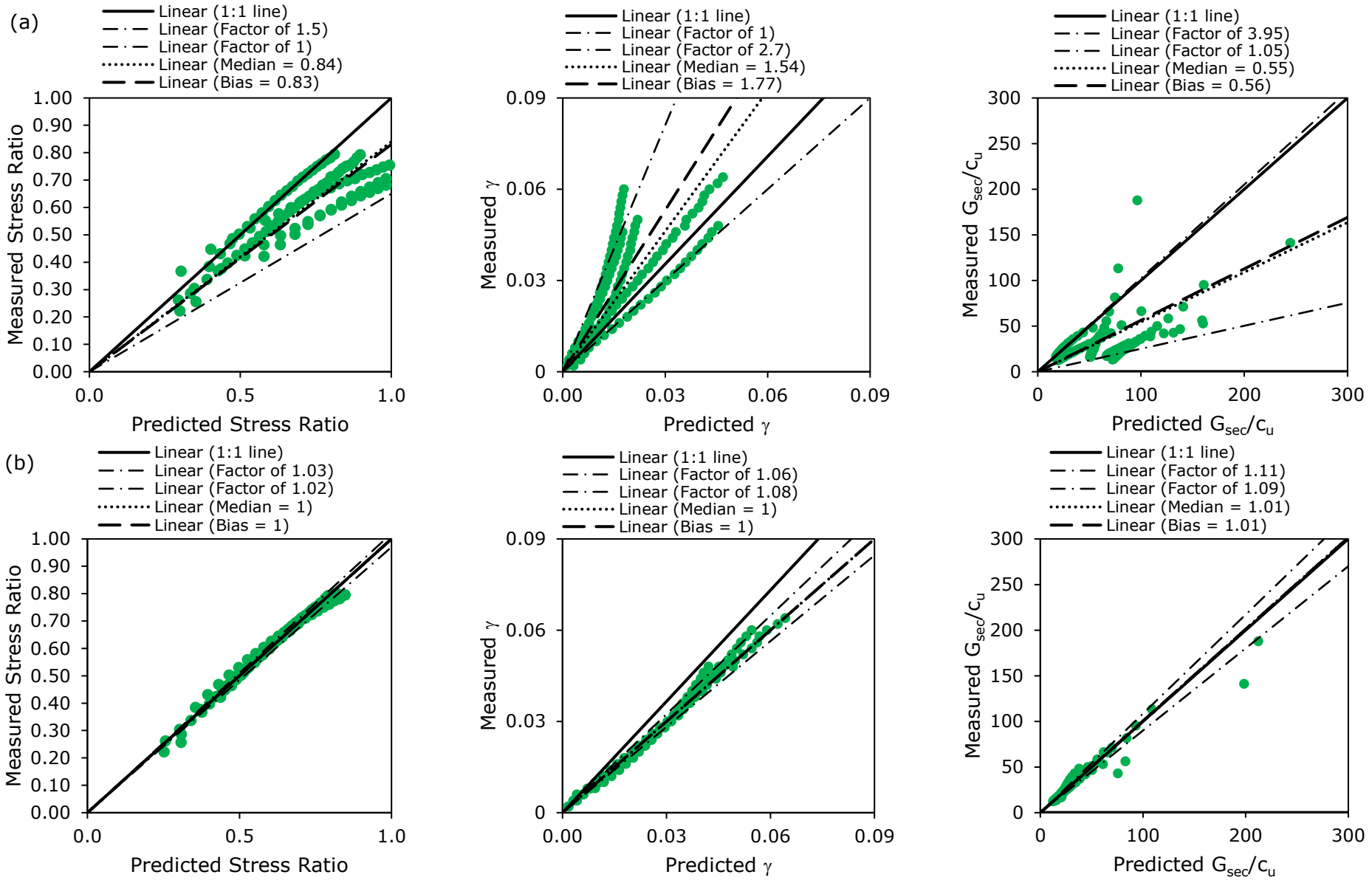

Figure 6- 37. Predicted-measured plots of *all new reconstituted Kaolin stress-strain data* between 20%≤*S*≤80% tested in CIUE (*n*=129 data points) predicted using: (a) Equation 4.14 (b) model parameters $\gamma_{50\ Power}$ and *b* of every triaxial test

6.5.3 Validated uncertainty estimation of fitted power-law functions

The model parameters fitted for each test are used to predict stress-strain in parts (b) of figures 6- 36 and 6- 37. This technique allows an estimate to made of the uncertainty due to model curve-fitting. The figures demonstrate that the new experimental data are not perfectly simulated by a power law function, as expected, and the model error due to the imperfect process of curve-fitting is similar to the error computed in chapter 4 (a factor error of about 1.15 to 1.2 when comparing predicted with measured values of G_{sec}/c_u throughout the moderate stress range).

6.5.4 Example: using the calibrated factor errors to estimate variable stress-strain behaviour

Using Equations 4.29 and 4.31, the parameters for strength mobilisation in RBOT- CIUE- 1.5- 99 can be estimated. Similarly, $(c_u/\sigma'_{v0})_{\text{CIUE}}$ and $\gamma_{50\ \text{Power CIUE}}$ could be estimated using Equations 4.14 and 4.27. The estimated parameters shown in Figure 6- 38 demonstrate that the use of factor errors, deduced from the calibration of empirical data as explained in chapter 4, may be valuable when assessing parameter variation when test data are questionable or scarce.

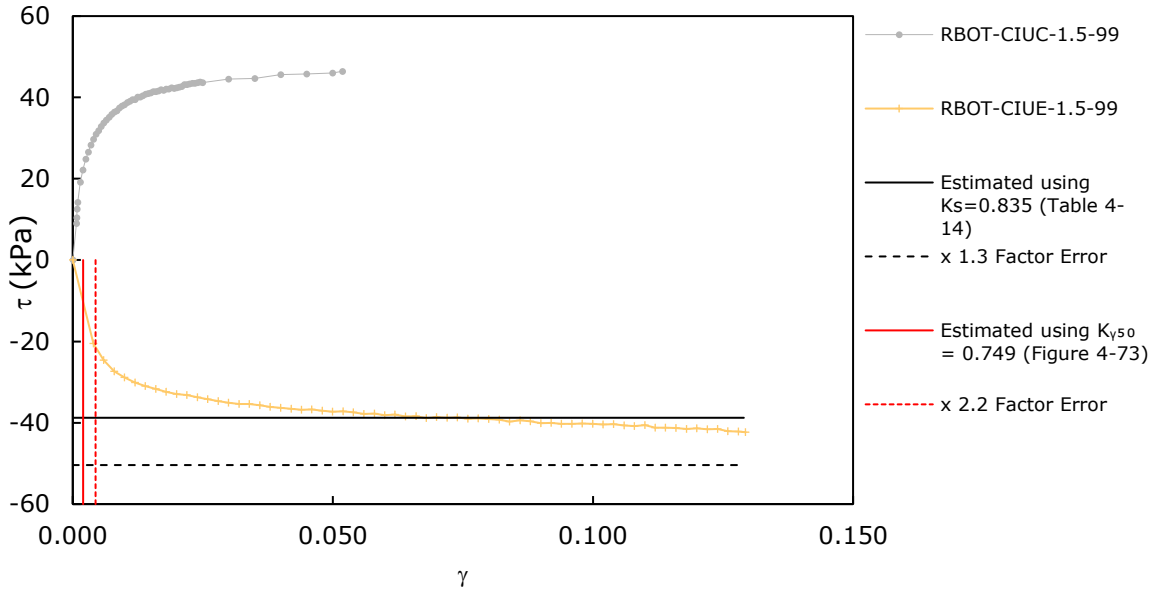

Figure 6- 38. Estimated peak undrained shear stress and $\gamma_{50\ \text{Power CIUE}}$ for test RBOT-CIUE-1.5-99

6.6 Conclusions

The results of a new experimental programme of CU triaxial and oedometer tests on reconstituted Kaolin, reconstituted Bothkennar, and intact Bothkennar have been presented in this chapter. The measurements of stress-strain and the fitted power-law model parameters for the moderate stress region have been compared with the results of the database analysis of RFG/TXCU-278 presented in chapter 4. The following conclusions can be made:

- The results suggest that isotropic consolidation parameters are sensitive to initial void ratio, which is likely to be the result of varying degrees of swelling during sample setup and saturation. Values of λ and κ from oedometer tests on non-preconsolidated material are less sensitive to initial void ratio and demonstrate convergence to the intrinsic compression line reported by Burland (1990).
- It appears that the type of load cap connection which forces the sample into vertical alignment at the start of shear can have a significant influence on the behaviour of Kaolin samples in the moderate stress region. When using the new extension cap 'Vacuum-2', compliance displacement at the start of shear occurred in the order of 0.13 to 0.4mm. It is highly probable that this was the direct cause of $\gamma_{50\ \text{Power CIUE}}$ measurements to be around the upper bound of expected values according to Equation 4.14 (factor error =1.7).
- For Kaolin, the variations of c_u/σ'_{v0} and $\gamma_{50\ \text{Power}}$ with overconsolidation ratio are described by positive trends in CIUC and CIUE test modes, which agree with the results of similar tests on reconstituted soils in RFG/TXCU-278 (presented in chapter 4). Equations 4.11 and 4.14 and Equations 4.22, 4.23, 4.26 and 4.27 have been validated with the new test results. Including strain rate as a variable for estimating c_u/σ'_{v0} proved to reduce the error of the estimate. Some caution is advised with Equations 4.11 and 4.14 since 50% of the new data plotted outside of the factor error bounds recommended in chapter 4.
- Several useful results in relation to parameter variability were found which were not possible to determine using the database analysis alone and required a new set of CU test results:

Adopting a different test procedure - identified by (a) or (b) - for reconstitution, saturation and consolidation of the Kaolin samples influenced the trends of c_u/σ'_{v0} and $\gamma_{50\ Power}$ with *OCR*. However, Λ is less sensitive to a change in procedure than Γ.

Up to 6%, 6% and 28% variation respectively in c_u, b and $\gamma_{50\ Power}$ can arise from the assumption of sample deformation shape (cylindrical versus parabolic).

The number of data points (n) used to derive the model parameters b and $\gamma_{50\ Power}$ is important since the values vary by 0% to +16% and -1% to +18% as n reduces from n>950 to 10<n<24 to n=3.

The factor errors of the strain parameter transformation models (Equation 4.14 for CIUC parameters with factor error of 1.75 and Equation 4.11 for CIUE parammeters with factor error of 1.70) are influenced predominantly by the inaccurate regression coefficients assumed to be representative for a specific material (particularly $\gamma_{50\ Power}$ at *OCR*=1). However, the variability due to test procedure and measurement uncertainty remains significant with calculated factor errors of up to 1.49 (CIUC) and 1.66 (CIUE) for tests performed on Kaolin samples over a range of *OCR*. Using this information, an engineer could make an informed decision about whether to use the parameter transformation model calibrated with the database and accepting the range in factor error that represents parameter variability of the various soils in the database, or to invest in more tests to achieve the estimated reduction in factor error for a particular soil.

- A limited assessment of soil constituents and destructuration effects on the model parameters of CIU tests (c_u/σ'_{v0}, $\gamma_{50\ Power}$, and b) can be made using the results presented in this chapter. Bothkennar has a higher silt content than Kaolin and the reconstituted Bothkennar samples were subjected to a lower preconsolidation stress range than the reconstituted Kaolin samples. With a higher initial void ratio before commencing undrained shear, the strain and strength parameters measured in compression demonstrated that Bothkennar in its reconstituted state is a stiffer and stronger material than Kaolin. The parameters measured for reconstituted

Bothkennar also surpass the upper bound of expected c_u / σ'_{v0} and lower bound of expected $\gamma_{50\ Power}$ according to Equations 4.22, 4.27 and 4.11. Reconsolidating the intact samples of Bothkennar to their estimated in-situ mean effective stress was achieved with a reduction in volume of 0.77% to 1.77% to give e_0=1.944, which exceeds the value of the material in its reconstituted state. As expected, the intact material is stronger when tested in CIUC but larger magnitudes of $\gamma_{50\ Power}$ were measured compared with the reconstituted material. The effect of reconstituting the material on the nonlinearity parameter *b* was to reduce the value from 0.730 to 0.476. Similarly, in chapter 3 it was observed that the parameter *b* reduced due to part destructuration in two pairs of CKUC and CKUE tests on intact Bothkennar samples reported by SERC (1989).

7. Footing settlement predictions with parameter variability assessment

Parts of this chapter have been included in the following publication:

Beesley M.E.W. and Vardanega P.J. 2020. "Variability of soil stress-strain non-linearity for use in MSD analyses using databases of triaxial tests on fine-grained soils". 10th International Symposium on Geotechnical Aspects of Underground Construction in Soft Ground (IS-Cambridge 2020). *Accepted*

7.1 Introduction

In the preceding chapters, a method was described to characterise the variability of soil stress strain in the moderate stress range ($0.2 \leq S \leq 0.8$). Results of the detailed statistical analysis of a database of reconstituted soils (RFG/TXCU-278) demonstrated that the variability of $\gamma_{50\ \mathrm{Power}}$, b and c_u/σ'_{v0} may be characterised by a large number of CU triaxial tests using empirical regression models ($\gamma_{50\ \mathrm{Power}}$ and c_u/σ'_{v0}) or average mean and standard deviation (b). In chapter 6, the results of new experimental data on reconstituted Kaolin and Bothkennar validated the range in behaviour observed in RFG/TXCU-278. In this chapter, a scenario analysis of undrained footing settlement examines the effect of the parameter ranges reported in chapter 4 on load-displacement predictions.

7.1.1 Research objectives

Further to the conclusions presented in chapters 4 and 6, the objectives of this chapter are:

(1) To investigate the effect of parameter variability on settlement design calculations

The scenario of a shallow footing serviceability design is used for demonstration.

7.2 Mobilisable Strength Design

The Mobilisable Strength Design (MSD) method has been the subject of considerable research in recent years. MSD is a performance-based design procedure for preventing undrained failure and excessive settlements of clay foundations. The method states that soil deformations induced by undrained loading are intrinsically linked to the proportion of mobilised undrained shear strength. To perform calculations, MSD relies on a representative soil stress-strain curve and assuming similarity with the load-displacement curve (Osman and Bolton 2005). For reliability- style calculations, a test curve needs to be replaced by a simple constitutive model of behaviour with the model parameters calibrated with large databases or characteristic distributions (cf. Vardanega and Bolton 2016a). MSD also relies on the accuracy of the modelled deformation field; kinematic plasticity-based solutions have been developed for retaining structures (Bolton and Powrie 1988, Bolton et al. 1990, Osman and Bolton 2004, Lam and Bolton 2011, Diakoumi and Powrie 2013, Lam et al. 2014, Bolton et al. 2014); deep foundations (Vardanega et al. 2012b, Vardanega 2015, Vardanega et al. 2018, Voyagaki et al. 2019); tunnels (Klar and Klein 2014); and shallow foundations (Osman and Bolton 2005, McMahon et al. 2014).

7.3 Design example

Taking the example from Osman and Bolton (2005) that was discussed in Vardanega & Bolton (2011a) for a rough shallow footing with a variable *b*-factor it can be shown that:

$$\left(\frac{\sigma_{mob}}{6.05\Delta\tau_{peak}}\right) = \frac{1}{2}\left(\frac{1.35w}{D\gamma_{50\ Power}}\right)^{b} \tag{7.1}$$

Where, w = undrained footing settlement; D = footing diameter, $\Delta\tau_{peak}$ = maximum change in average mobilised shear stress; σ_{mob} = vertical bearing pressure; and using a bearing capacity factor N_c=6.05 (Eason & Shield 1960).

Figure 7.1 shows field measurements from a pad loading test at Bothkennar reported by Jardine et al. (1995). Shown for comparison are predicted load-settlement curves using Equation 7.1 from 16 of the reported CKUC and CKUE triaxial tests performed on Bothkennar Clay (included in BTK/TXCU-

34 and reported by SERC 1989). Table 2 lists parameter values (Tests 1, 2 and 4) and mean values (by test mode) derived from the digitised test data (SERC 1989). An additional curve (Test 3) using mean b_{CKUE} demonstrates the use of Equations 4.29 and 4.31 to estimate variation of strain from a single triaxial compression test (Test 1) due to shear mode effects.

The predicted curves in Figure 7.1a indicate a range in nonlinearity of b = 0.307 to 1.304 for all test modes. This parameter range includes the effect of sampling depth, material variability, different sampling procedures, two strain rates, and measurement accuracy of two laboratories. Lowest b (0.298) was measured in CKUE mode after SHANSEP consolidation (to OCR=1, not shown in Figure 7- 1). A single CKUC test was undertaken on a specimen sampled from 1.61m – close to the characteristic depth (1.5m) used in the MSD case study of Osman and Bolton (2005). However, the b_{CKUC} value is very high (1.304) and Equation 7.1 predicts load-settlement that does not match field behaviour.

Figure 7- 1 shows that, using test results from sample depths of 2.62 to 9.02m below ground level and without accounting for maximum change in shear stress, the MSD-MSF method (Equation 7- 1) underpredicts w/D needed to mobilise stress ratio beneath the test pad. $\Delta\tau_{peak}$ has a noticeable effect on the prediction accuracy of Equation 7.1: predicted bearing pressures (Figure 7- 1b) for 0.8m embedment (Brinch Hansen 1970; following Osman & Bolton 2005) are a closer approximation of field measurements. A better prediction of nonlinear behaviour is achieved using the average strains of Tests 1 and 3 compared with Tests 1 and 2, with the result governed by $\Delta\tau_{peak}$. Note that the power-law model adopted here has been calibrated to a moderate bearing pressure range equal to $27 \leq \sigma_{mob} \leq 110$ kPa for the 2.2m square pad.

Using Equation 7.1, Figure 7- 2 demonstrates the range of strain expected for the data in RFG/TXCU-278 with varying values of b and average $\gamma_{50\ Power}$ values for OCR=1, 2 and 4 according to Equations 4.11, 4.14, 4.17, 4.20. Lower b values are associated with CIU and CKUE triaxial tests and higher $\gamma_{50\ Power}$ values are expected at a greater degree of overconsolidation. Using average $\gamma_{50\ Power\ CKUC}$, the envelope of normalised nonlinear behaviour is relatively narrow for CKUC test data on reconstituted soils compared with the other test modes. Larger envelopes of strain due to varying b, particularly where stress ratios exceed 0.5, are associated with higher $\gamma_{50\ Power}$ values.

Table 7- 1. Stress-strain model parameters for triaxial tests shown in Figure 7- 1 (mean values shown for depth range 2.62-9.02m, specimens from 'Laval' samplers only)

Parameter	$c_{u\ CKU}/\sigma'_{v0}$	$\gamma_{50\ Power\ CKU}$	$b_{\ CKU}$
Test 1	0.624	0.0036	0.814
Test 2	0.326	0.0070	0.453
Test 3	0.405	0.0189	0.490
(Test 4)*	(1.060)	(0.0235)	(1.304)
Mean CKUC n=8	0.506	0.0024	0.516
Mean CKUE n=6	0.242	0.0051	0.490

* Test 4 data not included in the mean values

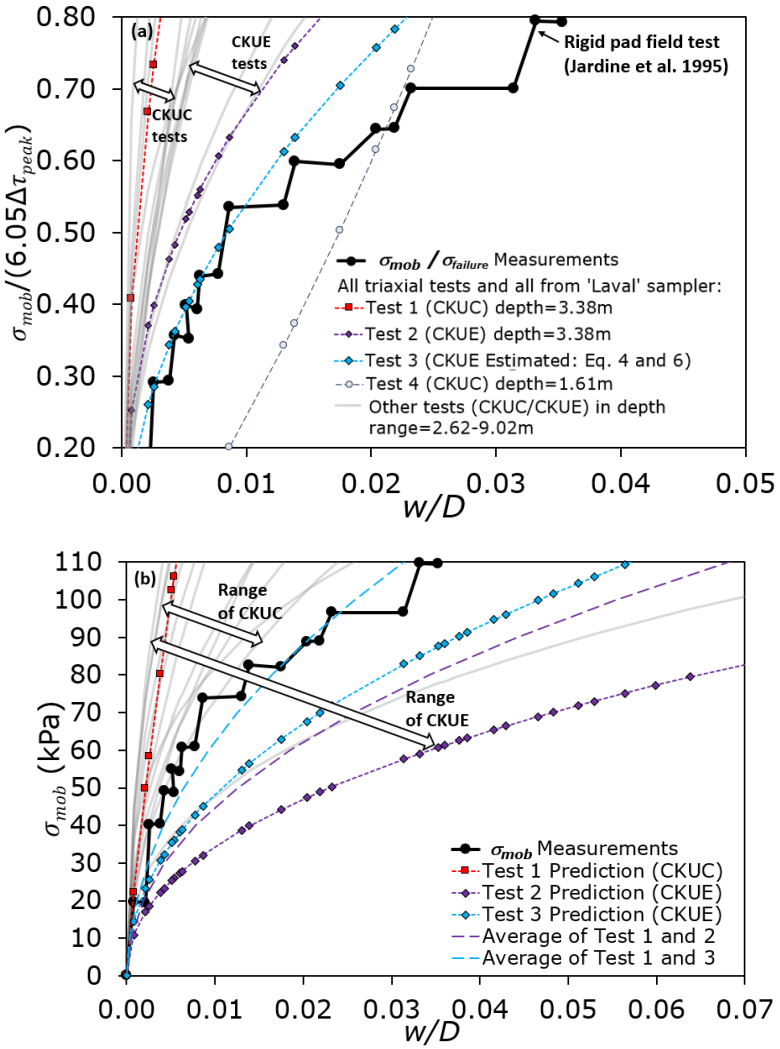

Figure 7- 1. Load-settlement predictions using MSD-MSF and data from SERC (1989) with comparison to field measurements (a) predicted stress ratio (b) predicted bearing pressure

Comparing Figures 7- 1a and 7- 2 and referring to Table 7- 1, the average values of $\gamma_{50\ \text{Power CKUC}}$ and b_{CKUC} for reconstituted soils are smaller than those of the reported tests on intact Bothkennar Clay for similar values of *OCR* (or *YSR*). However, in CKUE tests, parameters are similar; slightly higher values of b_{CKUE} define the narrower envelope shown in Figure 7- 1a compared with Figure 7- 2. The Bothkennar Clay was reconsolidated to in-situ stresses (σ'_{v0}=33-75kPa) (SERC 1989) lower than the consolidation stresses needed to achieve *OCR*=1 and 2 (minimum σ'_{v0}=142kPa) for the CKU tests in RFG/TXCU-278. Therefore, void ratio of the reconstituted soils would have been lower than the intact Bothkennar Clay. Notwithstanding this, the comparison of Figure 7-1a and Figure 7-2 shows that shear mode has a greater effect on the variation of stress-strain in reconstituted soils.

7.4 Design charts using MSD-MSF and implications for factors of safety

In Figure 7- 3, Equations 4.11, 4.14, 4.17 and 4.20 been used to plot ranges of strain per test mode according to the factor errors of the regression models i.e. the best estimate of $\gamma_{50\ \text{Power}}$ multiplied and divided by the factor error to find upper and lower values. In each plot, three curves are plotted with either a lower or upper bound *b*-value per test mode. Hence Figure 7- 3 demonstrates the strain envelope by increment of stress ratio that may reasonably be expected for a reconstituted soil according to the statistical analysis of RFG/TXCU-278. Each plot represents a reconstituted soil sample tested at the same *OCR* in four different triaxial test modes (CKUC, CKUE, CIUC and CIUE) to simulate a range of undrained load-displacement behaviour of a shallow footing (Equation 7.1).

The envelopes of stress-strain behaviour plotted in Figure 7- 3 demonstrate the variability of the undrained deformation parameters presented in this study. Although the parameter values may not be representative of intact materials, the plotted curves are useful for those wishing to assess the effects of *OCR* (less reported for studies on intact soils) and test mode. As demonstrated in chapter 6, the factor errors of the new transformation models (represented in Figure 7- 3 by the range of strain plotted per test mode) provide a useful indication of parameter variability related to the material variability of reconstituted soils (particularly at *OCR*=1) and the uncertain effects of different experimental procedures.

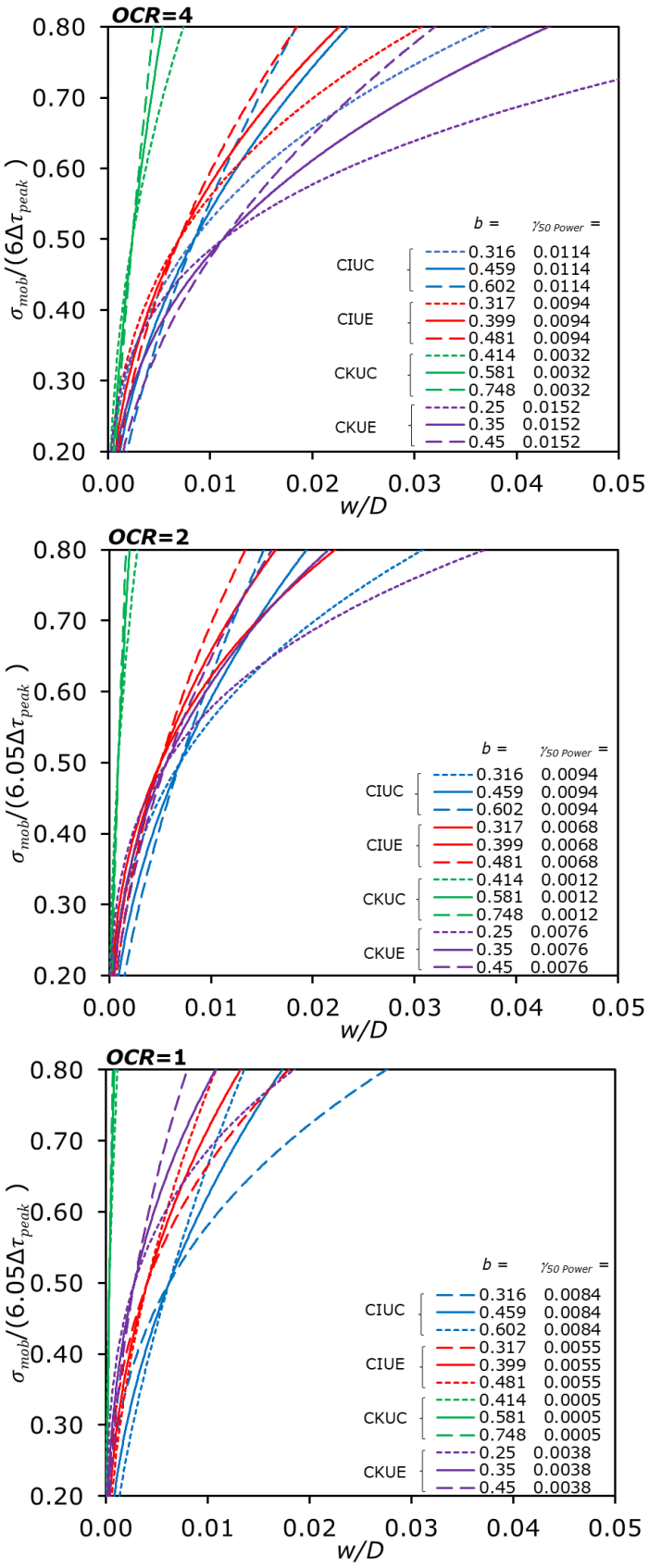

Figure 7- 2. Load-settlement predictions using MSD-MSF and data from RFG/TXCU-278: expected values by test mode of $\gamma_{50\ Power}$ for *OCR*=1, 2 and 4 using Equations 4.11, 4.14, 4.17, 4.20 and varying *b*-values using mean ± standard deviation

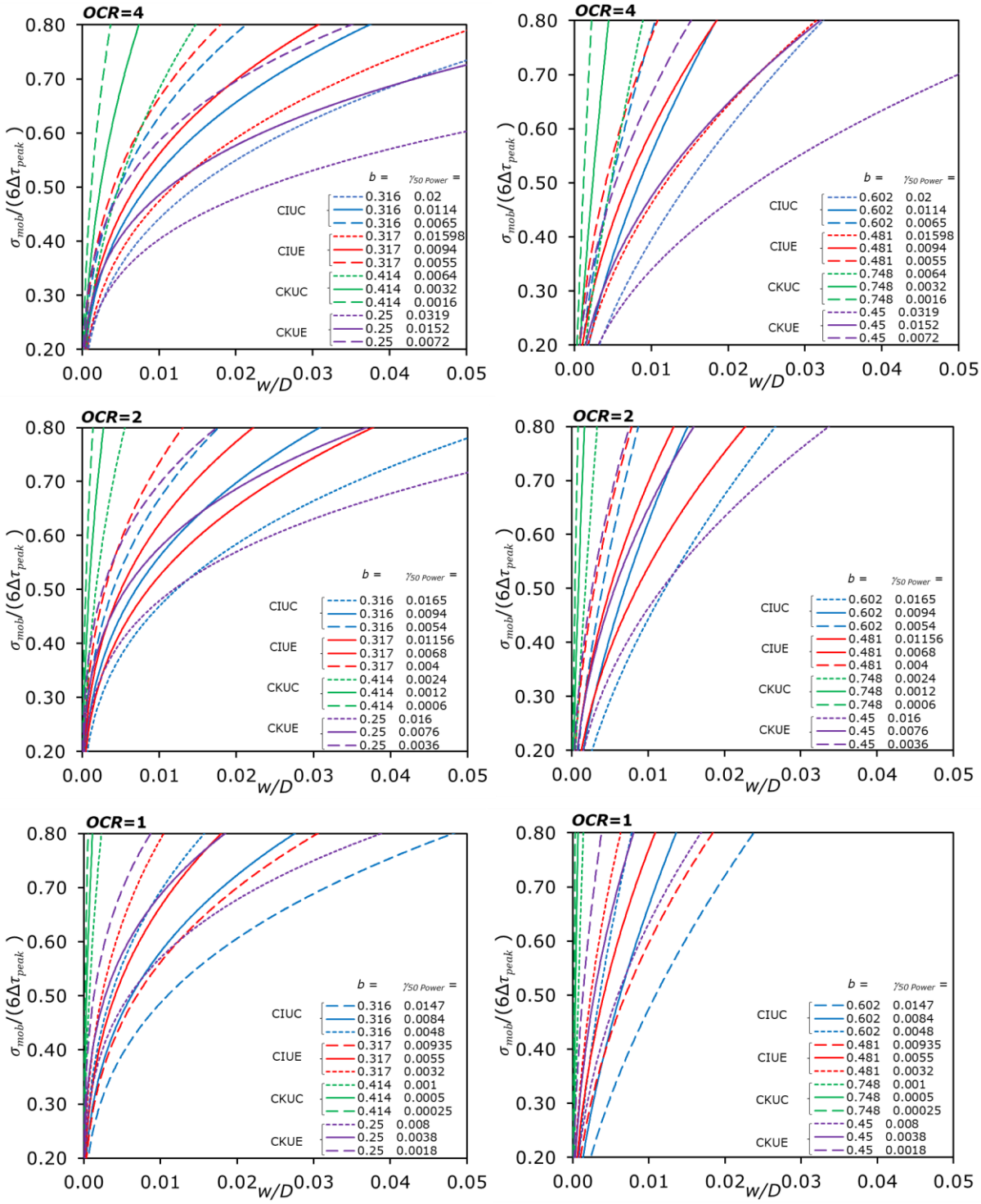

Figure 7- 3. Load-settlement predictions using MSD-MSF and data from RFG/TXCU-278: expected parameter ranges by test mode of $\gamma_{50\ Power}$ for *OCR*=1, 2 and 4 using the factor errors of Equations 4.11, 4.14, 4.17, 4.20 in combination with lower or upper *b*-values

In addition, Figure 7- 3 can be interpreted as a design chart to estimate the strains mobilised when reducing the factor of safety on undrained collapse from 5 to 1.25. The range of strain increases markedly below a factor of safety of about 3. When the scope of a ground investigation is limited or test data are considered unreliable, the necessary use of empirical estimates with a factor of safety of about 3 may be justified from these plots.

8. Conclusions and recommendations for future work

This study has demonstrated a method to characterise the variability of nonlinear soil behaviour at pre-failure loads in the moderate stress range ($0.2 \leq S \leq 0.8$). Two large databases of CU triaxial tests on reconstituted (RFG/TXCU-278) and intact (BTK/TXCU-34) soil samples have been compiled and categorised by consolidation mode (isotropic or K_0) and shear mode (triaxial compression or triaxial extension) to quantify the variability of undrained shear strength and shear strain. The "mobilisable strength" or "strength mobilisation" framework (e.g. Bolton 1993a) was adopted to investigate stress-strain behaviour at varying stress ratio, *S*. The concept of a mobilisation strain at *S*=0.5 (Vardanega and Bolton 2011a, Vardanega and Bolton 2016b) was also adopted to normalise the stress-strain data with respect to a reference stress and a reference strain. Three models based on exponential, power, and logarithmic functions were initially tested to evaluate the best fitting mathematical function to simulate nonlinear stress-strain, and the variability of the selected power law model parameters was then examined to establish insights into the causes of variable stress-strain behaviour. To do this, linear regression techniques were used to estimate association between the parameters (c_u/σ'_{v0}, $\gamma_{50\ Power}$, b) and other possible explanatory variables (*OCR*, strain rate, liquid limit, plastic limit). The same set of parameters, together with additional reference strains at *S*=0.3 and *S*=0.7, were then used to study the influence of shear-mode anisotropy on parameter variability.

The new database provides evidence that shear strain (like undrained shear strength) is sensitive to the consolidation and shear mode applied in the test. Analysis of RFG/TXCU-278 has shown that the reference strains mobilised at *S*=0.3, 0.5 and 0.7 vary with test mode and *OCR*. Strain anisotropy, expressed by the ratio K_γ, varies with stress ratio and with consolidation mode. Measured strains in K_0- consolidated samples of reconstituted soil are markedly more anisotropic in triaxial compression and extension than isotropically-consolidated samples. Strain anisotropy is also more variable in K_0-consolidated samples: at *S*=0.5, K_γ can vary by up to an order of magnitude for the same *OCR*. Despite this, for the materials included in the database, the mobilisation strain and measured strength obtained from a triaxial compression test can be used to predict the corresponding triaxial extension parameters to a reasonable accuracy (with a factor error of 1.3 to 2.2).

The parameters c_u/σ'_{v0} and $\gamma_{50\ Power}$ increase with *OCR* according to regression coefficients Λ and Γ, respectively, following the framework of Ladd et al. (1977) and Mayne (1980) for the variation of strength and a similar approach proposed for the variation of mobilised strain in reconstituted soils. New empirical transformation models have been developed to evaluate the variation and uncertainty of c_u/σ'_{v0}, $\gamma_{50\ Power}$, and b with a variety of statistical tools. In particular, this work has demonstrated the value of calculating factor errors of the parameters predicted using the transformation models since the factor errors provide a useful indication of parameter variability. The variation of parameters $\gamma_{50\ Power}$ and c_u/σ'_{v0} are described by empirical correlations with *OCR* and shear mode with factor errors of 1.15 to 2.1, dependent on test mode, quantifying the scatter of 80% of the data. Including strain rate in the regression model with *OCR* reduces the factor errors of c_u/σ'_{v0} but not $\gamma_{50\ Power}$. No reduction in error is achieved when liquid limit and plastic limit are added to the regression models. The nonlinearity parameter b does not correlate with any of the tested variables and the variability of b is therefore described using mean ± standard deviation per test mode.

The proposed empirical transformation models (Equations 4.11, 4.14, 4.22, 4.23, 4.26 and 4.27), based on the analysis of RFG/TXCU-278, have been validated with a new set of experiments on reconstituted Kaolin and Bothkennar Clay. Results of the CIU triaxial tests on Kaolin suggest that the factor errors of 1.75 for Equation 4.11 (CIUC) and 1.70 for Equation 4.14 (CIUE) are influenced predominantly by the inaccurate estimate of the regression coefficients for a specific soil (particularly $\gamma_{50\ Power}$ at OCR=1). However, using the observed coefficients for the new Kaolin tests still shows significant variability of $\gamma_{50\ Power}$ due to test procedure and measurement uncertainty - with factor errors of up to 1.49 (CIUC) and 1.66 (CIUE). Adopting one of two different test procedures (for the combined stages of reconstitution, saturation, and consolidation) influenced the magnitudes of c_u/σ'_{v0} and $\gamma_{50\ Power}$ and the fitted coefficients Λ and Γ in triaxial compression. Parameter sensitivity to procedure was not investigated in triaxial extension but $\gamma_{50\ Power}$ measurements were more variable and greater in magnitude than compression measurements. The likely reason for this is the compliance displacement caused during vacuum connection between the extension cap and sample. It would be valuable to repeat the extension

tests to assess the effect on parameter variability using either a modified version of the extension cap or an improved procedure that allows the connection to be made with less displacement.

Other useful results in relation to parameter variability were found from the experimental programme which were not possible to determine using the database analysis alone. Up to 6%, 6% and 28% variation respectively in c_u, b and $\gamma_{50\ Power}$ can arise from the assumption of sample deformation shape (cylindrical versus parabolic). These results confirm that the strength and deformation parameters, notably $\gamma_{50\ Power}$, are affected by measurement uncertainty in triaxial tests which may have a significant influence on design calculations. In addition, the number of data points (n) used to derive the model parameters b and $\gamma_{50\ Power}$ causes respective variations of up to +18% and +16% as n reduces from $n > 950$ to $10 < n < 24$ to $n = 3$. On average, b is more sensitive to n which explains to some degree the variability of b observed in RFG/TXCU-278 and its lack of correlation with variables other than $\gamma_{50\ Power}$.

RFG/TXCU-278 was compiled specifically from reconstituted soils tests to quantify the parameter variability associated with changes in soil composition, stress history, test mode, and the uncertain effects of different experimental procedures, excluding other important influences on the mechanical behaviour of natural soil samples (such as soil structure, ageing, cementation, weathering and sampling disturbance). For comparison, triaxial test results on intact Bothkennar Clay samples (BTK/TXCU-34) were compiled from a report by SERC (1989) to investigate the parameter variability associated more with the natural variations of a uniform deposit of soft clay and the uncertain effects of sampling. An examination of the test data of BTK/TXCU-34 suggests that the nonlinearity parameter b may be related to destructuration: lower values of b_{CKU} were measured when a sample tested using SHANSEP consolidation procedures was compared with a reconsolidated sample extracted from similar depths below ground level. Results of the experimental programme presented in chapter 6 identified a similar reduction in b_{CIUC} between a reconsolidated intact sample and reconstituted sample of Bothkennar Clay.

Comparisons with field measurements from a pad loading test at Bothkennar (reported by Jardine et al. 1995) were made with MSD-MSF predictions (Equation 7.1) to assess the sensitivity of predictions to the stress-strain model parameters of specimens sampled over a depth range of 1.6 to 9.2m

below ground level. Using Equation 7.1, the prediction of nonlinear behaviour in the moderate bearing pressure range of $27 \leq \sigma_{mob} \leq 110$ kPa is highly sensitive to $\Delta\tau_{peak}$ in addition to the deformation parameters b and $\gamma_{50\ \mathrm{Power}}$. Hence, to adopt the MSD-MSF method, ground characterisation of nonlinear undrained behaviour requires a reliable assessment of all three parameters. Any procedure based on strength mobilisation would require a reliable characterisation of the undrained shear strength and the nonlinear stress ratio-strain relationship.

Using the framework developed in this study, an engineer could make an informed decision about whether to use a parameter transformation model calibrated with a database and accept the range in factor error that represents parameter variability of the various soils in the database, or to invest in more tests to achieve the estimated reduction in factor error for a particular soil. For example, based on the limited tests presented in the experimental programme, comparing the use of Equation 4.11 with performing 7 triaxial tests to measure accurate regression coefficients for the Kaolin, achieves a reduction in factor error of 1.75 to 1.49. In this case, supposing an engineer would choose to use the parameter transformation models, a rational approach would be to use the best-estimate parameter values and to investigate the sensitivity of the predictions to the upper and lower bounds which are available from the calibrated factor errors. This approach has been demonstrated in Figure 7- 3, which shows the expected range in nonlinear stress ratio-strain due to the calculated variability in b and $\gamma_{50\ \mathrm{Power}}$.

When considering variability across large construction sites or regional ground models, the characterisation of a ground behaviour with one or two parameters is a useful tool. When preparing geotechnical ground investigation reports, plotting $\gamma_{50\ \mathrm{Power}}$ and b alongside other test parameters such as c_u and V_s presents an opportunity to understand the variability of nonlinear behaviour of the soils between the elastic region and plastic failure. The results presented for reconstituted soils and a single deposit of soft clay demonstrate the value in using test databases for geotechnical variability analysis which could be adopted for ground characterisation on large-scale infrastructure projects. It would be valuable to investigate the sensitivity of mobilisation strains and non-linearity to sampling disturbance and to natural geological variations in other deposits. To this end, the development of larger intact soil test databases is certainly warranted and the analytical framework developed in this thesis can be adopted.

However, using MSF, or indeed any other simple constitutive model to simulate stress-strain, has its drawbacks. It is highly unlikely that a “perfect” mathematical function exists to fit stress-strain test data. The evidence presented here confirms that the fitted model parameters are affected not only by the measurement uncertainty associated with the boundary conditions of the test (Table 3- 1), but also the test procedure and the number of data points (n) on the experimental curve. For consistency with the experimental results presented in this study, within the moderate stress range $10 < n < 24$ is recommended where possible. Moreover, when using the power law model, it should be acknowledged that the fitting error due to model approximation is stress ratio dependent. For a test in RFG/TXCU-278, the distribution of error shows that the power law model tends to underpredict stress ratio between 0.3 and 0.7 and to overpredict stress ratio towards S=0.2 and S=0.8. To quantify the error, model parameters fitted for each test can be used to predict stress-strain and all estimated values for multiple tests plotted against the measured values for the calculation of factor error about the 1 to 1 line. Using this technique, 80% of the secant modulus values in RFG/TXCU-278 are approximated by a power law to an accuracy of ·/1.15 to ·/1.3 dependent on test mode. Consequently, when using parameter transformation models (e.g., Equation 4.11) and a mean value of b (= 0.459) to estimate stress-strain behaviour (for all CIUC tests in RFG/TXCU-278), the factor error in the prediction of a parameter made using the model (1.75) is much lower than the factor error in the prediction of the stress-strain measurements (2.9) within the moderate stress range.

This points to an interesting new question: without model parameters to describe nonlinear stress-strain measurements, are reliability-based variability analyses of nonlinear soil behaviour from test data feasible? There is a trade-off to make between improving our understanding of parameter variability and simulating more nuanced soil behaviours. The approach taken in this work was to restrict the number of parameters (4) and tests (1) required for model calibration, thereby restricting the sources of parameter uncertainty per test to the measurement of consolidation stresses, measurement of undrained shear stresses and strains, data digitisation (owing to the nature of the database compilation), and model approximation. More complex, sophisticated constitutive models require a greater number of parameters and tests for model calibration which in turn present a greater challenge for variability characterisation. In the context of large infrastructure projects, simple but representative characteristic

parameters are highly desirable for examining the variability of soil behaviour on regional scales and assessing hazardous zones. The methods developed in this study explicitly acknowledge the inaccuracies of adopting simplified stress-strain models by quantifying model error. For nonlinear stress-strain parameters, the sources of parameter variability outlined in Figure 3- 1 should be extended to include Model in addition to Test and Material. Hence, the proposed methods enhance the application of reliability-based frameworks such as MSF, while the results of the database analysis and experimental investigation offer a critical appraisal and identify the following opportunities for further research:

- Triaxial extension test data are relatively scarcer than triaxial compression test data in the literature, particularly CKUE tests on reconstituted overconsolidated soils. The trends identified between mobilisation strain and *OCR* and with strain anisotropy need to be further investigated with additional CKUE tests.

- The parameter transformation models proposed in this study were based on the available information of the tests in the database. Variables such as void ratio and clay fraction were not available for all tests and could not be tested by regression analysis. As a result, it is possible that the calculated range of parameter variability for reconstituted soils could reduce if superior empirical correlations with other variables can be found.

- The extension load cap and connection procedure for conventional triaxial frames could be improved with less compliance affecting the initial stress-strain measurements. Parameter variability associated with alternative procedures for CIUE, CKUC and CKUE tests should be investigated.

- An assessment of parameter variability of CU triaxial tests due to procedures employed at different commercial laboratories would be useful information for geotechnical engineers.

- Parameter variability measured in intact soils was considered using only a single deposit (Bothkennar). To improve current knowledge on stress-strain variability in the moderate stress range, the intact test database needs to be expanded considerably. With this requires a reliable data storage and processing system and accurate parametric records, with a view to investigate the possible effects of

sampling disturbance and natural geological variability on the deformation parameters. A basic outline of the geotechnical test database design and management procedure has been described in chapter 3, however, the development of specialist platforms and data processing tools for large databases of hydrogeological, GIS, and test data is likely to be justified. The digital reporting of CIU and UU triaxial tests using AGS data should include stress-strain measurements in addition to strength measurements.

- Testing information such as assumed sample deformation shape, observed tilt, and effects of equipment on the measurements, should be reported as standard with any ground investigation test results so that information regarding measurement uncertainty is readily available.

References

Abdulhadi N., 2004. "*Triaxial testing on reconstituted London clay*". MSc thesis. Imperial College, London, UK.

Addenbrooke, T. I., Potts, D. M., and Puzrin, A. M., 1997. "The influence of pre-failure soil stiffness on the numerical analysis of tunnel construction". *Géotechnique,* 47(3): 693-712.

Allman, M. A. and Atkinson, J. H., 1992. "Mechanical properties of reconstituted Bothkennar soil". *Géotechnique*, 42, 2, 289-301.

ASTM, 2011. "*Standard Test Method for Consolidated Undrained Triaxial Compression Test for Cohesive Soils*". ASTM D4767-11, ASTM International, West Conshohocken, PA, United States, https://doi.org/10.1520/D4767-11.

Atkinson, J. H., 2000. "Non-linear soil stiffness in routine design". *Géotechnique,* 50(5): 487-508. https://doi.org/10.1680/geot.2000.50.5.487

Atkinson, J. H. and Little, J. A., 1988. "Undrained triaxial strength and stress–strain characteristics of a glacial till soil". *Canadian Geotechnical Journal*, 25(3): 428-439. https://doi.org/10.1139/t88-048

Baldi, G., Hight, D. W., and Thomas, G. E., 1988. "A reevaluation of conventional triaxial test methods". *Advanced Triaxial Testing of Soil and Rock*, ASTM STP 977, Robert T. Donaghe, Ronald C. Chaney, And Marshall L. Silver, Eds., American Society for Testing and Materials, Philadelphia: 219-263.

Banerjee, P. K. and Stipho, A. S., 1979. "An elasto-plastic model for undrained behaviour of heavily overconsolidated clays". *Int. J. Num. Met.,, in Geomech.*, 3(1): 97-103.

Banerjee, P. K., Stipho, A. S., and Yousif, N. B., 1985. "A theoretical and experimental investigation of the behaviour of anisotropically consolidated clay". *Developments in soil mechanics and foundation engineering* – 2, Stress-Strain modelling of soils, P. K. Banerjee and R. Butterfield (Eds), Elsevier Applied Science Publishers LTTD, Essex IG11 8JU, United Kingdom.

Basile, F., 2015. “Non-linear analysis of vertically loaded piled rafts”. *Computers and Geotechnics*, 63: 73-82, http://dx.doi.org/10.1016/j.compgeo.2014.08.011.

Beesley M.E.W., Vardanega P.J., Ibraim E., 2019. “Developing an Experimental Strategy to Investigate Stress-Strain Models Using Kaolin”. In: McCartney J., Hoyos L. (eds), *Recent Advancements on Expansive Soils, GeoMEast 2018*, Springer, Cham, Switzerland: 99-118.

Beesley, M.E.W. & Vardanega, P.J., 2019. “Parameter variability of undrained shear strength and strain using a database of reconstituted soil tests”. *Canadian Geotechnical Journal*. https://dx.doi.org/10.1139/cgj-2019-0424 (ahead of print)

Beesley M.E.W. and Vardanega P.J., 2020. “Variability of soil stress-strain non-linearity for use in MSD analyses using databases of triaxial tests on fine-grained soils”. *10th International Symposium on Geotechnical Aspects of Underground Construction in Soft Ground* (accepted)

Bialowas, G., 2017. “*Time and stress dependent mechanical properties of reconstituted chalk*”. PhD thesis, University of Bristol, Bristol, UK.

Bishop, A. W., and Henkel, D. J., 1962. “*The measurement of soil properties in the triaxial test*”. E. Arnold, London.

Bjerrum, L., 1972. “Embankments on soft ground”. In: *Proceedings of the Specialty Conference on Performance of earth and earth-supported structures*, Purdue University, Lafayette, Indiana, June 11-14, 1972, American Society of Civil Engineers.

Bjerrum, L., 1973. “Problems of soil mechanics and construction on soft clays”. State-of-the-art report. In: *Proceedings, 8th International Conference on Soil Mechanics and Foundation Engineering*, Moscow, 3: 111–159.

Bolton M. D., Springman S. M. and Sun H. W., 1990. “The behaviour of bridge abutments on clay”. *A.S.C.E. Conference on the Design and Performance of Retaining Structures*, P.C. Lambe and L. A. Hansen (Eds). ASCE, Reston, VA, USA, pp. 292-306.

Bolton, M., 1979. “*A guide to soil mechanics*”. M. D. Bolton and K. Bolton, Cambridge, 1991.

Bolton, M., 1993a. “What are partial factors for?” In: *The International Symposium on Limit State Design in Geotechnical Engineering*, 1993, Copenhagen, Denmark: 565-584.

Bolton, M., 1993b. “Mechanisms of ground deformation due to excavation in clay”. *Excavation in urban areas*, KIGForum 1993, Adachi (ed.).

Bolton, M.D. & Powrie, W., 1988. “Behaviour of diaphragm walls in clay prior to collapse”. *Géotechnique* 38(2): 167-189.

Bolton, M.D., Lam, S-Y., Vardanega, P.J., Ng, C.W.W. & Ma, X., 2014. “Ground movements due to deep excavations in Shanghai: Design charts”. *Frontiers of Structural and Civil Engineering*, 8(3): 201-236.

Braathen, N., 1966. “*Investigation of effects of disturbance on undrained shear strength of Boston Blue Clay*”. PhD thesis. Massachusetts Institute Of Technology, Cambridge, Massachusetts, USA.

Brinch Hansen, J., 1965. “Some stress-strain relationships for soils”. *Proc. 6th Int. Conf. Soil Mech.*, Montreal, 1: 231-234.

Brinch Hansen, J., 1970. “A revised and extended formula for bearing capacity”. *Danish Geotechnical Institute Bulletin*, 28: 5–11.

British Standards Institutsion (BSI), 1990. “*Methods of test for soils for civil engineering purposes*”. British standard BS1377. British Standards Institution, London, UK.

British Standards Institution (BSI), 1994. “*Code of practice for earth retaining structures*”. British standard BS8002, British Standards Institution, London, UK.

Brosse, A. M., Jardine, R. J., and Nishimura, S., 2017. “The undrained shear strength anisotropy of four Jurassic to Eocene stiff clays”. *Géotechnique*, 67(8): 653-671, https://doi.org/10.1680/jgeot.15.P.227.

Brosse, A., Jardine, R. J., Nishimura, S., 2016. “Undrained stiffness anisotropy from Hollow Cylinder experiments on four Eocene-to-Jurassic UK stiff clays”. *Canadian Geotechnical Journal,* 54(3): 313-332, https://doi.org/10.1139/cgj-2015-0320.

Burland, J. B., 1989. Ninth Laurits Bjerrum Memorial Lecture: “Small is beautiful” – the stiffness of soils at small strains. *Canadian Geotechnical Journal*, 26(4): 499-516.

Burland, J. B., 1990. “On the compressibility and shear strength of natural clays”. *Géotechnique*, 40(3): 329-378.

Casey, B., 2016. Closure to “Undrained Young’s Modulus of Fine-Grained Soils” by B. Casey, J. T. Germaine, N. O. Abdulhadi, N. S. Kontopoulos, and C. A. Jones. *Journal of Geotechnical and Geoenvironmental Engineering* 142(10): [07016024].

Casey, B., Germaine, J. T., Abdulhadi, N. O., Kontopoulos, N. S., and Jones, C. A., 2016. “Undrained Young’s Modulus of fine-grained soils”. *Journal of Geotechnical and Geoenvironmental Engineering*, 142(2): [04015070]. https://doi.org/10.1061/(ASCE)GT.1943-5606.0001382

Chandler, R. J., 1988. “The in-situ measurement of the undrained shear strength of clays using the field vane”. *Vane Shear Strength Testing in Soils: Field and Laboratory Studies*. ASTM STP 1014, A. F. Richards, Ed., American Society for Testing and Materials, Philadelphia, 1988: 13-44.

Chen, Y. and Kulhawy, F. H., 1993. “Undrained strength interrelationships among CIUC, UU, and UC tests”. *J. Geotech. Engrg*., ASCE, 119(11): 1732-1750.

Ching, J., and Phoon, K. -K., 2013. “Multivariate distribution for undrained shear strengths under various test procedures”. *Canadian Geotechnical Journal*, 50(3): 907-923. https://doi.org/10.1139/cgj-2013-0002

Ching, J., and Phoon, K. -K., 2014a. “Transformations and correlations among some clay parameters – the global database”. *Canadian Geotechnical Journal*, 51(6): 663-685.

Ching, J., and Phoon, K. -K. 2014b. Reply to the discussion by Mesri on "Multivariate distribution for undrained shear strengths under various test procedures". *Canadian Geotechnical Journal*, 51(3): 346–347. doi:10.1139/cgj-2014-0032.

Clayton, C.R., Hight, D.W. & Hopper, P.J., 1992. "Progressive destructuring of Bothkennar clay: implications for sampling and reconsolidation procedures". *Géotechnique*, 42(2): 219-239.

Clayton, C.R.I., Matthews, M.C., and Simons, N.E., 1995. "*Site investigation: a handbook for engineers*". Second Edition, Oxford, Blackwell Science, UK. Available online: [accessed 04/10/2019] http://www.geotechnique.info/

Conn, G. M., 1988. "*The two-way repeated loading of a silty clay*". PhD thesis. Loughborough University of Technology, Loughborough, UK.

Davies, M. C. R. and Newson, T. A., 1993. "A critical state constitutive model for anisotropic soil". *Proceedings of the Wroth Memorial Symposium*, 27-29 July 1992, G. T. Houlsby and A. N. Schofield (Eds), Predictive Soil Mechanics, Thomas Telford, London, 1993.

Diakoumi, M. & Powrie, W., 2013. "Mobilisable strength design for flexible embedded retaining walls". *Géotechnique*, 63(2): 95 –106.

Dumbleton, M. J. and West, G., 1996. "*The influence of the coarse fraction on the plastic properties of clay soils*". Road Research Laboratory, Ministry of Transport, Rrl Report No. 36. Available online: [accessed 10/10/2019] https://trl.co.uk/sites/default/files/LR036.pdf

Duncan, J. M., 1980. Comments on "Generalized stress-strain applications in geotechnical engineering". *Soil Stress Strain Applications*, Session 2: 333-335.

Duncan, J. M., and Buchignani, A. L., 1976. "*An engineering manual for settlement studies*". Univ. of California at Berkeley, Berkeley, CA.

Duncan, J. M., and Chang, C-Y., 1970. "Nonlinear analysis of stress and strain in soils". *Journal of the Soil Mechanics and Foundations Division*, Proc. of the ASCE: 1629-1652.

Escribano D.E., Nash, D.F.T. and Diambra, A., 2019. “Local and global volumetric strain comparison in sand specimens subjected to drained cyclic and monotonic triaxial compression loading”. *Geotechnical Testing Journal*, 42(4), [54]. https://doi.org/10.1520/GTJ20170054.

Fayad, P. H., 1986. “*Aspects of the volumetric and undrained behavior of Boston Blue Clay*”. MSc thesis. Massachusetts Institute Of Technology, Cambridge, Massachusetts, USA.

Gasparre, A., 2005. “*Advanced laboratory characterization of London Clay*”. PhD thesis, Imperial College, London, UK.

Gens, A., 1982. “*Stress-strain and strength characteristics of a low plasticity clay*”. PhD thesis, Imperial College, London, UK.

Georgiannou, V. N., Coop, M. R., Altuhafi, F. N., and Lefas, D. I., 2018. “Compression and strength characteristics of two silts of low and high plasticity”. *J. Geotech. Geoenviron. Eng.*, ASCE, 144(7): 04018041. DOI: 10.1061/(ASCE)GT.1943-5606.0001891.

Germaine, J. T. and Ladd, C. C., 1988. “Triaxial testing of saturated cohesive soils”. *Advanced Triaxial Testing of Soil and Rock*, ASTM STP 977, Robert T. Donaghe, Ronald C. Chaney, And Marshall L. Silver, Eds., American Society for Testing and Materials, Philadelphia: 421-459.

Graham, J., Wood, D. M., Yin, J. H. and Azizi, F., 1989. “Prediction of triaxial stress strain behaviour of Winnipeg clay using an anisotropic elastic plastic model.” *Proc. 42nd Canadian Geotech Conference*, Winnipeg MB: 280-288.

Grimstad, G., Andresen, L., and Jostad, H. P., 2011. “NGI-ADP: Anisotropic shear strength model for clay”. *International Journal for Numerical and Analytical Methods in Geomechanics*, 36: 483–497.

Hardin, B.O.,and Drnevich, V. P., 1972. “Shear modulus and damping in soils: Design equations and curves.” *J. Soil Mech. and Found. Div.*, 98(7), 667–691.

Hawkins, A.B., Larnach, W.J., Lloyd, I.M. and Nash, D.F.T., 1989. “Selecting the location and the initial investigation of the SRC soft clay test bed site”. *Q.J.Engng Geol*., 22(4): 281-316.

Head, K.H., 1982. "*Manual of Soil Laboratory Testing: Volume 2: Permeability, Shear Strength and Compressibility Tests*". Pentech Press Limited, Plymouth, Devon.

Hight, D. W, Boese, R., Butcher, A. P., Clayton, C. R. I., and Smith, P. R., 1992b. "Disturbance of the Bothkennar clay prior to laboratory testing". *Géotechnique,* 42(2), 199-217.

Hight, D. W., Bond, A J., and Legge, J. D., 1992a. "Characterization of the Bothkennar clay: an overview". *Géotechnique,* 42(2), 303-347.

Hight, D. W., Gens, A., and Jardine, R. J., 1985. "Evaluation of geotechnical parameters from triaxial tests on offshore clay". In: *Offshore Site Investigation: Advances in Underwater Technology and Offshore Engineering*, Springer, Dordrecht, Netherlands. vol 3: 253-268.

Hight, D. W., McMillan, F., Powell, J. J. M., Jardine, R. J., Allenou, C. P., 2003. "Some characteristics of London Clay". *Characterisation and Engineering Properties of Natural Soils*, Tan et al.(eds.), Swets & Zeitlinger, Lisse: 851-907.

Hollomon, J.H., 1945. "Tensile Deformation". *Transactions of the Metallurgical Society of AIME,* 162: 268-290.

Hong, Z. -S., Yin, J., and Cui, Y. -J., 2010. "Compression behaviour of reconstituted soils at high initial water contents". *Géotechnique,* 60(9): 691-700.

ISO, 2018. "*Geotechnical investigation and testing — Laboratory testing of soil — Part 9: Consolidated triaxial compression tests on water saturated soils*". BS EN ISO 17892-9:2018, ISO/TC 182 Geotechnics.

Jamiolkowski, M., Lancellotta, R., Pasqualini, E., Marchetti, S., and Nova, R., 1979. "Design parameters for soft clays." *7th European Conf. on Soil Mechanics and Foundation Engineering*, British Geotechnical Society, London: 27–57.

Jamiolkowski, M., Ladd, C. C., Germaine, J. T. and Lancelotta, R., 1985. "New developments in field and laboratory testing of soils". *Proceedings of the ISSMGE,* A.A. Balkema, San Francisco, California, 1: 57-153.

Jardine, R. J., Potts, D. M., Fourie, A. B. and Burland, J. B., 1986. "Studies of the influence of non-linear stress–strain characteristics in soil–structure interaction". *Géotechnique*, 36(3): 377-396. https://doi.org/10.1680/geot.1986.36.3.377

Jardine, R.J., Lehane, B.M., Smith, P.R., and Gildea, P.A., 1995. "Vertical loading experiments on rigid pad foundations at Bothkennar". *Géotechnique*, 45(4): 573-597.

Jardine, R. J., Symes, M. and Burland, J.B., 1984. "The measurement of soil stiffness in the triaxial apparatus". *Géotechnique* 34(3): 323-340.

Jovičić, V., and Coop, M. R., 1998. "The measurement of stiffness anisotropy in clays with bender element tests in the triaxial apparatus". *Geotechnical Testing Journal*, 21(1): 3-10.

Kamal, R. H., 2012. "*Experimental study of the geotechnical properties of UK mudrocks*". PhD thesis. Imperial College, London, UK.

Kamei, T. and Nakase, A., 1989. "Undrained shear strength anisotropy of K0-overconsolidated cohesive soils". *Soils and Foundations*, 29(3): 145-151.

Klar, A. and Klein, B., 2014. "Energy-based volume loss prediction for tunnel face advancement in clays". *Géotechnique*, 64(10): 776-786.

Konder, R. L., 1963. "Hyperbolic stress-strain response: Cohesive soils." *J. Soil Mech. and Found. Div.*, 89(1), 115–143.

Kootahi, K. and Mayne, P. W., 2017. "Closure to 'Index Test Method for Estimating the Effective Preconsolidation Stress in Clay Deposits' by Karim Kootahi and Paul W. Mayne". *Journal of Geotechnical and Geoenvironmental Engineering*, 143(10): [07017031]. https://doi.org/10.1061/(ASCE)GT.1943-5606.0001765

Koutsoftas, D. C., Karina, K., and Hashash, Y. M. A., 2017. "Discussion of 'Index Test Method for Estimating the Effective Preconsolidation Stress in Clay Deposits' by Karim Kootahi and Paul W. Mayne". *Journal of Geotechnical and Geoenvironmental Engineering*, 143(10): [07017031].

Krabbenhøft, K., Galindo-Torres, S. A., Zhang, X. and Krabbenhøft, J. 2019. AUS: Anisotopic undrained shear strength model for clays. *International Journal for Numerical and Analytical Methods in Geotechnics*, https://doi.org/10.1002/nag.2990. (Ahead of print).

Kulhawy, F.H. & Mayne, P.W. 1990. "*Manual on estimating soil properties for foundation design*". Report No. EL-6800, Electric Power Research Institute, Palo Alto, CA, USA.

Kvalseth, T., 1983. "Note on the R^2 measure of goodness of fit for nonlinear models". *Bulletin of the Psychonomic Society*, 21(1): 79-80.

Ladd, C. C., 1991. "Stability evaluation during staged construction". *Journal of Geotechnical Engineering*, 117(4): 540-615.

Ladd, C. C., Foott, R., Ishihara, K., Schlosser, F., and Poulos, H., 1977. "Stress-deformation and strength characteristics". In: *Proceedings of the 9th International Conference on Soil Mechanics and Foundation Engineering*, (Publications Sub-Committee of the Organizing Committee for the Ninth International Conference on Soil Mechanics and Foundation Engineering, Eds.) Japanese Society of Soil Mechanics and Foundation Engineering, Tokyo, Japan, 2: 421–494.

Ladd, C. C. and Bailey, W. A., 1964. Discussion to "The behaviour of saturated clays during sampling and testing" by Skempton, A. W. and Sowa, V. A., *Géotechnique*, 14(4): 353-358.

Lade, P.V., 2016. "*Triaxial testing of soils*". Hoboken, John Wiley & Sons Inc., 2016.

Lam, S.Y. & Bolton, M.D., 2011. "Energy conservation as a principle underlying mobilizable strength design for deep excavations". *Journal of Geotechnical and Geoenvironmental Engineering*, 137(11): 1062-1074.

Lam, S.Y., Haigh, S.K. & Bolton, M.D., 2014. "Understanding ground deformation mechanisms for multi-propped excavation in soft clay". *Soils and Foundations*, 54(3): 296-312.

Lam, W-K. and Tatsuoka, F., 1988. "Triaxial compressive and extension strength of sand affected by strength anisotropy and sample slenderness". *Advanced Triaxial Testing of Soil and Rock*,

ASTM STP 977, Robert T. Donaghe, Ronald C. Chaney, And Marshall L. Silver, Eds., American Society for Testing and Materials, Philadelphia: 655-666.

Lambe, T. W., 1973. "Predictions in soil engineering". *Géotechnique*, 23(2): 149-202.

Liu, Y., 2004. "*The stress-strain behavior of kaolinite clay in triaxial compression and extension tests at elevated pressures*". PhD thesis, University of Delaware, Newark, Delaware, USA.

Loudon, P. A., 1967. "*Some deformation characteristics of kaolin*". PhD thesis, University of Cambridge, Cambridge, UK.

Low, H. E., Landon Maynard, M., Randolph, M. F., and DeGroot, D. J., 2011. "Geotechnical characterisation and engineering properties of Burswood clay". *Géotechnique*, 61(7): 575–591. doi:10.1680/geot.9.P.035.

Malandraki V. and Toll D.G., 1994. "Yielding of a weakly bonded artificial soil". *Proceedings of the International Symposium on Pre-Failure Deformation Characteristics of Geomaterials*, Hokkaido, Japan Shibuya S., Mitachi T. and Miura S. (eds), Balkema, Rotterdam, Vol. 1: 315–20.

Malvern Instruments, 2019. Mastersizer 3000. Available online: [accessed 10/10/2019] https://www.malvernpanalytical.com/en/products/product-range/mastersizer-range/mastersizer3000?creative=311633610439&keyword=%2Bmastersizer%20%2B3000&matchtype=b&network=g&device=c&gclid=EAIaIQobChMI_Mfz3fub5QIVksjeCh3Zmwz_EAAYASAAEgKvj_D_BwE

Matlock, H., 1970. "Correlations for design of laterally loaded piles in soft clay". In: *Offshore Technology Conference*, Houston, Texas, USA. OTC 1204.

Mayne, P. W. and Holtz, R. D., 1985. "Effect of principal stress rotation on clay strength". In: *Proceedings of the 11th International Conference on Soil Mechanics and Foundation Engineering, San Francisco/ 12-16 August 1985*, (Publications Committee of XI ICSMFE, Eds.) A.A. Balkema, Rotterdam, Netherlands, vol. 2, pp. 579-582.

Mayne, P.W., 1980. “Cam-Clay predictions of undrained strength”. J. Geotech. Eng. Div., ASCE, 106: 1219-1242.

Mayne, P.W., 1985. “Stress anisotropy effects on clay strength”. *Journal of the Geotechnical Engineering Division*, 111(3): 356-366.

Mayne, P. W., 1988. “Determining OCR in clays from laboratory strength”. *Journal of Geotechnical Engineering*, 114(1): 76-92.

Mayne, P.W., Coop, M.R., Springman, S., Huang, A-B. & Zornberg, J., 2009. “State-of-the-Art Paper SOA-1. Geo-Material Behaviour and Testing”. In (Hamza, M. et al. Eds.) *Proceedings of the 17th International Conference on Soil Mechanics & Geotechnical Engineering*, Millpress/IOS Press, Rotterdam, The Netherlands, 4: 2777-2872.

McMahon, B.T., Haigh, S.K. & Bolton, M.D., 2014. “Bearing capacity and settlement of circular shallow foundations using a nonlinear constitutive relationship”. *Canadian Geotechnical Journal*, 51(9): 995-1003.

Mesri, G., 1989. “A reevaluation of $s_{u,mob} = 0.22\ \sigma'_p$ using laboratory shear tests”. *Canadian Geotechnical Journal*, 26(1): 162-164.

Miura, N., Murata, H. and Yasufuku, N., 1984. “Stress-strain characteristics of sand in a particle-crushing region”. *Soils and Foundations*, 24(1): 77-89.

Montgomery, D. C. and Runger, G. C., 2003. “*Applied statistics and probability for engineers*”. John Wiley and Sons, Inc.

Muir Wood, D., 1990. “*Soil behaviour and critical state soil mechanics*”. Cambridge University Press, Cambridge, UK.

Muir Wood, D., 2017. “Modelling and testing”. *Proceedings of the 19th International Conference on Soil Mechanics and Geotechnical Engineering*, Seoul 2017.

Nakase, A. and Kamei, T., 1983. “Undrained shear strength anisotropy of normally consolidated sohesive soils”. *Soils and Foundations*, 23(1): 91-101.

Nash, D. F. T., Powell, J. J. M., and Lloyd, I. M., 1992a. “Initial investigations of the soft clay test site at Bothkennar”. *Géotechnique*, 42(2): 163-181.

Nash, D. F. T., Sills, G. C., and Davison, L. R., 1992b. “One-dimensional consolidation testing of soft clay from Bothkennar”. *Géotechnique*, 42(2): 241-256.

O’Brien, A. S., Forbes-King, C. J., Gildea, P. A., and Sharp, P., 1992. “In situ stress and stiffness at seven overconsolidated clay and weak rock site – Part 2”. *Ground Engineering*, 25(7).

Ohta, H. and Nishihara, A., 1985. “Anisotropy of undrained shear strength and clays under axi-symmetric loading conditions”. *Soils and Foundations*, 25(2): 73-86.

Osman, A. S. and Bolton, M. D., 2005. “Simple plasticity-based prediction of the undrained settlement of shallow circular foundations on clay”. *Géotechnique*, 55(6): 435-447, https://doi.org/10.1680/geot.2005.55.6.435.

Osman, A.S. & Bolton, M.D., 2004. “A new design method for retaining walls in clay”. *Canadian Geotechnical Journal*, 41(3): 451-466.

Osman, A.S. & Bolton, M.D., 2006. “Ground Movement Predictions for Braced Excavations in Undrained Clay”. *Journal of Geotechnical and Geoenvironmental Engineering*, 132(4): 465-477.

Parry, R. H. G., 1956. “*Strength and deformation of clay*”. PhD thesis. Imperial College, London, UK.

Parry, R. H. G., 1960. “Triaxial compression and extension tests on remoulded saturated clay”. *Géotechnique*, 10(4): 166-180. https://doi.org/10.1680/geot.1960.10.4.166

Parry, R. H. G. and Nadarajah, V., 1974. “Observations on laboratory prepared, lightly overconsolidated specimens of kaolin”. *Géotechnique*, 24(3): 345-357. https://doi.org/10.1680/geot.1974.24.3.345

Paul, M. A., Peacock, J. D. and Wood, B. F., 1992. “The engineering geology of the Carse clay at the National Soft Clay Research Site, Bothkennar”. *Géotechnique*, 42(2): 183-198.

Pennington, D. S., Nash, D. F. T., and Lings, M. L., 1997. “Anisotropy of G0 shear stiffness in Gault Clay”. *Géotechnique*, 47(3): 391-398.

Pennington, D.S., 1999. “*The anisotropic small strain stiffness of Cambridge Gault clay*”. PhD thesis, University of Bristol, Bristol, UK.

Phoon, K-K. & Kulhawy, F.H. 1999a. Characterization of geootechnical variability. Canadian Geotechnical Journal 36(4): 612-624.

Phoon, K-K. & Kulhawy, F.H. 1999b. Evaluation of geotechnical property variability. Canadian Geotechnical Journal 36(4): 625-639.

Potts, D., Axelsson, K., Grande, L., Schweiger, H., Long, M., Sagaseta, C., Dolezalova, M., Anagnostou, G., Laue, J., Herle, I., and Battelino, D., 2002. “*Guidelines for the use of advanced numerical analysis*”. David Potts, Kennet Axelsson, Lars Grande, Helmut Schweiger and Michael Long (Eds), Thomas Telford Publishing, Thomas Telford Ltd, 1 Heron Quay, London E14 4JD.

Powrie, W., Pantelidou, H., and Stallebrass, S. E., 1998. “Soil stiffness in stress paths relevant to diaphragm walls in clay”. *Géotechnique*, 48(4): 483-494.

Puzrin, A. M. and Burland, J. B., 1996. “A logarithmic stress–strain function for rocks and soils”. *Géotechnique*, 46(1): 157-164.

Ratananikom, W., Yimsiri, S., and Likitlersuang, S., 2015. “Undrained shear strength of very soft to medium stiff Bangkok clay from various laboratory tests”. *Geotechnical Engineering: Journal of the SEAGS & AGSSEA*, 46(1): 64-74.

Roscoe, K. H. and Burland, J. B., 1968. “*On the generalized stress-strain behaviour of wet clays*.” Engineering Plasticity, Cambridge University press.

Sachan, A. and Penumadu, D., 2007. “Effect of microfabric on shear behavior of kaolin clay”. *Journal of Geotechnical and Geoenvironmental Engineering*, 133(3): 306-318.

Santucci de Magistris, F., Koseki, J., Amaya, M., Hamaya, S., Sato, T., and Tatsuoka, F., 1999. "A triaxial testing system to evaluate stress-strain behavior of soils for wide range of strain and strain rate," *Geotechnical Testing Journal*, GTJODJ, 22: 44–60.

Sarsby, R. W., Kalteziotis, N., and Haddad, E. H., 1980. "Bedding error in triaxial tests on granular media". *Géotechnique*, 30(3): 302-309, https://doi.org/10.1680/geot.198 0.30.3.302

Schofield, A.N., and Wroth, C.P., 1968. "*Critical state soil mechanics*". McGraw-Hill, London.

SERC, 1989. "Results of in situ and laboratory tests". Bothkennar 1989 Site Investigation Volume 2, *Internal Report.*

Sheahan, T. C., 1991. "*An experimental study of the time-dependent undrained shear behavior of resedimented clay using automated stress path triaxial equipment*". PhD thesis. Massachusetts Institute of Technology, Cambridge, Massachusetts, USA.

Sheahan, T.C., Ladd, C.C. & Germaine, J.T., 1996. "Rate-dependent undrained shear behavior of saturated clay". *Journal of Geotechnical Engineering*, 122(2): 99-108.

Sheng, D., Westerberg, B., Mattson, H. and Axelsson, K., 1997. "Numerical analysis of stress-strain inhomogeneities in a triaxial test specimen". In: *Proceedings of the Fourteenth International Conference on Soil Mechanics and Foundation Engineering*, Hamburg, Balkema Publishers, A.A. / Taylor & Francis: 403-407.

Silvestri, F., 2001. "Looking for objective criteria in the interpretation of laboratory stress-strain tests". *Pre-failure deformation characteristics of geomaterials*. Jamiolkowski, Lancellotta & Lo Presti (eds). Swets and Zeitlinger, Lisse, ISBN 9058090752.

Simpson, B., 2001. "Engineering needs". In: *Proceedings of the 2nd Int. Symp. On Pre-failure Deformation Characteristics of Geomaterials*, IS Torino 1999, M. Jamiolkowski, R. Lancellotta and D. Lo Presti (Eds), Swets & Zeitlinger, Lisse, ISBN 90 5809 075 2.

Skempton, A. W., 1951. "The bearing capacity of clays". *Building Research Congress*, London, 1: 180-189.

Skempton, A. W., 1954b. “The Pore-Pressure Coefficients A and B”. *Géotechnique*, 4(4): 143-147.

Skempton, A. W., 1954. “Discussion: sensitivity of clays and the c/p ratio in normally consolidated clays”. *Proc. Am. Soc. Civil Eng*. Separate 478: 19–22.

Skempton, A. W., 1957. “Discussion: further data on the c/p ratio in normally consolidated clays”. *Proc. Inst. Civil Eng*. 7: 305–307.

Smith, P. R., Jardine, R. J. and Hight, D. W., 1992. “The yielding of Bothkennar clay”. *Géotechnique*, 42(2): 257-274.

Stallebrass, S. E. and Taylor, R. N., 1997. “The development and evaluation of a constitutive model for the prediction of ground movements in overconsolidated clay”. *Géotechnique*, 47(2): 235-253.

Sukolrat, J., 2007. “*Structure and destructuration of Bothkennar Clay*”. PhD thesis, University of Bristol, Bristol, UK.

Tatsuoka, F., 1988. “Some recent developments in triaxial testing systems for cohesionless soils”. *Advanced Triaxial Testing of Soil and Rock*, ASTM STP 977, Robert T. Donaghe, Ronald C. Chaney, And Marshall L. Silver, Eds., American Society for Testing and Materials, Philadelphia: 7-67.

Toll, D. G., 1993. A Computer Control System for stress Path Triaxial Testing. In: *Developments in Civil Construction Engineering Computing*. (Ed: Topping, B. V.) Civil-Comp press, Edinburgh: 107-117.

Valls-Marquez, M., 2009. “*Evaluating the capabilities of some constitutive models in reproducing the experimental behaviour of stiff clay subjected to tunnelling stress paths*”. PhD thesis. University of Birmingham, Birmingham, UK.

Vardanega, P. J. and Bolton, M. D., 2011. “Strength mobilization in clays and silts”. *Canadian Geotechnical Journal*, 48(10): 1485–1503, https://doi.org/10.1139/t11-052 and *Corrigendum*, 49(5), 631, https://doi.org/10.1139/t2012-023.

Vardanega, P. J. and Bolton, M., 2016b. “Discussion of ‘Undrained Young’s Modulus of fine-grained soils’ by B. Casey, J. T. Germaine, N. O. Abdulhadi, N. S. Kontopoulos, and C. A. Jones”. *Journal of Geotechnical and Geoenvironmental Engineering*, 142(10): [07016023]. https://doi.org/10.1061/(ASCE)GT.1943-5606.0001571

Vardanega, P. J. and Bolton, M., 2013. “Stiffness of clays and silts: normalizing shear modulus and shear strain”. *Journal of Geotechnical and Geoenvironmental Engineering*, 139(9): 1575-1589.

Vardanega, P. J., Lau, B. H., Lam, S. Y., Haigh, S. K., Madabhushi, S. P. G., and Bolton, M. D., 2012. “Laboratory measurement of strength mobilisation in kaolin: link to stress history”. *Géotechnique Letters*, 2(1): 9–15. https://doi.org/10.1680/geolett.12.00003

Vardanega, P. J., Lau, B. H., Lam, S. Y., Haigh, S. K., Madabhushi, S. P. G., Bolton, M. D., and Mayne, P. W. 2013. “Discussion to ‘Laboratory measurement of strength mobilisation in kaolin: link to stress history’ ”. *Géotechnique Letters*, 3: 16–17. https://doi.org/10.1680/geolett.13.00005

Vardanega, P.J. & Bolton, M.D., 2016a. “Design of Geostructural Systems”. *ASCE-ASME Journal of Risk and Uncertainty in Engineering Systems*. Part A: Civil Engineering 2(1): [04015017].

Vardanega, P.J., 2015. “Sensitivity of simplified pile settlement calculations to parameter variation in stiff clay”. In (Winter, M. G., et al. eds.) *Geotechnical Engineering for Infra-structure and Development: Proceedings XVI European Conference on Soil Mechanics and Geotechnical Engineering*. ICE Publishing, London, United Kingdom, vol. 7, 3777-3782

Vardanega, P.J., Williamson, M.G. & Bolton, M.D., 2012b. “Bored pile design in stiff clay II: mechanisms and uncertainty”. *Proceedings of the Institution of Civil Engineers-Geotechnical Engineering*, 165(4): 233-246, Corrigendum, 166(5): 518.

Voyagaki, E., Crispin, J., Gilder, C., Nowak, P., O’Riordan, N., Patel, D. and Vardanega, P.J., 2019. “Analytical Approaches to Predict Pile Settlement in London Clay”. In: El-Naggar H. et al. (eds) *Sustainability Issues for the Deep Foundations, GeoMEast 2018*, Springer, Cham, Switzerland: 162-180.

Waters, T. J. and Vardanega, P. J., 2009. “Re-examination of the coefficient of determination (r2) using road materials engineering case studies”. *Road and Transport Research*, 18(3), 3-12.

Won, J. Y., 2013. “Anisotropic strength ratio and plasticity index of natural clays”. In: *Proceedings of the 18th International Conference on Soil Mechanics and Geotechnical Engineering*, Paris 2013: 445-448.

Wroth, C. P. and Loudon, P. A., 1967. “The correlation of strains within a family of triaxial tests on overconsolidated samples of kaolin”. *Proc. Geotech. Conf.*, Oslo, 1: 159-163.

Yimsiri, S. 2001. “*Pre-deformation characteristics of soils: anisotropy and soil fabric*”. PhD thesis, University of Cambridge, Cambridge, UK.

Zhang, Y. and Anderson, K. H., 2017. “Scaling of lateral pile p-y response in clay from laboratory stress-strain curves”. *Marine Structures*, 53: 124-135. https://doi.org/10.1016/j.marstruc.2017.02.002

Zhu, J.-G. and Yin, J.-H., 2000. “Strain-rate-dependent stress-strain behavior of overconsolidated Hong Kong marine clay”. *Canadian Geotechnical Journal*, 37(6): 1272-1282. https://doi.org/10.1139/t00-054

Appendices

Appendix 4-1

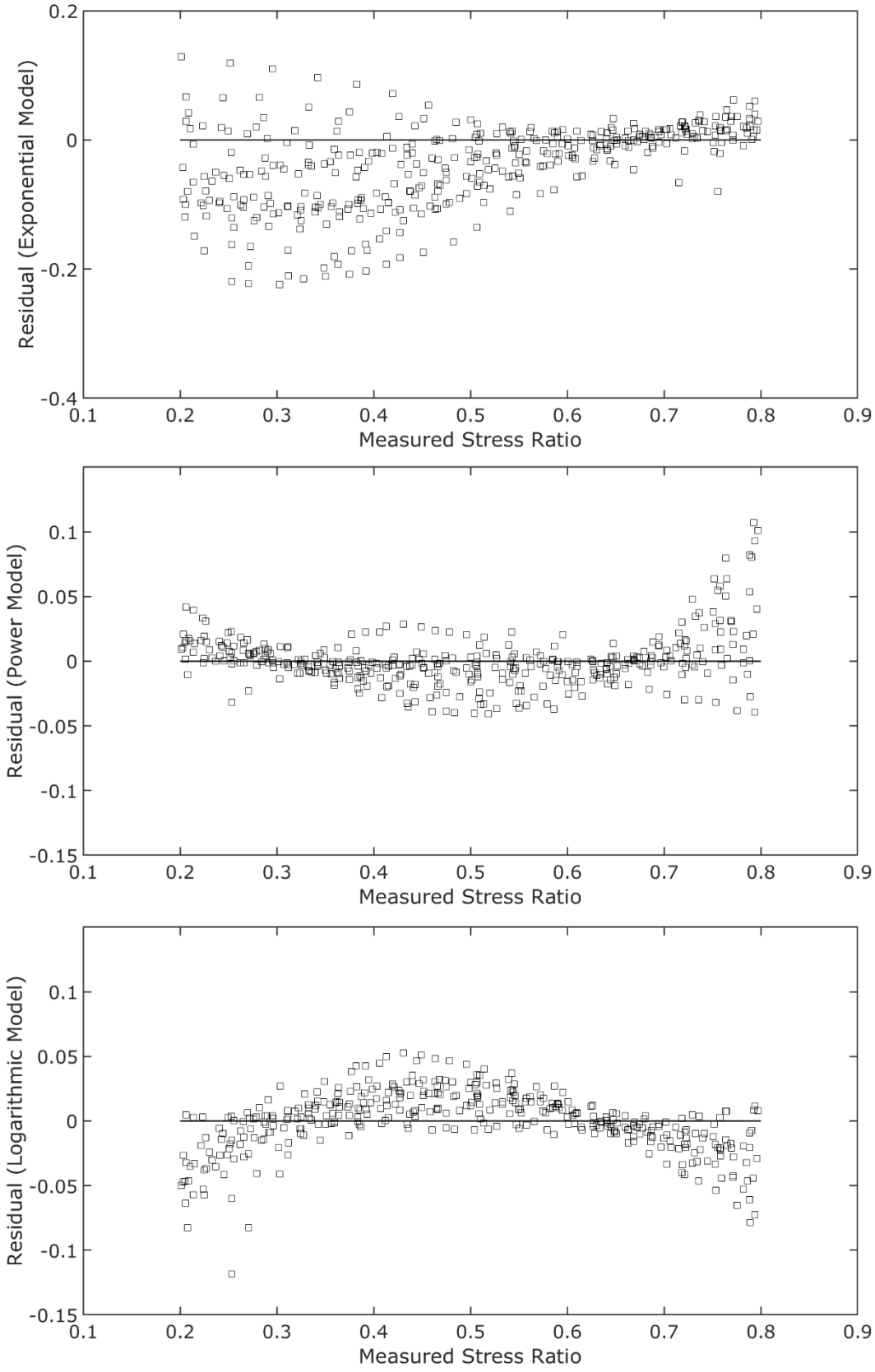

Figure A4-1. Residuals of observed stress ratio for the Intact Bothkennar CKUC tests (23 tests) by curve-fitting model: (a) Exponential law model (b) Power law model (c) Logarithmic law model.

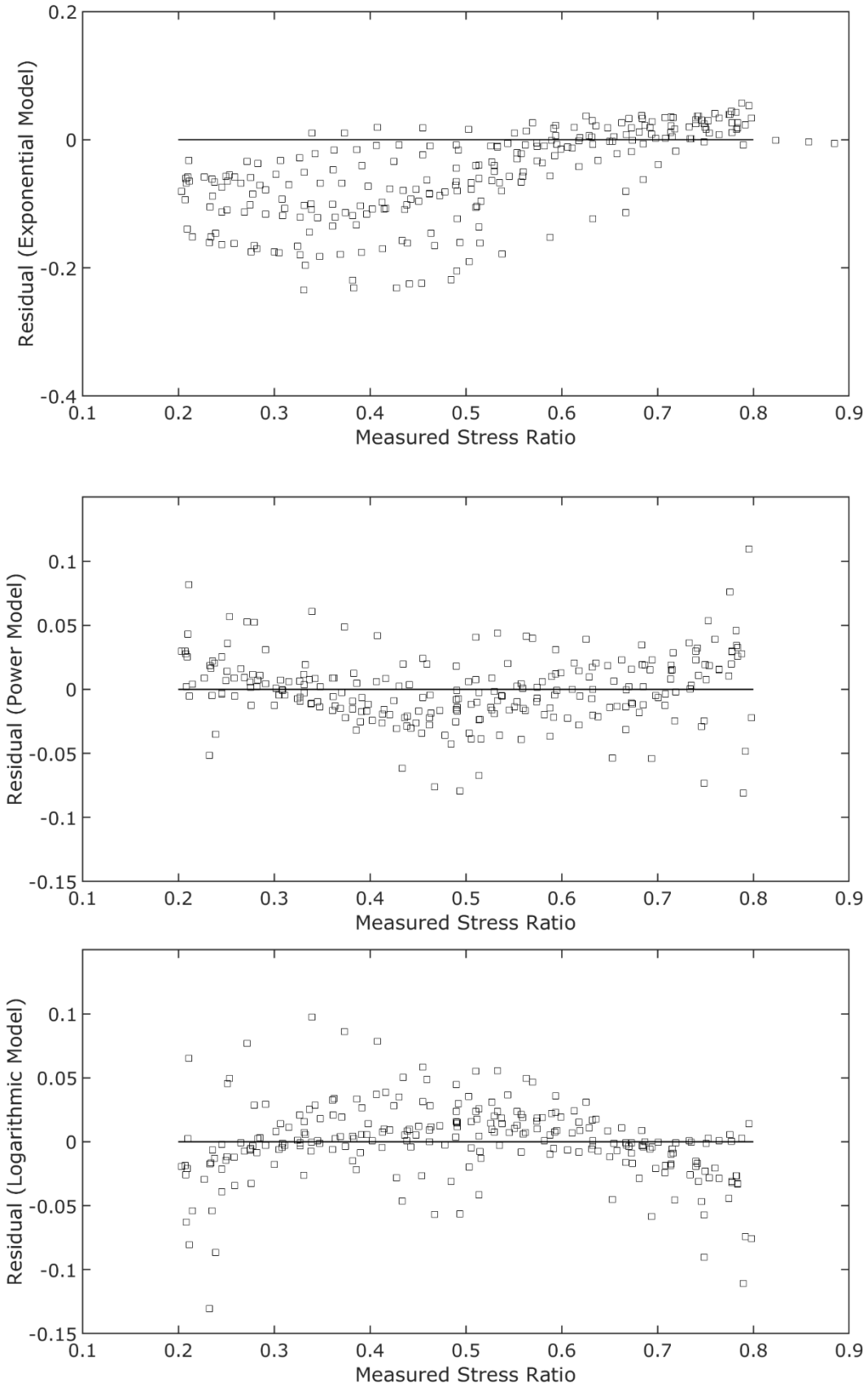

Figure A4-2. Residuals of observed stress ratio for the Intact Bothkennar CKUE tests (11 tests) by curve-fitting model: (a) Exponential law model (b) Power law model (c) Logarithmic law model.

Appendix 4-2

Residual errors from Model 2 (Power Law) and Model 3 (Logarithmic Law) for all shear modes by increment of stress ratio. Mean average and standard deviation shown for each increment of stress ratio.

Power Law model

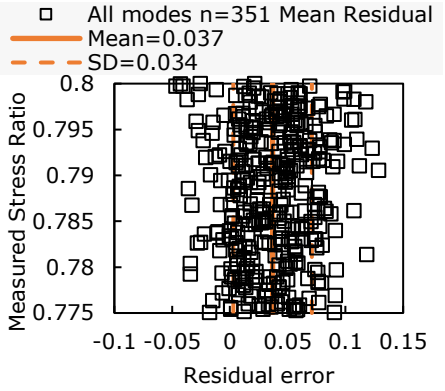

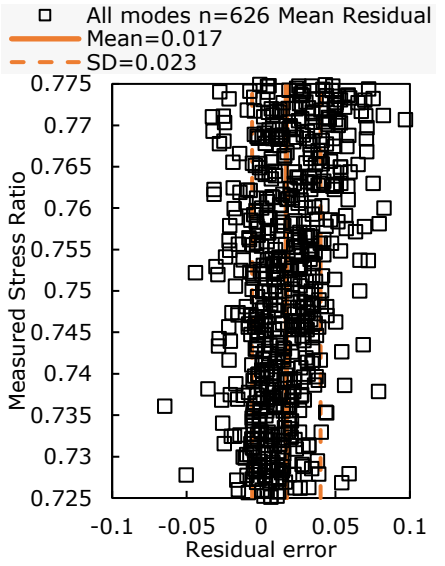

Logarithmic Law model

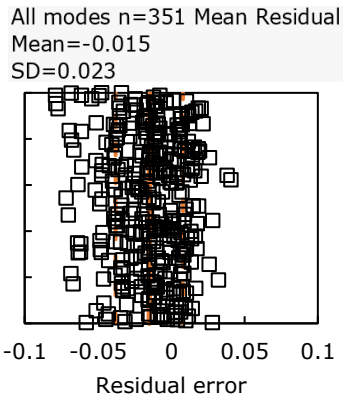

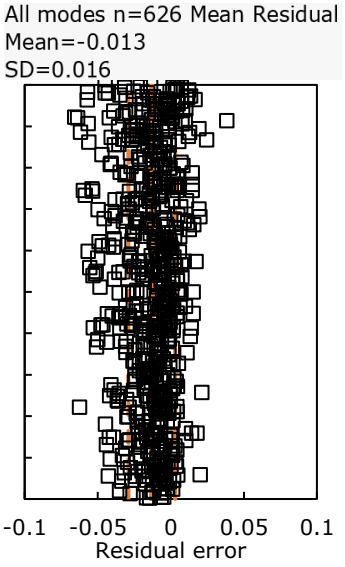

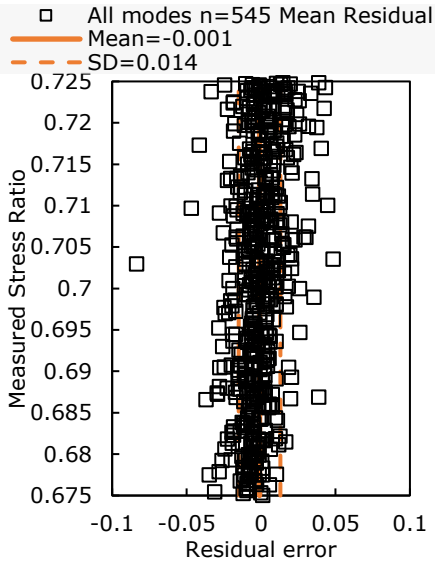
All modes n=545 Mean Residual
Mean=-0.001
SD=0.014
Measured Stress Ratio
0.725
0.72
0.715
0.71
0.705
0.7
0.695
0.69
0.685
0.68
0.675
-0.1
-0.05
0
0.05
0.1
Residual error

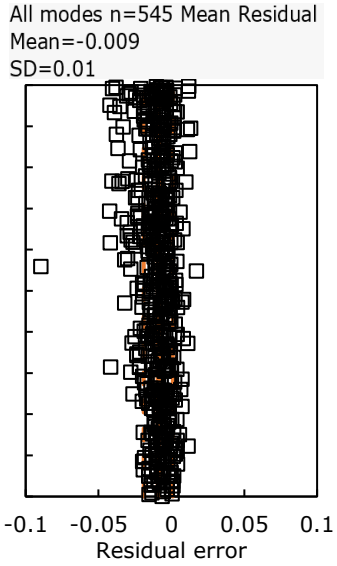
All modes n=545 Mean Residual
Mean=-0.009
SD=0.01
-0.1
-0.05
0
0.05
0.1
Residual error

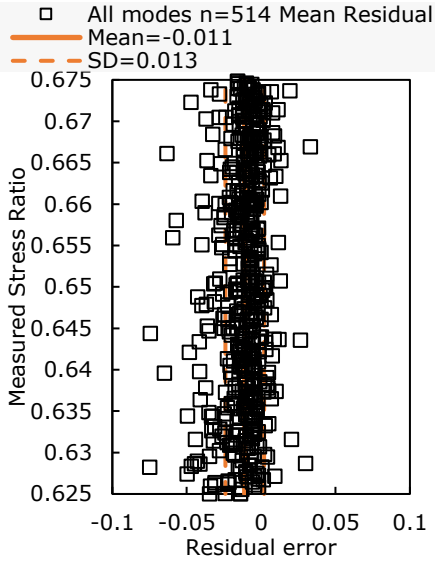
All modes n=514 Mean Residual
Mean=-0.011
SD=0.013
Measured Stress Ratio
0.675
0.67
0.665
0.66
0.655
0.65
0.645
0.64
0.635
0.63
0.625
-0.1
-0.05
0
0.05
0.1
Residual error

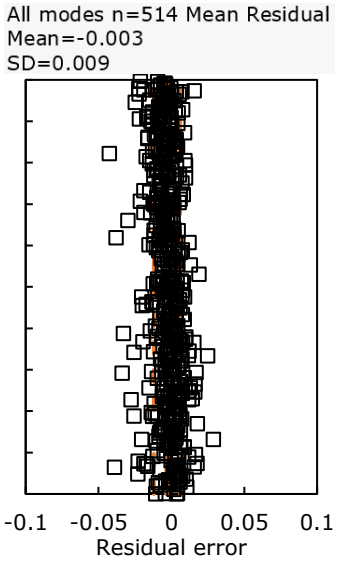
All modes n=514 Mean Residual
Mean=-0.003
SD=0.009
-0.1
-0.05
0
0.05
0.1
Residual error

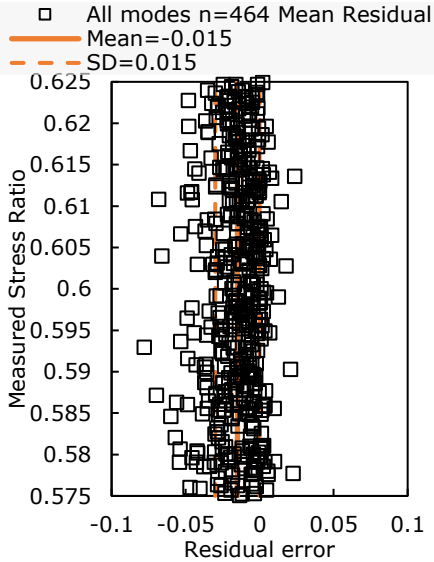
All modes n=464 Mean Residual
Mean=-0.015
SD=0.015
Measured Stress Ratio
0.625
0.62
0.615
0.61
0.605
0.6
0.595
0.59
0.585
0.58
0.575
-0.1
-0.05
0
0.05
0.1
Residual error

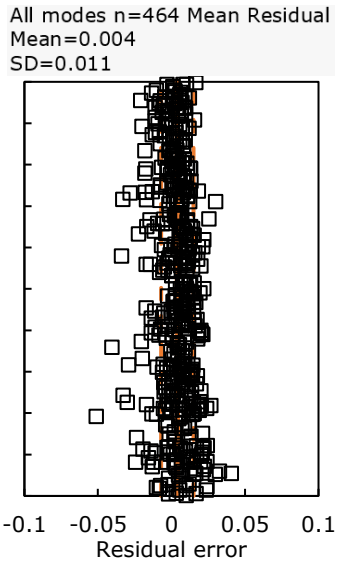
All modes n=464 Mean Residual
Mean=0.004
SD=0.011
-0.1
-0.05
0
0.05
0.1
Residual error

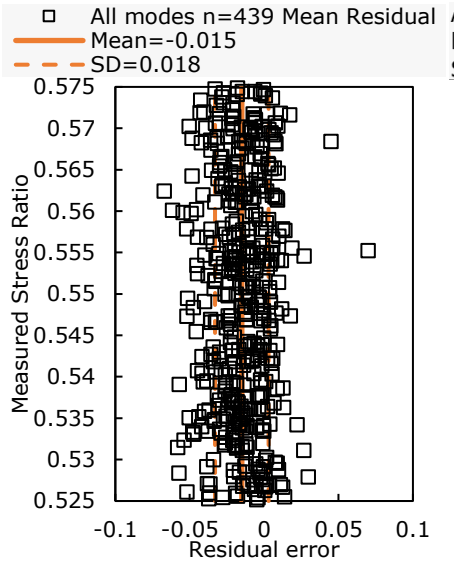
All modes n=439 Mean Residual
Mean=-0.015
SD=0.018
Measured Stress Ratio
0.575
0.57
0.565
0.56
0.555
0.55
0.545
0.54
0.535
0.53
0.525
-0.1
-0.05
0
0.05
0.1
Residual error

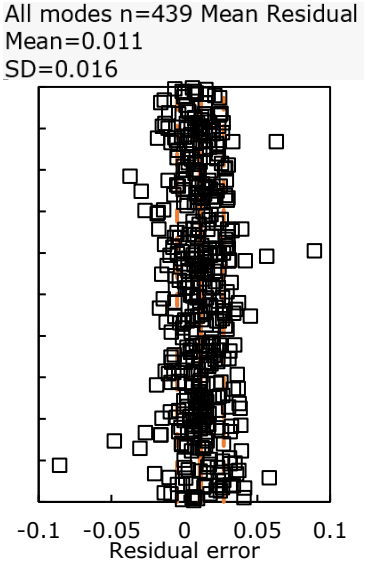
All modes n=439 Mean Residual
Mean=0.011
SD=0.016
-0.1
-0.05
0
0.05
0.1
Residual error

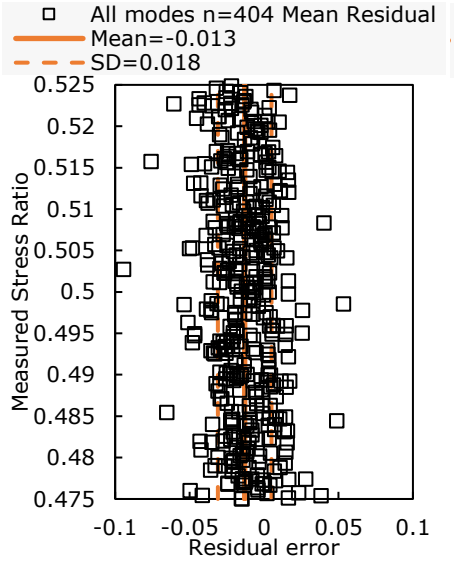
All modes n=404 Mean Residual
Mean=-0.013
SD=0.018
Measured Stress Ratio
0.525
0.52
0.515
0.51
0.505
0.5
0.495
0.49
0.485
0.48
0.475
-0.1
-0.05
0
0.05
0.1
Residual error

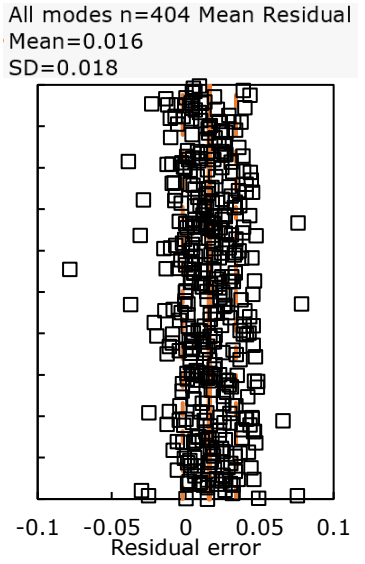
All modes n=404 Mean Residual
Mean=0.016
SD=0.018
-0.1
-0.05
0
0.05
0.1
Residual error

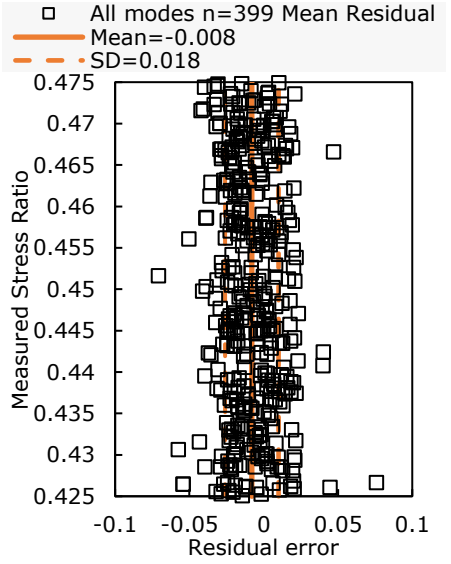
All modes n=399 Mean Residual
Mean=-0.008
SD=0.018
Measured Stress Ratio
0.475
0.47
0.465
0.46
0.455
0.45
0.445
0.44
0.435
0.43
0.425
-0.1
-0.05
0
0.05
0.1
Residual error

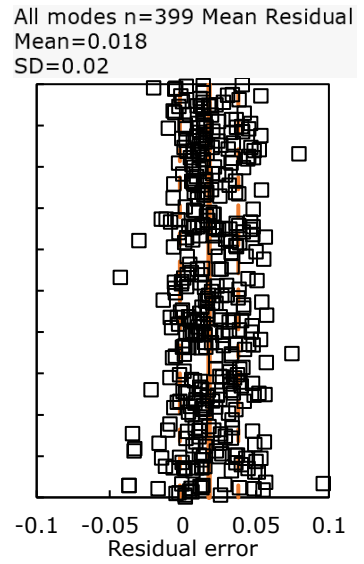
All modes n=399 Mean Residual
Mean=0.018
SD=0.02
-0.1
-0.05
0
0.05
0.1
Residual error

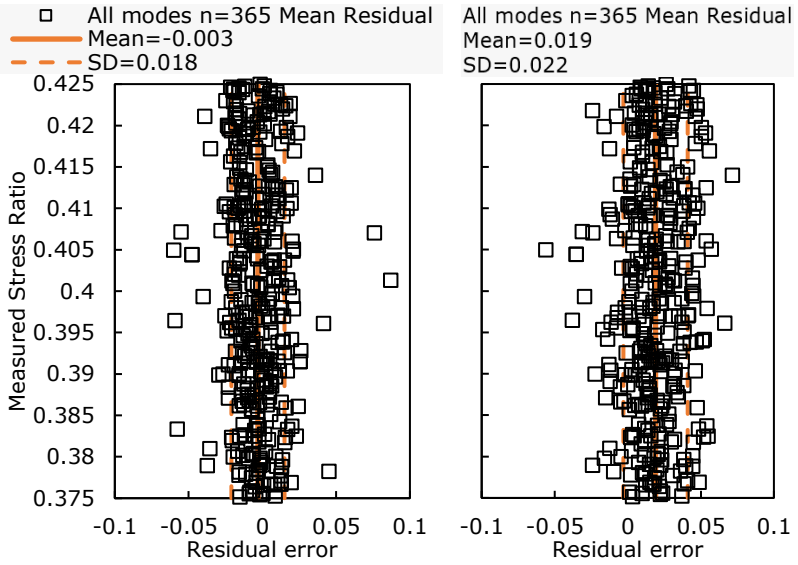
All modes n=365 Mean Residual
Mean=-0.003
SD=0.018
All modes n=365 Mean Residual
Mean=0.019
SD=0.022
Measured Stress Ratio
Residual error

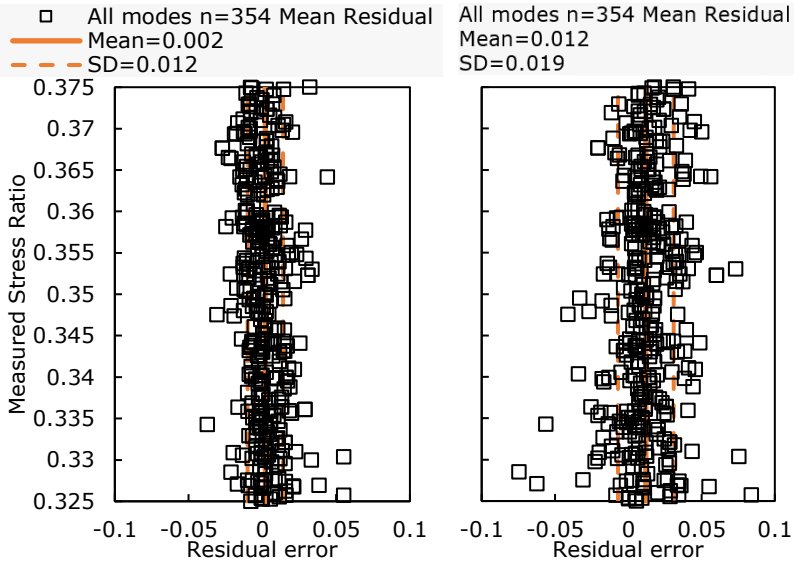
All modes n=354 Mean Residual
Mean=0.002
SD=0.012
All modes n=354 Mean Residual
Mean=0.012
SD=0.019
Measured Stress Ratio
Residual error

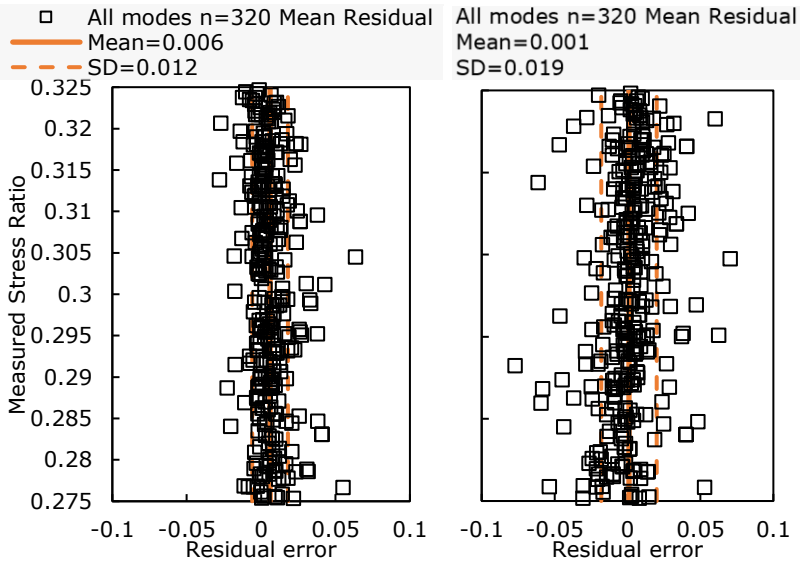
All modes n=320 Mean Residual
Mean=0.006
SD=0.012
All modes n=320 Mean Residual
Mean=0.001
SD=0.019
Measured Stress Ratio
Residual error

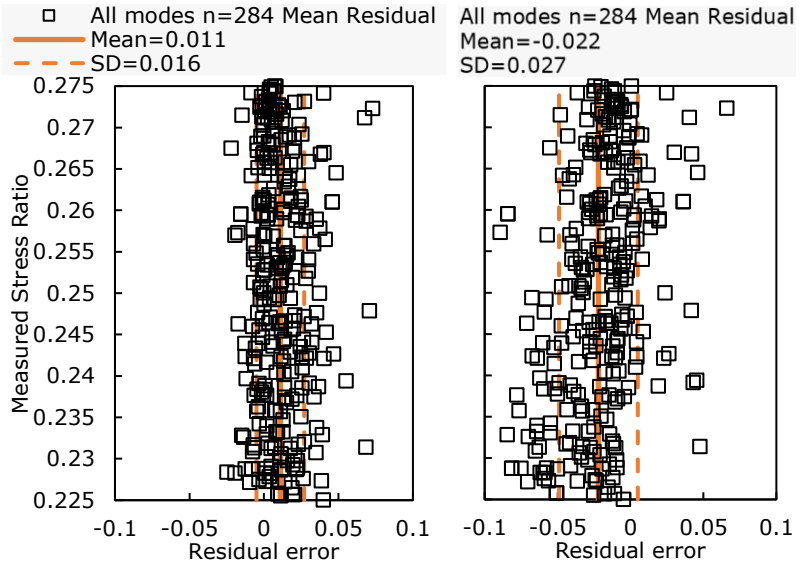
All modes n=284 Mean Residual
Mean=0.011
SD=0.016
All modes n=284 Mean Residual
Mean=-0.022
SD=0.027
Measured Stress Ratio
0.275
0.27
0.265
0.26
0.255
0.25
0.245
0.24
0.235
0.23
0.225
-0.1
-0.05
0
0.05
0.1
Residual error

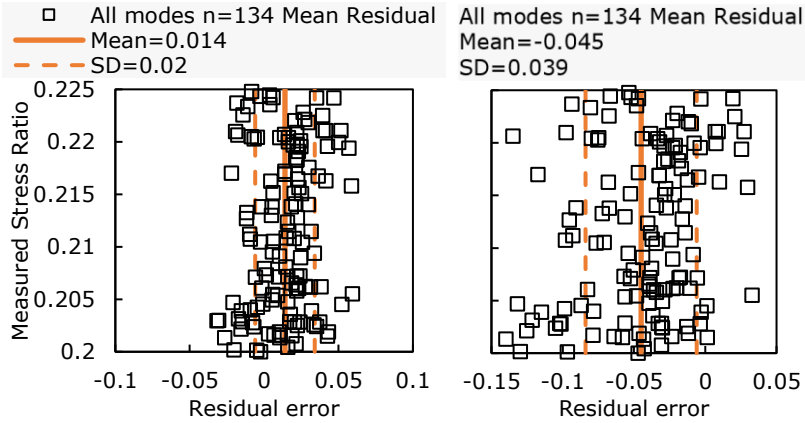
All modes n=134 Mean Residual
Mean=0.014
SD=0.02
All modes n=134 Mean Residual
Mean=-0.045
SD=0.039
Measured Stress Ratio
0.225
0.22
0.215
0.21
0.205
0.2
-0.1
-0.05
0
0.05
0.1
-0.15
-0.1
-0.05
0
0.05
Residual error

Appendix 5.1

The following general procedure was used for CIU triaxial tests:

SETTING UP Reconstituted Samples

(1) Prepare sample mould with thin layer of grease and weigh.
(2) Callipers and scales should be ready to use after the sample has been extruded.
(3) Reduce the applied consolidometer pressure to zero and extrude the sample into the mould quickly and carefully.
(4) Remove filter papers and porous stones and measure sample mass and dimensions. Note that:
    The consolidometer top cap will be attached to the sample following extrusion. While the sample is still in the mould, use a screwdriver or thin blade to carefully detach the top cap from the stone. Do not pull away roughly as this can disturb the sample.

SETTING UP Reconstituted Samples (Continued) And Intact Samples

(5) If using filter drains, prepare filter paper strips ready to attach to sample (vertical strips for compression tests). Note: filters were used only in preliminary tests, see Table 5- 1.
(6) Check that the O-rings are not over-stretched and will provide adequate seal.
(7) Ensure that there is sufficient water available in the air-water interface. (Apply vacuum to lower the pressure exiting the chamber, causing water to flow in from a water source.)
(8) Eliminate air in the back pressure system. Apply a small back pressure manually and bleed the back lines to the base and top platens using spare connectors and syringe.
(9) Apply vacuum to the membrane stretcher**.** Regulate the air pressure with a connected valve.
(10) The porous stones should be saturated (by boiling or placing under vacuum) before placing one onto the triaxial base platen. Flood with de-aired water from the back pressure system and remove excess surface water.
(11) Place the sample onto the base platen.
(12) With the vacuum still applied to the membrane stretcher, lower the stretcher over the sample. It may help to place small weights/discs on the base to provide a platform once lowered.
(13) Lower the top cap carefully onto the sample, ensuring the bender has correct alignment. Remove membrane stretcher. Note: bender elements were used but results are not reported.
(14) Fix horizontal clamp to base plate ready to fasten local axial LVDTs into position. Provide sufficient gap to allow LVDT and wire to exit round the base plate.
(15) Fasten LVDTs to the sample, ensuring vertical alignment, and check that the instrument is recording within the predetermined linear range of operation.
(16) Position and secure the cell onto the frame using the lifting eyes /chains and hoist.
(17) Fill cell with water. Release the valve to air at top to assist the filling process.

(18) Ensure all air-water interface chambers have sufficient water available. It is possible to use the head difference between cell water level and chamber or apply a vacuum to the chamber to fill the interface from the cell water.

(19) Flush the base porous stone, then the top stone, then from the base upwards through the membrane.

   a. Be careful to avoid flushing too much water into the base of the sample, as this can cause softening at the sample base.
   b. A small suction applied to the outgoing flush pipes assists the removal of air bubbles. This can be achieved using a syringe and extra piping.

(20) After flushing, reduce back pressure to 0kpa and reset back pressure channels. While cell pressure is 0kpa, reset the cell p channel.

SATURATION

(21) With the drain valve open, manually increase cell pressure and back pressure so that the sample experiences an isotropic effective stress of **5-30kPa**

(22) Increase cell pressure and back pressure simultaneously, using Triax control equations, at a rate of **25-50kPa/hour** until back=**200-250**kPa

(23) Close the drain valve and carry out a B check. Turn off control, and manually increase cell pressure by a known pressure increment (e.g. 25kPa). Allow up to an hour for the pore water pressure (PWP) transducers to respond to the increase in cell p. $\Delta pwp/\Delta cell = B\ value \geq 0.95$ (if this B value is not achieved, repeat steps 20-22 at a higher back pressure of up to 300kPa)

(24) Once a satisfactory B value has been achieved, lower the back pressure to the value recorded at the start of the B check (usually 200kPa). Reduce the cell pressure so that the current effective stress is maintained.

CONSOLIDATION

(25) With the drain valve now open, increase the cell pressure steadily using Triax control, at a continuous rate of **5-8kPa/hour**

(26) Continue until the effective maximum preconsolidation stress is reached ($\boldsymbol{p'_m}$). Allow the sample to continue draining at this stress, until a steady state of volume change is recorded.

(27) If swelling to an OCR>1, decrease the cell pressure steadily using Triax control, at a rate of -**5-8kPa/hour**

(28) Continue until the effective preshear stress is reached ($\boldsymbol{p'_0}$). Allow the sample to continue draining at this stress, until a steady state of volume change is recorded.

UNDRAINED SHEAR (Triaxial compression)

(29) Close the sample drainage line. Move the cell onto the triaxial frame platform, taking care to minimise aggravation to the cell/sample.

(30) Check position of the frame platform and adjust manually to ensure adequate displacement is available to complete required shearing of the sample.

(31) Take bender element readings.

(32) Place the triaxial frame loading bar into the correct position by adjusting the height with minimal possible aggravation to the triaxial cell.

(33) Adjust the load cell configuration to prevent any vertical displacement downward into the cell.

(34) Fix the load cell to the frame loading bar with the tapped connection rod. The load cell is now supported by the frame.

(35) Lower the load cell slowly and carefully downwards to almost reach contact with the sample-cap. Attached to the load cell is a ball bearing load-cap for compression tests.

(36) Start placement-controlled shear (upwards) at the required strain rate. Take bender element readings from initial contact at the required strain intervals.

END OF TEST

(37) Stop frame displacement. Reverse frame until sizeable gap is between load cell and top cap. Secure the load cell onto the triaxial cell. Remove the frame loading bar and move cell to a manageable height (e.g. to the work station).

(38) Empty cell water and remove the cell to expose the sample.

(39) Disassemble the sample (keeping membrane intact if possible, for later load-displacement testing).

(40) Measure sample dimensions, mass, dry mass.

UNDRAINED SHEAR (Triaxial extension)

(41) Close the sample drainage line. Move the cell onto the triaxial frame platform, taking care to minimise aggravation to the cell/sample.

(42) Check position of the frame platform and adjust manually to ensure adequate displacement is available to complete required shearing of the sample.

(43) Take bender element readings.

(44) Place the triaxial frame loading bar into the correct position by adjusting the height with minimal possible aggravation to the triaxial cell.

(45) Adjust the load cell configuration to prevent any vertical displacement downward into the cell.

(46) Fix the load cell to the frame loading bar with the tapped connection rod. The load cell is now supported by the frame.

(47) Lower the load cell slowly and carefully downwards to reach contact with the sample-cap. Attached to the load cell is the rotationally flexible load-cap which will accommodate a sample tilt of up to 12 degrees. The load-cap should be seated with a load of up to 10kPa. It is possible to achieve a sealed connection with a seating load of only 1 to 2kPa. However, it is of interest to minimise the probability of an unsuccessful attempt to seal the connection between load-cap and sample-cap. Therefore, a seating load of 5 to 10kPa is recommended.

(48) Adjust the external LDS to ensure adequate travel is available to record shear displacement.

(49) Connect the frame to the cell (e.g. by placing weights on the top of the cell).

(50) Quickly open the vacuum line to atmospheric pressure. If the connection seal is successful, the outflow of cell water through the vacuum line will stop, and the load cell will record an initial extension load (i.e. negative) that is dependent on the local compliance (i.e. the small extension displacement that occurs during the load-cap to sample-cap connection process) and the stiffness of the sample.

(51) Allow the sample load to stabilise

(52) Start displacement-controlled shear (downwards) at the required strain rate. Take bender element readings from initial contact at the required strain intervals.

END OF TEST

(53) Lower cell pressure to atmospheric pressure

(54) Release vacuum in extension cap by small pulse of positive air pressure (e.g. blow sharply into vacuum pipe)

(55) The load cell will then be released and can be raised to near the top of the cell. The cell is thus supported by the frame platform.

(56) Remove the cell-frame connection (e.g. hanging weights).

(57) Using load pulley system, move the cell off the triaxial frame and onto the bench securely.

(58) Empty cell water.

(59) Disassemble the sample (keeping membrane intact if possible, for later load-displacement testing).

(60) Measure sample dimensions, mass, dry mass.

Appendix 5.2

UU test procedure

(1) 38.1mm samples to be handled carefully to avoid disturbance. Wear gloves to reduce moisture loss due to handling.

(2) Apply thin silicon grease to the sample container and measure the mass. Extrude sample into container.

(3) Remove porous stones and filter papers from extruded sample. Measure mass of the sample + container with scales. Measure diameter and length of sample.

(4) Saturate the porous stones to be used during the test using a vacuum chamber and water vessel

(5) Saturate the pore water pressure pipes and zero the transducer

(6) Place a porous stone onto the base pedestal and flood, ensuring a puddle of water is formed on the surface. Then remove the excess water.

(7) Place filters onto the sample ends then position sample onto the saturated base porous stone

(8) Place top cap onto sample

(9) A brass tube with suction acting between the interface with the rubber membrane is placed over the sample, without touching it.

(10) Turning off the suction contracts the membrane over the sample and allows the membrane ends to be slipped off and fixed with O rings to the Perspex discs at each end. Check the axial alignment.

(11) Fill the cell with water.

(12) Apply the required cell pressure, corresponding to typical total vertical in-situ stress. E.g. 0.5σv or 10z, σv or 20z, and 2σv or 40z.

(13) Wait for the pore water pressure to increase due to the raised cell pressure, until a stable value is obtained.

(14) Raise the loading platform so the loading cap is ¼ inch or 6.35mm below the ram.

(15) The reading of the load cell is set to zero and the motor drive is started at the specified strain rate (1%/minute). Contact is indicated by a positive load measurement.

(16) Test is continued until deviator stress remains constant or begins to fall, although samples which fail with plastic yield (constant stress) show a slow rising load with strain at failure due to increase in sample area.

(17) Make note of the strain at which slip surfaces first appear.

AFTER THE TEST

(18) Drain the cell water.

(19) Remove the cell, remove loading cap and rubber membrane.

(20) Measure mass, diameter, length of sample. Sketch the mode of failure and measure inclination of slip planes (if any).

(21) Measure moisture content of the specimen.

Appendix 5.3

Oedometer test procedure

(1) Prepare apparatus: This involves checking alignments of the yoke and beam and measuring the inherent deformability of the apparatus.

(2) Prepare soil: For kaolin, the same maturing process is used as in 4.1.1, stage 1.

(3) Measure consolidation ring and porous stones: Diameter, height and mass

(4) Calculate hanger masses required for application of particular effective stresses: The hanger mass varies in accordance with the measured area of the consolidation ring

(5) Place specimen into ring and weigh: The kaolin slurry may be difficult to place in the ring without trapping air.

(6) Measure initial moisture content: A sample is taken from the remaining slurry.

(7) Assemble specimen into the oedometer load frame: The specimen is placed in the oedometer cell and screwed into a fixed position. The cell is then placed in the oedometer press. Finally, the top cap is placed atop the specimen very carefully to ensure no tipping occurs.

(8) Set up loading yoke and beam: The yoke must be aligned vertically; the top cap has a groove to guide the yoke but it may not always be correct. No additional load must be applied via the yoke to the specimen during this stage, as this will affect the results due to misalignment of the top cap.

(9) Adjust alignment of the dial gauge or LDS to the top cap and reset to zero.

(10) Apply first load increment to hanger: The load is applied while the beam is supported by the frame. The load is taken by the frame initially and not by the specimen, to prevent additional moment forces being applied.

(11) Transfer load to the specimen: With everything in place and provided that the hanger is motionless, the beam support is wound down and the load is transferred instantly to the specimen.

(12) Saturate specimen: Fill the cell with distilled water.

(13) Record settlement readings: A linear displacement transducer may be used for automatic readings. However, this requires calibration and must account for fluctuating voltage. Owing to the limited number of available transducers in the laboratory, it was deemed suitable to manually record the settlement readings from non-electric dial gauges. This also enabled multiple tests to be run at once. Settlement readings were taken in time intervals of 24 hours after load application. Over 90% consolidation occurred within this time in every case.

(14) Apply next load increment and repeat steps 10-13.